Université Montpellier 2
Science et Techniques du Languedoc

Thèse

présentée en vu d'obtenir le grade de
Docteur de l'Unversité Montpellier 2

Discipline: Informatique
Ecole Doctrale: Informations, Structures, Systemes (I2S)

par

Szymon Stoma

Modélisation du développement du méristème apical caulinaire d'*Arabidopsis*

sous la direction de:

Christophe Godin
Jan Traas

Thèse soutenue le 03.02.2009 devant le jury composé de:

M. Grégoire Malandain	INRIA	Présidente
M. Henrik Jönsson	Lund University	Rapporteur
M. Yves Couder	Universite Denis Diderot Paris 7	Rapporteur
M. Emmanuel Guiderdoni	CIRAD	Jury
M. Christophe Godin	INRIA	Directeur de thèse
M. Jan Traas	ENS Lyon	Directeur de thèse

Université Montpellier 2
Science et Techniques du Languedoc

PhD Thesis

submitted for the degree of
Doctor of Philosophy
in
Computer Science

by

Szymon Stoma

Modelisation of shoot apical meristem of *Arabidopsis*

Advisors:

Christophe Godin
Jan Traas

Thesis defended 03.02.2009 before the jury composed of:

M. Grégoire Malandain	INRIA	President
M. Henrik Jönsson	Lund University	Reviewer
M. Yves Couder	Universite Denis Diderot Paris 7	Reviewer
M. Emmanuel Guiderdoni	CIRAD	Jury
M. Christophe Godin	INRIA	Advisor
M. Jan Traas	ENS Lyon	Advisor

Dla tej, której zapach jest wiecznie przy mnie..

Acknowledgements

I would like to thank all the people who made writting of this thesis possible. First of all Jan and Christophe, whose help, determination and guidance was simply priceless. It is important to note, that Jan and Christophe are not only 100% professionals fully dedicated to their work, but they allowed me to recognize them as nice and friendly people on whom I could count in all situations. I consider this rare and I appreciate this very much. I would only wish to meet more people like them on my path. Thanks! Then I would like to mention all the members of Virtualplants team in Montpellier and RDP team in Lyon, who gave me a lot of inspiration on everyday basis. I was extremely lucky to spend the last three years with the people I do not call colleagues but definitely friends. Some of these people I would like to thank more explicitely since they were too important to be generalised:

Jerome - you are the one who knows the best how much I owe you (and how much you owe me ;]). Since you are very decent, I would not put it here (however, I will remember). Thank you for all this time we spend together in various conditions and places. You are the one, who has tough skin, but you also showed me your fragile belly, which I really appreciate. David – thanks for all your inputs to my life, I hope this will go much further, and maybe one day we both will find a place to rejoin on this magic world? You know, to do all the sports we tried together and finally, to invent a supa-booma b-game we will conquest the world with? Fred – I am really glad to have met you somewhere on my path. In short: thanks for all the coolness and chill-out you bring to the world even without noticing it, It was amazing feeling to watch you converting from black Moise into sensitive and loving father (which seems to suit you). Christophe – thanks for all your thoughts you shared with me during this time. If I would be God, I would really organize the world according to many ideas of yours. And please, tell your kids to practice Indian pool, since next time there will be no handicap. Sam – thanks for all the time we spend together, I can only regret we did not manage to organize any boat trip on the same ocean

and in the same time, Next time? Florence – I really regret I did not manage to know you better, since only from what I know you are a great woman, with terrible (the one I like) sense of humour.

During this thesis I was supported by tones of positive energy by almost every person in my closest surrounding which I consider as being extremely lucky. Without this positive feedback I would not be able to finish this thesis. This feedback was also coming from all my invisible friends, who are spread all around the world and I can only wish that somebody will finally invent teleportation, so we can be together and not skype together. Thank you guys! During all this period I was also supported by one of the most amazing human beings I met in my life – my girlfriend Magdalena – who bravely bared my everyday moods and was bringing rays of sun to my life, allowing me to skip the battles with myself. Thank you! And last, but not least I would like to thank my family, who supports me in everything whatever I do, accepting it or not, till I remember.

And thanks to Fate, because I really think I had more luck than I desire.

Thank You all!

Contents

List of Figures

List of Tables

Abbreviations

API application programming interface
CLV clavata
CMT cortical microtubules
CUC cup-shaped cotyledon
CZ centre zone
GUI graphical user interface
LFY leafy
MPI Max Planck Institute
MSS mass-spring system
PIN1 pin-formed1
PZ peripheral zone
REV revoluta
RAM root apical meristem
mRNA messenger ribonucleic acid
RZ rib zone
SAM shoot apical meristem
SEM scanning electron microscope
STM shootmeristemless
STN single and multi-cellular signal transduction networks
SVG scalable vector graphics
WUS wuschel

Abstract

The research presented in this thesis uses computational techniques to heighten our comprehension of shoot apical meristem (SAM) development, and in particular the process of regular organ initiation, called *phyllotaxis*. This work is focused on the role of an essential plant hormone, auxin, in SAM development. In this thesis, I introduce an auxin-transport model of phyllotaxis at cellular scale, which is able to reproduce spiral phyllotaxis patterns observed *in vivo*. The auxin-transport is mediated by special membrane carrier molecules, called PIN proteins. The polarization of PIN inside of the cell is regulated by the flux of auxin, as it was suggested in the original canalization concept proposed by Tsvi Sachs. The proposed flux-based model reproduces PIN distribution observed *in vivo* both, in L1 meristem layer and as well in the rib zone of the meristem. Second part of the thesis is dedicated to the simulations of growth. In this part, I introduce the physical-based framework to simulate growth of the meristem including tropisms. Since auxin modifies rigidity of cell walls leading to an increase in growth rates in the spots of its high concentration, the introduced framework is used to upgrade auxin transport-based model of phyllotaxis. In this upgraded model the transport-based patterning mechanism directly modifies the growth directions of the meristem, allowing us to study the coupling of growth, auxin and PIN distributions.

Introduction

A *meristem* is a section of a plant tissue characterised by continuous cell divisions and growth. It consists of incompletely or not differentiated cells functionally analogous to stem cells*[1] in animals. *Shoot apical meristem* (SAM) is located at the tip of the aerial part of the plant. It produces lateral organs and stem tissues. One of the most spectacular phenomena resulting from the meristem functioning is the process of regular organ initiation – *phyllotaxis*[2].

During plant *development*, the cells in the meristem interact with each other by sensing and emitting various molecules. This interaction is called *cell signalling* and it leads to specific, spatial and temporal gene expression patterns, creating a *dynamic patterning mechanism*. The phyllotaxis is driven by this *complex system*[3]. Due to their intricacy, a qualitative analysis of complex systems, is usually not possible. However, *computational modelling* provides a powerful means to test the behaviour of such systems.

During last years the development of methods enabling observation and analysis of plant cells rapidly progressed. In particular, the knowledge about cell signalling and patterns of gene expression significantly increased allowing us to gain a deeper insight into the mechanisms responsible for meristem functioning at a cellular level. Although relevant progress has been made in understanding how *morphogen*[4] distributions are changing during plant development, less is still known about how these distributions are related to *plant growth*.

Understanding how morphogens both influence and respond to growth can be also addressed using computational modelling. Using mechanistic computer models it is possible to generate *shape* changes and associated morphogen pat-

[1] Difficult words are marked with * if they are used more than once. Their definitions can be found in the Glossary in the Appendix B. If the word is used only once, the definition is given in the footnote.

[2] from the Greek (*phyllon* — leaf; *taxis* — order).

[3] A complex system is a system composed of interconnected parts that as a whole exhibit behaviour not obvious from the properties of the individual parts (Wikipedia).

[4] A morphogen is a substance governing the pattern of tissue development and, in particular, the positions of the various specialised cell types within a tissue (Wikipedia).

terns. The results can be compared with experimental observations of normal and mutant phenotypes and therefore, used to test and verify hypotheses.

This work is focused on the role of an essential plant hormone, *auxin,* in SAM development. The interest in this particular, biochemical substance arises from the experiments showing a direct influence of auxin on the process of organ initiation in SAM, as well as its correlation with cell growth intensity. It is believed, that auxin-based mechanisms are responsible for this remarkable, regular arrangement of organs that has been discussed since centuries.

It is assumed that phyllotaxis results from an uneven distribution of auxin caused by its *active transport* mediated by special molecules, called *membrane carriers.* These membrane proteins enable both the cell influx and efflux of auxin. Interestingly, recent findings suggest, that these carriers are regulated by auxin itself. This dependency creates a complex *feedback* loop, increasing the difficulty level of further analysis.

Present biomolecular methods do not allow us to tracking the auxin flow directly at the cellular level. However, there is a possibility (e.g. through staining of auxin carriers) to follow periodical patterns of these transporters during the meristem development. The auxin distribution can thus be accessed in an indirect way. Due to these obstacles in the auxin-based model explaining phyllotaxis, additional hypotheses describing the relation between auxin and its transporters are needed.

The main goal of this thesis is to increase the comprehension of such a Daedalian, biological process as phyllotaxis in the context of patterning and growth. This task is realized using computional modelling techniques.

In the context of this work, I developed a collection of dedicated computer simulation tools. They allowed me to convey *in silico* experiments focused on the meristem development and, in particular, on the hypothesised mechanisms governing the auxin transport driving the phyllotaxis, as well as to analyze the feedback between growth and auxin distribution.

Organization of the thesis

In the first chapter I introduce the meristem (1.1.1), describe its structure (1.1.2), gene expression during its development (1.3.2), and further I focus on its dynamics. Its development leads to a phyllotaxis (1.2), thus I present the terms required to analyze this process and review a subset of phyllotaxis models based on the concept of inhibitory field (1.2.3). In the context of phyllotaxis, a plant hormone *auxin* is explained (1.3). I discuss in details the biological data concerning auxin functions (1.3.1) and in particular its transport in the SAM (1.3.2). In the subsection 1.3.3 auxin transport model is formalized in the form of equation system. The chapter finishes with the comparision of recent phyllotaxis models based on the active transport of auxin and its concentration-based mechanism (1.4). The mathematical notation introduced and developed in this section is used to unify all auxin transport models reviewed and studied within this thesis (which importantly simplifies the in between comparisons).

In the second chapter auxin transport in the tissue and meristem is discussed in details. I present the original Sachs concept (the canalization hypothesis, and its generalization, *flux-based* mechanism) and its formalization proposed by Mitchison. In section 2.2 our work on *flux-based* auxin transport extending the Mitchison's simulations is presented. This work was used as a basis to study the *flux-based* mechanism in the context of phyllotaxis. In section 2.2, I describe this study, in which we show, that the *flux-based* hypothesis, together with a set of rules describing the development of the meristem creates a self-organising system, which is able to drive phyllotaxis. I describe the properties of this system and compare *in silico* images with *in vivo* ones. Finally, in the last section of this chapter (2.3), the *flux-based* phyllotaxis model is compared with the *concentration-based* models.

In the third chapter cell mechanics is studied. Firstly, I review the mechanical properties of cell wall in the context of growth (3.1), I present our work on a modelling framework, which allowed us to study the influence of the mechanical properties of the meristem on its developing form (3.2). We performed a series

of *in silico* experiments, in which we investigated the issues of a maintenance of the dome-like shape of *pin1* (3.3), the local variation of growth depending on the concentration of auxin in growing meristem (3.4), and finally the feedback between the *concentration-based* auxin transport model and auxin-dependent growth (3.5).

In the fourth chapter computer details concerning the modelling issues are discussed. I present the concept of $(DS)^2$ systems (4.1) and place tissue structures in this context. I review structures used to model various cellular processes (4.2) and introduce the WalledTissue, the data structure developed during this thesis (4.2.2).

In the appendices a short text on the solving of ODE and PDE equation in the context of this thesis is attached (A). Since this thesis is placed in the multidisciplinary field, a glossary containing difficult words was prepared (B). Also, original posters, covers and publications diffused during this thesis are attached (C).

Chapter 1

Development of the meristem

1.1 Meristems

1.1.1 The shoot apical meristem (SAM)

A plant develops and increases its size through the activity of small groups of undifferentiated cells called meristems. Different types of meristems are identified according to their function and localisation in the growing plant. The SAM is localized at the tip of aerial plant's axes, whereas the root apical meristem (RAM) at the tip of ground plant's axes. Cells in the SAM give rise to all plant organs above the ground, e.g. leaf or flower primordia, whereas the RAM initiates the subterranean portion of the plant. Moreover, the SAM has the ability to form as well lateral organs such as petals, floral bracts or bud scales. During vegetative growth of the plant the SAM continuously produces branches or leaves. When flowering begins, the SAM evolves into inflorescent meristem producing floral meristems [Solomon and Berg, 2007].

This thesis is focused on the shoot apical meristem and therefore further detailed discussion concerns this plant tissue. The figure 1.1 shows the SAM of *Antirrhinum* from the top and the side, taken using the scanning electron microscope (SEM). The side-view of SAM scheme is presented in the figure 1.2.

1.1.2 The structure of the SAM

In the shoot apical meristem an organisation into radial zones and layers is distinguished [Schmidt, 1924].

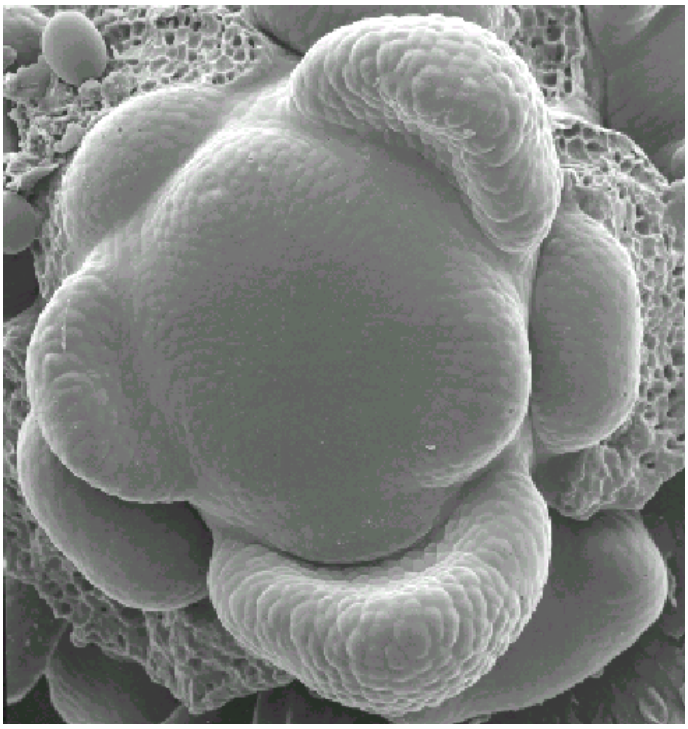

A

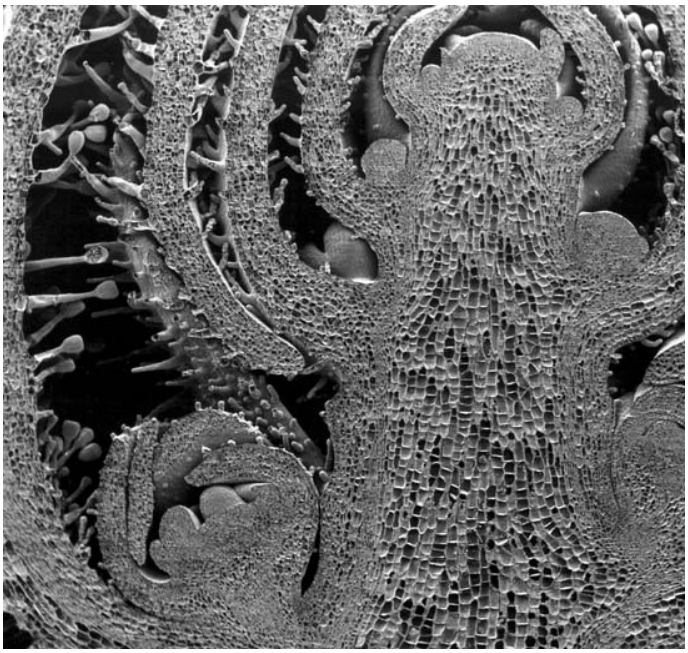

B

Figure 1.1: Electro scan microscope images taken of shoot apical meristems of Snapdragon (*Antirrhinum majus*).
Figure 1.1a shows the meristem seen from top. Image taken from Jan Traas (credits to John Doonan). Figure 1.1b shows a side view of the meristem. Image taken by P. Huijser (MPI, Koeln).

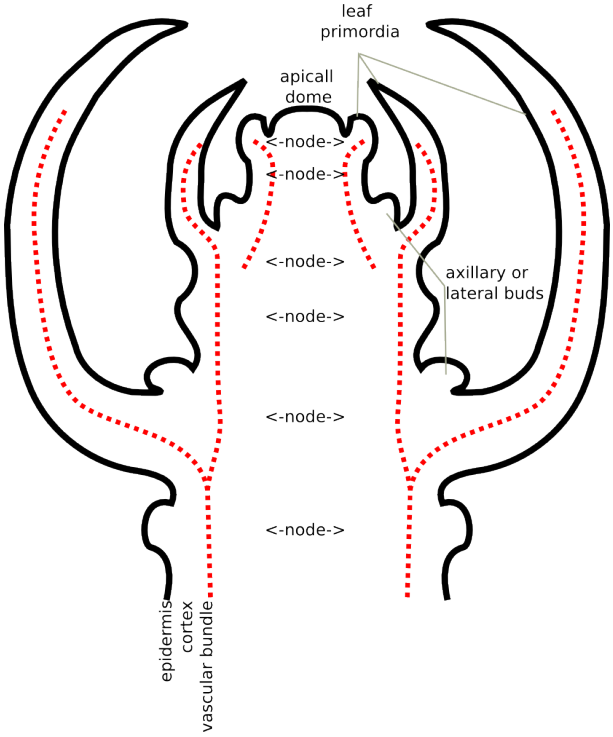

Figure 1.2: A scheme of a shoot apical meristem in side view. Apical dome, leaf primordia tips and lateral buds are zones of continuous divisions and internodes (marked as nodes) are the zones of cell elongation. Note, that the vascular strands are created very early, just after primordium initiation.

The layers of cells within the SAM form two regions: an external, known as the tunica, in many species subdivided into several layers (called L1, L2) and an inner defined as a corpus (in species with and L1 and L2 referred to as L3), figure 1.3. With respect to the surface, the cells within the tunica proliferate mostly perpendicularly, whereas within the corpus, they divide mostly parallel to it.

In *Arabidopsis*, the outermost layer L1, initiates the precursor cells of the epidermis, the L2 or subepidermal layers initiates the ground tissues and germ cells, while the L3 produces the vascular tissues and the inner portion of the leaves and flowers.

Despite this stereotypic organization, this laminal structure is dynamic. Growth creates a basipetal* displacement of the cells and, as a result their positions within the layers are not rigid [Gifford and Corson, 1971]. The laminal organisation of the meristem is maintained in the stem and lateral organs of the SAM [Dermen, 1953, Stewart and Burk, 1970]. Moreover, the number of layers varies between different types of plants [Barbier, 2005].

In addition, the SAM is divided into radial zones, characterised by specific rates of proliferation and cytohistological properties [Gifford and Corson, 1971, Steeves and Sussex, 1989].

At the tip of the SAM, within the central zone (CZ), cells are often relatively large with pronounced vacuoles and divide with lower frequency than the neighbouring cells [Kerstetter and Hake, 1997]. This zone produces cells that will enter the differentiation process while maintaining itself.

On the sides of CZ the peripheral zone (PZ) which initiates the lateral organs is discriminated. Within this zone the cells display higher rate of division, no prominent vacuoles and are smaller than the ones being a part of the CZ.

Third, the rib zone (RZ) expands at the bottom of the SAM, where cells proliferate fast and become a part of the stem tissues. The described zones are presented in figure 1.3.

1.1.3 Main genes expressed during organ initiation

1.1.3.1 Maintenance of the meristematic stem cells

Genetic analysis has identified a range of genes involved in meristem function. Genes encoding transcription factors of the so-called KNOTTED-LIKE-

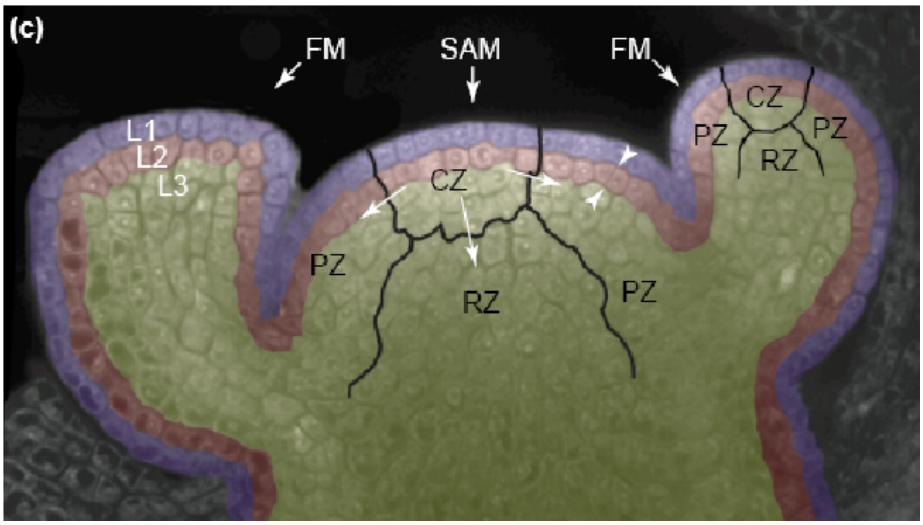

Figure 1.3: Confocal laser-scanning micrography through an *Arabidopsis* inflorescence SAM and its adjacent floral meristems (FMs).
The coloured domains depict the different cell layers: in *Arabidopsis*, the tunica corresponds to two layers of cells, the epidermal (L1) and subepidermal layers (L2), whereas the corpus corresponds to the internal layers (L3). The two arrowheads point at an anticlinal cell division occurring in L2. The black outlines represent the approximate boundaries between the different meristematic zones: the peripheral zone (PZ) contributes cells to the formation of lateral organs, the rib zone (RZ) contributes cells to stem growth and the central zone (CZ) acts as a "factory" of cells for the PZ and RZ, but also for its own replenishment with new cells. Although the cells of the PZ and the CZ are histologically distinguishable, there is no sharp boundary between each zone. The PZ and the CZ contain both tunica and corpus cells, whereas the RZ is "buried" beneath them in the deeper layers of the corpus. Figure taken from [Carles and Fletcher, 2003].

HOMEBOX (KNOX)[1] family. They prevent the meristem cells from differentiation [Heisler et al., 2005]. In *Arabidopsis thaliana*, a major homebox genes regulating meristematic activity is SHOOTMERISTEMLESS (*STM*). If, due to mutation, *STM* is not expressed, the plant fails to establish and maintain the SAM showing that this gene is required for sustaining the indeterminate character of the SAM stem cells [Barton and Poethig, 1993]. In many species its local downregulation is required for the initiation of the primordia in course of the plant embryogenesis [Long et al., 1996]. Indeed, *STM* is expressed in whole SAM with exception of the primordia [Lenhard et al., 2002].

1.1.3.2 Regulation of the central zone

Mutants where the so-called CLAVATA (CLV) genes are inactivated, are characterized by an enlarged SAM and the development of additional floral organs [Clark, 1993]. These changes result from a higher number of cells caused by a deficient transition of cells out of the central zone [Laufs, 1998]. The function of the *CLV* is to negatively regulate the size of central zone limiting an expansion of the undetermined meristematic cells of the SAM [Jeong et al., 1999].

In contrast to the *CLV* mutations, the SAM of the plants where the WUSCHEL (*WUS*) gene is inactivated, is flat and terminates prematurely after forming of a few organs [Laux et al., 1996]. Thus, *WUS* counterbalances the function of *CLV* promoting the production of undifferentiated cells [Laux et al., 1996, Mayer et al., 1998]. *WUS* also serves a complementary function with *STM*. *WUS* determines the meristematic cell pool, while *STM* prevents the SAM cells from undergoing differentiation [Carles and Fletcher, 2003].

1.1.3.3 CLV-WUS feedback loop

The coordination of the central zone controlled by *CLV* and *WUS* is a continuous antagonistic process. When the signaling of *CLV* is repressed, *WUS* expression increases [Schoof et al., 2000]. Conversely, mutants showing overexpression of the *WUS* gene, have a *clv*-phenotype. An opposite pattern results, if the *CLV* domain expands, repressing the *WUS* and producing a *wus*-like plant [Brand, 2000]. Therefore, it was proposed that this feedback loop is required to provide the equilibrium between the maintenance of the stem cells pool and production of cells designated for building new organs. This feedback loop is illustrated in figure 1.5.

[1] By convention, the names of the genes are noted in italics capital letters (e.g. *STM*), the names of proteins in capital letters (e.g. STM) and names of the phenotypes of genetic plant mutants in lower-case (e.g. *stm*).

Jonsson and Heisler [2006] presented a series of computer simulations demonstrating various properties of this feedback loop. Their simulations were based on reaction-diffusion mechanism in which an activator induces *WUS* expression. This model is able to organize the *WUS* expression domain, as observed in the experiments. In addition, the model predicts the dynamical reorganization seen in experiments where cells, including the *WUS* domain, are ablated with laser beam. It also predicts the spatial expansion of the WUS domain resulting from removal of the *CLV* signal.

1.1.3.4 Genes expressed during the initiation of primordia

The demarcation of boundaries between the SAM and primordium leads to development of new organ identity and is controlled by CUP-SHAPED-COTYLEDON (*CUC*): *CUC1, CUC2, CUC3* genes [Aida et al., 1997]. Though the mechanism of boundary positioning is still not well understood, gene families both associated with adaxial, facing the main axis, patterning such as REVOLUTA (*REV*) [Mcconnell et al., 2001, Otsuga et al., 2001, Emery et al., 2003] and abaxial, facing away from the axis, arrangement as *YABBY, KANADI* were discovered [Eshed et al., 2004, Kerstetter et al., 2001].

A mutation in PINOID (*PID*) encoding a protein kinase C–like protein, leads to decreased auxin transport [Bennett et al., 1995, Christensen et al., 2000], whereas the overexpression of *PID* gene leads to augmented growth consistent with increased auxin transport [Christensen et al., 2000, Benjamins et al., 2001]. The spacial expression of these genes during the meristem development is presented in figure 1.4.

1.2 Phyllotaxis

1.2.1 Introduction to phyllotaxis

Observing spikes of a cactus (1.6A), scales of a pineapple fruit (1.6B) or seeds within a sunflower head (1.6C) leads to an impression of symmetry. This striking regularity is due to the fact that during the growth of the plant organs emerge at well defined positions, forming phyllotactic patterns (figure 1.7). These patterns can be used to classify and distinguish plant species. During the study of phyllotaxis patterns, certain quantitative measures were introduced [Schimper, 1830, Braun, 1831, 1835].

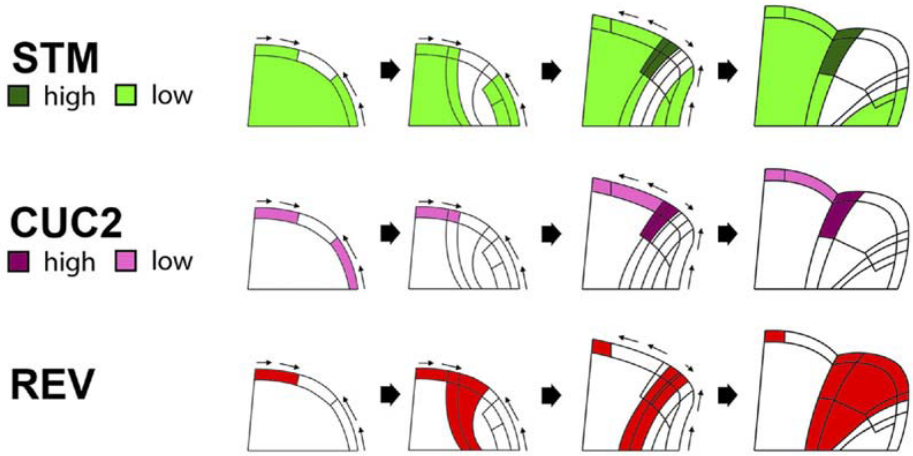

Figure 1.4: The schematic of spacial expression of genes during inflorescent meristem development.
Description in text, image taken from [Heisler et al., 2005].

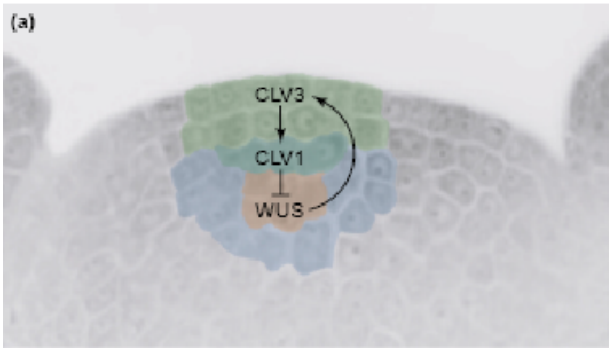

Figure 1.5: Stem cell regulation in the SAM via the *CLV–WUS* feedback loop. *CLV3* expression is restricted mainly to the L1 and L2 of the central zone, whereas *CLV1* mRNA can only be detected in the L3 of the central zone and rib zone. *WUS* is expressed in few central cells of the rib zone. The *CLV–WUS* feedback loop consists of a *WUS* mediated signal from the central zone that specifies stem cell identity in the outermost layers, which signal back via the *CLV* pathway to limit the size of the *WUS*-expressing CZ.Image taken from [Carles and Fletcher, 2003].

A

B

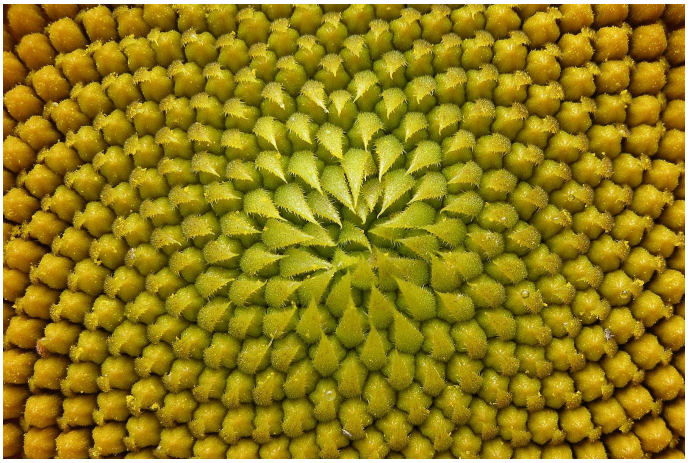

C

Figure 1.6: Examples of phyllotactic patterns.
The following figures shows spacial organisation of plant's organs: 1.6A spikes of a cactus *Trichocereus huascha* (Botanic garden, Montpellier), 1.6B scales of a young pineapple (Botanic garden, Berlin) and 1.6C seeds within a sunflower head (own cultivation, Montpellier). All these patterns show high level of organisation.

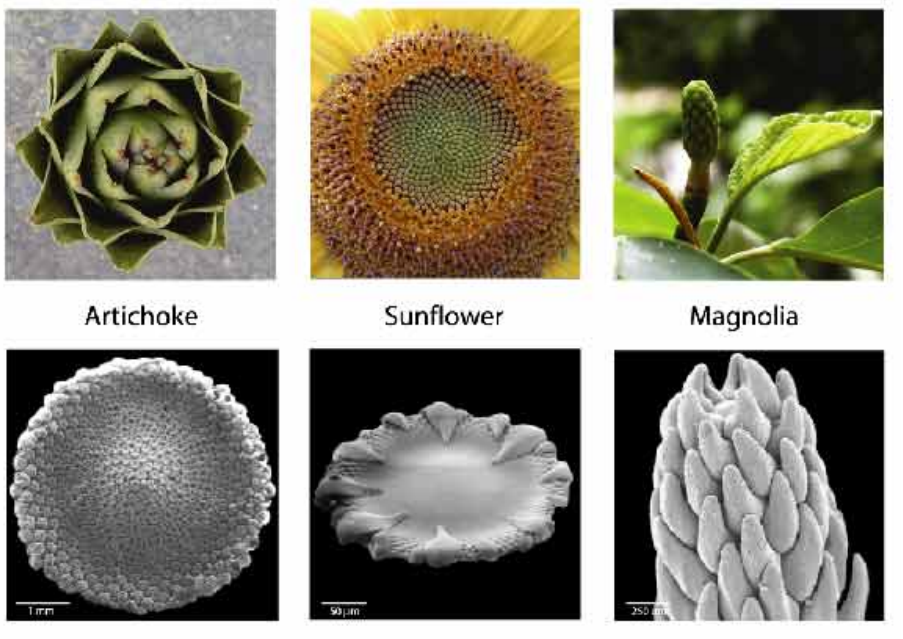

Figure 1.7: Meristem as a source of phyllotaxis.
The organisation of primordia in meristem resembles the mature organs.

1.2.1.1 Divergence angle

One of the main concepts used to characterise phyllotactic patterns is the divergence angle. It is defined as an angle between two organs that are formed consecutively. For example considering an arrangement of leaves appearing alternatively on opposite sides of a stem (figure 1.9C). The divergence angle of this pattern equals 180 degrees.

1.2.1.2 Parastichies

Another important parameter is derived from the concept of *parastichies* - imaginary lines connecting the centres of neighbouring organs. On the pinecone illustrated on figure 1.8 we can observe, that its scales are organised in concentric rows starting from its bottom 1.8B. For each scale we draw a line to the rightmost and leftmost adjacent scales from the consecutive row. As a result, clockwise and counter-clockwise spirals around the vertical axis of the pinecone emerge 1.8C, 1.8D. If we count these spirals, we obtain two numbers: $i = 8$ (for clockwise ones) and $j = 13$ (for anti-clockwise ones). These numbers are used to characterise this particular phyllotactic pattern.

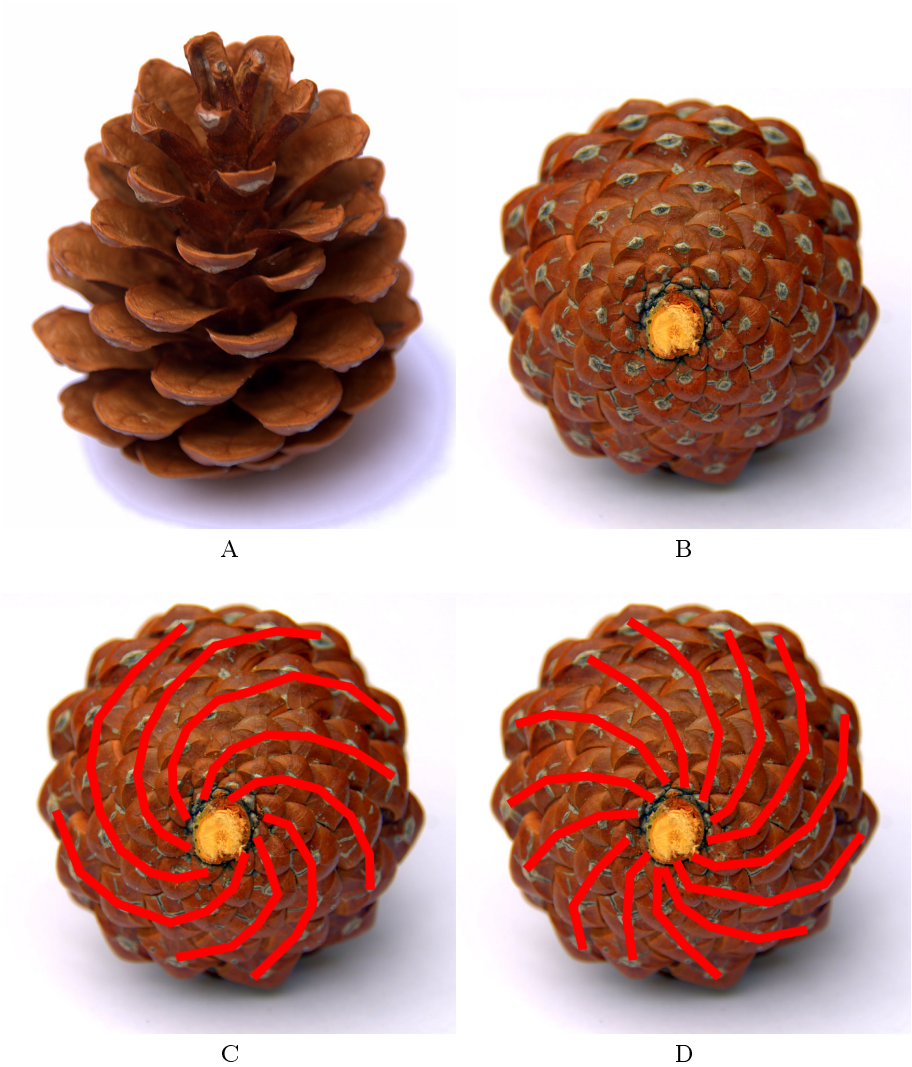

A B C D

Figure 1.8: Phyllotactic pattern of a pine cone.
1.8A presents side view of a pine cone, whereas 1.8B shows the bottom view of a pine cone. It can be observed that its scales are organised in concentric rows starting from its bottom 1.8B. In figures 1.8C, 1.8D spiral line are drawn starting from the pine cone bottom. For each scale we draw a line to the rightmost (1.8C) or leftmost (1.8D) adjacent scales from the consecutive row. As a result, clockwise and counter-clockwise spirals around the vertical axis of the pine cone emerge 1.8C, 1.8D. If we count these spirals, we obtain two numbers: $i = 8$ (for clockwise ones) and $j = 13$ (for anti-clockwise ones). These numbers are used to characterise this particular phyllotactic pattern.

1.2.2 Types of Phyllotaxis

The series of divergence angle along a stem or parastichy numbers allow us to classify systematically the phyllotactic patterns. Two groups of patterns are usually distinguished: *i*) patterns where primordia appear one at a time or *ii*) patterns for which more then one primordium appears simultaneously [Kuhlemeier, 2007].

The first group contains spiral patterns with one special case, alternate (distichous) pattern. The alternate pattern (figures 1.9C, 1.9D) is characterised by the consecutive organs' emergence on opposite sides of the growing tip, and therefore the divergence angle equals 180 degrees.

In spiral patterns (figures 1.9A, 1.9B) the divergence angles are constant during the plant development. As a result, the organs are positioned on a helix. This type of architecture corresponds to the most common leaf arrangement in nature.

The stunning phenomenon is that in many spiral patterns the number of parastichies i, j are two consecutive Fibonacci numbers (1, 1, 2, 3, 5, 8, 13, 21, ...)[2]. Even more intriguing is the fact that for such patterns, the divergence angle is close to the Golden Angle (about 137.5 degrees). This frequent arrangement is called Fibonacci phyllotaxis.

If more primordia emerge simultaneously at a node, a whorled phyllotaxis can be observed. A whorl is a structure, in which all the organs are attached at the same node and evenly distributed around the stem.

Let us denote α an angle between each consecutive organ in a whorl. In opposite (decussate, 2-whorl) pattern the successive layers of whorls with two organs are established. For this pattern α equals 180 degrees . Following whorls are rotated by an angle of 90 degrees, $\alpha/2$ (figures 1.9D, 1.9E).

When three primordia develop at one time, a tricussate (3-whorl) phyllotaxis is formed. In such an arrangement of organs, an angle of whorls rotation between consecutive nodes equals 60 degrees. In general, in k-whorl the angle α equals $360/k$ and the angle between consecutive whorls bisects the α angle and thus equals $360/2k$.

A more complicated phyllotaxis corresponds to multijugate patterns. A spiral is composed of k-whorls, and the rotation angle of the next emerging layer of whorls is constant as in spiral pattern (therefore each k-whorl pattern is a special cases of multijugate pattern where the rotation angle equals $360/2k$). In this

[2]Figure 1.10 contains a selection of mathematical properties of Fibonacci numbers.

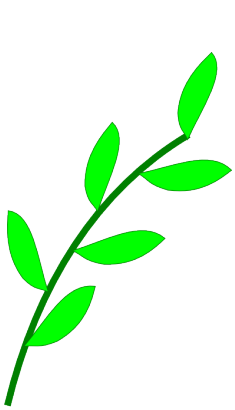

A

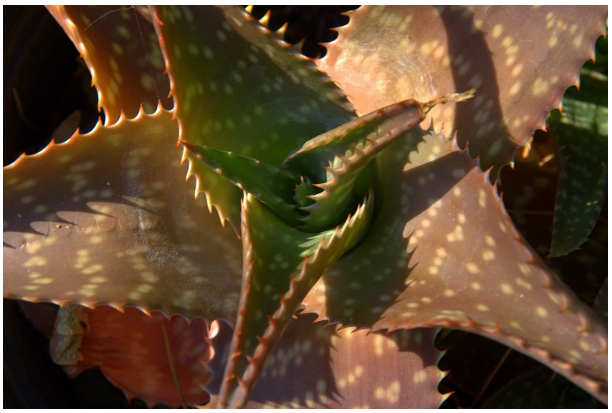

B

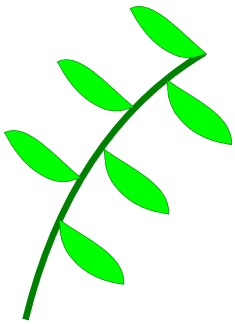

C

D

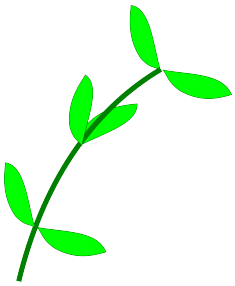

E

F

Figure 1.9: Basic phyllotactic patterns.
Figures 1.9A, 1.9B show spiral phyllotaxis.Figures 1.9C, 1.9D show decussate phyllotaxis (between the leaves). Figures 1.9E, 1.9F show 2-whorl phyllotaxis (between the stained leaves).

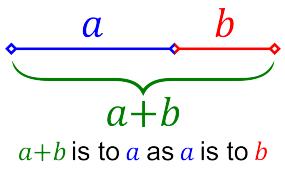

Figure 1.10: The golden section is a line segment sectioned into two according to the golden ratio.
The total length $a+b$ is to the longer segment a as a is to the shorter segment b: $\frac{a+b}{a} = \frac{a}{b}$.

In mathematics, the Fibonacci numbers are a sequence of numbers named after Leonardo of Pisa, known as Fibonacci [Fibonacci and Sigler, 2002]. The first number of the sequence is 0, the second number is 1, and each subsequent number is equal to the sum of the previous two numbers of the sequence itself, yielding the sequence 0, 1, 1, 2, 3, 5, 8, etc. In mathematical terms, it is defined by the following recurrence relation:

$$F_n = \begin{cases} 0 & if\ n = 0 \\ 1 & if\ n = 1 \\ F_{n-1} + F_{n-2} & if\ n > 1 \end{cases}$$

Like every sequence defined by linear recurrence, the Fibonacci numbers have a closed-form solution:

$$F_n = \frac{\varphi^n - (1-\varphi)^n}{\sqrt{5}}$$

where $\varphi = \left(1+\sqrt{5}\right)/2 \approxeq 1.61803$ and is called Golden ratio [Carr et al., 2008].

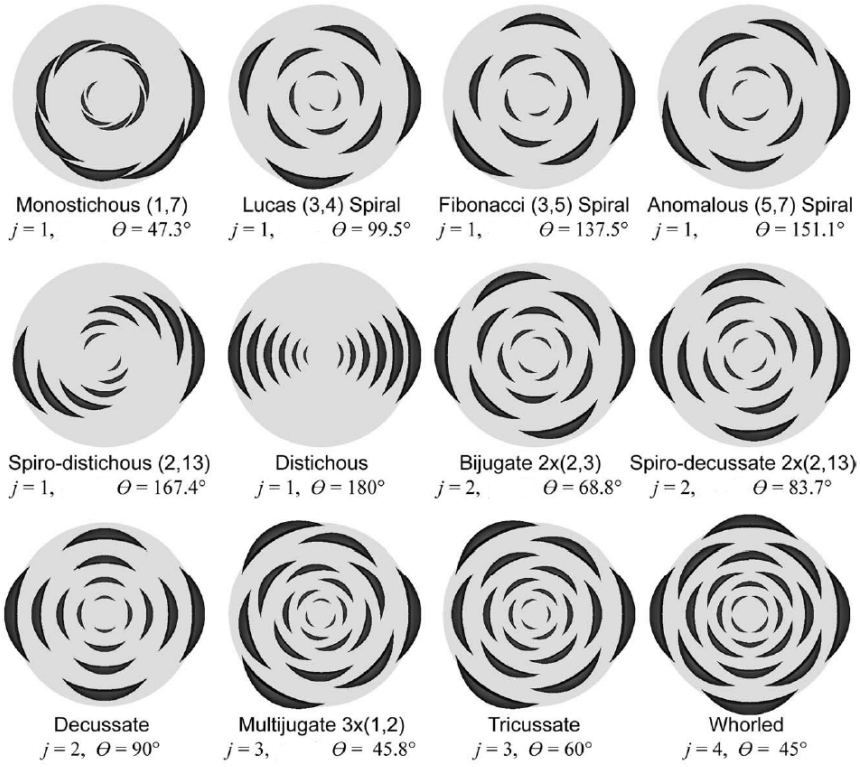

Figure 1.11: Review of phyllotaxis patterns.
Description in the text. For each pattern the name, divergence angle (θ) and jugacy (j) are given. For spiral patterns, numbers of opposed parastichies are given in parenthesis. Figure taken from [Smith et al., 2006b].

type of organ arrangement, if within one whorl two organs are established it is called bijugate, when three, it is referred to as trijugate.

The collection of different phyllotactic patterns is presented in figure 1.11 [Smith et al., 2006b]. It is important to note that the phyllotactic pattern may change during the growth of the plant either due endogenous or exogenous factors.

1.2.3 Phyllotaxis as the result of the inhibition of morphogens

In 1868 The German botanist Wilhelm Hofmeister proposed a rule describing the formation of a new primordium:

> "*Es ist eine durchgreifende Erfahrung, dass neue Blätter (oder Seitenachsen) an denjenigen Orten über den Umfang des im Zustande des Vegetationspunktes befindlichen Stängelendes (oder Stän-*

Ancient Egyptians were the source of Greek science, and as skilled observers probably knew about numbers and patterns in plants and the number t (look below).
370-285 BC Theophrastus wrote Enquiry into Plants which mentions leaves in regular series.
23-79 AD Pliny wrote Natural History which includes more detailed descriptions of plant patterns as a way of categorizing plants.
1202 Leonardo Fibonacci obtained the Fibonacci sequence as a solution to the problem of monthly population growth of rabbits. This sequence relates to t by the formula $\lim_{n\to\infty}(F_{n+1}/F_n) = t$.
1452-1519 Leonardo Da Vinci anticipated, in one of notebooks, the observation of spiral patterns in plants such as those made by Bonnet.
1571-1630 Johannes Kepler was fascinated by the number five and incorrectly concluded that the Fibonacci sequence propagated itself as the seeding capacity of plants, but did correctly surmise the intrinsic involvement of the sequence in plant growth.
1754 Charles Bonnet in his *Recherches sur l'Usage des Feuilles dans les Plantes* mentions the different phyllotactic arrangements of leaves, the genetic spiral, and one family of parastichies. He initiated observational phyllotaxis.
1830 Schimper introduced the concepts of the genetic spiral, the divergence angle, and the parastichy. He defined the divergence angle as a fraction by dividing the spiral arrangement into cycles and setting d = times around the stem per cycle/leaves per cycle.
1831, 1835 Alexander Braun observed conspicuous parastichies on pine cones, noting that the number of left and right parastichies were generally consecutive Fibonacci numbers.
1837 Auguste and Louis Bravais used a point lattice on a cylinder to represent leaf distribution, found the number of genetic spirals to be equal to the greatest common divisor of the numbers of secondary spirals, and defined the divergence angle as an irrational number related to the sequence from which the numbers of secondary spirals came.
1848 Lestiboudois found a connection between phyllotactic patterns and the phenomena of branching and ramification.
1868 Hofmeister proposed that new promordia form periodically at the apex boundary in the largest gap left by the preceding primordia.
1872 P. G. Tait rewrote and interpreted the Bravais brothers' results concerning the divergence angle and parastichy pair.
1873 Airy explained the arrangement of leaf primordia in a bud in terms of economy of space.
1875 Weisner theorized that the divergence between leaves evolved by natural selection as a way to maximize leaf exposure to light.
1878 Simon Schwendener described conspicuous opposed parastichy pairs, observed the changes in divergence angle and the ratio of internode distance to stem girth as the plant growth leads to higher phyllotaxes, and explained (incorrectly) that leaf arrangements are the result of contact pressure between primordia.
1882 Julius Sachs rejected the mathematical theory of phyllotaxis, seeing no significance in the continuous fractions for divergence angles.
1904 Church proposed an explanation for the phenomena of transitions between phyllotactic patterns, and that parastichies are lines of force. He rejected the genetic spiral and the cylinder model in favor of parastichies and a centric representation.
1907 van Iterson constructed a model of leaf primordia around a cylinder which assumed close packing.
1913 Schoute concluded that the dominance of the Fibonacci sequence over parastichy numbers was still unexplained and that Schwendener's work headed to the solution. He explained the placement of new primordia as a reaction to chemical inhibitors released by primordia to keep others from growing too close.
1917 D'Arcy Thompson proclaimed that there was no reason to prefer any one parastichy or family of parastichies and transformed the whole subject into speculation by concluding that there was an irreducible subjectivity to it.
1931 Mary and Robert Snow concluded from studying the effects of isolating leaf primordia that the positioning of new primordia is affected by adjacent, preexisting primordia.
1948, 1951 Richards introduced the idea of the plastochrone ratio and developed a system of equations to mathematically describe a centric representation using three parameters: plastochrone ratio, divergence angle, and the angle of the cone tangential to the apex in the area being considered.
1950 Plantefol concentrated on one family of spirals (foliar helices) and their biological reality without any mathematics.
1974 Adler wrote out the Fundamental Theorem of Phyllotaxis.
1983 Erickson rediscovered and extended van Iterson's analysis.
1984 Roger Jean reworked the Fundamental Theorem of Phyllotaxis.
1991 Levitov found and explained phyllotactic patterns in a flux lattice of a superconductor as a way of minimizing energy in the system.
1992 Douady and Couder found that drops of ferrofluid placed periodically in the centre of a dish produced phyllotactic patterns.
2000 Reinhardt and colleagues demonstrates that auxin accumulation is required and sufficient to trigger primordium development.
2003 Atela and colleagues formalized Hoffmaister's model in the form of a discrete dynamical system. The most frequent phyllotaxis patterns appear to be fixed points (orbits) in this system, as well as some patterns previously considered as random or chaotic, but appearing in the nature.
2003 Rainhardt and colleagues propose the explanation of phyllotaxy based on the active transport of auxin.
2006 Jonssen and colleagues propose a mechanism of PIN orientation based on the local concentration of auxin. This mechanism is compatible with 2003 model of phyllotaxis.
2006 Smith and colleagues demonstrate that the extension of Couder model (achieved by introducing second, time-related inhibitor) increase the stability of whorled and multijugate patterns.

Table 1.1: The history of the study of phyllotaxy. Green text updated by yours truly. Taken from `http://maven.smith.edu/~phyllo/`

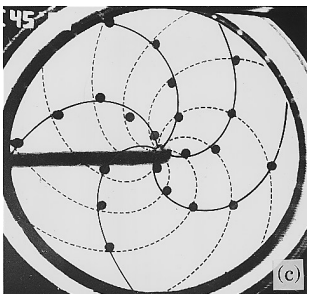

Figure 1.12: Set-up and results of the experiment described by Douady and Couder [1996b].
Image shows ferrofluid droplets on a dish filled with silicon oil. The droplets form regular, spiral patterns often found in the analysis of phyllotactic patterns. Imaginary spirals are marked with continuous (anticlockwise) or dashed (clockwise) lines. Image taken from [Douady and Couder, 1996b].

> *gelgürtels) hervortreten, welche am weitesten von den Seitenrändern der Basen der nächst benachbarten, bereits vorhandenen Blätter entfernt sind*" (Hofmeister 1868, pp. 482–483). [3]

This description led to a theory proposing that each new primordium develops on the tip of the growing stem at the spot that is the furthest with respect to all the older primordia. As the tip continues to grow from its centre, the primordia are pushed outwards leaving the space for new ones.

This hypothesis is one of the earliest attempts to model meristematic development. Together with the observation that the primordia usually appear in constant time intervals called plastochrones, it is possible to predict the phyllotactic pattern resulting from given parameters (like meristem growth description and plastochrone).

If the period between primordia formation is small, many primordia will be placed near to the apex. Whereas if the period is large, only few primordia will be closely localised to the centre zone. In particular, if the period is very large, only one primordium happens to be near to the apical ring, so that the new primordium will be formed on the side opposite to the previous primordium, just as in alternate phyllotaxis.

In 1992 physicists Stephane Douady and Yves Couder performed an experiment which basics resembled the system described by Hofmeister [Douady and Couder, 1992]. They let droplets of a ferromagnetic liquid fall into a dish that

[3] It is a common experience that new leaves (or axillary buds) emerge at those places in the circumference of the vegetative apex that are situated at the end of a stem (or at a node). These points are removed furthest from the margins of the bases of the next-adjoining leaves, already present on the apex [Kirchoff, 2003].

was filled with silicone oil and placed in a vertical magnetic field. This field had a weak radial gradient: it was minimal at the centre and maximal at the periphery. Thus, magnetic forces pushed the droplets towards the edge of the dish but made them repel one another.

When the droplets were added slowly, each one would move toward the side of the dish, directly opposite to the previously added drop. When added faster, the two most recently added droplets would both repel the new one. Instead of shifting to one side or the other, the new droplet would move in a third direction. For a certain experiment configuration (i.e. magnetic field strength, droplet mass, droplet frequency, etc.), a series of consecutive droplets formed a spiral pattern, with an almost constant divergence angle (figure 1.12).

The authors created a computer model allowing them to test varied configurations of such a system. The primordia in the model were represented by particles. Each particle produced a repulsive potential and the new particle appeared on a circle where the potential was at its absolute minimum. Their experiments together with the computer model indicated that the system based on the inhibitory field idea is consistent with the Hofmeister's hypotheses and is able to generate a whole range of phyllotactic patterns.

The limiting factor of inhibitory based model is the stability of whorled patterns. Douady and Couder [1996a] showed that these patterns are less stable then the spiral ones. However, in the world of plants, whorled patterns are observed frequently [Jean, 1994]. This discrepancy was investigated further by Smith et al. [2006b]. These authors proposed a modified concept of inhibition, where the strength of inhibition should also depend on time.

In the simulations which Smith et al. [2006b] performed, the primordium inhibition is inversely proportional to its distance from a given position and decreases exponentially with its age. Similar to the single inhibition system studied by Douady and Couder [1996a], at positions where the sum of the inhibitory effects exerted by the primordia falls below a predefined threshold, a new primordium arises. The model reproduces distichous and spiral patterns in a robust manner. The authors report that the introduction of a second inhibitory function that is similar to the first, except that it decreases rapidly over time, makes it possible to simulate decussate and whorled systems with high stability. Variation in the inhibition strength also allows for phyllotactic transitions, as in the original model of Douady and Couder [1996a]. Thus, the presence of temporal dependence of inhibition, makes it possible to reproduce all the important aspects of phyllotactic patterning.

To explain phyllotaxis also other concepts were proposed. In the context of this thesis particularly important is a model of mechanical buckling proposed by Green [1985]. Buckling involves two layers of cells at the tip of a plant: the rib zone (corpus), and the tunica (L1 and L2 layers). Green suggested that the tunica, as it grows faster than the corpus, buckles. Using stress analysis incising of growing heads of sunflower, Dumais and Steele [2000] gave some supporting evidence for buckling. The model based on buckling is capable of generating phyllotactic patterns and can explain transitions between patterns and the different primordia shapes that occur in plants [Green, 1985]. Surprisingly, the primordia initiation appears to be robust after meristem tissues are disrupted by laser treatments that presumably changes stress patterns to a high degree, which is incompatible with the model.

Turing [1952] proposed a system of equations describing a relation between two morphogens and leading to a patterning process. He called this system reaction-diffusion model. Referring back to the work of Turing [1952], Koch and Meinhardt [1994] introduced a reaction-diffusion version of the inhibitor model by incorporating an activator molecule as well as an inhibitor, allowing a continuous dynamical model. Reaction-diffusion involves chemical reaction and diffusion of a mixture of chemicals which, under certain conditions, result in non-homogeneous spatial concentrations of the different chemicals, and hence patterns. A long ranging inhibitor is responsible for the pattern in space and a second inhibitor poises once formed activator maxima, causing their breakdown. After a certain period they reappear at a displaced position. These models exhibit robust and dynamic pattern generation, including the initiation of new concentration peaks corresponding to primordia, however the exact molecular mechanism behind these models remains unknown and therefore, they are considered as highly speculative.

Most phyllotactic models are in some way guided by the concept of inhibition (e.g. realized by magnetic field in case the experiment performed by Douady and Couder [1996a]). Schoute [1922] first proposed the idea of lateral inhibition based on a diffusible chemical agent produced by each developing primordium that inhibits the initiation of neighbouring primordia.

A complementary idea of inhibitory field is based on the depletion of an organ initiation factor and was proposed by Chapman and Perry [1987]. Recent findings provide a considerable support for such a scenario. It has been shown recently, that the high concentration of plant hormone auxin is an essential activator for primordium formation [Reinhardt et al., 2000a]. Reinhardt et al. [2003] suggested, that new organs deplete auxin, therefore the concentration gradient of auxin mimics the abstract inhibitory fields.

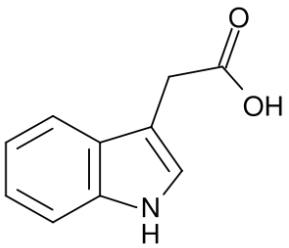

Figure 1.13: The indole-3-acetic acid (IAA) structure. It has the greatest importance among all native auxins.

1.3 Auxin

Auxins are plant hormones that play an essential role in the coordination of many growth and behavioural processes in the plant life cycle. The highest concentrations are found in young growing plant organs [Ljung et al., 2001, 2005]. Indole-3-acetic acid (IAA) is the most abundant auxin (figure 1.13).

1.3.1 Functions of auxin

IAA acts on entire plant inducing cell divisions and differentiation of cells and it contributes as well to a multitude of tissue-specific responses. It is fundamental for the embryonal axis development through directional distribution, leading to an arrangement and growth of primary poles and primordia of future organs [Friml, 2003].

The concentration of auxin and the type of tissue where it acts can lead to different responses [Cholodny, 1927, Thimann, 1948, 1977, Weyers et al., 1995]. For example, the same quantity of auxin may promote cell elongation in shoot, but inhibit it in root, due to dose dependent auxin-responses. At low concentration ranges, both in shoots as in roots, increasing auxin concentration causes an increase in growth, whereas, after an optimum is reached, any further increase of auxin concentration leads to decrease in growth. Due to higher sensitivity of root tissues, as compared to shoot tissues, physiological auxin doses appear to promote cell elongation in stem while inhibiting it in roots [Thimann, 1948].

Asymmetric distribution of auxin contributes to biological mechanisms known as tropisms understood as growth or turning and bending movement of plant or its organs, as a response to an environmental stimulus [Friml et al., 2002]. It participates in directional growth of organs e.g. towards light (phototropism), water (hydrotropism), in response to gravity (gravitropism). Auxin plays an

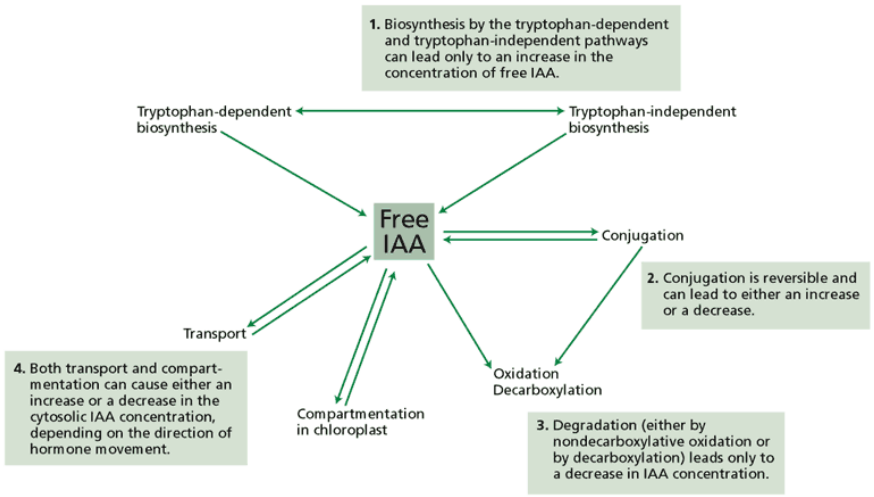

Figure 1.14: Factors that influence the steady-state levels of free IAA in plant cells.
Biosynthesis by the tryptophan-dependent and tryptophan-independent pathways can lead only to an increase in the concentration of free IAA. Degradation (either by nondecarboxylative oxidation or by decarboxylation) leads only to a decrease in IAA concentration, while conjugation is reversible and can therefore lead to either an increase or a decrease. Both transport and compartmentation can cause either an increase or a decrease in the cytosolic IAA concentration, depending on the direction of hormone movement. Image taken from [Normanly, 1997].

essential role in growth of lateral roots [Reed et al., 1998, Casimiro et al., 2001, Bhalerao et al., 2002, Lucas et al., 2008] and in process of phyllotaxis [Reinhardt et al., 2000b, Stieger et al., 2002, Reinhardt et al., 2003] described in detail in 1.4.

In mature regions of the plant IAA stays at equilibrium controlled by process of biosynthesis, conjugation, degradation and transport. In roots, leaves and cotyledons the levels of IAA can be elevated on two biochemical pathways: tryptophan-dependent and tryptophan-independent biosynthesis [Bartel, 1997, Woodward and Bartel, 2005]. Within the cell it can be stored in two forms as indole-3-butyric acid (IBA) or as IAA conjugated with sugars or with aminoacids and peptides. The main factors regulating auxins in the plants are presented in the figure 1.14.

1.3.2 General patterns of auxin distribution/transport pathways

Comparing different plant tissues, a continuous uneven pattern of auxin distribution can be found as shown in the figure 1.15. Firstly, it can be noticed that the basipetal* auxin gradient is decreasing from the growing tip to the base. IAA levels are high in the stalks. The developing leaves show higher IAA concentrations than the expanded leaves. The auxin levels increase from the leaf centre to its margins [Müller et al., 2002]. The meristematic growth zones are situated at the sites of higher IAA concentrations [Ljung et al., 2001].

The findings concerning the differentiated distribution of auxin together with the data demonstrating its circulation within a plant [Lomax et al., 1995] led to a development of a dynamic model of its transport. It is suggested that the auxin flow starts at young organs such as primordia and developing leaves [Ljung et al., 2001]. Further, IAA is distributed within the epidermis to the SAM and basipetally transported by phloem in the direction of the root. On its way auxin inhibits the growth of new lateral buds in the stem (apical dominance) and within the root it influences the development of lateral root primordia [Thimann and Skoog, 1934, Celenza et al., 1995, Lucas et al., 2008].

1.3.3 Chemiosmotic model of auxin transport

The chemiosmotic model of auxin transport was formulated by Rubery and Sheldrake [1974]. It states that the auxin can be transported between plant

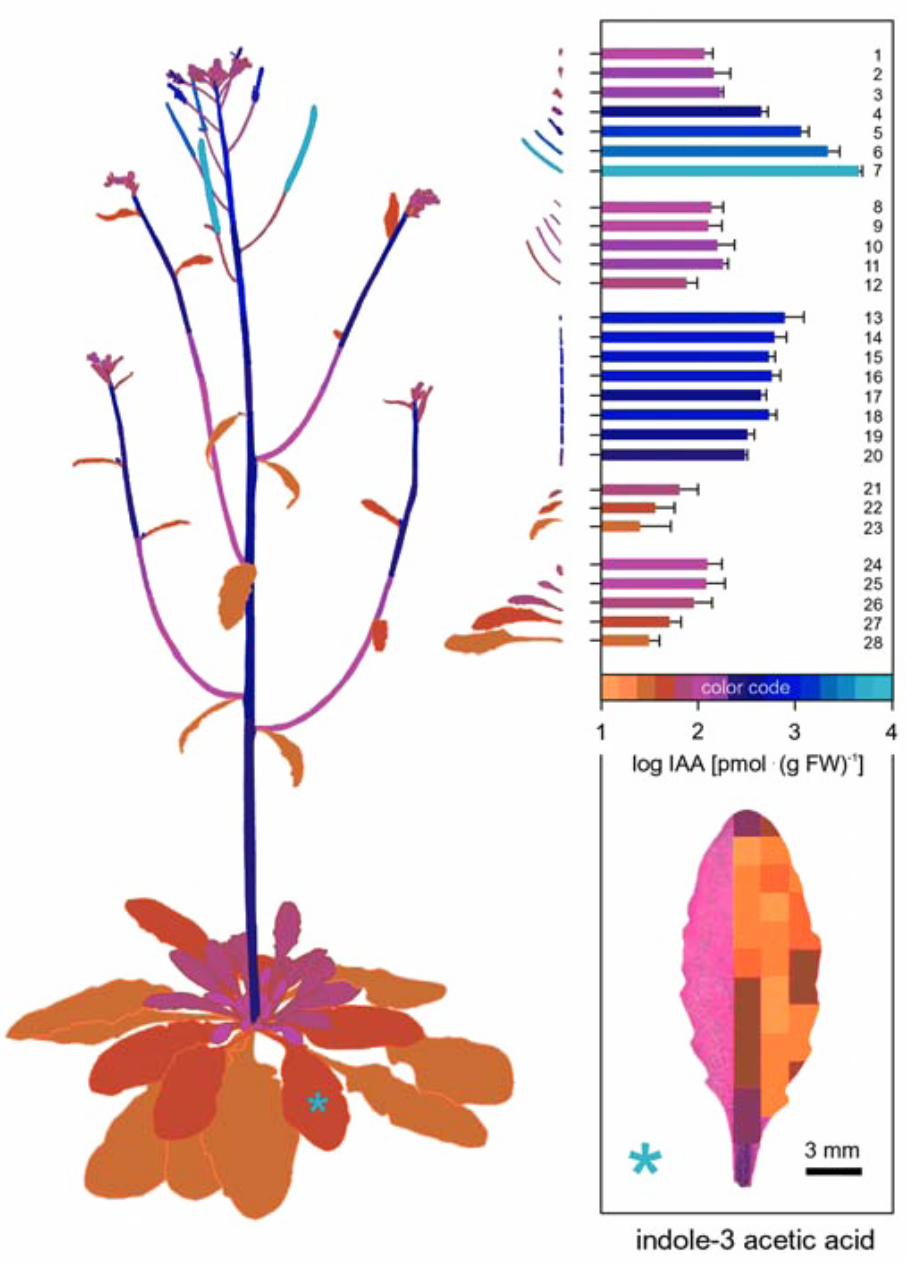

Figure 1.15: Organ-distribution map for indole-3-acetic acid.
The distribution of IAA levels in the whole *Arabidopsis thaliana* plant is colour-coded in the drawing. The same colour code applies to the bar diagram which gives the mean values with standard deviation for the individual plant parts of the main inflorescence stalk and the rosette. Figure taken from [Müller et al., 2002].

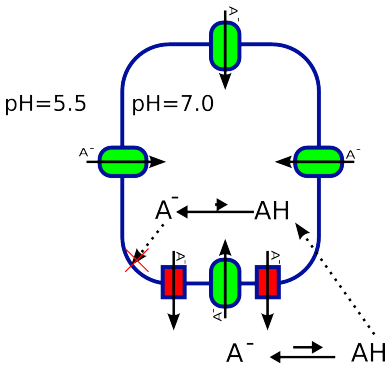

Figure 1.16: Schematic of chemosmotic model of auxin transport, based on the general description presented by Rubery and Sheldrake [1974].
Red rectangles depict efflux carriers with polar location within the cell. Green shapes depict auxin influx carriers together with the symoporters, uniformly located in the cell. Dotted arrows depict dominant direction of lipophylic diffusion. Description in text. Figure drawn by Tristan Bitard Feildel.

cells in a passive and active way[4]. The passive transport results from a diffusion process * while active transport requires the mediation of special proteins, placed in the plasma membrane, called efflux/influx carriers.

The auxin is a weak acid and can be found in the plant both in the undissociated (AH) and ionised (A^-) form. In the cell walls (apoplast) the pH is approximately 5.5 showing more acidic character than inside the cell (pH 7.0). The higher concentration of H^+ in the apoplast* leads to a shift of equilibrium towards the AH form. Thus, outside the cell the concentration of undissociated auxin is much higher then inside of the cell[5].

Facilitated by the auxin concentration gradient, the undissociated acid molecules enter the cell membrane by lipophilic diffusion [Titapiwatanakun and Murphy, 2008]. The auxin anions in the wall compartment are also mediated actively into the cell by the symporters*. In the more basic cytoplasm the undissociated auxin changes into A^-. Since the cell membrane is less permeable for the A^- than for the AH, auxin anions accumulate within the cell. The efflux of the anions from the cytoplasm to the apoplast is mediated by the active transport carriers. This process is summarized in figure 1.16.

It is important to note, that due to low AH/A^- ratio in the cytoplasm, the active transport factors are more important then the passive ones for creating

[4]Another possibility for a cell to transport auxin, is through microscopic channels connecting the adjacent cells, called plasmodesmata. The data concerning the importance of auxin transport by plasmodesmata are currently not available.

[5]The AH/A^- ratio in the wall compartment is $\sim 1/5$, whereas in the cell auxin is present almost only in A^- form [Titapiwatanakun and Murphy, 2008].

differences in spacial distribution of auxin [Kramer and Bennett, 2006, Kramer et al., 2007].

1.3.3.1 Efflux carriers PIN, PGP1/19

The most studied efflux carriers is the PIN-FORMED (PIN) family transporting auxin according to the electrochemical gradient [Blakeslee et al., 2005]. It is assumed that the PINs are a part of an auxin transporters complex together with P-GLYCOPROTEINS (PGP1) and PGP19 proteins, members of MULTIDRUG RESISTANCE P-GLYCOPROTEIN (MDR/PGP) family [Vieten et al., 2007]. Within the root both the locations of PIN PGP1 and PGP19 proteins are polar. In the plant stems PINs are mostly distributed as well in a polar way, whereas PGPs are oriented apolarly all around the cell membrane [Petrasek et al., 2006, Bandyopadhyay et al., 2007, Vieten et al., 2007].

For proper PIN1 location at the membrane in a polar or apolar way, PINOID (PID) proteins and of MODULATOR-OF-PIN (MOP) acting on post-transcriptional factors are required [Vieten et al., 2007]. Other considered mechanisms controlling the PIN distribution include the direct influence of auxin [Muday et al., 2003]. It was observed that in the absence of auxin, PIN1 undergoes endocytosis*. If auxin enters the cell, the endocytosis is reduced with help of calossin-like protein, renamed BIG, due to its enormous (560 kDa) size [Gil et al., 2001]. Its exact function is still no known [Paciorek et al., 2005].

1.3.3.2 Influx carriers AUX/LAX, PGP4

AUX1 and LIKE-AUX (LAX) proteins mediate the active IAA^- influx into the cells against IAA concentration gradients [Kramer, 2004, Swarup et al., 2004, Vieten et al., 2007]. Studies concentrating on AUX1 proteins reveal that the localisation of these transporters depends on the tissue type [Bandyopadhyay et al., 2007]. Within the root cap it can be polar and apolar, but in the epidermis of the distal growth zone of the root only apolar carrier distribution is found. The exact activity and function of LAX proteins is not yet fully understood [Kleine-Vehn et al., 2006, Reinhardt et al., 2003].

Another identified carrier of auxin active influx is P-GGLYCO-PROTEIN4 (PGP4), a member of MDR/PGP family [Geisler and Murphy, 2006]. The highest level of expression can be found in the root, although diverse PGP4 distribution patterns can be found in different root tissues. In the root cap its expression is apolar, however in the basal part of the growth zone and in the cells of epidermis PGP4 has polar location [Geisler and Murphy, 2006].

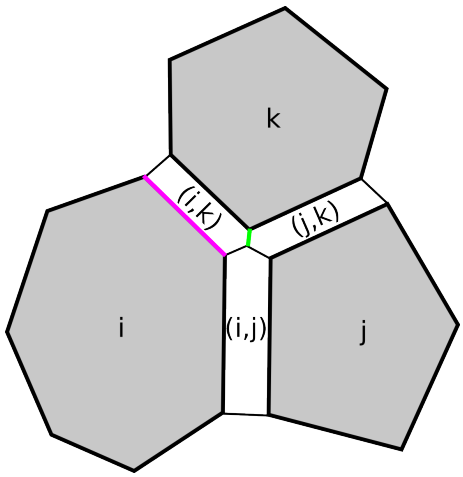

Figure 1.17: Cell and wall compartment model.
Description in the text. Neighbours of cell compartment i are cells j, k, which is denoted as $N_i = \{j, k\}$. Neighbours of wall compartment i, j are wall compartments j, k and i, k, which is denoted as $N_{i,j} = \{(j, k), (i, k)\}$. Magenta line depicts the contact surface between cell compartment i and wall compartment i, k denoted as $S_{i,k}$. Green line depicts the contact surface between wall compartment i, k and wall compartment j, k denoted as $S_{(i,k),(j,k)}$.

1.3.3.3 Chemiosmotic model formalization

The chemiosmotic model of auxin transport is described in 1.3.3. Based on this description it is possible to formulate a system of equations describing the auxin transport. The system describes an active and passive transport across membranes and diffusion within the cell walls. This model is derived from concepts proposed by Goldsmith et al. [1981] and Mitchison [1981], revised by Jönsson et al. [2006].

To describe the auxin transport in a tissue certain simplifications are needed. Firstly, the cytosol is assumed to be a single compartment, thus spatial variations of auxin within the cell is neglected. As suggested by several authors [Jönsson et al., 2006, Kramer et al., 2007], a subcompartization is not very important assuming the average cell sizes in the meristem and the auxin diffusion constant. Also, each part of the wall, being in contact with cells i and n is assumed to be a single compartment (figure 1.17).

In the equations, a_i denotes the auxin concentration in the cell i, and $a_{i,n}$ denotes the auxin concentration in wall compartment between cell i and n, V_i stands for a volume of cell i, $V_{i,n}$ signifies volume of wall compartment i, n, $S_{i,n}$ is the area of interface of cell i with wall compartment in, $S_{(i,n),(k,l)}$ denotes the area of interface between wall compartment i, n and wall compartment k, l. The

set of cell neighbours of cell i is denoted as N_i and the set of wall neighbours of wall i,n is described as $N_{i,n}$ (figure 1.17). Therefore, the auxin variation in cells and walls can be formalized:

$$\frac{\partial a_i}{\partial t} = \sum_{n \in N_i} \frac{S_{i,n}}{V_i} J_{i \to (i,n)} \tag{1.1}$$

$$\frac{\partial a_{i,j}}{\partial t} = -\left(\frac{S_{i,j}}{V_{i,j}} J_{i \to (i,j)} + \frac{S_{j,i}}{V_{i,j}} J_{j \to (i,j)} \right) + \sum_{(k,l) \in N_{i,j}} D_w \frac{S_{(i,j),(k,l)}}{V_{i,j}} \left(c_{k,l} - c_{i,j} \right) \tag{1.2}$$

Where D_w describes the diffusion constant of auxin in the cell wall and $J_{i \to (i,n)}$ is the net unitary flux from cell i to wall compartment i,n. For means of simplification, it is assumed that the diffusion of both form of auxin in the walls is similar.

As it was described in 1.3.3, AH can much easier penetrate the membrane passively then A^- (see [Kramer et al., 2007]), therefore the passive flux is approximated assuming the lipophylic diffusion of AH form only. As a result, the anions A^- move between cell and wall compartment only by active transport influx and efflux carriers.

The reaction $AH \rightleftharpoons A^- + H$ is faster then the transport itself, thus in the equations the pH dependent equilibrium fractions are used [Kramer, 2004, Kramer and Bennett, 2006, Kramer et al., 2007]. The pH is different for cytoplasm and for walls, therefore the proportions of different forms of auxin vary in the wall compartment and in the cell (as described in 1.3.3). The concentration of A^- in the wall i,j or in the cell i are called respectively by $a_{i,j}^{A^-}$ and $a_i^{A^-}$; The concentration of AH in the wall i,j or in the cell i as respectively $a_{i,j}^{AH}$ and a_i^{AH}[6].

The $J_{i \to (i,n)}$ can be denoted as $J_{i \to (i,n)} = I_{(i,n) \to i} - E_{i \to (i,n)}$, where $I_{i \to (i,n)}$ stands for influx from wall compartment i,n to cell i and $E_{i \to (i,n)}$ means the efflux from cell i to wall compartment i,n. According to chemosmotic model, both efflux and influx have passive and active part. Unitary passive efflux from cell i to wall compartment i,j is equal to $D_m a_i^{AH}$, and influx in opposite direction $D_m a_{i,j}^{AH}$, where D_m is membrane permeability for AH particles. The unitary active efflux and influx depend on the active transporters and is described respectively as $\breve{E}_{i \to (i,n)}$ and $\breve{I}_{(i,n) \to i}$. Therefore, in the general form $J_{i \to (i,n)}$ can be denoted as:

[6] The concentrations of the different auxin forms in cell i in steady state can be estimated using the equations: $\left[a_i^{A^-}\right] 10^{pH} = K_d \left([a_i] - \left[a_i^{A^-}\right] \right)$ and $[a_i] - \left[a_i^{AH}\right] 10^{pH} = K_d \left[a_i^{AH}\right]$, where pH describes the pH in cell compartment and K_d is auxin dissociation constant.

$$J_{i\to(i,n)} = \breve{I}_{(i,n)\to i} + D_m a_{i,j}^{AH} - \left(\breve{E}_{i\to(i,n)} + D_m a_i^{AH}\right)$$

1.3.3.4 Simplified chemiosmotic auxin model for meristem

The general model proposed in 1.3.3.3 depends mostly on the fluxes generated by active transport ($\breve{I}_{(i,n)\to i}$ and $\breve{E}_{i\to(i,n)}$). PIN and PGP1/PGP19 protein families are the most important auxin efflux carriers (see 1.3.3). PIN family members are distributed polarly in the meristem, whereas PGP1/PGP19 are distributed uniformly.

As mentioned before, an auxin transport mutant *pin* (i.e mutant not expressing PIN carrier family members) presents several developmental changes concerning auxin dependent processes (e.g. phyllotaxis). It suggests an important role of this protein type in auxin transport.

In the case of influx carriers (AUX, LAX, PGP4) all carriers have fairly uniform distribution. The *aux* plant mutant (not expressing AUX) has only minor problems with auxin dependent processes (e.g. it develops organs not in the regular spiral patterns).

These observations were raised as arguments to simplify the auxin transport model in the meristem (figure 1.18) Barbier de Reuille et al. [2006], Jönsson et al. [2006], Smith et al. [2006c]. Due to symmetric distribution of influx carriers, the wall compartments are omitted in the simulation and the auxin intake is approximated by the diffusion between cell compartments. The active efflux transport (realized by PIN molecules distributed in a polar way) is simulated as a direct flux of auxin from cell to cell with omission of the wall compartment. It was reported that the simplified model have qualitative properties similar to the one explicitly simulating the chemiosmotic model [Heisler et al., 2006, Jönsson et al., 2006]. In this thesis a similar simplification scheme was adopted.

1.3.4 Molecular basis of auxin signaling

1.3.4.1 ARF/TIR proteins

Once auxin enters the cell a cascade of rapid gene transcription follows [Ulmasov et al., 1997, Guilfoyle et al., 1998, Okushima et al., 2007]. The expression of auxin sensitive genes is regulated by antagonistically acting transcription factors, the Auxin Response Factors (ARF) and Auxin/Indole-acetic acid

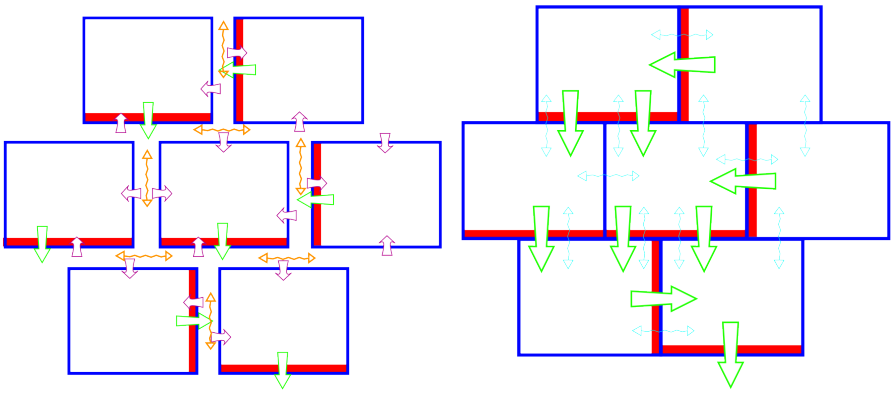

Figure 1.18: The schematic of auxin transport model in the tissue.
The chemosmotic model of auxin transport proposes that the influx carriers (violet arrows), efflux carriers (green arrows), and the diffusion in the apoplast (orange arrows) are the most important for auxin transport in the SAM (1.18A). The biological data suggest also that the influx carriers are evenly distributed in SAM tissue, therefore this schematic may be simplified. In the reduced model, the inter-cellular spaces might be omitted (1.18B). Figure drawn by Tristan Bitard Feildel.

(Aux/IAA) genes[7]. When the intracellular concentration of auxin is high, ARFs bind to a promoter sequence Auxin Response Element (ARE) and the expression of auxin sensitive genes is induced. If the auxin concentration is low, Aux/IAA proteins associate with the ARFs making the gene induction impossible. At high intracellular auxin levels, the hormone will interact with the Transport Inhibitor Response 1 protein (TIR1)[8]. This protein is part of a complex that, when activated by auxin, will target the Aux/IAA factors to the proteosomes by poly-ubiquitination [Guilfoyle, 2007]. Genes activated by ARF are important in regulation many processes, such as the cell-cycle and cell-wall remodelling [Delker et al., 2008].

1.3.5 Specific patterns of influx/efflux carriers in the SAM

In the SAM as well as in other already described plant tissues, active auxin carriers are found. In the L1 layer of the meristem epidermis and vascular bundle underneath the growing primordia both AUX1 and PIN1 are expressed at increased levels (look at figure 1.21). AUX1 shows mainly apolar distribution in the SAM cells, however meristem imaging studies reveal higher concentration

[7] The abbreviation Aux/IAA should not be confused with AUX transport proteins.
[8] an element of SCF TIR1- protein ubiquitin ligase complex.

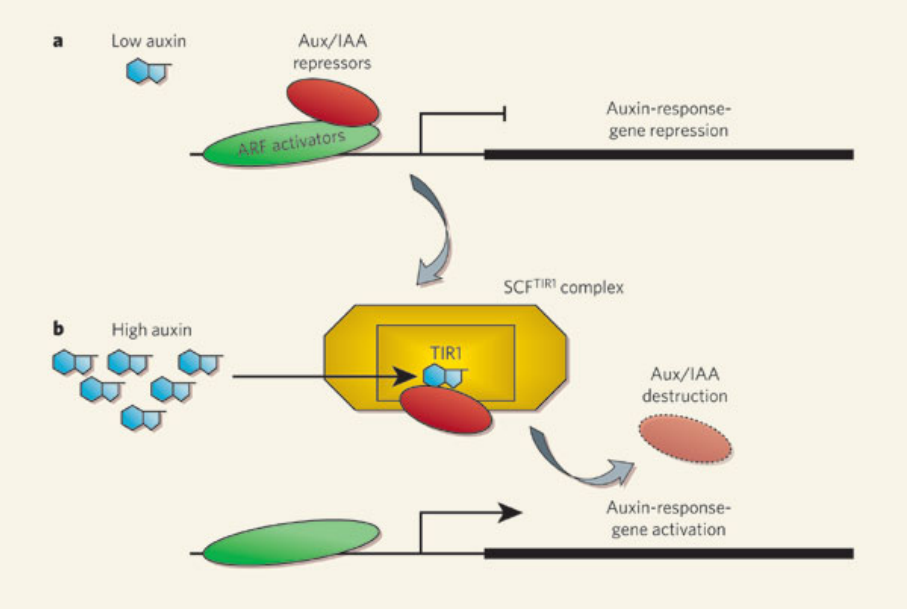

Figure 1.19: Auxin signalling pathways.
ARFs activators bind to auxin-response elements in promoters of auxin-response genes. When auxin concentration is low, Aux/IAA repressors associates with the ARF activators and represses gene expression. When auxin concentration increases, auxin binds to TIR1 receptor in the SCF[TIR1] complex, leading to recruitment of Aux/IAA in the SCF[TIR1] complex. Once recruited, Aux/IAA are targeted for proteasomic* destruction. The subsequently liberated ARFs then activate transcription. Image taken from Guilfoyle and Hagen [2007].

Figure 1.20: Wild-type *Arabidopsis thaliana* and the AXR2-1 mutant. AXR2-1 is a dominant gain-of-function mutation in an *Aux/IAA* gene that confers reduced auxin response. The mutant AXR2-1 protein constitutively represses auxin response because it cannot be targeted for proteolysis by the SCFTIR1 ubiquitin ligase. Image taken from Gray [2004].

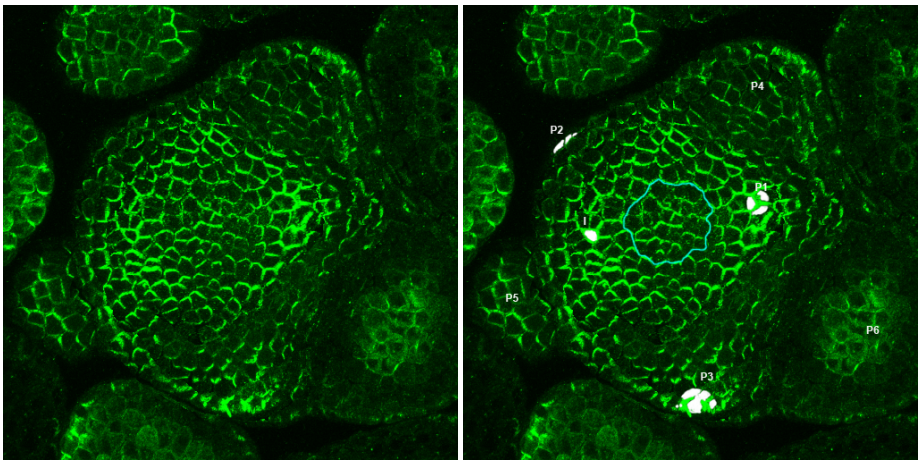

A B

Figure 1.21: Patterns of PIN distribution in SAM of *Arabidopsis*.
PIN signal is marked with green colour. The centre of the meristem is encircled with blue line, primordia are marked with consecutive numbers prefixed by "P". Description in text. The image was taken by Marianne Schaedel, ENS Lyon.

of AUX1 molecules at the bottom of the L1 layer (look at green arrows in figure 1.22A). PIN1 at the membrane of L1 cells points in the direction of the closest primordium or the meristem centre. Inside young organs PIN1 proteins are located basipetally (figure 1.22).

These pieces of information lead to a map of auxin flux in the SAM (look at figure 1.23). According to this map, auxin is actively transported acropetally into the meristem through L1 layer. When expression of a new organ begins, auxin flows from the neighbouring cells and as well from those situated at the periphery into the developing primordium. This is followed by the activation of auxin transport in the inner tissues, where auxin seems be transported away from the primordium.

As mentioned before, a variant of the inhibitory field concept, based on competition or depletion of a organ-promoting factor was proposed by Chapman and Perry [1987]. Recent findings suggest the plausibility of this depletion scenario. It has been shown that the suppression of auxin transport leads to a pin-formed phenotype characterised by a lack of primordium development. This phenotype develops into normal plant when auxin is applied, which results in primordium generation (figure 1.24) [Reinhardt et al., 2000a]. This suggests that localised auxin is necessary for the development of primordia.

Reinhardt et al. [2003] proposed a model of phyllotaxis, where the auxin is a primordium activator that is depleted from regions surrounding the primordia via

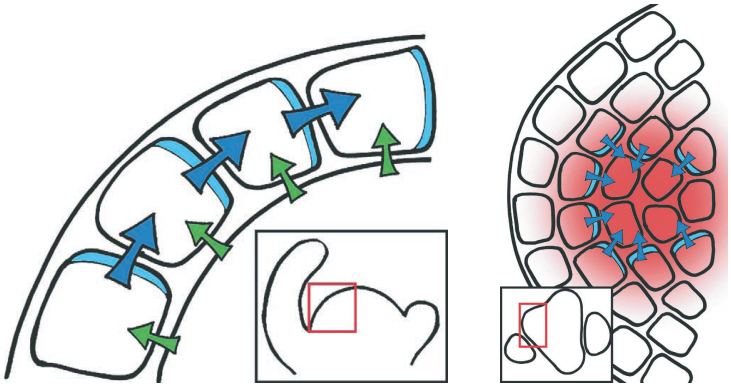

Figure 1.22: Auxin transport in the SAM.
Figure 1.22A shows auxin transport in the epidermal L1 layer of the shoot meristem. L1 cells express the presumptive auxin influx carrier AUX1, leading to the accumulation of auxin in L1 (green arrows). PIN1 is also expressed in the L1 layer, where it is localised to the upper side of the cells (light blue). This results in the acropetal* transport of auxin towards the meristem centre (blue arrows). Inset: the depicted area in the context of the apex. Figure 1.22B shows PIN distribution around the primordia. PIN1 expression is induced in young primordia. It becomes localised to the side of the cells that points to the centre of the primordium (light blue). This results in auxin withdrawal from the surrounding cells (blue arrows). The resulting auxin flux (red) confers positional information to the cells allowing them to establish organ and boundary identity. Inset: Location of the P1 position in the context of the apex. Figures taken from [Reinhardt et al., 2005].

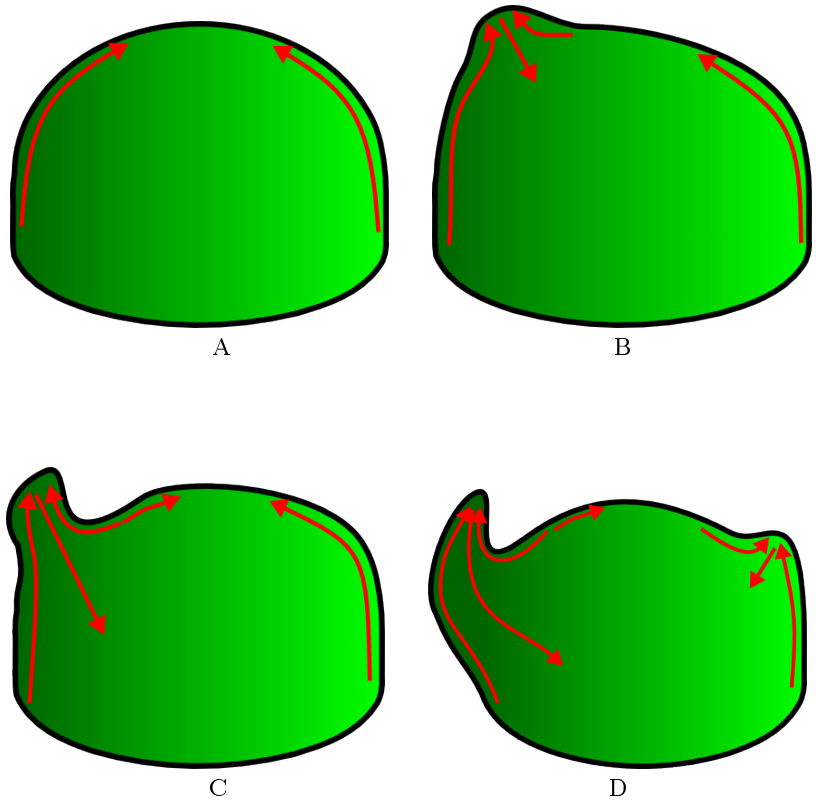

Figure 1.23: The schematic of auxin fluxes in the SAM during its development.

The fluxes are derived by observing the organised reorientation of PIN proteins. Figures show a schematic representation of an apex in longitudinal section through P1 and I1 at different stages of incipient primordium formation. Polar auxin flux is indicated with red arrows. Figure 1.23A shows acropetal auxin flux, as observed in *pin* mutant or plants with inhibited auxin transport (e.g. NPA). If the young primordium is present, acropetal auxin flux is still observed, however the PIN pumps in L1 are directed to this primordium in its closest neighbourhood. Also the vascular strand is starting to form in L3 below the primordium (figure 1.23B). After a certain time, due to the meristem growth, P1 is moving away from the meristem centre, and the reversal of PIN from the primordium towards the meristem summit is observed (figure 1.23C). Further outgrowth, leads to the configuration which prevents the auxin to accumulate on the left flank of the meristem, while it can reach the right flank (I1). The accumulation of auxin at I1 promotes primordium formation, and establishment of a new primordium, which attracts fluxes from L1 and redirects them to L3 (figure 1.23D).

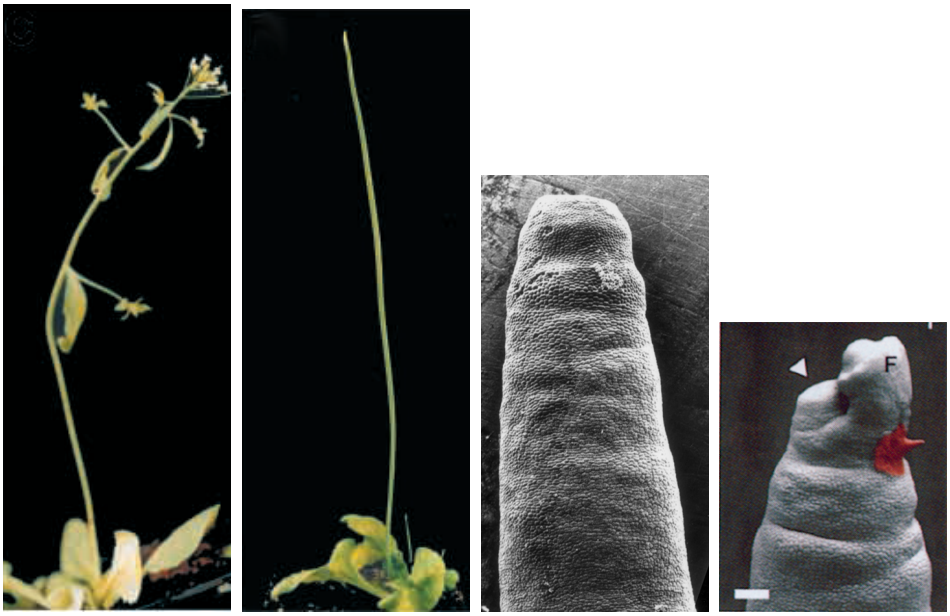

A B C D

Figure 1.24: The PIN1 mutant and its reaction for external application of auxin.

Figure 1.24A shows wild type *Arabidopsis* phenotype, while 1.24B shows *pin1* mutant. Figure 1.24C SAM of the mutant phenotype, and figure 1.24D shows primordium initiation triggered by the application of external auxin. Images taken from [Reinhardt et al., 2000a, Vernoux et al., 2000, Reinhardt et al., 2003].

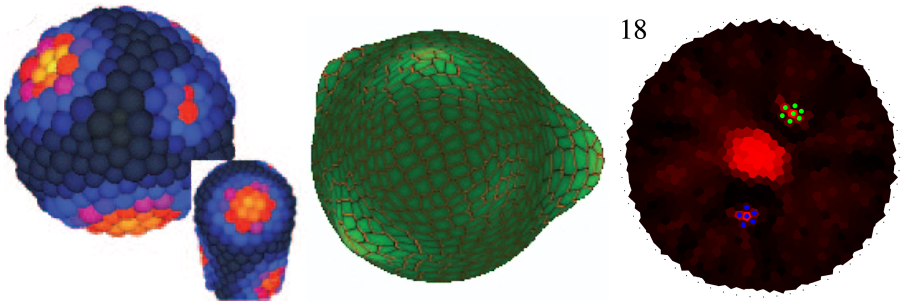

Figure 1.25: Auxin transport-based models of phyllotaxis.
Images taken from [Jönsson et al., 2006, Smith et al., 2006c, Barbier, 2005] respectively.

PIN1-dependent auxin transport. As a result, the auxin concentration maxima, required for primordium initiation, appear at points maximizing the distance from the previous primordia.

The analysis of PIN expression patterns in the L1 layer was presented by Barbier de Reuille et al. [2006]. The computional modelling of auxin fluxes on the digitized PIN expression patterns confirmed that auxin flows to the young primordia or meristem centre.

The results showed also an unexpected accumulation of auxin in the meristem summit, which was confirmed in additional experiments [Barbier de Reuille et al., 2006]. The authors suggested, that the centre of meristem might play an important role in the auxin-based control of phyllotaxis.

One of the key questions concerning the model proposed by Reinhardt et al. [2003], is how the auxin transport itself is regulated. Since at the molecular level no such a process is currently identified, a hypothetical mechanism, coherent with the biological data concerning auxin and its transport, was proposed *ad hoc* by two recent models of phyllotaxis [Jönsson et al., 2006, Smith et al., 2006c].

1.4 Comparative analysis of auxin transport-based models of phyllotaxis

Recently, a series of computer simulations of phyllotaxis inspired by the concept proposed by Reinhardt et al. [2003] were presented [Barbier, 2005, Jönsson et al., 2006, Smith et al., 2006c]. These simulations include passive and active

transport of auxin, meristem growth and a mechanism of PIN allocation to the cell membranes. The active transport of auxin creates the auxin concentration gradients in the tissue. These gradients, together with the growth of the meristem, lead to a patterning mechanism. The models are able to generate different types of phyllotactic patterns.

The equation describing models are presented in figure 1.26. All three models share the following framework. The concentration of auxin in a cell i is denoted as a_i. Its variation in a cell i depends on the net unitary auxin flux between this cell and neighbouring cells $n \in N_i$, denoted as $J_{i \to n}$ and auxin synthesis and decay, regulated respectively by α_a and β_a (equations 1.3, 1.7, 1.11). The net flux $J_{i \to n}$ between cell i and n depends on the diffusion between these cells, characterized by diffusion constant D and the active transport (equations 1.4, 1.8, 1.12). Active transport is modulated by the PIN transporting auxin from cell i to cell n (PIN concentration is denoted as $p_{i,n}$) and its efficiency A. The concentration of PIN available for allocation in cell i is denoted by p_i (equations 1.5, 1.9, 1.13). One of the key differences between the models is the mechanism responsible for the PIN allocation (equations 1.6, 1.10, 1.14).

Despite many similarities, the models are different in some important aspects:

1. **Auxin transport and its regulation aspects:**

   (a) **The PIN polarization mechanism**

   Barbier [2005] abstracts the nature of the actual process of PIN allocation. In his model, based on the work of Barbier de Reuille et al. [2006], it is assumed that the primordia and meristem summit attract fluxes. This is achieved, by introducing an imaginary, "magnetic" attraction between the PIN molecules and the primordia centres and the meristem summit. In this model, each cell allocates all its PIN proteins to only one cell membrane (equation 1.14).

   Two other models propose different approaches. In both the Jönsson et al. [2006] and Smith et al. [2006c] models, the amount of PIN allocated to the cell membrane depends on the local gradient of auxin. As a result, they propose a mechanism, in which every cell senses the concentration of auxin in its neighbours and transports the hormone to the neighbour with the highest concentration. It results in increased auxin fluxes towards the cells with high auxin concentration and depletion of auxin in their neighbourhood. Auxin peaks emerge at regular distances. These auxin maxima are used to determine the locations of primordia. This mechanism can break an approximately uniform auxin distribution by forming a spatial pattern of

Jönsson et al. [2006]:

$$\frac{\partial a_i}{\partial t} = \sum_{n \in N_i} \frac{S_{i,n}}{V_i} J_{n \to i} + \alpha_a x_i - \beta_a a_i \tag{1.3}$$

$$J_{i \to n} = D\left(a_i - a_n\right) + T\left(p_{in} \frac{a_i}{1 + a_i} - p_{ni} \frac{a_n}{1 + a_n}\right) \tag{1.4}$$

$$p_i = 1.0 \tag{1.5}$$

$$p_{i,n} = p_i \frac{\alpha_p a_n}{\beta_p + \frac{\alpha_p}{|N_i|} \sum_{j \in N_i} a_j} \tag{1.6}$$

Smith et al. [2006c]:

$$\frac{\partial a_i}{\partial t} = \sum_{n \in N_i} \frac{S_{i,n}}{V_i} J_{n \to i} + \frac{\alpha_a}{1 + a_i} + \alpha'_a \left[i \in Pr\right] - \beta_a a_i \tag{1.7}$$

$$J_{i \to n} = D\left(a_i - a_n\right) + T\left(p_{in} \frac{a_i^2}{1 + a_i^2} - p_{ni} \frac{a_n^2}{1 + a_n^2}\right) \tag{1.8}$$

$$\frac{\partial p_i}{\partial t} = \frac{\alpha_{p0} + \alpha_p a_i}{1 + p_i} - \beta_p p_i \tag{1.9}$$

$$p_{i,n} = p_i \frac{3^{a_n}}{\sum_{j \in N_i} 3^{a_j}} \tag{1.10}$$

Barbier [2005]:

$$\frac{\partial a_i}{\partial t} = \sum_{n \in N_i} \frac{S_{i,n}}{V_i} J_{n \to i} + \alpha_a [i \in B] - \left(\beta_a - \beta'_a \left[i \in Pr \vee i \in Cz\right]\right) a_i \tag{1.11}$$

$$J_{i \to n} = D\left(a_i - a_n\right) + T\left(p_{i,n}\left(1 - e^{-a_i}\right)\left(1 - e^{-k_a + a_i}\right) - p_{n,i}\left(1 - e^{-a_n}\right)\left(1 - e^{-k_a + a_n}\right)\right) \tag{1.12}$$

$$p_i = 1.0 \tag{1.13}$$

$$p_{i,n} = \begin{cases} p_i & if \;\; \psi\left(i,n\right) \\ 0 & otherwise \end{cases} \tag{1.14}$$

Figure 1.26: Figure shows equation used in auxin-based models of phyllotaxis presented in the text.
The symbols denote: a_i concentration of auxin in cell i; x_i concentration of morphogen X in cell i; $J_{i \to n}$ unitary net flux of auxin from cell i to cell n; p_i concentration of PIN in cell i; $p_{i,n}$ concentration of PIN in the interface transferring the auxin from cell i to cell n; D auxin diffusion constant; T auxin active transport constant; $\alpha_{a/p}$ auxin/PIN synthesis constant; $\beta_{a/p}$ auxin/PIN decay constant; Pr set containing primordia cells; Cz set containing central zone cells; B set containing border cells; k_a auxin saturation threshold; $\psi(i,n)$ holds when the wall is the "closest" cell wall to any of the primordium or meristem summit; V_i denotes volume of cell i; S_{in} the surface of membrane interface i,n. Square brackets are used as proposed by Iverson (look at 2.2.5.1).

auxin concentrations. The magnitude and spacing of concentration maxima are parameter depend.

The concept of PIN allocation in the cell membranes according to the concentration of auxin in the neighbouring cells will be called in this thesis the *concentration-based* mechanism/polarization.

Smith et al. assumes that PIN concentration in the interface from cell i to its neighbour n is positively regulated by auxin concentration in cell i (equations 1.9, 1.10), whereas Jönsson et al. assumes that this positive regulation is due to the concentration in cell n (equations 1.5, 1.6).

As mentioned before, in both Jönsson et al. and Smith et al. models, the distribution of PIN in a cell membrane of cell i depends on the local auxin gradient. According to Smith et al. this is regulated by a non-linear function: the amount of PIN in cell i that is localised in the membrane towards cell n is proportional to 3^{a_n} (equation 1.10). In the simulations presented by Jönsson et al., the relationship is linear. Therefore, in the same situation as described above, the amount of PIN in the membrane will be proportional to a_i (equation 1.6).

(b) **The relation between active auxin transport and auxin concentration**

In all models, the rate of active auxin transport depends on auxin concentration. In the Jönsson et al. model, the relationship is linear with a saturation term (equation 1.4), while according to Smith et al., the transport rate is proportional to the square of the auxin concentration (equation 1.8). According to Barbier, the transport is decreased when auxin is both saturated or depleted (equation 1.8).

(c) **The auxin balance law**

Jönsson et al. propose that auxin is produced proportionally to the concentration hypothetical morphogen X (denoted as x in the equation 1.3). This morphogen is produced everywhere in the meristem except for the meristem summit (equation 1.3).

Smith et al. suggests that auxin is produced in every cell in the meristem. However, its production in the cell can slow down, if auxin concentration in this cell is relatively high (equation 1.7).

In Barbier's model the auxin enters the meristem only via the periphery (equation 1.11).

Smith et al. and Jönsson et al. assume that the auxin particles decay in all cells in the meristem (equations 1.7, 1.3). Barbier hypothesizes

that the auxin is removed only in the primordia and meristem summit (equation 1.11).

2. **Simulation aspects**

   (a) **The function of the primordia**

   To increase the model's stability, the Smith et al. make *ad hoc* assumption that within primordia, PIN1 polarization is up-regulated (equation 1.11). In Barbier's model it is required that the primordium emits a "magnetic" attraction changing the polarity of PIN in closest cells (equation 1.14). Contrary, Jönsson et al. make no additional assumptions about primordia functioning is made.

   (b) **Cell representation and growth of the structure**

   For each of the models different tissue representations is used. In Jönsson et al. model cells as spheres, which centres are layed on a dome-like shape. The growth is driven by forces, since the cell centres are connected with springs and repel each other.

   Smith et al. uses polygonal cells creating 2-manifold mesh. The growth is achieved using the method based on the relative elementary growth rate introduced by Nakielski and Hejnowicz.

   Barbier uses a 2D cell representation based on Dirichlet domains. The growth is realized using displacement field, as described by Douady and Couder [1996a].

   Both Jönsson et al. and Barbier admit that their representation introduce cell sliding and random changes of cell neighbourhood, which are not observed in meristem tissues.

   (c) **Definition of the central zone**

   Biological experiments show, that the cells in the central zone are not able to initiate primordia [Reinhardt et al., 2000a]. In Smith et al. and Barbier [2005] models, this is expressed explicitly by forbidding primordia formation in the central zone.

   In Jönsson et al. model, the difference between the zones is defined implicitly by using a molecule X that is produced only outside an apical region and degraded everywhere else. This molecule is allowed to diffuse and it induces auxin production (equation 1.3). The morphogen X-dependent auxin production is used to break the symmetry and to decrease the probability of peak formation in the central zone.

   (d) **Emerging patterns**

The Jönsson et al. [2006] model shows the principle of the patterning mechanism and its possible application for phyllotaxis. However, the observed patterns have limited stability.

Confronted with the same problem, Smith et al. [2006c] introduced a non-linear dependencies on auxin concentration, which increased the phyllotactic patterns stability. Moreover, an additional equation was introduced to increase PIN polarization exclusively within the primordia. With these modifications, the model starts from a radially symmetric embryo, produces opposite cotyledons and gradually shifts towards spiral phyllotaxis. The patterns are stable and reproduce in vivo measured angles within one standard deviation. The model is capable of reproducing whorled phyllotaxy, although the stability of this pattern is limited to 15 primordia (personal communication with R. Smith).

The model of Barbier [2005] is able to produce unstable spiral patterns, though the author mentions that the patterning capabilities were not exhaustively explored (P. Barbier de Reuille, personal communication).

Chapter 2

Flux-based model of phyllotaxis

2.1 Canalization-based models of auxin transport

2.1.1 Original Mitchison's model

While studying vascular strand formation in pea Sachs [1969], suggested,that vasculature development is induced by auxin, as it flows through a tissue. He postulated that veins are formed in a feedback process, in which the differentiation of cells increases their ability to transport auxin and auxin itself induces this cell differentiation. As a result of this mechanism, the signal inducing vein differentiation is "canalized" into paths in a process that is frequently compared with "water carving riverbeds in soft terrain" [Sachs, 2003]. Since then this concept has been called the *canalization* hypothesis. This is in line with more recent work by Reinhardt et al. [2003] who studied the forming vascular strands below each primordium and observed that the strand positions corresponds to a path of cells in which PIN is strongly expressed.

The concept of canalization was formalised by Mitchison [Mitchison, 1980a,b, 1981]. In his model, following the Sachs [1969] concept, the auxin transport efficiency in cells increases with the auxin flux. The auxin transport in the model is mediated by imaginary carrier particles, placed in the cell membrane, and transporting the auxin from cell to cell. These particles dynamically change their location in the membrane, depending on the auxin flux. **To empha-**

size the difference of this patterning mechanism and the previously described *concentration-based* concept, we call it a *flux-based* transporter polarization[1].

To test Sachs' hypothesis, Mitchison developed a computer model with cellular resolution. In this model, a tissue is represented as a grid of square cells. The cells in a bottom row remove auxin (i.e. they act as sinks and for each such a cell i, $i \in Si$), whereas the top layer cells synthetize auxin (i.e. they act as sources, and $i \in So$). Auxin is then actively and passively transported in the tissue. The equation system to model this process can be denoted as:

$$\frac{\partial a_i}{\partial t} = \left(- \sum_{n \in N_i} J_{i \to n} + \alpha_a \left[i \in So \right] \right) \left[i \in Si \right] \tag{2.1}$$

$$\frac{\partial p_{i,n}}{\partial t} = \Phi \left(J_{i \to n} \right) + \alpha_p - \beta_p p_{i,n} \tag{2.2}$$

$$J_{i \to n} = \gamma_a \left(a_i p_{i,n} - a_n p_{n,i} \right) \tag{2.3}$$

$$\Phi_C(x) = \begin{cases} \kappa x^2 & x \geq 0 \\ 0 & x < 0 \end{cases} \tag{2.4}$$

where the conventions from the concentration-based models presented in 1.4 are used. Boundary conditions proposed by Mitchison were: a constant influx α_a of external auxin into the top row of cells (source cells), zero auxin concentration in the bottom row (sink cells) and no flux across the left or the right boundary of the tissue. At the beginning of the simulation, an initial graded distribution of auxin concentrations is set up in such a way that the auxin concentration is growing linearly with the distance from the sink cells [Mitchison, 1981].

In the original Mitchison's model a strand of increased transporter polarization emerges, following the destabilisation of the initially linear auxin concentration gradient. The destabilization is achieved by injecting an additional portion of auxin to the selected epidermis cell at the beginning of simulation.

The strand is formed in the following way: the initial destabilization of auxin concentration in randomly selected epidermis cell, called c, results in increased flux to its neighbouring cell c_2 in L2, located directly below c. This flux induces

[1] Or in short: *flux-based* mechanism, *flux-based* polarization. The auxin transport model using a variant of this hypothesis to allocate PIN in the cell membranes is called *flux-based* model.

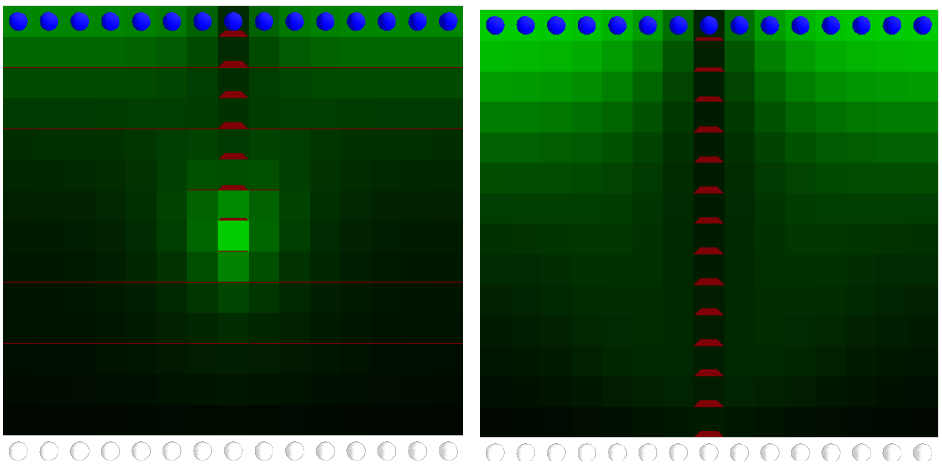

Figure 2.1: Simulation of the vascular vein formation.
White dots mark sink cells, blue cells mark cells producing auxin. Auxin concentration is depicted with green (the brighter the green the higher auxin concentration). All the parameters used for the simulation are exactly the same as in original Mitchison paper Mitchison [1981].

the allocation of PIN in the membrane of cell c being an interface to c_2. As a result, auxin flows efficiently to the cell c_2, but leaves this cell slower, due to the low number of membrane transporters. It leads to an accumulation of auxin in the cell c_2. However, the flux downwards increases with time inducing the PIN allocation at the bottom of cell c_2, allowing the cell c_2 to pump out its auxin to its closest neighbour in L3. This process continues creating a path of highly polarised membranes connecting the epidermis (source cells) with the internal tissues (sink cells). During this process, a local maximum of auxin appears in each cell forming the future strand, just before its PIN concentration in its bottom location rises (figure 2.1A). As a result, a "wave of auxin", traversing the tissue is observed. This prediction was indeed observed in plants [Goldsmith et al., 1981]. When the process is finished, a vascular strand can be observed (2.1B). The strand has high flux but low concentration of auxin. The results of reproduced Mitchison's simulation are presented in figure 2.1.

2.1.2 Extended Mitchison's model

One of the domains, where the concept of Sachs [1969] was extensively explored is leaf morphogenesis, and the process of leaf venation in particular. Veins in the leaf consist of vascular tissue and form so-called venation networks that are located in the spongy layer of mesophyll*. Plant species show a variety

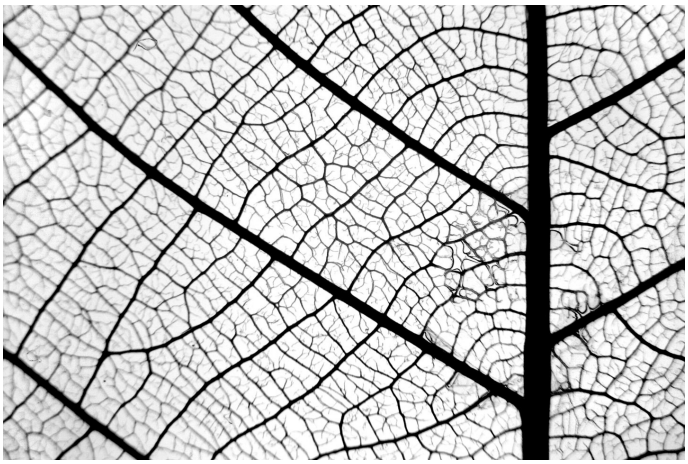

A

B

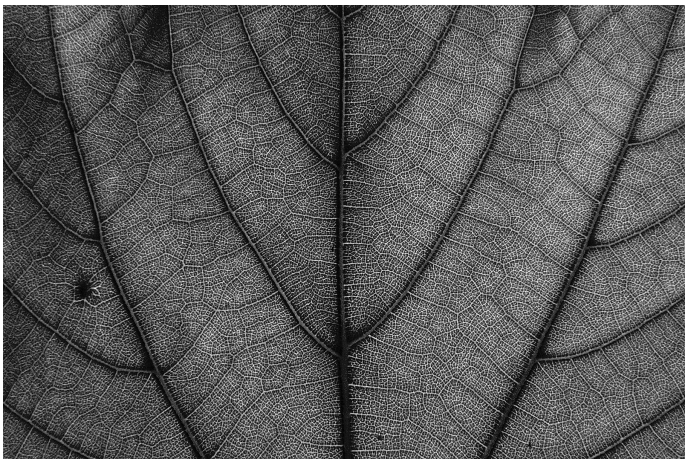

C

Figure 2.2: Examples of the venation patterns in leafs.
2.2A image of the Horse Chestnut (*Aesculus hippocastanum*) leaf blade coming from Botanic garden in Montpellier taken using light table technique, 2.2B macro image of the Common Hazel (*Corylus avellana*) tree taken in Botanic garden in Berlin and 2.2C macro image of the Common Grape Vine (*Vitis vinifera*) taken in Castelnau-le-Lez.

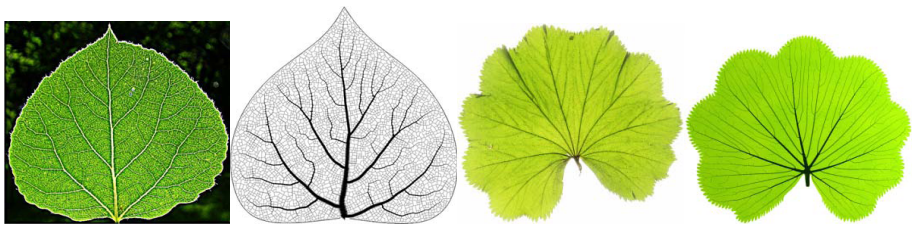

Figure 2.3: Examples of *in silico* generated venation.
Two first pictures present reticulate patterns of poplar leaves (first real leaf, second simulation result), two second ones present venation of lady's mantle venation (first real leaf, second simulation results). Images taken from Runions et al. [2005].

of leaf venation patterns, which are often used for classification (look at figure 2.2, for review Hickey [1979]). Our current understanding of venation suggests that vein formation depends on auxin and its transport [Avsian-Kretchmer et al., 2002, Mattsson et al., 1999, Sieburth, 1999]. Computer simulations showed that the canalization concept has patterning capabilities able to reproduce venation (figure 2.3) [Runions et al., 2005].

Since the formalization of original Mitchison's model and until the identification of the PIN transporters by Gälweiler et al. 1998 there was no evidence of the existence of any membrane carriers able to transport auxin. Only recently, Rolland-Lagan and Prusinkiewicz [2005] reproduced and re-examined the Mitchison's simulations in the context of leaf morphogenesis and in the light of new experimental data.

2.1.2.1 Single vein model

Analysis of vein patterning at the pre-procambial stage [Scarpella et al., 2004] suggests that the primary vein is formed acropetally (from leaf base to leaf tip), in spite of auxin being transported basipetally (from tip to base). The original canalization model does not reproduce this behaviour (compare with figure 2.1a). Rolland-Lagan and Prusinkiewicz [2005] proposed that the phenomenon of basipetal strand formation can be reproduced assuming that the formation of the primary vein is sink-driven rather than source driven. They reported, that with a single sink cell at the bottom of the tissue and an incoming flux of auxin along the entire top edge of the tissue, a strand of increased flux developed acropetally from the sink towards the top of the tissue.

Rolland-Lagan and Prusinkiewicz [2005] also showed that the destabilization of the system, leading to strand formation, can be achieved not only by one-time injection of an additional portion of auxin to a randomly chosen cell c of

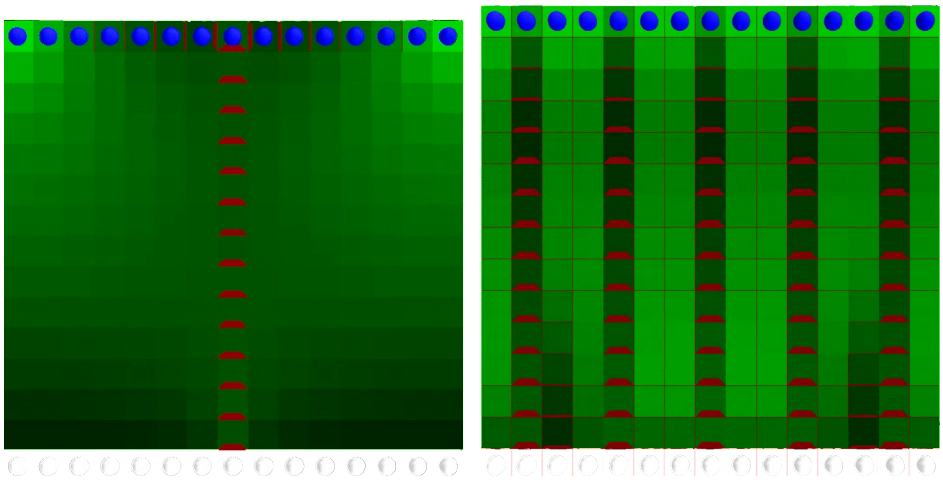

A B

Figure 2.4: Extensions of Mitchison simulations. Description in the text.

epidermis (as in the Mitchison's model). It is also possible to trigger strand initiation by additional, constant synthesis of auxin in the cell c during entire simulation.

According to these authors, the *flux-based* mechanism is not only able to create a single vein, like in the original model, but also a network of veins can develop. The introduction of multiple sinks, consecutively appearing during the simulation led to a network of veins containing loops, which correspond to aureoles* in leaves.

We investigated further the Mitchison's model and its modified variants (e.g. simulations from Rolland-Lagan and Prusinkiewicz [2005]) to test, whether the *flux-based* polarization is compatible with other experimental data concerning the PIN and auxin.

Constant synthesis of auxin in selected epidermic cell vs. one-time injection We repeated the modification of Mitchison's simulation in which the destabilization is achieved by constant auxin synthesis, instead of one-time auxin injection. We confirm, that this type of destabilization may lead to the formation of vein. Furthermore, when auxin is constantly synthetized, the rate of synthesis determines the number of strands. If only a small quantity of auxin is added, no strand is created. When the amount is moderate, one strand appears (this is the case for the parameter values proposed by Mitchison) and if the amount is high, more strands develop starting from the selected cell (2.4B).

Basipatal vs. acropetal vein formation Experimental data suggest that in the early stages of leaf formation, there are no localised auxin sources in the leaf margin [Avsian-Kretchmer et al., 2002]. It is possible, that auxin is synthetized relatively homogeneously in the whole apex [Ljung et al., 2001, 2002]. Therefore, we decided to exchange the axiom of auxin synthesis localized in the epidermis cells, by the homogeneous auxin synthesis in every cell (except the sink cells). In this case, the equation 2.1 becomes:

$$\frac{\partial a_i}{\partial t} = \left(- \sum_{n \in N_i} J_{i \to n} + \alpha_a - \beta_a \right) [i \in Si]$$

According to the performed simulations, this modification was sufficient to cause the primary vein to be formed acropetally. This result suggests, that according to *flux-based* model vein can form acropetally not only when auxin enters the system by epidermis, but also when it is synthetized in whole meristem. Thus, the simulations give another proof, that there is no contradiction between an acropetal development of the mid-vein and the *flux-based* polarization mechanism.

Auxin concentration in the vein It is commonly stated, that Mitchison's model produces veins with high auxin flux, but low concentration of auxin in the vein [Feugier et al., 2005, Rolland-Lagan and Prusinkiewicz, 2005]. The experimental data suggest however, that the concentrations of auxin in the vascular precursor cells are high [Mattsson et al., 1999]. Therefore, this observation is a common argument used against the plausibility of *flux-based* mechanism in leaf morphogenesis [Rolland-Lagan and Prusinkiewicz, 2005, Merks et al., 2007].

Our simulations reveal, that this statement is only true when a distance between the epidermis (source of auxin) and sink cells is small. In more general case, when the system stabilizes, a constant concentration of auxin in a strand is observed. However, the concentration in the tissue gradually decreases from epidermis to the row of sink cells. Hence, if the distance between the epidermis and sink cells is sufficient, that the concentration in the vein close to the sink is higher than in the surrounding cells. This situation is illustrated in figure 2.4B. The concentration of auxin in the vein does not have to be lower than in the surrounding tissue, although the ratio between the auxin concentration in the vein and the auxin concentration in vein surrounding increases with the distance from source.

Feugier et al. [2005] provided an alternative explanation of this issue. They demonstrated, that the concentration of auxin in the canals crucially depends

on the detailed properties of the mechanism distributing efflux carriers within a cell. According to this model, if the number of membrane carriers is controlled independently in different parts of a cell, as is the case in Mitchison's model, the canals will have a lower concentration of auxin than the surrounding tissue. By contrast, the canals might have a higher auxin concentration than the adjacent tissue when two additional assumptions are made: *i*) the number of carrier proteins in a cell is fixed or slowly changing, *ii*) different sides of a cell compete for the allocation of carrier proteins from the available pool.

Resolution of the equations In the original Mitchison model and its extensions proposed by [Rolland-Lagan and Prusinkiewicz, 2005] the transporter concentrations ($p_{i,j}$) were capped[2]. For the set of parameters chosen by Mitchison, when the concentrations are left uncapped, the system requires extremely short integration steps and is less stable due to huge differences in transporter concentrations. Capping of the transporters is difficult to explain with respect to any known chemical reaction dynamics.

The partial solution of this issue is to change the equation 2.4 by introducing the saturation component [Michaelis and Menten, 1913]. After introducing a saturation component, we did not observe any qualitative change of the system's behaviour. However, the integration steps had to be reduced (depending on simulation up to 10 folds), which importantly increased the simulation's time.

Sensitivity of the model The original Mitchison model is sensitive to a variation of several parameters. For example, for the parameter set proposed originally by Mitchison, an increase of source strength by 4 folds changes remarkably the number of strands (2.4B). Similarly, the final number of strands is influenced by size and shape of a grid representing the tissue (it was also reported by Rolland-Lagan and Prusinkiewicz [2005], Feugier et al. [2005]).

2.1.2.2 Modelling regeneration of vasculature with *flux-based* model

In the L1 layer of the meristem a fast reallocation of PIN transporter molecules is observed after the initiation of the primordium. In this moment, PIN molecules in the neighbourhood of the primordium switch their position to conduct auxin towards the new primordium. One of properties of *flux-based* mechanism is the ability of the transporter molecules to dynamically relocate, adapting to changes in the system system. We modified the Mitchison model to perform simulations

[2] it means that while solving the equation system, if the value of $p_{i,j}$ exceeds certain threshold t, the value is automatically set to the threshold value t.

and to test if the *flux-based* mechanism is compatible with the experiments showing dynamic changes in PIN polarization.

Regeneration of vascular tissue following its disruption by wounding is a prime process, which requires reorganization of an adult tissue and has been the basis for a formulation of the canalization hypothesis [Sachs, 1969]. Classical experiments investigating the polarity during regeneration and *de novo* formation of vascular tissue were performed in pea (*Pisum sativum*) [Sachs, 1981]. Recently, to observe changes in PIN distributions during vascular tissue regeneration, Sauer et al. [2006] repeated Sachs' experiment on pea and monitored the distribution of PIN. The experiment is described in the following way:

> *Twenty-four hours after disruption of the existing vasculature by wounding, PsPIN1 (in following PIN1) lost its basal polarity above the wound (figure* 2.5A*, around the asterisk) but remained basally localised below the wound in cells accompanying the vasculature, identical to the control situation (data not shown). After 2 days, PIN1 became ectopically expressed above the cut in a relatively large field of tissue, with a pronounced sub-cellular lateral orientation facing the central part (figure* 2.5B*). After 3 days, the field of cells ectopically expressing PIN1 became narrower, and stronger expression levels were constricted to inner cells of the field (figure* 2.5C*). The field of cells expressing PIN1 was oriented around the wound with PIN1 polarity lateral above the wound, and gradually becoming basal at the position of the wound itself. After 5 days, the field of cells expressing PIN1 had narrowed down to only a file of cells and new vasculature (morphologically distinguishable by tracheary elements) had formed next to these cells (figure* 2.5D*). Thus, the regeneration of new vasculature is preceded temporally and spatially by differential expression of PIN auxin transport components, and its polarity is preceded by the concerted gradual establishment of PIN polarities in each individual cell.*

To simulate the regeneration of the vasculature we adapted the original Mitchison model:

1. The equation 2.1 is changed, by introducing auxin degradation β_a in every cell:

$$\frac{\partial a_i}{\partial t} = \left(- \sum_{n \in N_i} J_{i \to n} + \alpha_a \left[i \in So \right] - \beta_a \right) \left[i \in Si \right]$$

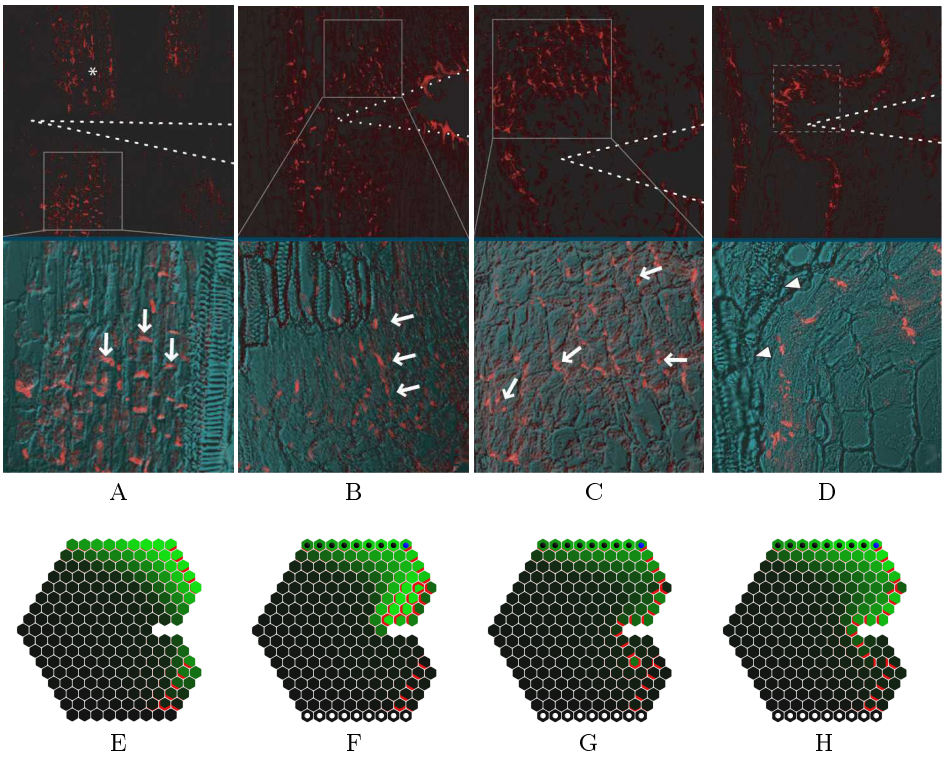

Figure 2.5: Vein formation after wounding an organ: reality and *in silico* experiment.
Figures (2.5A-2.5D) taken from [Sauer et al., 2006] and show the consecutive stages of their experiment (detailed description of the experiment in the text). Figures (2.5E-2.5H) show the corresponding stages of *in silico* experiment using the *flux-based* polarization hypothesis to orient the PIN.

This modification is inspired by biological data suggesting that the cell constantly degrade auxin [Ljung et al., 2002].

2. The cell membranes which reach the maximum concentration of PIN, remove the PIN slower. This modification is discussed in the following paragraph. It is equivalent to the modification of equation 2.2:

$$\frac{\partial p_{i,n}}{\partial t} = \Phi\left(J_{i\to n}\right) + \alpha_p - \beta_p p_{i,n}\left[p_{i,n} < p'_{max}\right] - \beta'_p p_{i,n}\left[p_{i,n} \geq p'_{max}\right]$$

Where β'_p is a constant describing PIN removal from the membrane and it holds $\beta'_p \ll \beta_p$; p'_{max} is only a little smaller than PIN capping threshold p_{max}.

3. The tissue geometry is changed. In this simulation the cells are represented by hexagons (look at virtual tissues in figure 2.5). This modification is introduced to allow auxin to be transported in more than only four directions, as in the grid build up from squares.

4. The simulation is adjusted to the new tissue geometry: the cells in a bottom-most row act as sinks ($i \in Si$), the cells in a top-most row act as auxin sources ($i \in So$), the right-most top cell is producing additional auxin (similar to the original model in order to develop vascular strand).

The beginning of the simulation is similar to the original Mitchison experiment. During the simulation, the right-most top cell is constantly synthesising additional auxin. This leads to the establishment of the vascular tissue, passing all the right-most cells of the tissue. After the vein is established (the system has reached a stable state at this moment), a part of the tissue, together with the middle segment of the vein is removed to simulate wounding.

After removing the part of the tissue (figure 2.5E) a sequence of events quantitatively similar to the one observed *in vivo* can be followed. Firstly, auxin reaches the zone where the part of the tissue was removed, and due to its flux in all directions, induces PIN activation in the whole zone (figure 2.5F). This corresponds to the extensive expression of PIN above the cut in a relatively large field of tissue facing mostly the central part of the tissue (figure 2.5B). Secondly, PIN expression becomes concentrated to a single strand, wrapping around the wound and searching for the fastest path to the sink (figure 2.5G). This is again consistent with the *in vivo* observation, where the field of cells laterally expressing PIN1 becomes narrower and stronger expression levels are constricted to inner cells of field. The new vascular strand joins the remaining,

basal vascular strand and thus, reuses this medium to fully connect the source with the sink (figure 2.5H). Once again, it resembles the real observations, where PIN expression zone narrows down to only a file of cells creating a new vasculature. It is important to note, that in this process we observe a strand formation from source to sink.

Finally, we show that *flux-based* polarization is able to reproduce the sequence of events observed during the pea wounding experiments. Both *in vivo* and *in silico* experiments, show qualitatively similar auxin-dependent changes in PIN polarity preceding *de novo* formation or regeneration of vascular tissue and the establishment of new vasculature.

During the development of vasculature after wounding of the tissue, PIN proteins change their basal localisation and gradually establish a new polarity, which guides the development of vascular tissue. This mechanism is able to change the polarity of PIN completely, in this particular case from basal to lateral locations in the cells. This situation is similar to the primordium initiation in the SAM, where rapid PIN reversal is observed in the direction of young primordium [Reinhardt et al., 2003].

The model requires slower removal of PIN by cell membranes with its maximal concentrations (assumption 2). Without this condition the high PIN polarization disappears in the place of old vascular tissue and below the cut. If PIN polarization vanishes completely in this location, the vein passing the wound proceeds directly down, without "reusing" the old strand. This is not in line with experimental data showing that the new vasculature joins the lower part of the old vein.

It is important to underline, that auxin is a sufficient signal to trigger the whole sequence of vein development events (assuming the interaction with its membrane carrier PIN) required for the vasculature regeneration.

2.1.3 Canalization and branching patterns

Feugier et al. [2005] performed a further analysis of canalization models. The authors showed, that if auxin is produced uniformly in a sufficiently large grid of cells, the *flux-based* model yield to different types of PIN patterns. In their models the type of self-enhancement described by the function Φ, has a strong effect on the possibility of generating the branching patterns. For response functions with acceleration in the increase of carrier protein numbers compared to the auxin flux, branching patterns are likely to be generated. For linear or decelerating response functions, no branching patterns are formed.

Fujita and Mochizuki [2006] studied a related canalization-type mechanism and introduced a hypothetical, diffusible enhancer molecule produced according to the net auxin flux. Their model produces branching venation patterns like Feugier's model and reticulate[3] patterns. The authors point out, that these patterns lack important features of real venation, such as the presence of closed loops or hierarchical vein orders.

A recent "constant production hypothesis" by Dimitrov and Zucker [2006] is a variant of the *flux-based* interpretation of the canalization hypothesis. The authors assumed that the auxin is produce in every cell, contrary to Mitchison [1981], who assumed specific auxin synthesis locations in the tissue. The model explains side-vein formation as the shortest, steepest path draining an auxin maximum, formed in the centre of the aureoles in a balance between constitutive auxin production and drainage by the veins.

2.1.4 Conclusions

Implementing Mitchison's model and its variants allowed us to validate the simulation framework prepared for meristem simulation. The proposed framework made it possible to reproduce Mitchison's model and to perform certain modifications to test additional auxin transport hypotheses.

The putative auxin efflux transport protein PIN1 is the first known molecular marker for both plant organ primordia and pre-procambial tissue. Thus, phyllotaxis and vascular patterning are very closely related at the molecular level, providing further support for the idea that the two processes may have directive roles on each other.

We showed that the *flux-based* mechanism is able to create veins both, acropetally and basipetally. Acropetal vein formation can be triggered by assuming a homogeneous auxin synthesis. The original Mitchison model requires fixed tissue size and PIN capping. Initialisation of vein formation in the original Mitchison model can be triggered either by localised, constant, additional production of auxin or by a single auxin injection.

The *flux-based* mechanism has patterning properties allowing PIN to dynamically adapt to changes in the system configuration e.g. appearance of new auxin sinks or sources or a change in tissue geometry. The dynamics of these changes is compatible with the PIN dynamics observed during the wounding of already developed vasculature in the epidermis.

[3] A leaf with reticulate venation has its veins arranged in a pattern such that larger veins give rise to progressively smaller veins. The end branches of the veins define small areas called aeroles.

The performed simulations imply that the *flux-based* mechanism could provide an explanation for the development of vasculature below the primordia. Since this mechanism could also explain laminar PIN distributions, as observed on the surface of the SAM, it could possibly explain as well the distributions of PIN observed in the L1 layer. Together with an ability of dynamic reorientation, these observations suggest, that *a flux-based* mechanism could be responsible for auxin transport in whole meristem, thus also for the process of phyllotaxis.

2.2 *Flux-based* transport enhancement as a plausible unifying mechanism of auxin transport in meristem development

This chapter contains the article published in the October issue of PLOS Computational Biology journal in 2008.

Flux-based Transport Enhancement as a Plausible Unifying Mechanism for Auxin Transport in Meristem Development

Szymon Stoma[1,2], Mikael Lucas[1], Jérôme Chopard[1], Marianne Schaedel[2], Jan Traas[2,*], Christophe Godin[1,*]

[1] INRIA, Virtual Plants Project-Team, UMR DAP, TA A96/02, 34398 Montpellier, France.

[2] Laboratoire de Reproduction et Developpement des Plantes, Universite de Lyon1, INRA, CNRS, ENS-Lyon, 46 allee d'Italie 69364 Lyon Cedex 7, France.

*Corresponding authors: christophe.godin@inria.fr, jan.traas@ens-lyon.fr

Abstract (250-300 words) Plants continuously generate new organs through the activity of populations of stem cells called meristems. The shoot apical meristem initiates leaves, flowers and lateral meristems in highly ordered spiralled or whorled patterns via a process called *phyllotaxis*. It is commonly accepted that the active transport of the plant hormone auxin plays a major role in this process. Current hypotheses propose that cellular hormone transporters of the PIN family would create local auxin maxima at precise positions, which in turn would lead to organ initiation. To explain how auxin transporters could create hormone fluxes to distinct regions within the plant, different concepts have been proposed. A major hypothesis, *canalization*, proposes that the auxin transporters act by amplifying and stabilizing existing fluxes, which could be initiated, for example, by local diffusion. This convincingly explains the organised auxin fluxes during vein formation, but for the shoot apical meristem a second hypothesis was proposed, where the hormone would be systematically transported towards the areas with the highest concentrations. This implies the co-existence of two radically different mechanisms for PIN allocation in the membrane, one based on flux sensing and the other on local concentration sensing. Since these patterning processes require the interaction of hundreds of cells, it is impossible to estimate on a purely intuitive basis if a particular scenario is plausible or not. Therefore, computational modelling provides a powerful means to test this type of complex hypotheses. Here, using a dedicated computer simulation tool, we show that *flux-based* polarization hypothesis is able to explain auxin transport at the shoot meristem as well, thus providing a unifying concept for the control of auxin distribution in the plant. In addition, the simulations lead to testable predictions that should be able to distinguish between *flux-based* polarization and other hypotheses. Therefore, the flux-based polarization

mechanism provides a unifying concept for the control of auxin distribution in plants.

Author's summary (150-200 words) Plants continuously generate new organs through the activity of populations of stem cells called meristems. The shoot apical meristem (SAM) initiates leaves, flowers and lateral organs in highly ordered, spiralled or whorled arrangements via a process called phyllotaxis. Auxin, a plant hormone, plays an essential role in this process. It is actively transported from cell to cell by specific membrane associated transporters. In the SAM, this coordinated transport creates organized auxin fluxes resulting in hormone accumulation at precise positions, where organ formation is triggered. One key question in this process is to understand how auxin transport is coordinated. To address this issue, we have investigated a specific hypothesis, the canalization hypothesis, whereby every cell senses and attempts to stabilize existing hormone fluxes. Since such a patterning process would require the interaction of hundreds of cells, it is impossible to estimate on a purely intuitive basis whether it would be able to generate the observed organ positions. We, therefore, developed a computational approach to test this hypothesis and showed that a flux based mechanism is indeed able to generate phyllotactic patterns and is consistent with biological data describing meristem development.

2.2.1 Introduction

During plant development, organs are continuously created by small populations of cells called *apical meristems*. The so-called shoot apical meristem (SAM) generates all the aerial parts of the plant. The SAM is a highly organised structure, composed of a central zone required to maintain the meristem and a surrounding peripheral zone, that is competent to initiate new organ primordia [Reinhardt et al., 2000a]. The young organs are usually initiated in highly ordered spiralled or whorled patterns. This remarkable arrangement of organs is called phyllotaxy and varies according to particular plant species and growth conditions. Over the last two centuries, phyllotaxy has been extensively studied and different models for this patterning process have been proposed. From a mechanistic point of view, it is now widely accepted that phyllotaxy emerges from a process of local lateral inhibition: each primordium creates an inhibitory field in its vicinity where no other primordium can develop. This basic inhibitory field hypothesis (see Douady and Couder [1996a] for a review), is potentially able to generate a wide range of phyllotactic patterns Snow and Snow [1962], Douady and Couder [1996a], Atela et al. [2002], Shipman and Newell [2004], Smith et al. [2006a].

Hypotheses concerning the physiological nature of these inhibitory fields were proposed only recently Reinhardt et al. [2003]. They rely on the signalling role of a key hormone called *auxin*, that plays a crucial role in primordium formation Reinhardt et al. [2000a]. Auxin is actively transported throughout the plant from cell to cell by carriers that are located at the cell plasma membranes Vieten et al. [2007]. During auxin transport influx carriers of the AUX/LAX family, facilitate auxin import into the cells. This is in contrast to the PIN-FORMED (PIN) proteins, which facilitate efflux [Petrasek et al., 2006]. Interestingly, PIN proteins often accumulate on one particular side of the cell, thus suggesting that auxin is evacuated preferentially via that side. Importantly, PIN carriers often show locally coherent orientations between groups of neighbouring cells, indicating that PIN orientation is coordinated at the level of tissues Reinhardt et al. [2003], Barbier de Reuille et al. [2006]. It is therefore possible to imagine how cells could transport auxin from cell to cell throughout the plant, thereby creating fluxes that lead to local hormone maxima and minima Reinhardt and Kuhlemeier [2002], Kuhlemeier [2007]. These differences in concentration would subsequently be interpreted in terms of differential gene expression and growth rates.

At the SAM, auxin importers and exporters are mainly expressed at the meristem surface [Reinhardt et al., 2003]. When auxin transport is inhibited, organ initiation is severely affected or even totally absent [Okada et al., 1991]. In addition, the cells at the SAM orient their PIN proteins towards the young primordia and it is now currently thought that organs are initiated at auxin accumulation points, while the hormone is depleted in their neighbourhoods [Reinhardt et al., 2003]. The young primordia would thus create drainage basins in their vicinity which would be equivalent to the inhibitory fields proposed previously. While the coherent behaviour of PIN proteins in cell populations is well established, the actual mechanism behind this phenomenon is still not well understood. So far two basic concepts have been proposed.

A first hypothesis is based on the pioneering work of Sachs (1969) on vascular tissue differentiation in plants Sachs [1969]. Sachs proposed that auxin transport is facilitated during the process of vascular tissue induction. He suggested that the positive feedback between flux and transport is able to amplify small fluxes and can potentially create *canals* of auxin between auxin sources and sinks that subsequently differentiate into vein tissues. This positive feedback between flux and transport is at the basis of the *flux-based* polarization mechanism we study in this work. The *canalization* hypothesis was then formalized by Mitchison Mitchison [1980a, 1981] who developed a mathematical model of this process that increases membrane permeability of cell plasma membrane on

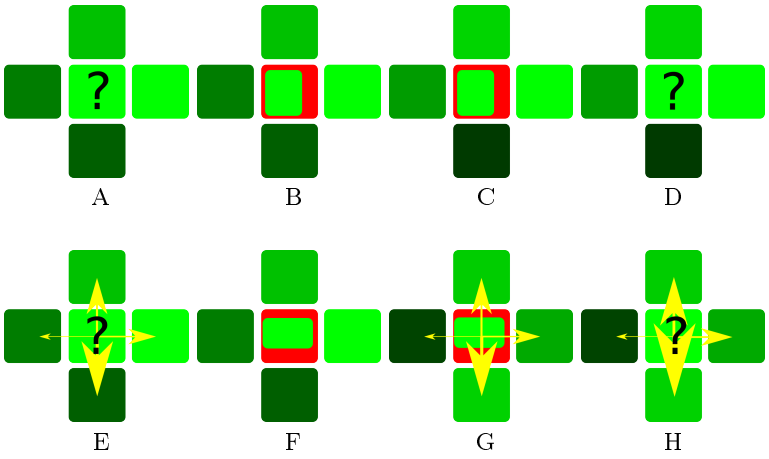

Figure 2.6: Comparison of two PIN orientation hypotheses. The concentration of auxin in the cells is marked with green (the brighter green, the higher the concentration), the fluxes are depicted with yellow arrows and PIN concentration at the membranes are indicated by red lines with variable thickness (the thicker the line the higher the concentration). Note, that the fluxes might be independent from the concentrations. Figures 2.6A-2.6D show the principle of the *concentration-based* hypothesis and figures 2.6E-2.6H show the principle of *flux-based* polarization hypothesis. In both cases the key question is how the cell marked with "?" should allocate the PINs to its membranes (2.6A, 2.6E). In the case of the *concentration-based* hypothesis this cell makes the decision based on the *concentrations* in the neighbouring cells. The higher its neighbours auxin concentration, the more PIN will be inserted in the membrane (2.6B). *Flux-based* polarization depends on the *net flux* between neighbouring cells. The higher the net flux to its neighbour the more PIN will be inserted in the membrane (2.6F). In both cases the newly allocated PINs change the concentrations and fluxes (2.6C, 2.6G), leading to the next iteration of the scenario (2.6D, 2.6H).

the sides where the net flux of auxin is positive. This model was then further studied in the context of leaf venation pattern by several authors Feugier et al. [2005], Rolland-Lagan and Prusinkiewicz [2005], Runions et al. [2005], Dimitrov and Zucker [2006] who interpreted the *canalization* hypothesis as a feedback mechanism between auxin fluxes and PIN transporters and studied the properties of such a coupling both on a fixed shape and during leaf development. From the biological point of view, recent experiments tend to support the *canalization* hypothesis, at least in the inner tissues of the plant Scarpella et al. [2004, 2006], Sauer et al. [2006]. However, whether it could also account for the behaviour of auxin transporters in other parts of the plant such as the shoot and root apical meristem or leaf margins remains an open question.

More recently, a second concept was proposed to explain auxin transport at

the SAM surface Jönsson et al. [2006], Smith et al. [2006b]. Based on the observation that PIN carriers point to primordia initiation sites in the SAM which supposedly correspond to auxin maxima, it was hypothesized that relative concentrations of auxin in neighbouring cells differentially drive the polarization of PIN1 to the corresponding portion of the membrane between each cell and its neighbours [Jönsson et al., 2006]. The cells would thus tend to export auxin against the auxin concentration gradient (referred to here as *concentration-based* hypothesis), thus amplifying differences in local auxin concentrations and creating *local maxima* or *spots* of auxin Scarpella et al. [2006]. The comparision of *concentration-based* and *flux-based* polarization hypothesis is presented in Figure 2.6, Using computational modelling, several authors were able to show that *concentration-based* hypothesis can produce spiralled and whorled phyllotactic patterns. In a recent article, Merks et al. proposed a modified *concentration-based* hypothesis Merks et al. [2007]. Although it requires further development, it is potentially able to explain the formation of veins in internal tissues. Could it, therefore, represent a unifying mechanism for the control of auxin fluxes throughout the plant? A major argument against this idea is that the model does not seem to be compatible with the presence of stable auxin maxima in tissues. This is typically the case at the root meristem, where a continuous, stable auxin maximum is maintained with incoming and outgoing fluxes Grieneisen et al. [2007]. In a recent study, Sauer et al. suggested that cell-type specific factors could decide whether one or the other mechanism would be used Sauer et al. [2006], but this remains to be proven.

Since the *concentration-based* hypothesis can not, on its own, provide a unifying mechanism for the control of auxin fluxes in the plant, we investigated whether *flux-based* polarization hypothesis, as the other major concept in the field could provide a realistic alternative. Since such cell-cell signalling based patterning processes involve the interactions between hundreds of cells it is impossible to estimate on a purely intuitive basis if a particular scenario is plausible or not. In this context, computational modelling provides a powerful means to test this type of hypotheses. We therefore designed a set of models and showed that the *flux-based* polarization mechanism is able to:

1. generate spiral phyllotactic patterns observed in the SAM,
2. produce pro-vascular strands below primordia in the sub-epidermal meristem layers,
3. reproduce stable auxin maxima as observed in the root meristems.

We therefore conclude that flux-based polarization could provide a unifying principle for the guidance of auxin fluxes in the plant. In addition, our model

leads to a set of testable predictions, that should be able to distinguish between the *flux-based* and *concentration-based* polarization hypotheses.

2.2.2 Models

2.2.2.1 Biological assumptions

To model auxin transport in a tissue we used a set of auxin related hypotheses derived from biological observations taken from the literature (see also introduction):

1. **The Auxin quantity in a cell changes as a result of active transport and diffusion between cells and local creation/degradation** [Edelstein-Keshet, 1988], as in previous models Smith et al. [2006b], Barbier de Reuille et al. [2006], Jönsson et al. [2006].

2. **Auxin is created locally in every cell** (suggested by Reinhard et al. Reinhardt et al. [2005], also used in other models Feugier et al. [2005], Smith et al. [2006b], Jönsson et al. [2006]). At this stage all precise locations of auxin synthesis is not well defined, but several of the YUCCA genes involved in auxin synthesis are expressed at the shoot meristem [Cheng et al., 2006].

3. **Auxin is degradated locally in every cell.** e.g. see Ljung et al. [2002].

4. Auxin is transported from the cell into the inter-cellular space according to the chemiosmotic model [Rubery and Sheldrake, 1974]. Briefly, this supposes that it is difficult for auxin to leave the cell by diffusion because of the neutral pH of the cytoplasm, whereas it can enter it more freely from the acidic inter-cellular space. Therefore, the plant has developed a system of transporters that facilitates the transport from cell to cell [Geldner et al., 2001, Vieten et al., 2007]. At the meristem, only PIN transporters seem to be polarized, while the AUX/LAX influx carriers are homogeneously distributed over the membrane. We model this overall transport process using a simplified system. First, we assume direct flux of auxin from cell to cell by omitting the wall compartment. Second, due to the symmetry of influx carriers, only PIN is simulated explicitly. Therefore **we model auxin redistribution in the meristem as a result of passive diffusion between cells and polar transport which is governed by PIN.** A similar approach was also used in other transport models Feugier et al. [2005], Smith et al. [2006b], Jönsson et al. [2006], Barbier de Reuille et al. [2006], Merks et al. [2007].

5. **PIN concentration in a cell membrane is up-regulated by auxin flux through this membrane** Sachs [1969]. This hypothesis is explained in detail in the Mathematical Formalization section.

To design the model of phyllotaxis, we extended the auxin related hypotheses with a set of hypotheses related to phyllotaxis:

1. The shoot apical meristem is a dome shaped structure, containing up to thousands of cells. **We distinguish the epidermal layer, called L1, that is one cell thick from the sub-epidermal cells that makes up the rest of the dome.**

2. **The L1 layer is itself composed of a central zone surrounded by a peripheral zone (also called competence zone).** These zones exhibit different properties Steeves and Sussex [1972] as explained below.

3. **Primordia can appear only in the peripheral zone of the meristem Reinhardt et al. [2000a].** Once a primordium is initiated, it moves away from the meristem summit following a radial trajectory, due to cell growth throughout the L1 Douady and Couder [1996a], Reddy et al. [2004].

4. **In the L1, primordium cells act as sinks by redirecting auxin from the L1 layer downwards.** This hypothesis is justified by the presence of vascular strands below each primordium which would transport auxin downwards [Reinhardt et al., 2003]. We assume that a primordium can easily remove any amount of auxin (the saturation level is much higher than the amount of auxin available in meristem).

5. Longitudinal sections show that pro-vascular strands are approximately three cells wide (data not shown). Therefore we assume that **a primordium is constructed from a central cell and all its direct neighbours.**

6. **A new primorium is formed as a response to high auxin accumulation in a cell of the competence (peripheral) zone** Reinhardt et al. [2000a].

7. **Auxin and PIN reallocation are fast processes. PIN proteins can be reallocated within one or two hours ([Sauer et al., 2006], our own unpublished results). Growth occurs at a slower timescale. Typically, a cell doubles its volume in 24h [Grandjean et al., 2004].** Therefore, as a simplification, we consider auxin concentrations and PIN localisation to be in equilibrium at the time scale used to model growth.

8. **Auxin is concentrated in the L1 and accesses the inner layers via primordia.** Because of the presence of **AUX/LAX** auxin importers, it has been proposed that auxin is concentrated in the L1 layer. It is mainly transported to the inner tissues via the pro-vascular strands in the primordia.

2.2.2.2 *Flux-based* polarization model

The model is essentially based on the *flux-based* polarization hypothesis derived from the *canalization* concept, introduced by Sachs Sachs [1969] who suggested that auxin transport is increased during the vascular induction by the auxin flux itself, leading to the canalization of the flux (for earlier mathematical formalizations see also Mitchison [1980a, 1981], Feugier et al. [2005], Rolland-Lagan and Prusinkiewicz [2005], Fujita and Mochizuki [2006]. The model is inspired by the original Mitchison model revisited by Rolland-Lagan and Prusinkiewicz [Mitchison, 1981, Rolland-Lagan and Prusinkiewicz, 2005].

Conservation law for the transport of auxin. We denote a_i $(mol.m^{-3})$ the concentration of auxin in a cell i and $p_{i,n}$ $(mol.m^{-2})$ the concentration of PIN proteins in the membrane facilitating transport from cell i to cell n. V_i (m^3) denotes cell volume and N_i denotes the set of neighbouring cells of cell i. If i and n are two neighbouring cells, then $S_{i,n}$ (m^2) denotes the exchange surface between these two cells. We assume that the auxin variation rate results from the combination of three processes i) diffusion ii) active transport of auxin by PIN and iii) local cell auxin synthesis and decay (see Auxin Hypotheses 1-4).

$$\begin{aligned} \frac{\partial a_i}{\partial t} &= -\frac{1}{V_i}\sum_{n\in N_i} S_{i,n}J^D_{i\to n} + \\ &\quad -\frac{1}{V_i}\sum_{n\in N_i} S_{i,n}J^A_{i\to n} + \alpha_a - \beta_a a_i, \end{aligned} \tag{2.5}$$

where $J^D_{i\to n}$, $J^A_{i\to n}$ are the fluxes of auxin $(mol.m^{-2}.s^{-1})$ due to diffusion from cell i to its neighbouring cell n, active transport from cell i to n respectively. By convention, out-going fluxes are positive, incoming fluxes are negative. α_a $(mol.m^{-3}.s^{-1})$ is a constant that describes the rate at which auxin is produced in cells and β_a (s^{-1}) defines the rate of auxin decay. Diffusion is modelled using Fick's First Law, $J^D_{i\to n} = \gamma_D\,(a_i - a_n)$ where γ_D is the constant of permeability reflecting the capability of auxin to move across the membrane $(m.s^{-1})$. In his original paper from 1981, Mitchison proposed to model

the flux due to active transport across a *membrane* between cells i and n as $J^A_{i\to n} = \gamma_A \left(a_i p_{i,n} - a_n p_{n,i}\right)$ where γ_A $(m^3.mol^{-1}.s^{-1})$ characterizes the transport efficiency of the PIN pumps. Hence the auxin variation rate in a cell i can be expressed as:

$$\begin{aligned}\frac{\partial a_i}{\partial t} &= -\frac{1}{V_i}\sum_{n\in N_i} S_{i.n}\gamma_D\left(a_i - a_n\right) + \\ &\quad -\frac{1}{V_i}\sum_{n\in N_i} S_{i.n}\gamma_A\left(a_i p_{i,n} - a_n p_{n,i}\right) + \\ &\quad +\alpha_a - \beta_a a_i. \end{aligned} \tag{2.6}$$

***Flux-based* polarization** According to Sachs' original concept, *canalization* relies on a feedback mechanism from the auxin fluxes on its transporters. More precisely, we assume that the concentration of PIN proteins $p_{i,n}$ in cell i transporting auxin to cell n changes due to i) insertion in the *membrane* induced by the flux ii) background insertion and removal of PIN from the *membrane*. The net flux of auxin that crosses *membrane* from cell i to cell n is $J_{i\to n} = J^D_{i\to n} + J^A_{i\to n}$.

$$\frac{\partial p_{i,n}}{\partial t} = \Phi(J_{i\to n}) + \alpha_p - \beta_p p_{i,n}, \tag{2.7}$$

where Φ defines the intensity of PIN insertion into the *membrane* due to the feedback of the auxin flux, α_p $(mol.m^{-2}.s^{-1})$ describes the rate of background PIN insertion into the *membrane*, and β_p (s^{-1}) the background removal rate from the *membrane*. Depending on the nature of the Φ function, different types of canalization regimes can be obtained (Feugier et al. [2005] and see below). In this paper we use two types of functions: a linear function $\Phi_L\left(J_{i\to n}\right) = \kappa(J_{i\to n}/J_{ref})$ and a quadratic function $\Phi_Q\left(J_{i\to n}\right) = \kappa\left(J_{i\to n}/J_{ref}\right)^2$, where κ $(mol.m^{-2}.s^{-1})$ is a constant parameter and J_{ref} $(mol.m^{-2}.s^{-1})$ is an arbitrary reference flux that makes it possible to keep constant units in the equation. For a negative net flux the Φ functions are truncated to 0, which means that no additional PIN is inserted in the *membranes* for which more auxin particles come in than particles come out.

2.2.2.3 SAM model

As mentioned above we suppose that auxin flows essentially in two separated conduits: the L1 layer and the sub-epidermal layers. The two systems meet at

the primordia cells. This very localised coupling between epidermal and sub-epidermal domains makes it possible to model the transport in each pathway independently and to account for their interaction at the sites of primordia only.

Epidermal model We represent the L1 layer by a set of polygonal cells forming a 2D surface. Similarly to other models of auxin transport at the SAM Smith et al. [2006b], Jönsson et al. [2006], the inter-cellular space was not modelled as a compartment of its own (however see Kramer and Bennett [2006]) and the contact between cells was abstracted as a single separation (referred to as *membrane*) allowing auxin molecules to flow between adjacent cells and PIN molecules to accumulate on either side. To model phyllotaxis we included certain topological and geometrical assumptions. We identify a particular point z as the meristem centre. Different zones of the meristem are defined relatively to this centre z. The centroid of each cell i is denoted by o_i. The central zone, $\mathcal{Z}$, is the set of cells whose centroids have a Euclidean distance to the meristem centre z less than or equal to the constant radius $R_{\mathcal{Z}}$. Similarly, a cell i belongs to the peripheral (or competence) zone $\mathcal{C}$ when the distance between its centroid o_i and the meristem centre z is less than or equal to $R_{\mathcal{C}}$ and greater than $R_{\mathcal{Z}}$. Cells i in the peripheral zone can be promoted to primordia cells (which is denoted by $i \in \mathcal{P}$).

Sub-epidermal model Second, to model the vascular pathways below the primordia, we designed a 2D model of a longitudinal section of the SAM where the connection between the epidermal and sub-epidermal layers could be explicitly represented. In the sub-epidermal layer, the definition of the zones $\mathcal{Z}$, $\mathcal{C}$, and of primordia cells $\mathcal{P}$ is analogous to that of the epidermal model. Cells are also represented as 2D planar polygons whose edges represent cell *membranes*.

Growth of the SAM To simulate meristem dynamics, we used a purely kinetic description of meristem growth Smith et al. [2006b]. We explicitly defined the velocity v of every point at the meristem surface in a reference frame attached to the meristem centre z. The velocity $v(x)$ of a point x at the meristem surface is assumed to be proportional to its distance to the meristem centre: $v(x) = \rho\,|x - z|$, thus simulating isotropic radial growth Douady and Couder [1996a]. The constant ρ defines the relative elementary growth rate in the radial direction [Nakielski and Hejnowicz, 2003]. Due to this global kinetic process, the vertices of each cell move toward the meristem periphery with a velocity growing exponentially. This makes the cells grow smoothly as they move away from the meristem centre. As soon as a cell surface exceeds a constant threshold

S_{max}, the cell divides by creating a new wall inside. The position of this wall is computed using a modification of the optimization criterion introduced by Nakielski [2000], *i.e.* finding a wall that both minimizes the distance between two opposite walls of the cell and that divides the cell into two polygons with the same surface. Then, similarly to Smith et al. [2006b], the cell vertices of newly created walls are slightly moved toward each other to provide a more realistic aspect. After a cell division event, the auxin concentration and PIN concentration in the *membranes* are inherited by the daughter cells from their parent. Primordium identity is inherited by randomly choosing one daughter of the primordium cell as the new primordium cell. The new *membrane* is initialized with α_p/β_p concentration of PIN on both sides. Finally, to keep a constant size of the overall simulation, a cell i that is too far away from the meristem centre z (its centroid o_i is at a distance greater than R_{sim}) is removed from the simulation.

In order to integrate in a single model the different processes involved in the system, *i.e.* auxin transport, cell growth, division, PIN allocation, and cell differentiation, we assume that these processes take place at different scales. Auxin transport is supposed to be much faster than growth and cell differentiation so that in the growing meristem, auxin concentrations are always at equilibrium.

2.2.2.4 Practical aspects of simulation

Numerical solving The non-linear system of equations describing the *flux-based* polarization model is integrated using the Scipy package designed for ODE solving Jones et al. [2001]. The integration algorithm uses the Adams predictor-corrector method in the non-stiff case Curtiss and Hirschfelder [1952]. Solver iterations are performed until a stable state is obtained, *i.e.* until change in auxin concentration becomes less than a predefined threshold value ϵ_{min} in every cell.

Boundary and initial conditions The boundary conditions for every simulation are specified in the supplementary material. In most simulations boundary cells do not receive any auxin flux from the outside and we assume fixed, null concentration in sinks. In all simulations we assume that the initial auxin concentrations are null and PIN concentration on both sides of the *membrane* are initiated with a basic amount of PIN α_p/β_p.

Visualisation and simulation environment The visualization of tissue simulations was carried out with PlantGL, an open-source graphic toolkit for

the creation, simulation and analysis of 3D virtual plants [Pradal et al., 2007] available in the OpenAlea software platform for plant modelling [Pradal et al., 2008].

General convention for figures In all figures representing 1D or 2D tissues, we adopted the following graphical conventions: the absence of auxin in a cell is represented by black while the highest concentration is shown in bright green. Intermediate concentrations are represented by interpolations between these two extremes (see supplementary materials). PIN transporters at the *membrane* of a cell i are represented as a red line. The thickness of this line is proportional to the amount of PIN.

Supplementary materials For every figure showing a dynamic system, we provide a corresponding movie to capture system dynamics. Movies are available as supplementary materials and named after the figures. Supplementary text is provided, specifying equations, parameters, boundary and initial conditions and display specific conventions.

2.2.3 Results

The study of systems controlled by *flux-based* polarization is not straightforward as the process relies on a feedback loop between auxin concentrations and auxin fluxes in tissues. To address this problem, we first defined different remarkable properties of the *flux-based* polarization that are essential in the generation of patterns. These properties are illustrated on simplified 1D or 2D "virtual tissues". The sensitivity of the model for different parameters was tested. As expected, the system was more dependent on certain parameter values, but overall the results were robust (see supplementary materials). Based on this analysis, we then investigated the ability of *flux-based* polarization to produce phyllotactic patterns at the SAM in a way that is consistent with the current biological knowledge and observations.

***Flux-based* polarization amplifies fluxes** The *flux-based* hypothesis, proposes that any small flux between two cells in the system will reinforce itself by increasing the local amount of PIN, thus initiating a positive feedback loop. Initial fluxes may typically be generated by diffusion between zones with different concentrations. We illustrated this phenomenon on a 1-dimensional tissue with two perfect auxin sinks at both extremities (Figure 2.7A). Auxin is produced in every cell except the sink cells. Initially, the highest flux appears close to

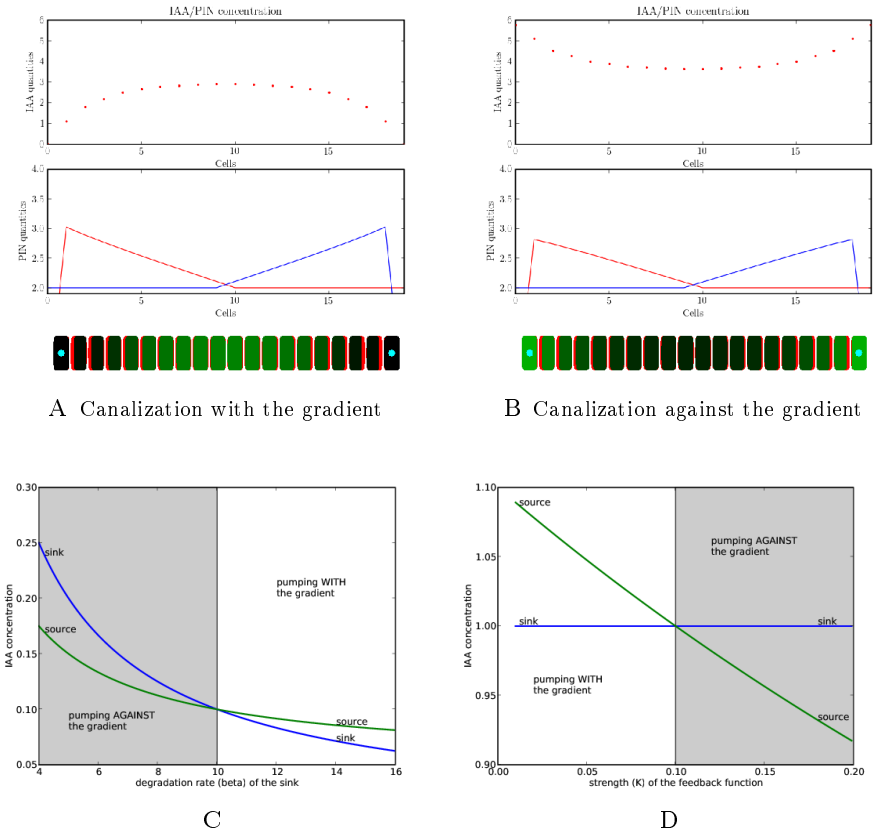

A Canalization with the gradient

B Canalization against the gradient

C

D

Figure 2.7: Canalization in a 1-dimensional cellular system.
Figures 2.7A-2.7B show the system consists of 20 linearly aligned cells. Boundary cells are acting as sinks, hence they evacuate or degrade auxin. At the start of the simulation the cells do not contain auxin. Then the simulation runs until a stable state emerges. On the two first plots (2.7A and 2.7B) the blue and red lines correspond to PIN concentrations at the right and left side of the *membranes* respectively. The two systems differ only by the way auxin is removed: in 2.7A we assume that the removal in the sink cells is very efficient whereas in 2.7B the removal efficiency is limited. This difference leads us to two different stationary patterns in which the auxin gradients are opposite and the sink cells are minima of auxin 2.7A or maxima 2.7B. Figures 2.7C and 2.7D present a further analysis of the conditions leading to pumping against or with the gradient. For this purpose a system of two cells sharing one *membrane* was analysed. Figure 2.7C presents the concentrations of auxin in the two cells in the stable state as a function of the degradation rate β of the sink. The green curve corresponds to auxin concentrations in the source cell, the blue curve corresponds to auxin concentrations in the sink cell. In the grey region, pumping is carried out against the auxin gradient, while in the white region, pumping follows the gradient. Figure 2.7D shows similar curves for the variation of the feedback strength κ of flux on PIN synthesis.

the sink cells, due to diffusion. This small initial flux is subsequently reinforced by a polar allocation of PIN transporters favouring the evacuation of auxin in the direction initiated by the original flux. If the auxin sink is maintained, the auxin flux reaches a stable state with the maximum concentration of auxin appearing at the maximal distance from both sinks (Figure 2.7A). Figure 2.7A shows that the concentration of PIN at each cell *membrane* linearly increases from the location of the auxin maximum up to the sinks. This is because each cell is producing auxin at a constant rate α_a and in the stationary state the amount of removed auxin must be balanced by auxin synthesis (if we neglect auxin degradation). It implies that the auxin flux should grow linearly in the direction of the closest sink. If the feedback function Φ is linear, this results in a linearly increasing allocation of PINs to the cell *membranes* in the direction of the closest sink.

Flux-based polarization allows auxin to flow with or against auxin gradients Although the molecular mechanism underlying PIN polarization is still unknown, PIN proteins can polarize either *with* or *against* the gradient of auxin Heisler et al. [2006], Scarpella et al. [2006], Vieten et al. [2007]. If a unique transport mechanism is operating in the plant it should thus be able to reproduce this property. In the previous example, auxin fluxes were amplified from regions of high concentration of auxin to regions of low concentration (Figure 2.7A). Auxin thus flowed *with* the auxin gradient.

To show that *flux-based* polarization can also lead to flow against the gradient, we modified the above 1-dimensional model by weakening the sinks in such a way that they were only able to degrade auxin at a finite constant rate. This simple modification produces a drastic change in the system's behaviour. The auxin gradient is now reversed in the stable state, with highest concentrations at the sink locations and lowest in the places *maximizing* the distance to all sinks (Figure 2.7B).

To study the conditions for either pumping *with* or *against* the gradient, we considered a system of two cells sharing a *membrane*. One cell is a source of auxin while the other acts as a sink destroying auxin at a constant rate. Once this system reaches a stable state, the net flux across the *membranes* separating the two cells is exactly equal to the rate at which the source creates auxin and leads to a polarization of PIN from the source to the sink. Depending on the model parameters, the system can reach different levels of concentration in both cells. Two regimes may be obtained as shown by the graphs (Figures 2.7C and 2.7D). The transition between both regimes, pumping *with* or *against* the gradient, can be obtained by varying different parameters of the model such as

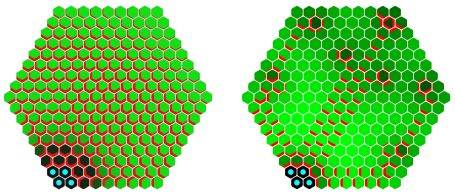

Figure 2.8: Weak and strong regimes on 2D hexagonal lattices. The sink cells are tagged with blue dots. Figure 2.2.3 shows the stable state in case of a weak regime. At the end of the simulation the auxin concentration is progressively increasing with the distance from the sink. PIN, marked in red, is present in all cells leading to a laminar flow over the entire surface. Figure 2.2.3 shows the stable state of a strong regime with one sink leading to the formation of canals (where PIN is present) and patches of cells without transporter. This system corresponds to the original *canalization* concept.

the feedback strength and the degradation rate (Figure 2.7).

***Flux-based* polarization has two different regimes (*weak* and *strong*)** Initially, the *flux-based* polarization hypothesis was introduced to model the formation of vascular canals in stem and leaf tissues, as an integral part of the *canalization* concept Mitchison [1980a, 1981], Feugier et al. [2005], Runions et al. [2005], Fujita and Mochizuki [2006]. Using this mechanism in the meristem may seem in contradiction with the absence of canals at the meristem surface. Feugier et al. Feugier et al. [2005] demonstrated that a *fluxed-based* polarization mechanism where the feedback function Φ was linear did not result in the formation of canals in a tissue. We further confirmed this by comparing the behaviour of auxin transporters in a 2D sheet of cells showing weak or strong feedback. When the feedback function Φ is non-accelerating (increasing linearly or less rapidly than linearly) the process creates laminar flows transported by homogeneous arrangement of PINs and converging to the sink (Figure 2.2.3). We refer to such a system as a *weak* regime. Conversely, when the feedback function Φ is *accelerating* (increasing more rapidly than linearly), canals appear, creating branching structures in the 2D tissue (Figure 2.2.3). We will call such a system a *strong* regime. In both cases, fluxes may be oriented with or against the gradient, depending on the model parameters and boundary conditions.

The *weak* regime can produce fields of lateral inhibition of varying intensities As explained earlier, the most widely accepted theory of phyllotaxy relies on the formation of inhibitory fields around each primordium. Recent models propose that these fields are in fact zones where auxin is depleted [Snow

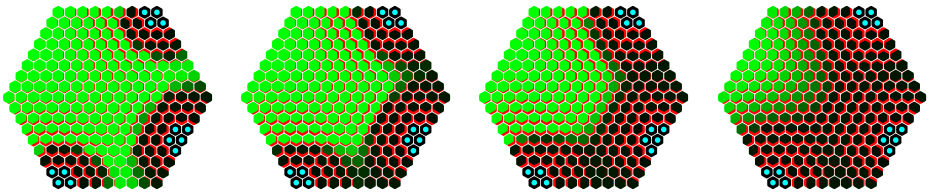

Figure 2.9: Inhibitory fields induced by a *flux-based* polarization system. The size of the field changes according to the value of parameter κ which regulates the feedback of fluxes on PIN pumps synthesis.

and Snow, 1962, Douady and Couder, 1996a, Smith et al., 2006a]. To show that *flux-based* polarization can indeed be considered as a plausible mechanism, we demonstrate that it can generate such inhibitory fields with varying intensities.

A *weak* regime (as in Figure 2.2.3) leads to the formation of a zone around the sink where auxin is depleted. The intensity of the auxin depletion fields around sinks can be changed by tuning the parameter κ that controls the feedback level of auxin fluxes on PIN insertion in the *membranes*. Figure 2.9 shows the extent of inhibitory fields (in black) around the blue sinks for increasing values of parameter κ. PIN is regularly distributed throughout the tissue, with a polarity that is determined by the relative distance of the cell to the different sinks. The weak regime thus makes it possible to vary the auxin depletion level around sinks. It therefore provides a plausible explanation for the formation of inhibitory fields during organ initiation at the SAM.

***Flux-based* polarization as a source of patterning in a growing structure** The mechanism that controls PIN orientation in cells takes place in a growing structure. Therefore we constructed a dynamic model with dividing and growing cells. As before, we assume that all cells create auxin except for a limited number of cells marked as sinks in which auxin concentration is fixed at 0. To produce phyllotactic patterns, the combination of *flux-based* polarization hypothesis and tissue growth should therefore show a recurrent, temporal patterning property. We show this property in a simplified 1D model by introducing a sink creation threshold, *i.e.* an auxin concentration at which a new auxin sink is created. In a growing system, neighbouring auxin sinks are pushed apart. Due to the weakening of the sink influence and the constant local hormone production the level of auxin increases in the zone between these two sinks. At a particular auxin threshold (the sink initiation threshold ω), the amount of hormone is sufficient to initiate a new sink at the location which is the farthest from the two sinks, Figures 2.10A-2.10B. As a result of sink cre-

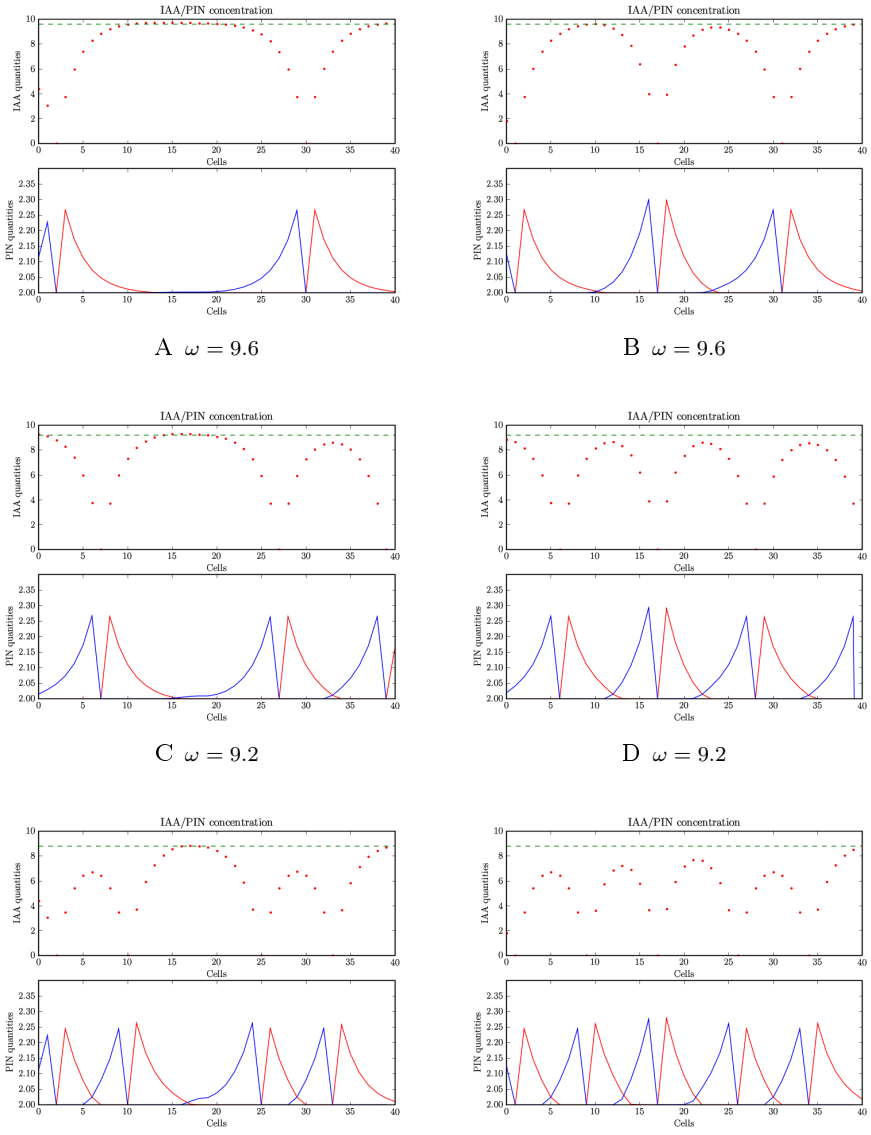

A $\omega = 9.6$ B $\omega = 9.6$

C $\omega = 9.2$ D $\omega = 9.2$

E $\omega = 8.8$ F $\omega = 8.8$

Figure 2.10: Dynamic patterning with *flux-based* polarization. Figures 2.10A-2.10B, 2.10C-2.10D and 2.10E-2.10F present three simulations with different thresholds ω for primordium initiation. Figures 2.10A, 2.10C, 2.10E present the step just before primordium initiation and Figures 2.10B, 2.10D, 2.10F present the step just after primordium initiation. The frequency of primordium initiation increases with a decrease of the initiation threshold ω.

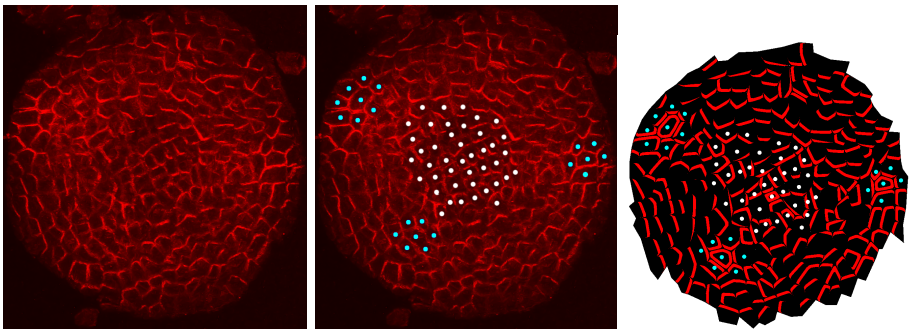

A B C

Figure 2.11: SAM digitalization.
Figure 2.11A shows the PIN distribution in a real meristem obtained using immunolabelling (top view). Figure 2.11B shows the same image with marked primordia cells (blue dots) and central zone cells (white dots). Figure 2.11C shows the reproduction of PIN distribution and polarity in a digitized version of the same image.

ation, some of the PIN pumps reverse toward the new sink, with PIN and auxin patterns similar to that of the previous sinks. By changing the sink initiation threshold ω, it is possible to augment or to decrease the initiation frequency, Figures 2.10C-2.10D and 2.10E-2.10F. In the supplementary materials we show in details how the initiation frequency depends on different model parameters.

***Flux-based* polarization model can reproduce observed PIN maps and realistic influence zones** In Barbier et al. (2006), we showed that the distribution of PIN at the SAM (called "PIN map") has a number of specific features [Barbier de Reuille et al., 2006]. As illustrated in Figure 2.11, PIN labelled membranes are pointing towards their nearest primordium (blue dots in Figures 2.11B-2.11C). In addition, a significant number of cells appear to transport auxin to the meristem summit. A plausible model of phyllotaxy should be able to reproduce similar distributions of PIN.

To determine to what extent the *flux-based* polarization model could reproduce realistic PIN maps, we digitized the cell walls on the images of real meristems, immunolabelled to visualize PIN. We recorded the PIN orientation in each cell as described in Barbier de Reuille et al. [2006] (called *real PIN maps* as in Figure 2.11C). The position of each primordium could be clearly identified as indicated by the convergence of PIN toward particular cells and the presence of vascular strands below these primordia seen on other sections of the same meristem (blue dots in Figure 2.11B, longitudinal image data not shown). We also designated a central zone of about 6 cells in diameter at the meristem summit. This zone

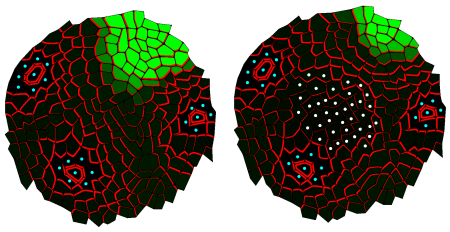

A B

Figure 2.12: Simulation of auxin transport in a digitized meristem based on the *flux-based* polarization hypothesis.
The cells and primordia of the real meristem shown in Figure 2.11 were used to initialize the system, and the virtual PIN maps were then calculated based on the *flux-based* polarization hypothesis. Green intensity is proportional to the virtual auxin concentration. Figure 2.12A shows a simulation where the centre plays no special role in the auxin flux. Figure 2.12B shows a simulation where the centre degrades auxin.

is usually free of primordia in the wild type *Arabidopsis* SAM.

We then simulated the emerging arrangement of PIN distributions according to the *flux-based* polarization hypothesis on the digitized maps. Primordia were considered as perfect sinks while all other cells in the meristem were assumed to produce auxin at a fixed rate according to Equation 2.6. The resulting PIN distributions are shown in Figure 2.12. Close to the primordia, the simulated PIN arrangements are converging towards the sink cell and look similar to the PIN arrangements on the real PIN maps (Figure 2.11A). Besides, auxin accumulates at the position where one would expect the next initium in a spiral phyllotaxy (Figure 2.12A). However, contrary to real PIN maps, virtual PIN patterns did not show any significant converging tendency towards the centre of the meristem. To overcome this discrepancy, we made a second simulation, where the cells in the meristem centre were assumed to degrade auxin at a higher rate. While the convergence of PIN toward the primordia cells is preserved, an additional convergence of PIN toward the centre is now observed, reflecting more faithfully the observed distributions of PIN in the immunolabelling images (compare Figures 2.11c and 2.12b). The same result were obtained by reducing the synthesis of auxin in the central zone of the meristem (result not shown).

To go beyond a simple visual inspection for similarity, we computed the so-called *influence zones* of the primordia and of the central zone in the real meristem and compared them to those in the simulated meristems. The influence zone of a region (i.e. a cluster of cells) is the set of meristem cells that are connected to a cell of the considered region through a path of PIN arcs oriented in the direction of this region. Figure 2.13 shows the influence zones of different regions (centre

and primordia) on real (Figures 2.13A-2.13D) and simulated (Figures 2.13E-2.13L) PIN maps. In real maps, pumps are distributed in such a way that auxin can reach the central zone from all the directions between each pair of primordia (with a small auxin pathway between primordia P_0 and P_2, a larger one between primordia P_0 and P_1 and the largest pathway between P_1 and P_2). Influence zones of the primordia are restricted to the neighbourhood of each primordium and do not extensively overlap with the cells of the central zone. We then computed the influence zones from the first simulation where the central zone did not act as a sink. This showed important differences with the real maps. For the central zone , only two auxin pathways of equivalent width could be observed while the pathway between P_0 and P_2 had disappeared (Figure 2.13E). In addition, the influence zone of P_0 largely crossed the meristem centre in 2.13F in contrast to what was observed on the real map. The influence zones of the simulations with auxin depletion in the centre showed better agreement with the influence zones computed from real PIN maps: with three auxin pathways of gradually increasing width going to the meristem centre and the influence zones of primordia being almost non-overlapping with cells in the central zone (Figures 2.13I-2.13L).

Formation of phyllotactic patterns and pro-vascular strands Based on the preceding results, we designed a dynamic model of phyllotaxy using the *flux-based* polarization hypothesis. The epidermal and sub-epidermal layers were assumed to be relatively independent, except at the primordia were the two interact by exchanging auxin. This assumption was based on the generally accepted hypothesis that auxin is accumulated in the L1 layer due to the presence of influx carriers of the AUX/LAX family on the cell membranes [Reinhardt et al., 2003]. This made it possible to simulate auxin transport at the surface and in internal layers separately and to summarize their interactions as boundary conditions. Since in the L1 layer no channels of auxin transport are observed, we supposed that the weak regime prevailed at the surface. For vein formation in inner tissues, we supposed that a strong regime was active.

The simulations using the model characteristics described above resulted in a dynamic pattern of auxin distribution and primordium formation. The following general scenario was observed. In the L1 layer, each primordium evacuates auxin by its pro-vascular system to the inner parts of the meristem. In the L1, the primordium can thus be considered as a sink depleting auxin in its immediate neighbourhood. This in turn inhibits the formation of new primordia close to the existing ones (Figure 2.14A). Due to cell growth, primordia progressively move away from each other, which allows the accumulation of auxin in cells

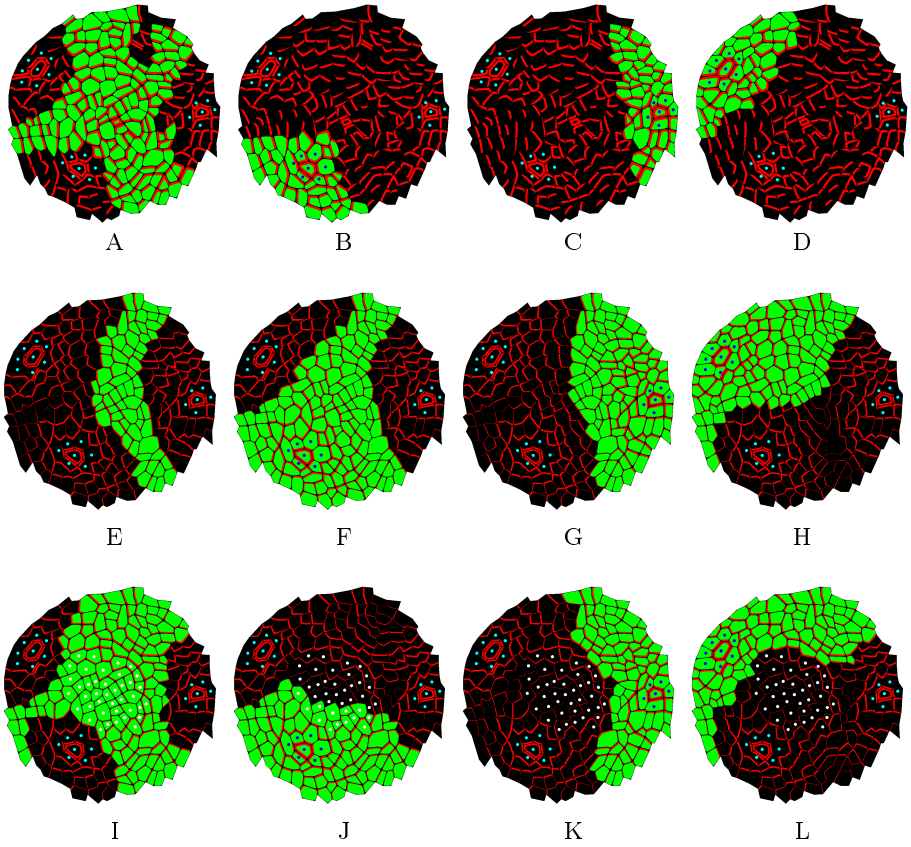

Figure 2.13: Influence zone analysis.
The influence zones calculated for the central zone (first column), P_0 (second column), P_1 (third column), P_2 (fourth column) in real and simulated maps. Figures 2.13A-2.13D show the influence zones in a real map. Figures 2.13E-2.13H show the influence zones in digitized maps where PIN labelling was calculated based on the *flux-based* hypothesis. In this simulation, cells in the central zone are identical to other cells. Primordia (blue cells) are perfect sinks. Figures 2.13I-2.13L shows a simulation based on the *flux-based* polarization hypothesis, but here both primordia and cells in the central zone (white cells) are removing auxin. Note that qualitatively the last simulation shows a better match with the original real map.

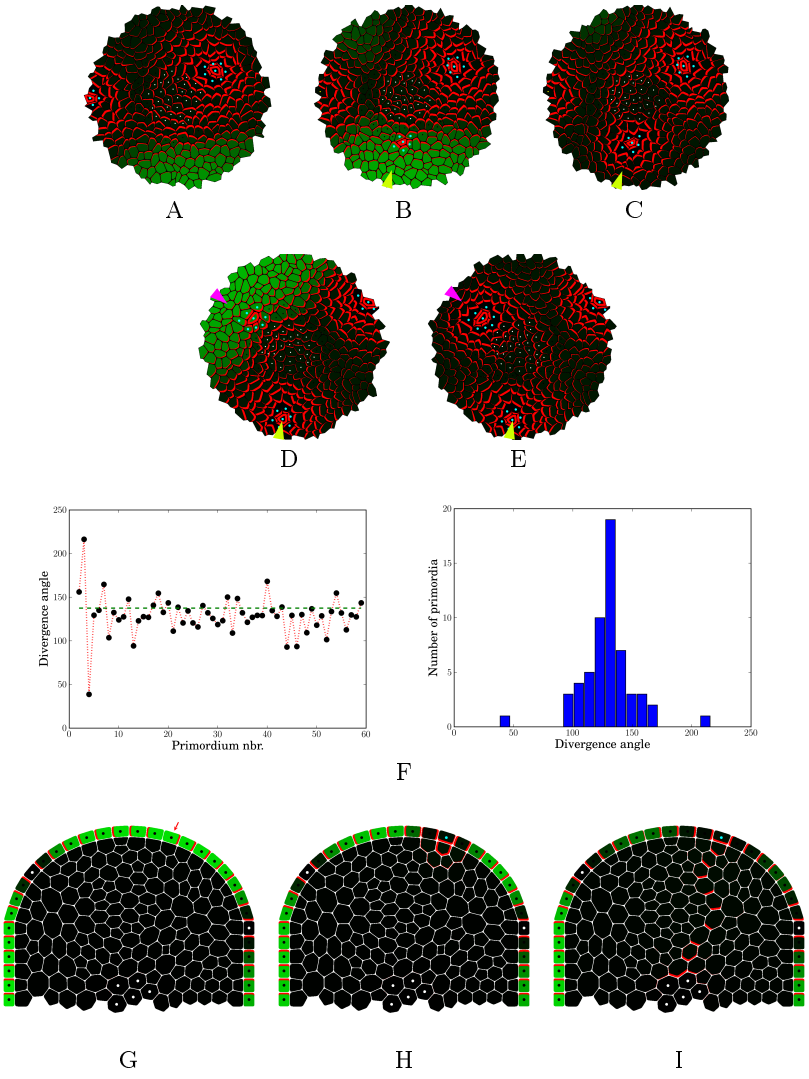

Figure 2.14: Dynamic models.
Figures 2.14A-2.14E, 2D top view of a virtual meristem following the *flux-based* model showing the dynamics of PIN distribution, auxin concentrations and primordia initiation. The sequence shows the initiation of two consecutive primordia (arrowheads). The sequence starts with auxin accumulation in the zone that is the farthest away from the existing primordia. When a threshold is reached, the maximum acquires primordium identity and becomes a sink. Figure 2.14F shows the variation of the angles between 65 consecutive primordia. Note that the mean value is close to the golden angle (137°5) typical for spiralled phyllotaxis as observed in Arabidopsis. Figures 2.14G-2.14I, 2D transversal cut of a virtual meristem following the flux-based model showing the dynamics of PIN distribution, leading to the formation of a pro-vascular strand of cells that transport auxin downwards. Detailed description in the text.

sufficiently distant from these young organs. As a result a new maximum of auxin concentration gradually appears in the region maximally separated from all primordia, thus defining the location of the next initium (Figure 2.14G). As soon as the auxin concentration exceeds a predefined threshold in a cell belonging to the competent zone surrounding the central zone, this cell and its immediate neighbours acquire primordium identity (Figure 2.14B). This implies that auxin can leak at the initium location into the inner layers, which triggers the creation of the primordium vascular strand (Figure 2.14H). The vein being formed below the initium drains the auxin out from the L1 layer and converts the initium into an auxin minimum (Figures 2.14C, 2.14H). The flux induced by this process reverses pump polarizations in the direction of the initium in the L1 (Figures 2.14C, 2.14I). Then, due to tissue growth, new space becomes available allowing the system to generate a new initium. (Figures 2.14D-2.14E). This system is able to produce a stable phyllotactic pattern, with a mean angle close to the golden angle, 137°5 (Figure 2.14F) observed in Arabidopsis and characteristic for spiralled phyllotaxis.

An obvious simplification in this model is the assumption that an instant drop in the auxin concentration occurs when cells of L1 acquire primordium identity. However, modifying the rate at which the auxin concentration changes at the initium showed that an immediate drop gives qualitatively the same patterns as a gradual reduction over time (simulation not included). Since this would add another parameter to the model we kept this simplification.

2.2.4 Discussion

We show here that *flux-based* model provides a realistic explanation for phyllotaxis, predicting patterns of PIN distribution that are very similar to the observed ones. The model leads to a classical inhibitory field scenario where the very young primordia pumps auxin towards the inner tissues, draining the hormone away from their immediate vicinity. As long as these sinks are close to the competence zone, no new primordia can be formed. However, as growth drives the sinks away, auxin concentration can build up again locally because of synthesis and transport, creating a new auxin maximum. The model proposes that the import capacity of the L1 layer at the surface is overridden when a certain auxin concentration threshold is reached after which the hormone starts to leak away to inner tissues. This initial diffusion-driven flux will be reinforced by *flux-based* polarization. This in turn will rapidly create an auxin transport channel connecting the local surface maximum to the inner vasculature and transforming it into a sink. The main requirement here is that *flux-based* polar-

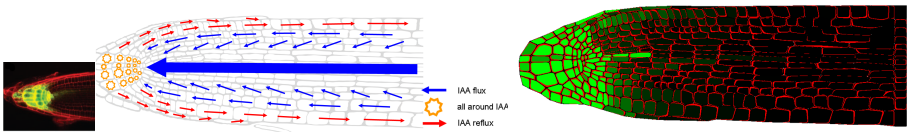

A B C

Figure 2.15: *Flux-based* polarization model of the root meristem. *Flux-based* polarization hypothesis is compatible with the maintenance of an auxin maximum and with the general organisation of PIN at the root tip. Figure 2.15A shows the existence of a stable auxin maximum at the root tip as evidenced by the DR5:GFP marker [Okada et al., 1991, Grieneisen et al., 2007]. At the shoot apex, the general organisation of the different PIN transporters in the different tissues suggests a flux going downward via the vascular tissues and than spreading out over superficial layers "like a fountain" (Figure 2.15B). Figure 2.15C shows a digitized root apex based on a real optical section from an *Arabidopsis* root (not shown, image taken by Tom Beeckman). Similarly to PIN maps at the shoot apex, the polarity of PIN was recorded in each cell. This PIN map was used as an initial condition for the simulation. The cellular system was provided with a fixed global quantity of auxin initially divided equally over the tissue. In addition, two border cells of the epidermis were chosen as auxin sinks, to comply with the biological assumption that a fraction of auxin is evacuated from the root tip along the epidermis [Swarup et al., 2005]. Auxin arriving in these sink cells is completely depleted at each simulation step. In addition, a permanent auxin source was added on the border of the central vascular system providing auxin in a constant fashion, in accordance to biological auxin source localisation in the vascular bundle. Simulations revealed that transporter dynamics based on *flux-based* polarization are sufficient to enable and maintain auxin accumulation in the collumella and quiescent centre Figure 2.15C, as observed in Figure 2.15A. Additionally, realistic transporter distribution profile was maintained by the *flux-based* polarization mechanism.

ization should be relatively weak at the surface, switching to a strong regime in inwards directed fluxes. This switch from one regime to the other could directly depend on the amount of auxin flowing through the cell, but it could also be activated indirectly as part of the differentiation process induced by high auxin concentrations. In such a scenario even a small leakage from the surface to the inner parts would be very rapidly amplified.

***Flux-based* polarization hypothesis as a unifying concept** *Flux-based* polarization provides an alternative explanation for phyllotaxis. Indeed, since it allows for transport with and against gradients, it also provides a plausible explanation for the stable auxin maxima observed in roots and leaves. This is illustrated in Figure 2.15 where we have reproduced PIN and auxin distributions in the root meristem using the flux based hypothesis. An important caveat is that two different regimes are required in the model. As shown previ-

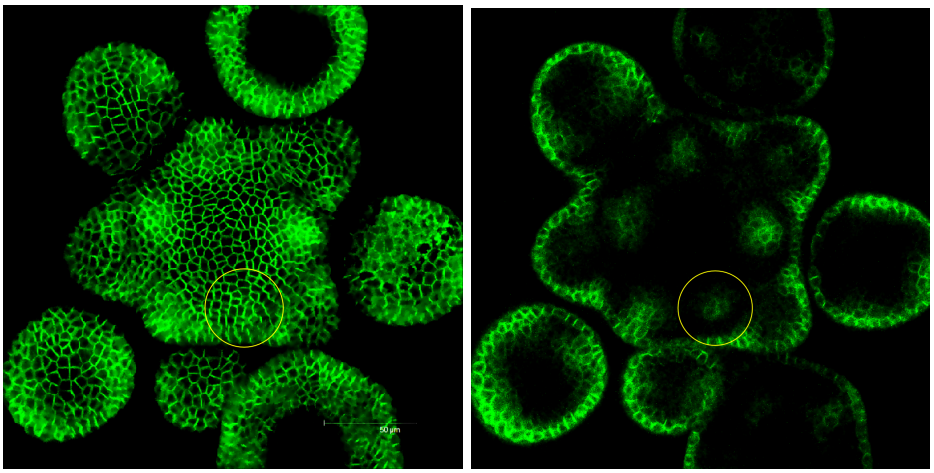

A B

Figure 2.16: Confocal image of a living meristem expressing a fluorescent version of PIN (PIN1:GFP, a generous gift of J. Friml).
Figure 2.16A shows the higher expression of PIN at the surface around new primordia is clearly observed. The yellow circle indicates the site where the next organ will be initiated. The images show no very obvious reorientation of PIN orientation at this site, although a pro-vascular strand expressing PIN is clearly observed at this site (yellow circle on the individual section of the same meristem in (2.16B).

ously by Feugier et al., only the weak regime can explain the absence of canals as observed at the meristem surface [Feugier et al., 2005]. In this context it is important to note that the weak regime has some characteristics in common with diffusion. In particular, both processes can lead to auxin transport down the gradient. However, as auxin cannot freely diffuse between the cells, the weak regime is fundamentally different and can only function if the cell is able to sense fluxes. As long as the precise mechanism of PIN localisation is not known, it will be difficult to predict whether each regime would require a completely different cellular mechanism which would go against the idea of a unifying concept. However, it seems reasonable to propose that both regimes correspond to different states of the same flux sensing mechanism. We therefore conclude that the *flux-based* hypothesis remains a potential unifying mechanism for auxin transport throughout the plant.

Confronting the *flux-based* polarization hypotheses with experimental results Having established that the *flux-based* polarization model can reproduce phyllotactic patterns, it now becomes important to test the hypothesis as rigorously as possible. We have made a first step towards this procedure by

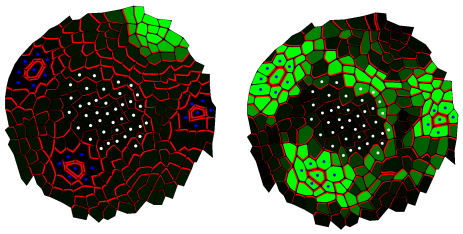

A B

Figure 2.17: The simulation 2.12b showing the predicted levels of auxin concentration (2.17A) and flux intensity (2.17B).
Note the sharp peaks observed in (2.17B), comparable to DR5rev:GFP peaks observed in vivo [Barbier de Reuille et al., 2006].

comparing the predicted PIN protein patterns with the observed ones. While this in itself is a stringent test, so far not performed on other models, the *flux-based* model should also be coherent with other existing data. In the following paragraphs we will discuss a number of its implications.

Auxin concentrations at the L1 layer Like the *concentration-based* model, the *flux-based* model requires that the patterning process mainly occurs in the L1 layer. This is based on the idea that auxin is concentrated there by auxin importers (AUX1 and LAX proteins) that are strongly expressed in the L1. In addition, the highly organised distribution of PIN at the meristem surface also indicates that the patterning process mainly occurs in the L1 layer. This might seem contradictory with the phenotypes of mutants where the auxin importers are impaired and which are still able to generate primordia. It should be noted, however, that other factors such as the human multiple drug resistance/P-glycoproteins (MDR/PGPs) are also involved in auxin influx [Blakeslee et al., 2007] and could guarantee the presence of sufficiently high levels of auxin in the L1 layer when the AUX/LAX proteins are inactivated. We therefore conclude that overall our model is in line with the experimental data supporting a major role of the meristem surface in phyllotaxis.

Auxin and the central zone An intriguing aspect of our model concerns the central zone (CZ) cells. Like the *concentration-based* model, the *flux-based* model does not require any particular property of this zone, other than a lack of competence to generate a primordium. We could, however, only obtain realistic patterns of PIN distribution when we attributed a sink function to this zone. This is in line with earlier observations by Barbier et al. (2006) who provided evidence that the CZ receives auxin fluxes [Barbier de Reuille et al., 2006].

However, the sink function of the CZ required by the *flux-based* model seems in contradiction with the same study showing the presence of relatively high auxin levels there. It is therefore important to note that in the *flux-based* model the concentration in the CZ is not much lower than in the other peripheral zone cells, and is certainly significantly higher than in the primordium cells. Therefore on average the model would predict higher concentrations in the CZ than in the periphery as reported by Barbier et al. (2006)). As a result there does not appear to be any conflict between earlier observations and the *flux-based* hypothesis.

Auxin concentrations and PIN dynamics The primordia in the *flux-based* model could be maxima or minima of auxin concentration with pumps oriented towards them. If they are maxima, however, auxin concentration in the meristem would decrease slowly from the maximum value (at the primordia location) to lower values as we get further away from the primordia. In this context, the point that is the furthest from all of the primordia in the competence zone would be a minimum of auxin concentration, therefore new initium could not be formed there. It is thus a requirement of the *flux-based* model that the primordia are rapidly transformed into minima of auxin concentration to obtain phyllotactic patterns.

The *flux-based* model scenario proposes that a relatively broad auxin peak leads to an inward flow which rapidly leads to the formation of an auxin minimum. It is the formation of this minimum that will reorient the PIN transporters in surrounding cells. This scenario seems in contradiction with earlier observations suggesting that (i) the reorientation of PIN transporters precedes the initiation of the young organ and (ii) that an auxin maximum is maintained at the young primordium. There are several explanation for these apparent contradictions.

First, it has not been unambiguously established that the PIN transporters orient before the initiation of the inward flux marked by the formation of the pro-vascular strand. Heisler et al. [2005] showed that there is some reorganisation of PINs before this strand is formed but did not report clear converging transporters. In accordance with this, we have observed the presence of PIN in the internal tissues at a moment where the transporters were not clearly converging (Figure 2.16). We therefore conclude that the precise timing has not been sufficiently well established to draw clear conclusions.

Second, the supposed stable auxin maximum at the young initium has been revealed using the so-called DR5rev promoter driving the green fluorescent protein (GFP). This promoter contains an auxin responsive element and is activated by

auxin responsive transcription factors. While it is often presented as a quantitative auxin sensor, it is in fact only a very indirect marker which not only depends on the amount of hormone but also on the capacity of cells to react to it. In addition the fluorescent GFP marker can be stable for prolonged periods, and could therefore mask rapid changes in the activity of the promoter. It is therefore possible that the precise fluctuations in auxin concentrations at the primordium have not been unambiguously established. In addition, DR5rev might not only mark high auxin concentrations but could also be activated by other factors or even by high auxin fluxes. Indeed, in principle high fluxes could, in terms of the number of particles reaching the nuclear receptor, be equivalent to high concentrations. Interestingly, our simulations show that a *flux-based* activation of DR5rev would give sharp maxima, very comparable to what is observed in vivo (Figure 2.17).

General conclusion In this study we have shown that the *flux-based* polarization model is a plausible alternative to the existing *concentration-based* model for phyllotaxis. Fortunately, both models make different predictions regarding the sequence of events, the maintenance of auxin maxima or the presence of auxin sinks at particular sites. In particular, the *flux-based* polarization model requires the rapid conversion of an auxin maximum into a minimum. Further experimentation should therefore make it possible to distinguish between the two models. A careful and quantified description of cell behaviour (e.g. PIN distribution) should be part of this approach. We are further testing this by using transgenic approaches aimed at modifying the capacity of these cells to transport auxin or by changing the auxin content in the same cells. A major scientific question concerns the actual mechanism involved in auxin transport. Indeed a better insight into the process might also help to validate one or the other polarization hypothesis. It is important to note, that both the *flux-based* and *concentration- based* models are obvious abstractions of reality. They both do not, for instance, take into account inter-cellular spaces nor do they indicate how auxin fluxes or auxin concentration gradients are sensed. A process like the *flux-based* polarization mechanism described here could, therefore, be much more complex than just PIN proteins sensing auxin particles flowing through the cell. What is important here is that the overall behaviour of the system can be described accurately by flux-based polarization model with predicted, testable properties.

Acknowledgements

The authors thank Olivier Hamant, Teva Vernoux, Laurent Laplaze, Pradeep Das as well as the reviewers for their fruitful comments on the initial version of the manuscript. Figure 2.16 was provided by Isabelle Courseau. This study was funded by the EU RTN SY-STEM project and the ANR Virtual Carpel project.

2.2.5 Supplementary materials

2.2.5.1 Simulation overview

Conventions

Notations: In the equations describing changes in PIN and auxin concentrations we use the Iverson notation Iverson [1962], Knuth [1992]: if ψ denotes a logic statement then,

$$[\psi] = \begin{cases} 1 & \text{if } \psi \text{ is True} \\ 0 & \text{otherwise} \end{cases}$$

Supplementary movies: For each figure demonstrating a system changing in time, a movie showing the process dynamics is provided. These movies are named after the Figures with supplementary letter "S" at the beginning (e.g. the movie corresponding to Figure 2B is called "`VideoS2B.avi`").

PIN display conventions: The thickness of the line representing the PIN accumulation at a cell membrane is proportional to the computed PIN concentration at this membrane. However, high values are truncated to allow better inspection of visual results. The minimal displayed value of PIN concentration is always equal to α_p/β_p, whereas the higher value corresponds to the maximum displayed concentration of PIN, which is $2\alpha_p/\beta_p$. All values of PIN exceeding this value are capped to $2\alpha_p/\beta_p$, allowing a ratio of 200% between extreme values.

Auxin display conventions: Auxin concentrations below minimal (resp. above maximal) threshold a_{min} (resp. a_{max}) are depicted in black $RGB(0,0,0)$ (resp. in green $RGB(0,255,0)$). Intermediate values of auxin concentrations are depicted with a double linear interpolation function: a percentage p_{mid} of the visible auxin range $[a_{max}, a_{min}]$ defines the auxin concentration a_m for which the colour should be intermediate $RGB(0,127,0)$. Colours are then linearly interpolated between a_{min} and a_m and a_m and a_{max} respectively to render the colour of any auxin concentration within the interval $[a_{max}, a_{min}]$. Values for parameters p_{mid}, a_{max}, a_{min} are defined for each simulation in table 2.1.

Integration: The number of snapshots was specified for each simulation, as well as fixed step h which describes the time between each two consecutive timepoints used for integration. For each simulation a number of steps is also given.

This number is used to integrate the system with a given h between taking a snapshot. For some simulations the number of steps may vary if the objective is to obtain a quasi stable state between the snapshots (e.g.. simulation of phyllotaxis). A stable state is reached when the change in IAA concentrations in every cell becomes less than a predefined threshold value ϵ_{min} (using L_∞ norm). In such a case the time interval between each snapshot may be different. If it is the case it is specified in the simulation details.

At each step a non-linear system of equations describing the flux-based polarization process is integrated using the SciPy package designed for ODE solving Jones et al. [2001]. This package wraps ODE PACK, which is a collection of Fortran solvers for the initial value problem for Ordinary Differential Equation systems Hindmarsh [1983]. This solver allowed us to specify the precision on given integration interval (the step size is then adjusted automatically by solving algorithm).

2.2.5.2 Sensitivity analysis of the 1D flux-based polarization model

To test the sensitivity of the model results to variations of the model parameters, we made a sensitivity analysis on the 1D dynamic models of the type presented in Figure 5 in the main text and depicted in 5F simulation described below. We assume that the 1D medium is growing at constant velocity v_0 from the 1D tissue centre. Let us call f the frequency at which a new primordium is generated during a particular simulation. f typically depends on the model parameters: $\alpha_p, \beta_p, \alpha_a, \beta_a, \gamma_a.\gamma_d.\omega, CZ_{size}$. We define a reference frequency f_0 as the frequency corresponding to the model parameters defined in simulation 5F. To perform the analysis each parameter of the model is independently augmented by a factor $k\epsilon$ where $k \in [-3, -2, ..., 5]$ and $\epsilon = 10\%$. The competence zone size was also included in the tests, but due to its discrete nature it was augmented by a specific factor (see Figure 2.18 for the exact values). The Figure 2.18 shows the dependency of the relative change in frequency f/f_o with respect to each parameter change.

The sensitivity analysis confirms a number of intuitive predictions:

1. The increase of auxin synthesis α_a (or decrease of auxin decay β_a) increases f. Results suggest that the model is very sensitive to the amount of auxin in the meristem. Too low auxin synthesis (change by more than 10%) or too high degradation (change by more than 20%) stops the formation of patterns. This can be noted by observing α_a, β_a curves.

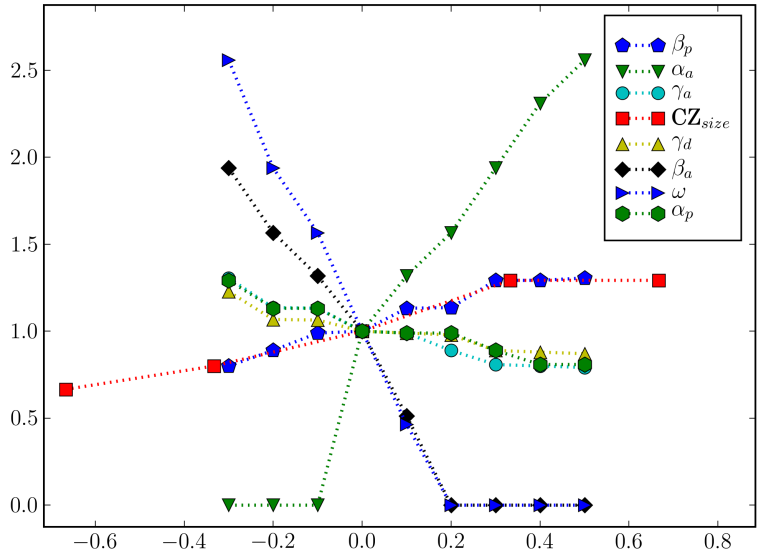

Figure 2.18: Plot showing the influence of the parameter change on the relative change in frequency f/f_9 in a 1D model.
On x-axis: k, on y-axis: f/f_0.

2. The increase of auxin transport (passive γ_d or active γ_a) decreases f. More efficient transport depletes the auxin faster from the meristem surface, increasing the inhibitory range of the primordium and increasing the time between the initiation of the consecutive primordia.

3. The increase of PIN background insertion into the membrane α_p (or decrease of PIN removal β_p) increases the strength of the active transport, therefore it decreases f. This can be observed in α_p, β_p curves.

4. The increase of competence zone size CZ_{size} leads to an increase of f. This observation is consistent with biology and other inhibitory field model predictions [Douady and Couder, 1996a, Smith et al., 2006a].

5. The increase of the primordium initiation threshold ω decreases f.

The sensitivity analysis of 1D flux-based dynamic system shows that *i*) the patterning capabilities of the model are kept for a range of parameter values *ii*) auxin synthesis, auxin decay and the primordia initiation threshold have the the biggest impact on the frequency f.

2.2.5.3 Sensitivity of the 2D flux-based polarization model to noise

The proposed mechanism of dynamic patterning depends on the detection of the locations where the auxin concentration exceeds a given threshold ω. The cells at this location differentiate and become sinks. We tested how sensitive this model is to the random auxin fluctuations in the system. This was achieved by i) adding noise to the already established auxin patterns and checking at what level the noise was able to perturb the PIN polarization pattern (in a non-growing tissue), ii) change the primordia initiation threshold ω in each cell by adding a noise with controlled amplitude to check the stability of primordium formation during development. The tests were performed on a system that was able to generate spiral phyllotaxy (equations and parameters were set according to Simulation 9A).

Let $m_{i\to j}$ be the membrane in cell i at the interface with cell j and M denote the set of all the membrane interfaces in the considered tissue. For each time t, we denote $P_m(t)$ the concentration of PIN in this $m \in M$ at time t.

In the first case, the arbitrary frame of Simulation 9A was chosen. This frame was describing system state at reference time t_0. Then auxin concentration was modified in each cell by adding a white noise of amplitude $\delta = k5\%$ (for $k \in \{1, 2, .., 5\}$). Then the system of equations describing the PIN and auxin dynamics was resolved, until a new stable state was reached. Then, the new PIN distributions $P'_m(t_0)$ were compared with the initial distributions $P_m(t_0)$ for every $m \in M$. The comparision between the simulation was done by comparing the average difference of PIN concentration $s = (1/|M|) \sum_{m\in M} |P'_m(t_0) - P_m(t_0)| / P_m(t_0)$, where $|M|$ denotes the size of M. As a result, we could observe that, the average difference of PIN concentration s was increasing with increasing values of k. However, for each k, s was found less than 5% and the system reached a state that was close to the original configuration. This showed that the flux-based model is fairly robust to auxin level perturbation throughout the meristem.

In the second case the simulation was performed exactly as in Simulation 9A, with one exception: the primordium initiation threshold ω_i was defined in every cell i as a mean threshold ω modified by an additive white noise of amplitude $\delta = \omega 2k\%$ ($k \in \{1, 2, .., 5\}$). This threshold noise was modified at every step of the simulation. By increasing the noise with a fixed primordium initiation threshold, we structurally change the speed at which primordia are detected, which results in a change in the phyllotactic pattern. To avoid this situation, the primordium initiation threshold ω was increased by $\omega\delta$. The results showed that the system is robust for low noise amplitudes: for $k \in \{1, 2\}$ the system was able to reproduce the spiral pattern with minor errors. These errors corresponded

to occasional changes in spiral orientation (chirality) during development. The system was fragile for higher noise ($k > 2$). In such cases, spiral patterns were not maintained. This suggests that flux-based polarization may require an additional mechanisms to achieve high robust behaviour.

2.2.5.4 Simulations

The basic system of equations

The basic system of equations equations, which we use in the simulations are defined as in the article:

$$\frac{\partial a_i}{\partial t} = -\sum_{n \in N_i} \frac{S_{i \to n}}{V_i} J_{i \to n} + \alpha_a - \beta_a a_i \tag{2.8}$$

$$\frac{\partial p_{i,n}}{\partial t} = \Phi\left(J_{i \to n}\right) + \alpha_p - \beta_p p_{i,n} \tag{2.9}$$

$$J_{i \to n} = \gamma_a \left(a_i p_{i,n} - a_n p_{n,i}\right) + \gamma_d \left(a_i - a_n\right) \tag{2.10}$$

$$\Phi_L(x) = \begin{cases} \kappa x & x \geq 0 \\ 0 & x < 0 \end{cases} \tag{2.11}$$

$$\Phi_C(x) = \begin{cases} \kappa x^2 & x \geq 0 \\ 0 & x < 0 \end{cases} \tag{2.12}$$

In the forthcoming sections we report which basic equation is used and which is modified for a particular simulation. The parameters for the system can be found in the supplementary Table 2.1.

Figure 2A

Specification: The cells which belong to Si were selected as described in the main article. The simulation was run for a fixed amount of steps. The system reached stability before the last step.

Model: We use equations 2.9, 2.11, we redefine 2.8, 2.10:

$$\frac{\partial a_i}{\partial t} = \left(- \sum_{n \in N_i} J_{i \to n} + \alpha_a - \beta_a a_i \right) [i \notin Si]$$

$$J_{i \to n} = \gamma_a \left(a_i p_{i,n} - a_n p_{n,i} \right),$$

And we assume that $\Phi = \Phi_L$.

Figure 2B

Model: The simulation differs from 2.2.5.4 only by modifying equation 2.8 in the following way:

$$\frac{\partial a_i}{\partial t} = - \sum_{n \in N_i} J_{i \to n} + \alpha_a - \left(\beta_a + \beta'_a [i \notin Si] \right) a_i$$

All the parameters are exactly the same and can be found in the Table 2.1.

Figure 3A

Specification: The cells which belong to Si were selected and the simulation was run for a fixed amount of steps. The system reached stability before the last step.

Model: We use equations 2.9, 2.10, 2.11, we redefine 2.8:

$$\frac{\partial a_i}{\partial t} = \left(- \sum_{n \in N_i} J_{i \to n} + \alpha_a - \beta_a a_i \right) [i \notin Si]$$

And we assume that $\Phi = \Phi_L$.

Figure 3B

Specification: The cells which belong to Si were selected and the simulation was run for fixed amount of steps. The system was stable after the last step. The figure presented in the text is not the last step of the simulation. The system still develops and creates more complex vein pattern (with loops). This evolution can be observed on the supporting movie.

Model: We use equations 2.9, 2.10, 2.12, we redefine 2.8:

$$\frac{\partial a_i}{\partial t} = \left(- \sum_{n \in N_i} J_{i \to n} + \alpha_a - \beta_a a_i \right) [i \notin Si]$$

And we assume that $\Phi = \Phi_C$.

Figure 4A-4D

Model: We use equations 2.9, 2.10, 2.11, we redefine 2.8:

$$\frac{\partial a_i}{\partial t} = \left(- \sum_{n \in N_i} J_{i \to n} + \alpha_a - \beta_a a_i \right) [i \notin Si]$$

And we assume that $\Phi = \Phi_L$.

Figure 5A-5F

Model: We use equations 2.9, 2.10, 2.11, we redefine 2.8:

$$\frac{\partial a_i}{\partial t} = \left(- \sum_{n \in N_i} J_{i \to n} + \alpha_a - \beta_a a_i \right) [i \notin Pr]$$

And we assume that $\Phi = \Phi_L$.

Figure 7A-7B

Specification: The simulation was run in two variants: with and without a centre. In case of " the simulation with a centre a subset of cells which belong to Cz was chosen. These cells were degrading the auxin. The initial geometry of the cells was acquired from confocal images. The simulation was run for 60 steps until it reached a stable state with a visible auxin maximum in the place of the future initium.

Model: We use equations 2.9, 2.10, 2.11, we redefine 2.8:

$$\frac{\partial a_i}{\partial t} = \left(- \sum_{n \in N_i} \frac{S_{i \to n}}{V_i} J_{i \to n} + \alpha_a - \left(\beta_a + \beta'_a \left[i \notin Cz \right] \right) a_i \right) [i \notin Pr]$$

And we assume that $\Phi = \Phi_L$.

Figure 9A-9E

Specification: To simulate the influence of old primordia, each primordium 'leaving the virtual meristem through growth tagged the closest neighbour cell with a special cell identity (yellow dots).. This property was propagated over a given time. The cells tagged as such were acting as sinks but the sink strength was gradually decreasing with time

Model: We use equations 2.9, 2.10, 2.11, we redefine 2.8:

$$\frac{\partial a_i}{\partial t} = \left(- \sum_{n \in N_i} \frac{S_{i \to n}}{V_i} J_{i \to n} + \alpha_a - \left(\beta_a + \beta'_a \left[i \notin Cz \right] \right) a_i \right) \left[i \notin Pr \right]$$

And we assume that $\Phi = \Phi_L$.

Figure 9G-9I

Specification: Cells with white dots are simulating old primordia and they belong to Si set, cells with black dots are L1 cells and they belong to $L1$ set, the cell with a blue dot is a new primordium and belongs to the Pr set (note: it belongs to $L1$ set as well). We assume that the L1 cells are separated from the inner cells except for the primordium cell. This cell is allowed to exchange the auxin with both L1 and inner cells. The feedback from flux on PIN polarisation in L1 and inner cells is different and it is modelled with a change inΦ function. Also, the cells in L1 layer produce much more auxin than inner layer cells.

Model: We use equations 2.10, 2.11, 2.12 we redefine 2.8, 2.9:

For cells i such as $i \in L1$:

$$\frac{\partial a_i}{\partial t} = \left(- \sum_{n \in N_i} \frac{S_{i \to n}}{V_i} J_{i \to n} \left[n \in L1 \vee i \in Pr \right] + \left(\alpha_a + \alpha_{L1} \right) - \beta_a a_i \right) \left[i \notin Si \right]$$

$$\frac{\partial p_{i,j}}{\partial t} = \Phi_L \left(J_{i \to j} \right) \left[j \in L1 \right] + \Phi_L \left(J_{i \to j} \right) \left[j \notin L1 \right] + \alpha_p - \beta_p p_{i,j}$$

For cells i such as $i \notin L1$:

$$\frac{\partial a_i}{\partial t} = \left(- \sum_{n \in N_i} \frac{S_{i \to n}}{V_i} J_{i \to n} \left[n \notin L1 \vee i \in Pr \right] + \alpha_a - \beta_a a_i \right) \left[i \notin Si \right]$$

$$\frac{\partial p_{i,j}}{\partial t} = \Phi_C\left(J_{i\to j}\right) + \alpha_p - \beta_p p_{i,j}$$

Parameters: $\alpha_{L1} = 0.3$

Figure 10C

Specification: The simulation was run until the system reached a stable state. In this state an auxin maximum was established in the root apex.

We use equations 2.10, 2.9, 2.12 we redefine 2.8:

$$\frac{\partial a_i}{\partial t} = \left(-\sum_{n\in N_i}\frac{S_{i\to n}}{V_i}J_{i\to n} + \alpha_a - \beta_a a_i\right)[i \notin Si]$$

And we assume that $\Phi = \Phi_C$.

Initial conditions: $\forall i \notin Si.a_i = 0.3; \forall i \in Si.a_i = 0.0; p_{i.j} = 1.0\, if\, PIN\, exists\, in\, vivo\, else\, 0$

Parameter	2A	2B	3A	3B	4A-D	5A-F	7A-B	9A-E	9G-I	10C
α_a	0.1	0.1	0.1	0.1	0.1	0.1	0.1	0.3	0.01*	0.0
β_a	0.01	0.01	0.01	0.01	0.01	0.01	0.01	0.03	0.01	0.0
β'_a	-	0.1	-	-	-	-	-/0.08	0.06	-	-
α_p	0.1	0.1	0.1	0.1	0.1	0.1	0.1	0.1	0.1	0.0
β_p	0.05	0.05	0.01	0.01	0.01	0.05	0.01	0.01	0.01	0.5
γ_a	0.1	0.1	0.1	0.1	0.1	0.1	0.1	0.125	0.1	100.0
γ_d	-	-	0.03	0.03	0.03	0.001	0.03	0.03	0.03	0.001
Φ	L	L	L	C	L	L	L	L	L+C	C
κ_L	0.15	0.15	0.2	-	1.3/1.5/1.7/2.0	0.15	0.18	0.11	0.09	-
κ_C	-	-	-	1.3	-	-	-	-	1.1	0.2
h	2.2	2.2	1.0	0.025	1.0	1.0	0.25	1.0	1.0	0.1
ϵ_0	-	-	-	-	-	0.01	-	0.01	-	-
init a_i	0.0	0.0	0.0	0.0	0.0	0.0	0.0	0.0	0.0	0.3
init $p_{i,j}$	$\frac{\alpha_p}{\beta_p}$	$\frac{\alpha_p}{\beta_p}$	$\frac{\alpha_p}{\beta_p}$	$\frac{\alpha_p}{\beta_p}$	$\frac{\alpha_p}{\beta_p}$	$\frac{\alpha_p}{\beta_p}$	$\frac{\alpha_p}{\beta_p}$	$\frac{\alpha_p}{\beta_p}$	$\frac{\alpha_p}{\beta_p}$	*
PIN max	-	-	2.0	1.0	2.0	-	2.0	2.0	2.0	1.0
snapshots	100	100	60	240	120	400	60 + 60*	*	30 + 80*	2500
steps	100	100	10	400	10	-	10	-	10	10
$[a_{min}, a_{max}]$	-	-	[0, 5]	[0, 5]	[0, 5]	-	[0, 4.8]	[0, 6.8]	[0, 12]	[0, 1]
p_{mid}	-	-	0.94	0.94	0.94	-	0.9	0.7	0.6	0.5

Table 2.1: The simulation parameters.
The "*" is used when the parameter is changed in complex way (which is explained in details in the text), the "/" means alternative values used in simulation and "-" means that the value is not included in the experiment equations. The units for the parameters were specified in the main article, however to adjust them to cellular world all the m should be exchanged by μm and mol by μmol.

2.3 Comparison of *flux-based* and *concentration-based* models in the context of *phyllotaxis*

Both, the *concentration-based* and *flux-based* models are able to reproduce phyllotactic patterns [Jönsson et al., 2006, Stoma et al., 2008]. This process of consecutive primordia formation can be seen in a simplified way as a mechanism which requires four separated components: *i*) growth, making the space for new organs *ii*) finding a position for a new initium *iii*) supplying auxin to this location *iv*) development of vascular tissue below the initium. It is important to note, that these components might not be sequencial, e.g. finding the position of a primordium might be realized by concentrating auxin in a particular location, thus these two components are rather *parallel* than *sequential*. Both, the *concentration-based* and *flux-based* models are based on the same mechanism to determine the position of the new primordium i.e the detection of auxin accumulation. However, the models differ by the way auxin is supplied towards the centre of initium and by how the vasculature is developed. This difference led us to a set of different predictions and requirements of the models which will be explained in the following paragraphs.

2.3.1 Initiation of primordia

In the *flux-based* model each primordium acts as a sink. It therefore lowers the concentration of auxin in its closest neighbourhood. The concentration of auxin in primordia is lower than in its neighbourhood. Due to growth of meristem primordia move away from each other (2.19F). This movement gradually increases the concentration of auxin in the location between them (2.19G). When the concentration of auxin exceeds a certain threshold, the cell identities in this zone change (2.19H). This identity change allows auxin to leak into L2 below initium, which induces vascular formation (2.19I). The vasculature drains auxin, which lowers its concentration in the initium (2.19J), and induces a flux towards the future primordium. The initium acts as a sink and the flux towards it reverses pump polarisations on the surface in the direction of the initium (2.19K).

In the *concentration-based* model each primordium acts by attracting auxin towards it. The constant drainage of auxin towards a primordium lowers the concentration of auxin in its neighbourhood. Since a removal of auxin from the L1 must be smaller then an auxin net flux flowing to it[4], the concentration

[4]if the auxin removal would be bigger, and as a consequence auxin concentration in the primordium would be lower, then PIN would not be point in the direction of primordia, which is in contradiction with the observations.

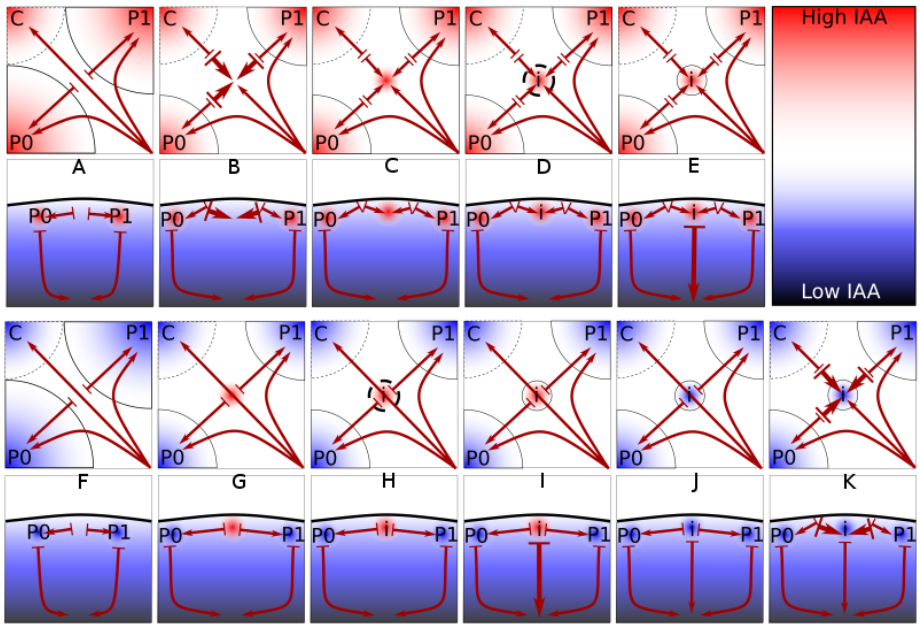

Figure 2.19: Comparision of phyllotaxy models based on *concentration-based* and *flux-based* polarization hypothesis.
Description in text.

of auxin in primordia is higher than in its neighbourhood. Due to growth of the meristem primordia move away from each other (2.19A). When the distance between primordia is sufficient, a spot with higher auxin concentration will spontaneously appear in the place maximising the distance between all primordia (due to local synthesis). The development of this spot causes a reversal of PIN pumps in the L1 towards it. (2.19B). This reversal further increases the maximum of the concentration of auxin (2.19C). The concentration of auxin exceeding certain threshold induces the change of the cell identities in the zone of maximum concentration of auxin (2.19D). The change of cell identities in the initium stimulates a formation of vasculature (2.19E).

2.3.2 Mechanism of the development of vasculature

In the *flux-based* model the development of vasculature below initium requires a change in the "regime" of Φ which regulates the influence of auxin flux on PIN allocation and which must "accelerate" to guarantee vascular formation. It is important to note, that despite this change, this mechanism still depends on the flux of auxin [Feugier et al., 2005, Stoma et al., 2008].

In the first publications introducing the *concentration-based* model, no mech-

anism for vasculature development was proposed [Jönsson et al., 2006, Smith et al., 2006c]. Recently, Merks et al. [2007] demonstrated that an extension of the Jönsson et al. [2006] model with the hypothesis of auxin dependent PIN synthesis in the cell allows to create auxin maxima "travelling" across the tissue. The authors suggest, that such a mechanizm can be used to create veins, thus explains the development of the vasculature below the initium.

The simulations show, that the model indeed can create auxin maxima "travelling" across the tissue Merks et al. [2007]. However, these simulations give the impression, that the path of the "travelling" auxin maxima is random, therefore to create a vein from the initium directly towards the internal vasculature of the meristem another mechanism to guide the vein would be required. Another problem is the preservation of high PIN polarization. According to the model equation, PIN polarization on the path of travelling maximum should disappear when this maximum is leaving the cell, since high concentration of auxin is required to keep high level of PIN. This suggests, that a mechanism preserving PIN in the cells for which its expression reaches high levels is required (e.g similar to the one proposed in the 2.1.2.2),

Another idea was proposed by Richard Smith in his thesis [Smith, 2007]. His idea is based on the observation, that auxin-dependent PIN targeting to a specific side of the cell depends on cell type-specific factors, as different cell types display different preferences for auxin-dependent changes in PIN polarity [Kleine-Vehn et al., 2006]. This could actually resolve a discrepancy between the *flux-based* and *concentration-based* models. Given a cell type-specific decision about PIN orientation in response to auxin, *flux-based* and *concentration-based* models may actually be facets of the same general mechanism by which feedback-driven directional auxin transport eventually leading to self-establishing developmental patterns. As a final solution, Smith [2007] propose a model (called dual-polarization model) which is switching between *flux-based* and *concentration-based* PIN polarization depending on auxin concentration, which is indirectly tissue-dependent.

2.3.3 Auxin concentration in the primordium

The supposed stable auxin maximum at the young initium has been identified using the DR5 promoter driving the green fluorescent protein (GFP). This marker is often described as a quantitative auxin sensor, however it not only depends on the amount of hormone but also on the capacity of cells to react to it (e.g. cells in the central zone of meristem do not respond to this marker as shown by Barbier de Reuille et al. [2006]). In addition, the fluorescent GFP marker

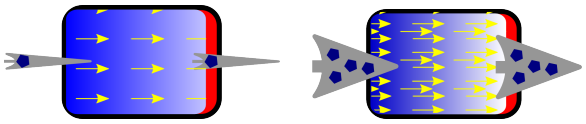

Figure 2.20: The directional flux strength influences the auxin gradient inside the cell.
The intensity of blue depicts the concentration of auxin. In the figures the size of grey arrow depicts the intensity of directional flux (caused by active transport) and the number of yellow arrows depicts the diffusion flux inside of the cell. The average concentration in both cells are identical, however according to Fick's First Law the diffusion flux is bigger in the Figure 2.20B than in the Figure 2.20A due to higher auxin gradient.

can be stable for prolonged periods, and could therefore mask rapid changes in the activity of the promoter. This is also important to note, that DR5 might not only mark high auxin concentrations but could also be activated by high auxin fluxes. This issue was already raised by other authors [Rolland-Lagan and Prusinkiewicz, 2005].

A high directional flux leads to a strong auxin gradient inside the cell ([Kramer and Bennett, 2006]) which according to Fick's First Law should in turn lead to a high auxin diffusion flux inside the cytoplasm (figure 2.20). Since, in the presence of a high diffusive flow it is more likely for an auxin particle to encounter its receptor, mainly localised in the nucleus of the cell, high flux could as well lead to increased signalling and DR5 activation (figure 2.21). Interestingly, our simulations show that, by combining *concentration-based* and *flux-based* activation of DR5 sharp peaks are obtained, very comparable to what is observed *in vivo* (figure 2.22).

2.3.4 Fluxes towards the centre

Inmunolabelling suggest, that the fluxes of auxin are directed towards meristem summit [Barbier de Reuille et al., 2006]. The *flux-based* model is compatible with the presence of these fluxes [Stoma et al., 2008], provided that the auxin undergoes endocytosis in the centre.

The compatibility of *concentration-based* models with these fluxes remains an open question. The authors of original models did not include these fluxes [Jönsson et al., 2006, Smith et al., 2006c]. A possible solution to force the fluxes to converge towards the centre of the meristem is to maintain the auxin maximum in this location. However, this option interferes with the stability of

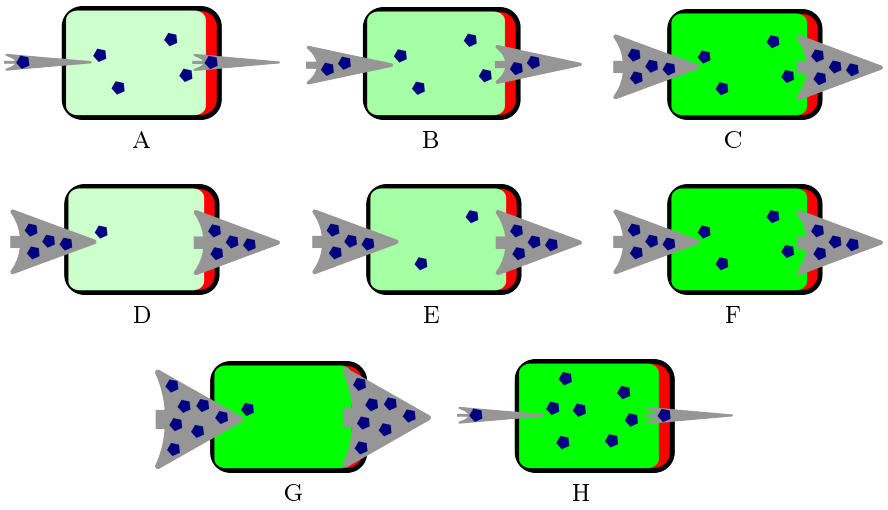

Figure 2.21: Flux and concentration inducing DR5::GFP marker.
The intensity of green depicts the strength of GFP response. The figures show the flux intensity (size of grey arrows) and concentration in the cell (blue pentagons). The GFP response increases with an increase of flux (Figures 2.21A-2.21A) or with an increase of concentration (Figures 2.21D-2.21D). However, it is important to remark that with high flux we may get strong GFP response even for small concentration (2.21H). The similar situation can take place for high concentration and small flux (2.21G).

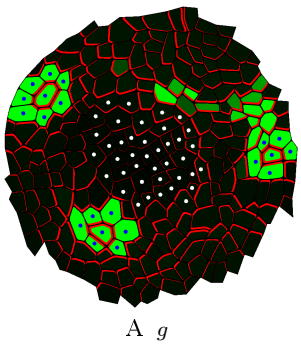

A *g*

Figure 2.22: Figure shows a *concentration-based* and *flux-based* activation of DR5 signal in the meristem studied in the paper.
More details can be found in the text.

phyllotactic patterns, since the simulations show, that the *concentration-based* model with an auxin maximum in the centre generates phyllotactic patterns with more noise than the same model without an auxin maximum in the centre (Richard Smith, personal communication). It is important to note, that in the model of Jönsson et al. [2006] it is required to preserve an auxin minimum in the centre. These results show, that the compatibility of *concentration-based* models with auxin fluxes towards the centre is not straightforward and has to be studied more carefully.

2.3.5 Conclusions

To summarize, both models make different predictions regarding the sequence of events, and in particular, the maintenance of auxin maxima in primordia, a difference in the order of PIN reversal on the surface and the development of vasculature. In particular, the *flux-based* model predicts a rapid conversion of an auxin maximum into a minimum, parallel to the development of vasculature below primordium. The *flux-based* model is compatible with the fluxes converging to the centre of meristem, whereas this compatibility remains to be verified for *the concentration-based* model. In case of the *flux-based* model the development of the vein requires a change of the function regulating the dependency between the flux and PIN allocation, whereas in case of the *concentration-based* model a different concept, is required involving a travelling wave hypothesis.

Further experimentation focused on these issues should therefore make it possible to distinguish between the two models.

Chapter 3

Towards coupling of physiology and growth

3.1 Cell wall mechanics

The presence of cell walls represents one of the structural features distinguishing a plant cell from an animal cell. Cell wall acts as a rigid shell, and from the mechanical point of view it is a dominant component responsible for the overall plant structure [Solomon and Berg, 2007]. The presence of walls allow plant cells to develop higher turgor pressure than their animal counterparts. By putting cell walls under tension stress, turgor functions like a hydroskeleton thus, contributing significantly to mechanical properties of young plant organs. Wilting for example, is a collapse of plant tissue due to the lack of internal pressure in individual cells[1].

Plant cell walls are composed of a variety of polymers that differ in their biochemical and biomechanical properties. The dominating component of a cell wall is cellulose, which forms microfibrills (figure 3.1) [Solomon and Berg, 2007]. Their arrangement determines the cell wall's capacity to resist to forces in different directions, as shown by measurements of the anisotropic extensibility of single-layer tissues [Kerstetter et al., 2001]. Microfibrills, if arranged parallel, would only be able to resist strength efficiently in their longitudinal direction.

While understanding and modelling static cellular architecture represents already a challenge, a new dimension is added when considering the dynamic

[1] Plants wilt not only when they lose water through evaporation but also when they are surrounded by an aqueous solution of common salts (e.g. potassium chloride, magnesium chloride) (Wikipedia).

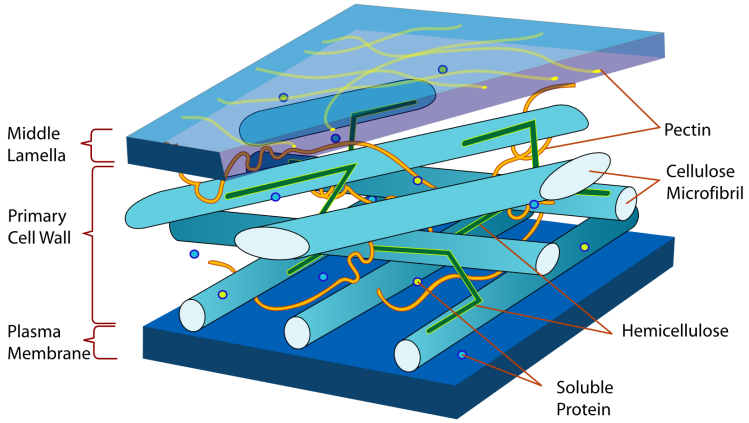

Figure 3.1: Molecular structure of the primary cell wall in plants (Wikipedia).

processes that change cell shape. Contrary to many animal cells that are able to migrate, most plant cells have a shape that does not change once functional maturity is achieved. This process is generally accompanied by numerous processes that involve a remarkable increase in cell size and significant changes in cell shape, both of which are based on the irreversible expansion of cell walls [Solomon and Berg, 2007].

This expansion is generally considered to be driven by a turgor-controlled volume increase and involves stress relaxation and polymer creep in cell walls [Cosgrove, 1997, Cosgrow, 2000]. Walls of growing cells have unique rheological* properties that may be measured in various ways [Cosgrove, 1993]. It is important in this context to distinguish between elastic (reversible) and plastic (irreversible) deformation of the cell wall [Proseus et al., 1999].

Depending on the tissue type, cellular morphogenesis produces a particular tissue shape. While the amount of turgor can affect growth velocity [Proseus et al., 2000], pressure is a non-directional force. Therefore, it cannot by itself produce shape deformations other than isotropic ones. To produce anisotropic shape changes, and thus particular spatial growth patterns, the cell wall has to exhibit regions that are more easily deformable than others. This is generally considered to be produced by a combination of the following: *i*) a non-uniform distribution of cell wall components with different physical properties, *ii*) a divergent localization of the insertion points of new cell wall material, or *iii*) an anisotropic expansibility determined by the orientation of fibrils in the wall [Geitmann and Anja, 2006].

Individual cell wall components were analyzed in vitro [Jarvis, 1984] and cell wall extensibility was investigated by measuring the deformation of cells encountered

in response to externally applied force [Cosgrove, 1993]. Such investigations revealed several factors that affect cell wall extensibility. For example, stress relaxation in cell walls was accelerated by pretreating the tissues with auxin [Masuda, 1990] and expansins increased the rate of long-term cell wall extension under acidic conditions [Cosgrove, 1996].

Since the discovery of cortical microtubules (CMT), various models for their implication in microfibrills orientation process were proposed [Giddings and Staehelin, 1991]. The CMT are microtubules localised at the "cortex" of the cell and attached to the plasma membrane. It is thought, that these microtubules orient the cellulose microfibrills in the extracellular matrix or cell wall. These microtubules (and their orientation) are, therefore, very important in the control of the plant shape. The other, the non-cortical microtubules play a role in the transport of organelles inside the cell. However, while the recent research has shown that the cortical microtubules clearly participate in the regulation of anisotropic cell wall expansion, their precise role in microfibril alignment has been intensively discussed [Baskin, 2001, Himmelspach et al., 2003]. An overview of the principles of the anisotropic expansion within plant cell walls including the role of microtubules has recently been published by Baskin [2005].

Numerous studies were focused on the role of the orientation of microfibrills for cell growth. Early models include the concept of "multinet growth" [Green, 1960]. According to this model, cylindrical cells add new microfibrils by apposition in a transverse direction to their inner cell wall. These microfibrils are building up separated layers, in which the most recently added microfibrils are located in the most internal layer. Additionally, during the growth, the microfibrils in older layers passively reorient themselves and loosen due to the stretching of a cell wall. This model explains different orientation of microfibrils found in the cell wall layers of many cells. Since the multinet model explains only how the microfibrills are deposed, it is an interesting question how is the oriented deposition of microfibrills controlled.

Due to the fact that the cell walls play an important role in the development of plants, we extended a modelling framework used to simulate phyllotaxis (Chapter 2). In current chapter, to simulate meristem dynamics physical-based approach was used.

Unlike descriptive models, physically-based growth models have the potential to generate apex and primordium shapes as emergent properties of the model. It enables the modelling of the processes that lead to these shapes and in particular the interaction between growth and resulting shape. For phyllotaxis, physically-based growth models may have a special significance as many authors pointed

out that physical forces may play a direct or indirect role in primordia positioning (for example Dumais and Steele [2000], Shipman and Newell [2004]).

Physical-based approach allowed us to vary growth intensity in different location of the meristem and to study the influence of the mechanical properties of the meristem on its developing form. Using this framework we performed a series of *in silico* experiments, in which we investigated the issues of *i*) a maintenance of the dome-like shape of *pin1* *ii*) the local variation of growth depending on the concentration of auxin in growing meristem *iii*) the feedback between the *concentration-based* auxin transport model and auxin-dependent growth.

3.2 Mechanical framework

3.2.1 Representation

In the model we suppose, that the meristem's external cell layer plays a crucial role both, in meristem functioning [Kessler et al., 2006] and in determining the mechanical properties of whole meristem [Savaldigoldstein and Chory, 2008]. We also assume, that the tissue has both, elastic and plastic properties [Cosgrove, 1997, Wei et al., 2001]. The turgor pressure generated and experienced by the cells in the rib zone occurs in all directions, since each cell is surrounded by walls of its neighbouring cells. However, the cells in L1 also interfere with the environment. To balance the forces resulting from this difference of external and internal medium, the outer wall of epidermis is thicker than inner walls (up to 5-10 folds) [Savaldigoldstein and Chory, 2008]. Thus, the turgor pressure is mostly supported by the epidermal cell layer is also a limiting factor for growth. Additionally, the pressure exerted on the L1 layer is approximately uniform [Hejnowicz, 2000].

In the model the mechanical constraints of the L1 layer are approximated by its external, periclinal* cell wall. To build up a mechanical model of the meristem, we construct a polygonal mesh* (figure 3.2). Each face* of the mesh corresponds to an external, periclinal cell wall of L1 cell c, and is surrounded by the edges that stand for the projection of cell c anticlinal* cell walls. The initial geometrical configuration of the tissue can be acquired from real meristem images using a protocol proposed by Barbier [2005], or can be artificially generated (for the details see 4).

To represent the rib zone we use the following abstraction: the influence of all inner cells of the meristem is summarised by an overall turgor pressure Π

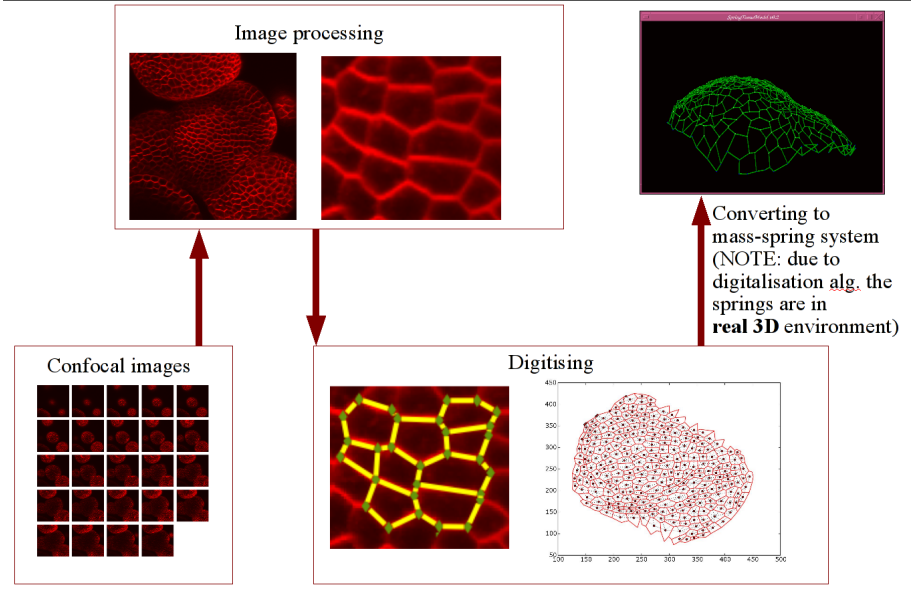

Figure 3.2: Protocol of mass system initiation from real image stack.
In the "Digitising" box, yellow segments depict edges, and green dots vertices.

that exerts perpendicular force on the surface and prevents the L1 layer from collapsing (figure 3.3), and provides a stress required for the growth.

3.2.2 Mechanics

To include mechanical properties, the representation described above is expressed in terms of a mass-spring system (MSS) (similar to the concept proposed by Prusinkiewicz and Lindenmayer [1990], Smith et al. [2006a]). Each edge e has an associated spring, while masses are attached to the vertices. The mechanical properties of each spring are characterised by two parameters: a stiffness K_e and a rest length l_e^0. Each spring in the system contributes to an elastic force F_e^E proportional to its tension and acting on the vertices:

$$F_e^E = K_e \left(l_e^0 - l_e\right)$$

At the junction of springs, vertices are submitted to these elastic forces. In addition to the forces on a vertex v due to springs F_v^E, a uniform force representing the internal turgor pressure F_v^Π is included in the model which acts along the direction of the surface normal at each vertex v.

A plant is able to control its growth direction e.g. to grow towards the light or to adapt to other environmental factors. In the model, each of such processes

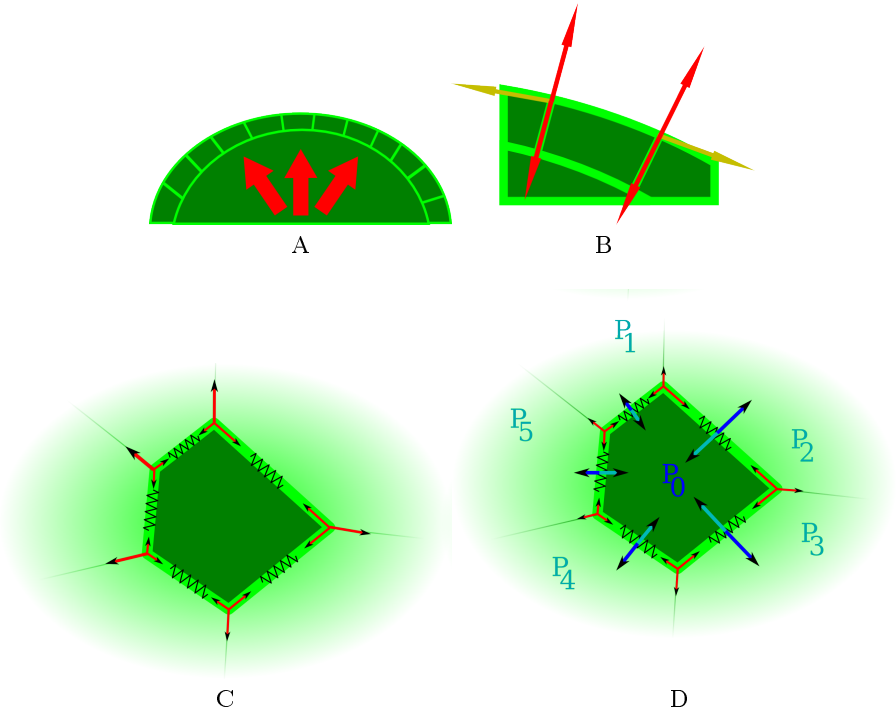

Figure 3.3: Meristem representation.
Figure 3.3A shows the schematics of the meristem representation. Red arrows depict forces exerted by turgor on L1. Figure 3.3B shows the close up. The presence of turgor pressure Π exerts forces stretching a cell (depicted with brown). Figure 3.3C shows the top view of L1 cell. Each wall of the cell has elastic properties, depicted by springs in the walls. The stretching forces and spring forces are depicted with red arrows. Figure 3.3D shows the forces caused by turgor pressure.

may be expressed with a directional force F_v^D acting on groups of vertices and leading to more intensive local growth in the force direction. It is important to note, that this force allows us to express growth tropisms in the model, however it abstracts from the source of these tropisms.

For each vertex v, all elastic forces F_v^E exerting on it are added together with the pressure forces F_v^Π and directional forces F_v^D and the system evolution is traced using particle solver system, until the steady-state of the system is determined (see 3.2.3) [Witkin, 2001]. Combining the various components, the total force F_v acting on a vertex v is:

$$\begin{cases} F_v^E = \sum_{e \in \{(x_1,x_2):x_1=v \vee x_2=v\}} F_e^E \\ F_v = F_v^E + F_v^D + F_v^\Pi \end{cases}$$

To allow the model to simulate development, we introduced a growth model, in which material is added to cell walls under tension. It is realized by increasing the rest lengths of springs representing the cell walls i.e. a change of length l_e^0 depending on the current spring tension:

$$\frac{dl_e^0}{dt} = \begin{cases} 0 & \text{if} \quad l_e(t) - l_e^0 < \text{threshold} \\ G_e\left(l_e(t) - l_e^0\right) & \text{otherwise} \end{cases} \tag{3.1}$$

where G_e is a growth rate. If the difference between spring length and its rest length is bigger than a given threshold, then its rest length is increased proportionally to this difference. In the case of cells with increased growth, this increase is larger either due to the directional force F^D (leading to bigger spring deformation $l_e\,(t)$), or due to the increase in growth rate G_e.

Since cell growth constantly increases cell sizes, a cell division rule, according to which a cell is divided when its size exceeds given threshold, has been integrated in the system. The location of a new wall is chosen to minimise two conditions: the difference between cell sizes of two daughter cells and the length of the new wall. Additionally, the rest length of a spring related to the new cell wall is shorter than this wall. This results in "pinching" the cell and makes the daughter cells less sliver. This idea was introduced by [Nakielski, 2000], who suggested that this rule corrects the visual look of the tissue. Further details concerning cell divisions are described in 4.2.3).

Moreover, we assume that the cell walls of cells distant from the meristem summit change their structure and become rigid. In the model the cell walls of the cells with an Euclidean distance to the meristem tip exceeding a certain threshold σ (further we call them "distant cells") resist all turgor and elastic

forces.

3.2.3 Physical simulation

In the real meristem growth is parallel to physiological processes (e.g. diffusion of morphogens). In the simulations, due to discrete nature of computation, it is required to assume a sequential order between these processes (however the processes can interlace). Physiological processes studied in this thesis are usually much faster than the growth. For example, we know that PIN proteins can reorient within a time-span of the order of an hour (e.g. in the root after gravistimulation). Estimated transport and even diffusion rates are estimated in uM/sec [Kramer and Bennett, 2006, Kramer et al., 2007], whereas the duration of a cell cycle is about 24 hours. Therefore, it seems reasonable to suppose that the auxin transport system is in equilibrium when comparing it to growth dynamics.

In the case of the growing apex model, we assume that growth is a quasi stable process. At the beginning of each time step the meristem is in a mechanical equilibrium state. Growth, which changes the rest lengths of the springs, alters this equilibrium. The MSS is then iterated until a new equilibrium is reached. This means that in general, there are many iterations of the physical simulation for each growth step of the model.

Given the total force F_w on a vertex w as defined earlier, the following equations (derived from Newton's Laws) describe the change in vertex velocity v_w and vertex position p_w over time. They can be used to compute the system's equilibrium:

$$\begin{cases} \frac{dv_w}{dt} = \frac{F_w}{m} - Dv_w \\ \frac{dp_w}{dt} = v_w \end{cases}$$

where D is a damping constant, which allows us to avoid system oscillations and guarantees a system convergence towards stationary state. In the equations we assume additionally that the point masses of points equal to 1, since this assumption does not change the equilibrium state reached by the model. The numerical integration of these equations is performed using one of the methods introduced in the appendix A.

Principles of equation integration The physics integration in each growth step is a separate simulation within the main program loop, which has its own

time step and method routines. This simulation is iterated until an equilibrium state is reached. We consider that this equilibrium is reached once the velocity of all points falls below a given threshold, since the velocities will go to zero when the system is at a steady-state. The threshold value can be used to control the iterations.

Since only the equilibrium state of the physics simulation is sought at each time step of growth, a relaxation method can be used without considering velocity. Instead of calculating displacement as a derivative of velocity, vertices can simply be moved in the direction of the total force by some amount proportional to the magnitude of the force. This allows us to decrease the number of differential equations to solve (for each point we have only one equation instead of two). The system is then iterated until the norm of the sum of the forces approaches zero. In the models presented in this chapter both approaches have been used, and both methods produce qualitatively similar results. It is important to note, that in the case of relaxation method, in our simulations Runge-Kutta of order four was more efficient than Euler method (in case of our simulation up to 3 folds).

3.3 Simulating regular growth of *pin1* mutant phenotype

The shoot apical meristem of *Arabidopsis* mutant phenotype *pin1* has a dome-like shape (figure 1.24). Since its shape is less complex than the wild type's one, we started our study by describing the mechanical constraints required and sufficient to reproduce this type of development.

The simulations showed, that the proposed framework is sufficient to reproduce the shape corresponding to the form of a pin-shaped meristem. For a given set of growth parameters (like turgor pressure Π, growth rate G, meristem size) the system could reach a dynamic equilibrium, in which the growth of the meristem was continuous, and the radius of the meristem dome was constant (figure 3.4).

If the internal pressure was too small, the meristem summit was continuously decreasing to reach a form of small dome, with low number of not growing cells. The intensity of meristem growth in this case was decreasing with time.

The assumption of fixing cell walls of distant cells was required. Without this condition the growth of the meristem was similar to inflating a balloon (figure 3.5), and the characteristic dome-like shape could not be maintained.

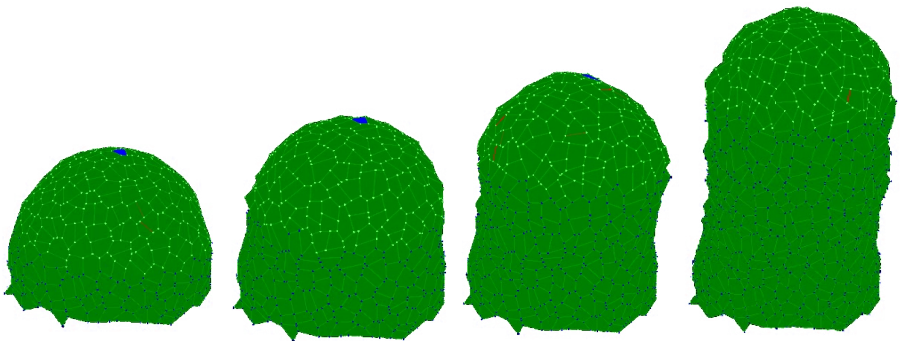

Figure 3.4: The model demonstrating the development of the meristem of *pin*1 mutant phenotype.
Growth of cells located too far from the meristem tip is limited by the secondary cell walls, thus in the simulation these cells are fixed (the vertices of such cells are marked with blue dots).

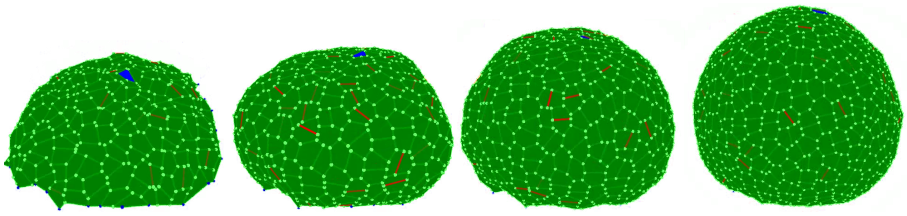

Figure 3.5: The model demonstrating the development of the meristem of *pin*1 mutant phenotype without the assumption, that the cell walls of distant cells are resisting turgor pressure.
Contrary to the simulation with this assumption, the meristem has an overall balloon-like form instead of observed *in vivo* dome-shaped form.

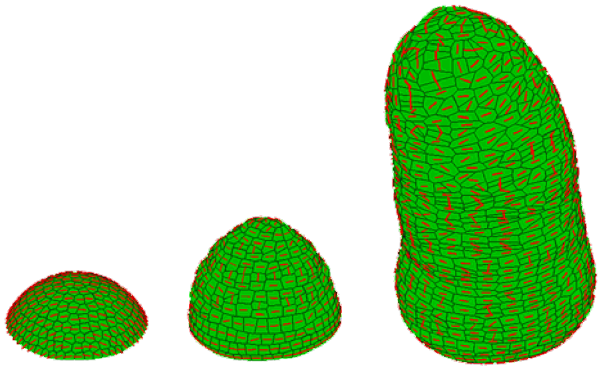

Figure 3.6: Simulation of meristem growth represented by pressure vessel. Time sequence of a simulation with the stress-feedback model generating a growing stem. Microtubules (depicted by red segments in the cells) align mainly orthoradially on the stem which has a regular shape [Hamant et al.]. Image taken from [Hamant et al.].

The simulations have shown, that the particular form of pin-shaped meristem could be the result of isotropic growth of cells together with the process of hardening of cell walls. The hardening of cell walls could be related to the development of secondary cell wall, which indeed takes place in cells at the bottom of the meristem. At the border of SAM, cell walls are thicker and grow slower Kwiatkowska and Dumais [2003].

An alternative explanation was given in a study of [Hamant et al.]. The authors were investigating the correlation between the cortical microtubules (CMT) and mechanical stress. They proposed a similar MSS model, however it was extended by including microtubules. CMT in the model acted by modifying the cell anisotropy, and as a consequence, prohibiting a cell from growing in the direction parallel to their orientation. In the model authors hypothesised, that microtubules orient themselves to resist stress. They have shown that during the growth of the pin-formed meristem, the CMT orientations were random and somewhat unstable at the apex, while these orientations on the stem stabilised in a mainly orthoradial pattern. It is important to note, that the CMT were required and sufficient to preserve the continuous growth of the pin-shaped meristem (figure 3.6).

These studies give the evidence that a non-directional turgor pressure together with a simple mechanical mechanism (either CMT or wall hardening) is sufficient to create a system with a an overall axial direction of growth. In reality it is likely that these mechanism act together to provide redundancy and increase the stability of such a biological system.

3.4 Simulating the development of primordium triggered by auxin

To investigate, how the regular growth of a pin-shaped meristem can be altered, we extended the model presented in 3.2 to include the influence of a morphogen on the intensity of growth. Auxin was chosen as a model morphogen, since it appears that meristem tissue is highly responsive to auxin-induced wall extensibility and elongation. Cells with high auxin concentration grow faster, due to the change in the mechanical properties of their walls [Kutschera, 1992]. Additionally, Reinhardt et al. [2000a] has described an experiment in which a patch of auxin applied on the surface of the meristem triggers the initiation of primordia in the region close to SAM apex of tomato:

> *We applied small amounts (...) of lanolin paste containing (...) auxin to various positions on the NPA pins, particularly on the flank (...). Treatment with auxin (...) induced the formation of bulges, whereas lanolin alone had no effect. These bulges, which always coincided with the radial position of IAA application, differentiated into leaf primordia. In the longitudinal (apical–basal) dimension, the primordia always formed at a fixed position from the summit, that is, within a ring-shaped zone roughly equivalent to the peripheral zone in untreated meristems (Steeves and Sussex, 1989; Lyndon, 1990, 1998). (...)*
>
> *The size of induced leaf primordia depended on the concentration of auxin. Whereas lower concentrations (...) induced primordia of approximately normal size, higher concentrations (...) induced primordia that were wider than normal and, in some cases, encompassed the entire meristem. The frequency of primordium initiation was also dependent on auxin concentration.*
>
> Reinhardt et al. [2000b]

These experiments show that the NPA pins contain functional meristems capable of leaf formation when supplied with auxin. The site of auxin treatment determined the location of primordium formation in the radial position. The concentration of auxin determined the number of cells recruited into primordia. These authors performed also similar experiments on the *pin1* mutant of *Arabidopsis* leading to the same conclusions.

We performed *in silico* variant of this experiment, where a framework similar to that described in 3.2 was used. The model was extended by the assumption,

that cell walls of cells which perceive a high concentration of auxin (called "auxin-positive" cells) grow faster. This was realized by substituting the growth constant G_e of these cell walls by G_e^{IAA} which was 3 folds bigger.

The patch of auxin was manually placed on the virtual meristem using the GUI*. The patch was 3 cells wide. The auxin-positive property was inherited by both daughter cells after the cell division.

This model reproduced the change of shape of the *Arabidopsis pin1* mutant described by Reinhardt et al. [2000a] (figure 3.7). Faster, local growth in the auxin-positive region (in red in the figure 3.7E), led to the formation of a bump shaped structure matching the appearance of a young primordium. If the springs in auxin-positive region were growing too slow, the bump was not well defined or not developed at all (figure 3.8). An alternative way of creating the bump was to include the directional force F_v^D for the vertices v below auxin-positive region, since it corresponded to an increase of growth rate in the rib zone below the primordium. Both variants led to qualitatively similar results.

The model highlighted particular stress in the boundary zone (which is the zone including the cells closest to the forming primordium). The stress in this zone was dominating in the circumferential directions (in light green in the figure 3.14A). The main growth direction follow the direction of the stress in the model. As a result of this directional stress, the cells in the boundary zone were elongated mainly in this particular direction.

To reproduce the development of the primordium it was sufficient to loosen the cell walls in the auxin-positive region or to assume an increased growth rate below the auxin-positive region. If the intensity of growth was insufficient and the directional force was too small, the bump was not well defined or did not emerge at all. The presence of different, circumferential stress in the boundary zone together with a specific gene expression in this location illustrates the possibility of the interaction between mechanical constraints and gene expression. Since the model reveals different mechanical properties in the boundary zones and biological data shows the expression of pBOUND promoter in this zone (figure 3.9), a hypothetical link between these two events can be suspected (similarly to other known examples of mechanical gene induction [Howard et al., 2008]). This hypothesis would need to be further investigated experimentally.

A similar experiment was performed by [Hamant et al.] within the framework described in 3.2. Alternatively in their model, primordia growth was initiated by a local decrease of wall stiffness leading to the outgrowth of a well defined bump. Since these authors included the microtubules in the model together with the hypothesis of their orientation according to stress, as the simulated primordium

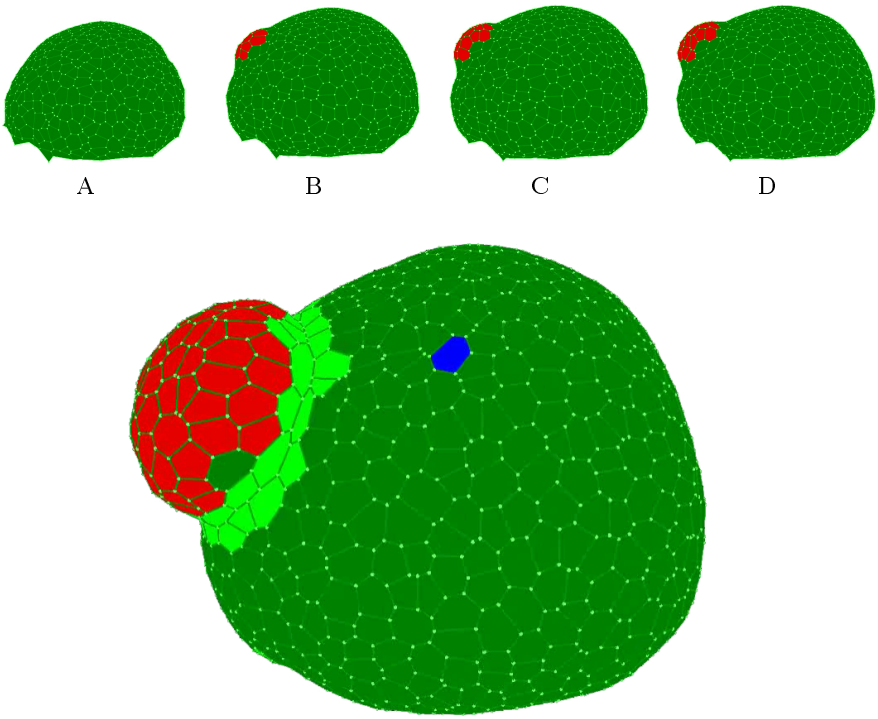

Figure 3.7: Model of primordium development.
This figure shows consecutive steps of a simulation demonstrating the emergence of the primordium as a response to an external application of auxin. Auxin-positive cells are marked in red.

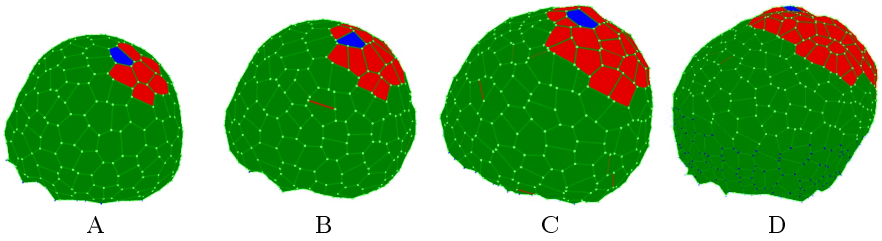

Figure 3.8: Model of primordia development similar to 3.7.
The pressure under the primordium was not increased. As a result, a bump was not able to properly form.

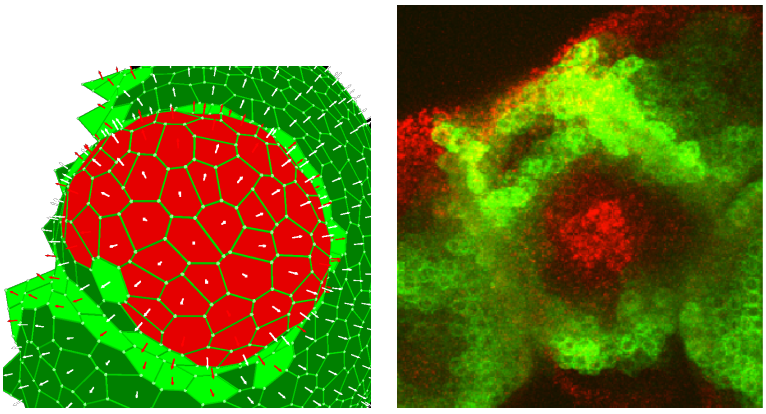

A B

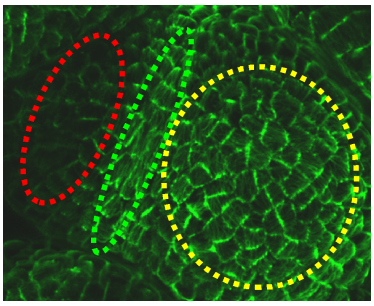

C

Figure 3.9: External application of auxin on PIN1 mutant.
Figure 3.9A shows the top view of meristem presented in 3.14A. The model reveals particular stress in this zone (in the cells marked with light green). Figure 3.9B shows in green GFP signal from the expression of pBOUND promoter (which is a part of the STM promoter, active in the boundary zone only). Figure 3.9C shows the image of CMT in different zones of the meristem: red in the primordium zone, light green in the boundary zone, yellow in the meristem centre. CMT in the boundary zone are oriented in circumferential directions.

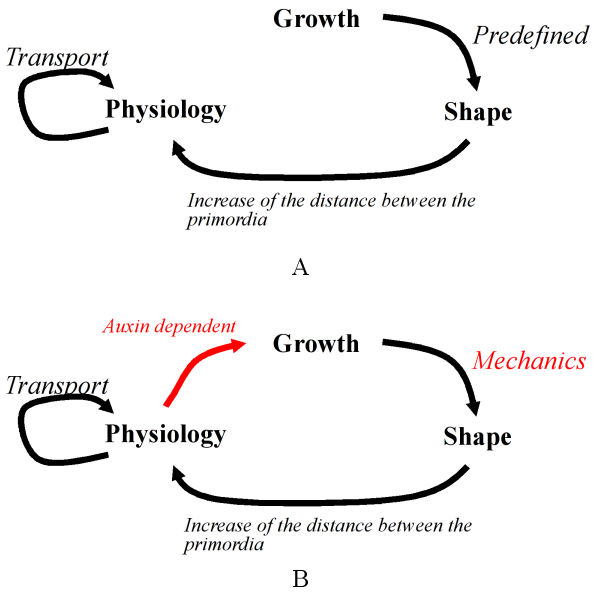

Figure 3.10: Model framework comparision.
Figure 3.10A shows the schema used for simulation of meristem development in models proposed by Barbier [2005], Jönsson et al. [2006], Stoma et al. [2008]. Figure 3.10B shows the schematics including the feedback between auxin and growth of the meristem, as in the model described in 3.5.

formed, the model predicted an orthoradial CMT orientation around the simulated primordium as observed in reality.

3.5 Coupling of growth with auxin transport

In the real meristem, growth is increased in the primordia. Therefore, a patterning mechanism responsible for phyllotaxis is able to function despite the anisotropic growth in the meristem. In the phyllotaxis model presented in Chapter 2 a descriptive growth was used to simulate meristem development. In such a model auxin-transport is independent from growth and including the growth anisotropy is cumbersome (figure 3.10a). Here we present a physical-based model containing a feedback loop between auxin concentration and growth (figure 3.10b).

To perform simulations, the framework described in 3.2 was used. The feedback from auxin concentration on growth is realized by extending the approach described in 3.4. The cell walls of auxin-positive cells instead of growing with increased, fixed ratio G_e^{IAA} grow with a ratio proportional to the auxin concen-

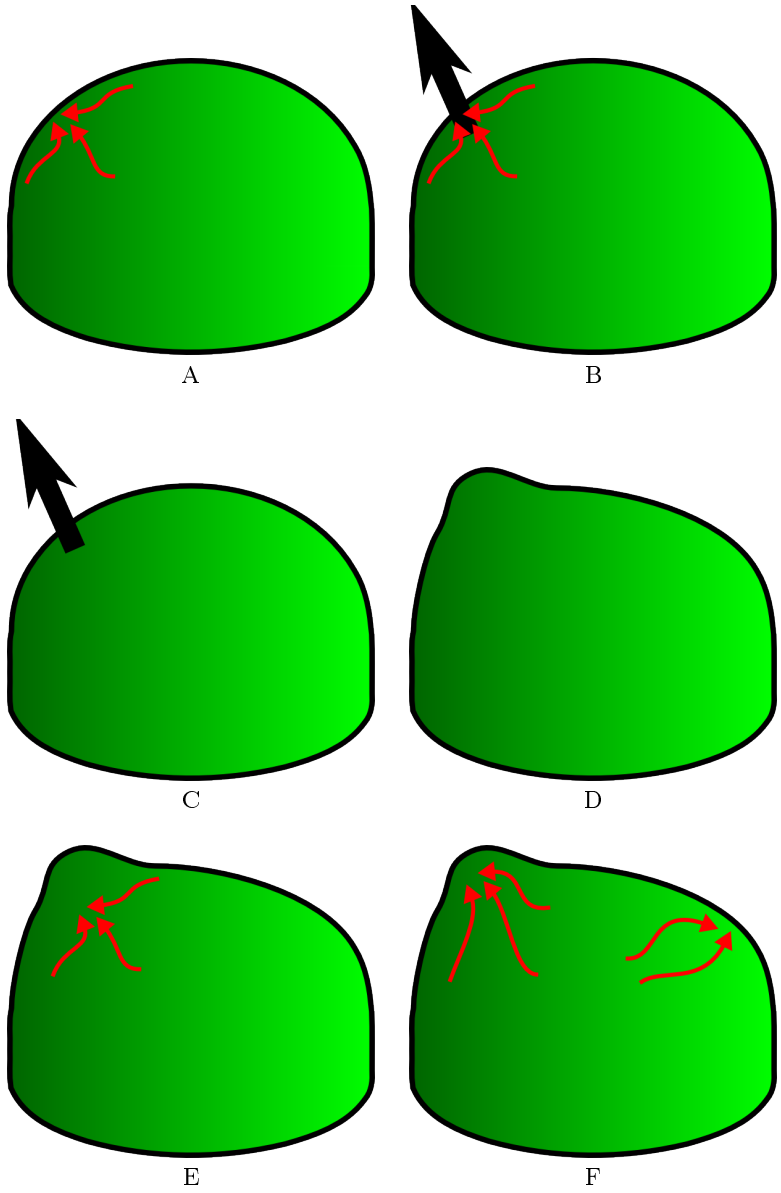

Figure 3.11: Feedback between the form and physiology on the example of auxin signalling in the SAM.
The red arrows depict the direction of fluxes of auxin, whereas the black arrows depict physical forces, leading to a change of meristem shape. Figure 3.11A shows the auxin fluxes converging in certain location l in the meristem. High auxin flux changes the properties of the cell walls in the location l (figure 3.11B). Since the cell walls in location l are loosen (figure 3.11C), they are deforming easier, which leads to a formation of a bump (figure 3.11D). The change of the form of the meristem, influences the auxin fluxes (figure 3.11E), leading to their reconfiguration (figure 3.11F).

tration in these cells. Therefore, for each edge e in the cell c the constant G_e is an auxin dependent function:

$$G_e = \alpha \left[IAA\right]_c$$

where α is a growth intensity constant. In the simulations auxin is distributed using the model described by Jönsson et al. [2006], therefore a *concentration-based* mechanism of PIN allocation is used. This framework together with the mechanical-based growth model allow us to build up a phyllotaxis model (comparision of the auxin growth dependent model with non-dependent one is presented in figure 3.12).

It was possible to maintain the long and stable development of meristem. During the simulations short series of consecutive primordia were following spiral phyllotaxis patterns, however it was impossible to obtain stable phyllotaxis (figure 3.13).

The growth in this physical-based is less regular than the descriptive growth used in the model described in Chapter 2. It is one of the reason why regular, stable phyllotaxis patterns are not observed. However, in real *Arabidopsis* plant the precision in primordia placement is limited to approximately 15^o (360 divided by approximately 24 cells). Thus, a robust mechanism is needed to initiate and maintain phyllotactic patterns in spite of a relatively large departure in the placement of individual primordia from their mathematically ideal positions. It is possible that in real plants phyllotaxis is not governed by a single mechanism, but represents a combined effect of several factors. This complexity may be required to generate phyllotactic patterns in the presence of noise. The problem of generation of phyllotactic patterns in the context of an irregular geometry was not studied until now.

3.6 Conclusions

The mechanical behaviour of an organism depends on the physical properties of the individual cells. In plant cells, these are largely determined by the interaction between the turgor pressure and the cell wall. However, knowledge about the structural function of the cytoskeleton in these cells requires further investigation. The availability of more structural and mechanical data should allow us to establish new and more realistic biomechanical models. The challenge will be to integrate all mechanical components and thus contribute to the understanding of development from a mechanical point of view.

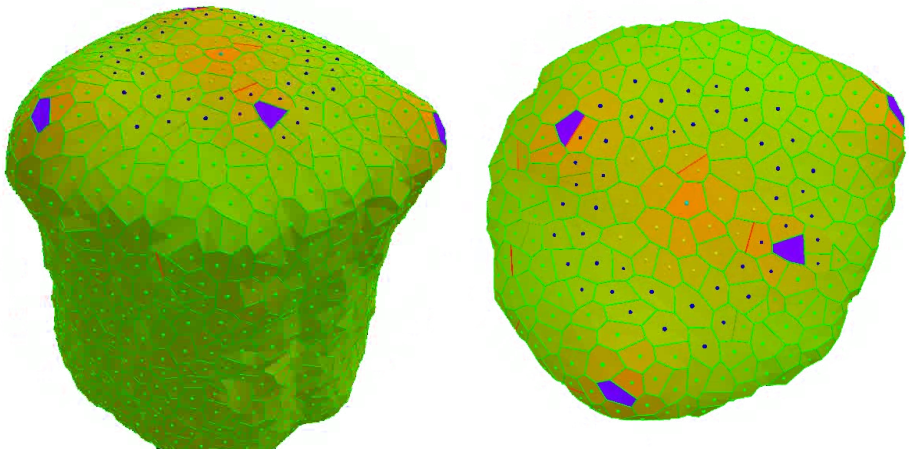

A B

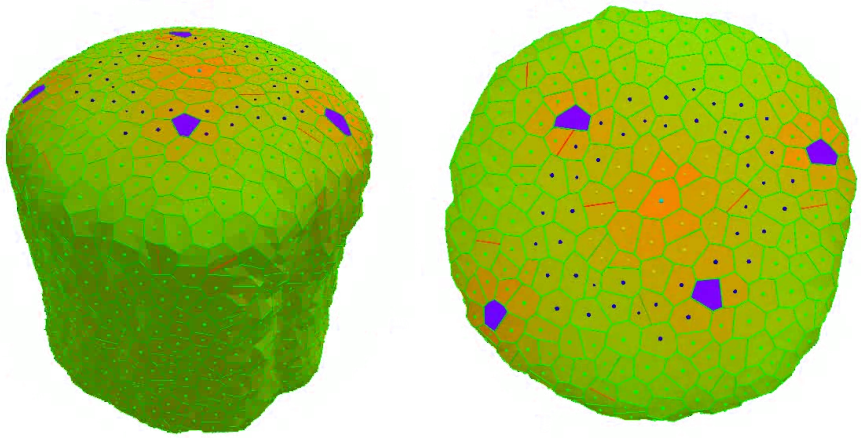

C D

Figure 3.12: Simulations with feedback between the auxin concentration and mechanics.

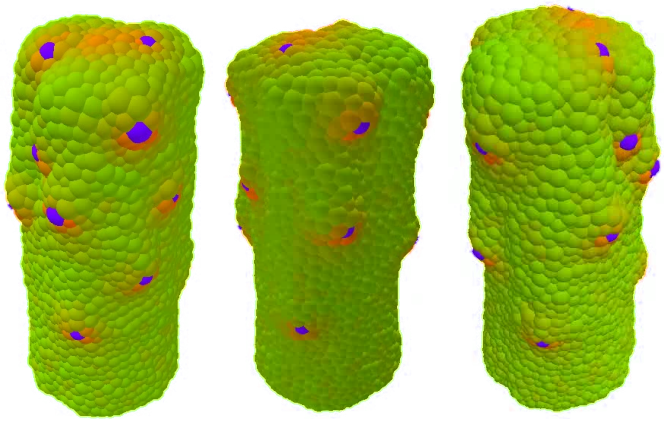

Figure 3.13: Developed *in silico* meristem modelled with the feedback of auxin on the growth.
The auxin transport is modelled using *concentration-based* mechanism. Unstable phyllotaxis is observed. Figures 3.12A and 3.12B show the meristem with 4 developed primordia without mechanical interaction between the growth and auxin transport. Figures 3.12C and 3.12D show the same simulation, however the feedback of auxin concentration on growth speed is present. In this case we can observe, that the primordia have bigger outgrowth.

Modelling only surface cells with 1D walls as springs is an efficient way to address meristem shape modelling. It allows for fast computation of the emergence of various meristem shapes when testing different parameters of this complex system. However, this approach has also important disadvantages.

From a mechanical point of view, cell walls in plants play an important role in the ability to resist not only tensile stress, which allows for the establishment of the turgor-based hydroskeleton. Secondary cell walls, typical for sclerenchymatic tissue, are constructed in a way to resist also compressive stress. In this case, the living protoplast and thus the turgor are dispensable for the cell's mechanical functioning and fully differentiated cells are often devoid of any cell component other than the cell wall [Geitmann and Anja, 2006]. The implicit representation of the inner cells as a generalised pressure makes it difficult to simulate the compression forces and thus, to generate more complex shapes, which may require compressive stress to form. For example, to model a crest instead of a bump using the MSS framework we need to explicitely represent the interior of the meristem, since the compression forces are important for this type of development (figure 3.14).

The use of MSS becomes also less straightforward when dealing with more complex deformations, like the young carpels formed by the *Arabidopsis* flower. The

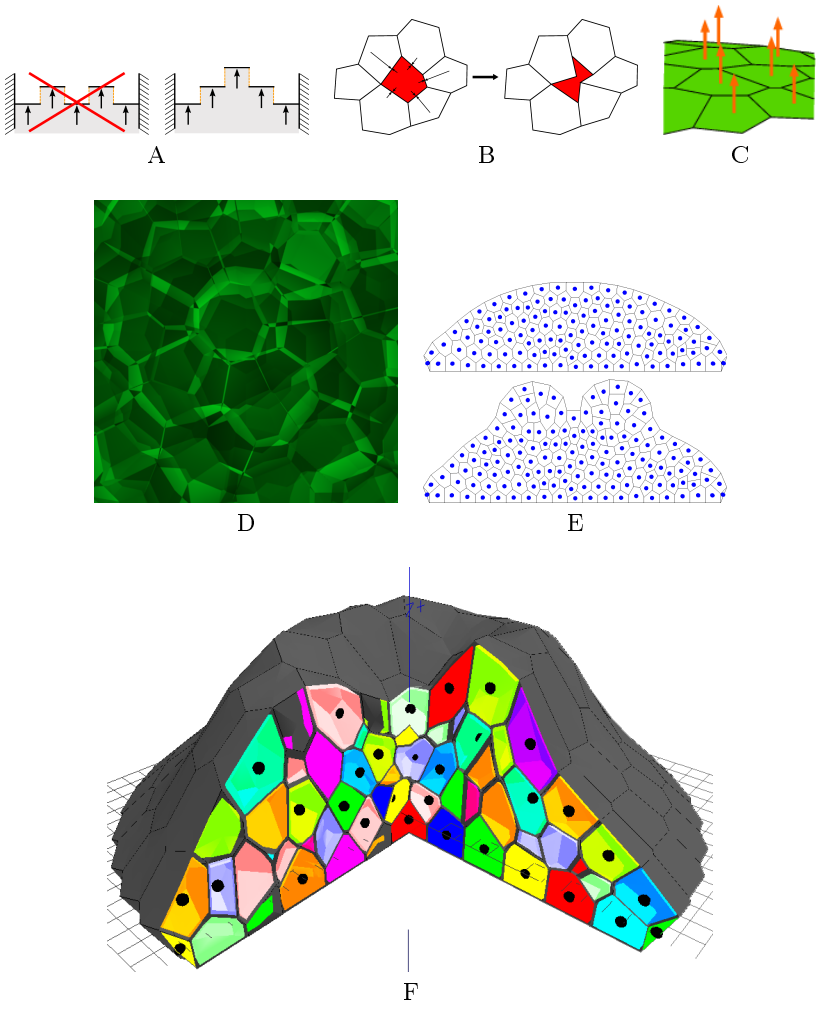

Figure 3.14: Issues with modelling complex shapes with MSS.
Figure 3.14A shows solid bars (horizontal segments, in black) are linked by elastic springs (vertical segments, in yellow). Extremities of the system are fixed. A pressure applied from bottom on the system will push all the bars to top. Crest formation is thus impossible. The red cell in figure 3.14B collapses due to the load of its neighbours. The explicit L1 layer representation (green polygons) with implicit inner cells (represented as pressure force – orange arrows) in figure 3.14C. Figure 3.14D shows 3D meristem representation where cells appear as polyhedra. Representing each cell wall by a set of springs is cumbersome. Figure 3.14E shows a simulation of carpel development. From an initial state (on top) with a bump shaped meristem, the simulation runs to a crest shaped tissue (on bottom). Figure 3.14F shows 3D representation of the final state of the simulation showing the development of the *style tube*. Carpel simulations were performed by Jerome Chopard.

carpels arise as a cylindrical shape on the top of the floral meristem. During the carpel development, some cells grow out more quickly than their neighbours, which is caracterized by a more rapid extension of the cell walls in the model. Dealing with a 3D MSS representing this type of development is a cumbersome task.

Simulations of phyllotaxis implemented on the shoot apex with physically-based growth require considerably more computation time than the simulations using descriptive growth described in Chapter 2. This is because each growth step requires that the mechanics simulation be iterated until equilibrium is reached. The relaxation method provides improvement of this situation, however the time required for growth steps is always longer than in the simulation with descriptive growth.

Despite this drawback, the physically-based models of the shoot apex and young developing primordia presented here provide a good framework for further work. One of the strongest point of physical-based approach is the straightforward way to add growth tropisms and model the emergence of complex shapes. This allows us to model objects which are not only radially symmetric, but develop into leaves, flowers, or other organs. Providing a descriptive model of growth for such shapes is a cumbersome task. Overally, physically-based model of the shoot apex provides an interesting platform to study the mechanisms of primordium boundary definition, including the possible gene-mechanics interactions.

Chapter 4

Computer representation of tissue

4.1 Dynamic systems with dynamic structures

4.1.1 Dynamic systems

A concept of a *dynamic system*[1] is a mathematical formalisation for describing system evolution in *time*. Time can be measured by integers, by real or complex numbers or can be a more general algebraic object without any relation with its physical origin. At any point in time, a dynamic system is characterised by its *state*. The state is represented by a set of *state variables*. Changes of the state over time are described by a *transition function*[2], which determines a next state of the system as a function of its previous state and, possibly, values of external variables (called *input* to the system). This progression of states forms a *trajectory* of the system in the *space of states*.

Many natural phenomena can be modelled as dynamical systems, for example, a motion of mass point on a spring. In this system, where phase space describes all possible position of a mass point, a state variable is the current position of the mass point, and inputs are mass and elasticity constant of a spring, and transition function is given by Hook's and Newton's Law equations [Carr et al., 2008]. If we assume no friction and dumping, solving the equation of transition function makes it possible to describe the trajectory of the system in an *analytic form* (in this example it will be a sinusoidal function). Unfortunately, in more

[1] This chapter is based on Giavitto et al. [2002], Giavitto and Michel [2003], Prusinkiewicz.
[2] or *evolution function*

complex cases, analytic formula representing trajectories of the system may not exist. In such cases, the behaviour of the system can be studied using computer simulations. However, dynamical systems often describe objects having a complex structure thus, it is desired to include this structure in the formal system description.

4.1.2 Structured dynamic systems

If a dynamical system can be decomposed into parts, the change of a state of the whole system can be viewed as a result of an advancement of all states of its components. Formally, we use a term *structured dynamical system*[3] to denote a dynamic system divided into *component subsystems*. The set of state variables of the whole system is then the Cartesian product of the sets of state variables of the component subsystems. Accordingly, the state transition function of the whole system can be described as the product of the transition functions of these subsystems.

In many cases, the transition function of each subsystem depends only on a subset of the state variables of the whole system. If the components of the system are discrete, these dependencies can be depicted as a *directed graph* with the nodes representing the subsystems and the arrows indicating the inputs to each subsystem. We say that this graph denotes the *topology* of the structured dynamical system and call *neighbours* the pairs of subsystems directly connected by arrows.

4.1.3 Dynamical systems with dynamic structures

Let us consider a dynamical system in which not only the values of state variables, but also the set of state variables and the state transition function changes over time. This can be captured using an extension of structured dynamic systems, in which the set of subsystems or the topology of their connections may be an argument for the transition function. We call these systems *dynamical systems with a dynamic structure* or $(DS)^2$-systems in short Giavitto and Michel [2003].

The development of an organism can be expressed with $(DS)^2$-system. We assume that the organism is modelled using a structured dynamic system, where each cell is a component subsystem. Firstly, the organism is composed of a single cell, which becomes larger and divides into two daughter cells. This

[3] or *dynamical system with structured state.*

process continues, until a mature, multicellular organism is build. To capture this development, a number of component subsystems must grow in time. Let us assume also that i) the cells can move in the medium ii) two cells are neighbours, if they are sufficiently close to each other iii) the state of a single cell depends on the state of its closest neighbours. Therefore, the movement of cells constantly changes the topology of the system. The constant change in the number of component subsystems and their changing topology require to model a $(DS)^2$-system to capture the system evolution.

From the computer science point of view, simulation of $(DS)^2$-systems raises the problem of finding a programming methodology well suited to the specification of such systems. The key difficulty is that, in $(DS)^2$-systems, not only the values of variables that describe the system, but also the entire set of variables and its topological organization and equations that relate them, change over time. If the number of these changes is small, they can be specified explicitly. In general a formalism that supports these changes in an automatic manner is required.

4.1.4 Meristem tissue as $(DS)^2$-systems

A meristem tissue can be seen as a multicellular, constantly growing medium. If we additionally assume, that the number of cells increases during this growth, the meristem modelling requires dealing with $(DS)^2$-systems. The consequences of this fact are therefore studied further in this thesis in respect to data structure design (4.2) and to the modelling of the study of meristem physiology (A).

4.2 Tissue representation

Modelling a complex system such as vegetal meristematic tissue requires developing specific data structures. This data structure must be adjusted for the system dynamics (e.g. development vs steady-state morphogen simulations), scale (e.g. root-shoot interaction vs cellular-level shoot simulations), accessible information (e.g. model parameters derived from measurements vs. invented parameters validated *a posteriori*), available resources (e.g. parallel/distributed computing vs local computing paradigm). As described in the goals of the thesis, my main modelling targets are:

- modelling of cell signalling with focus on auxin transport at the scale of meristem,
- modelling of meristem development with focus on the feedback between the shape changes and the physiology.

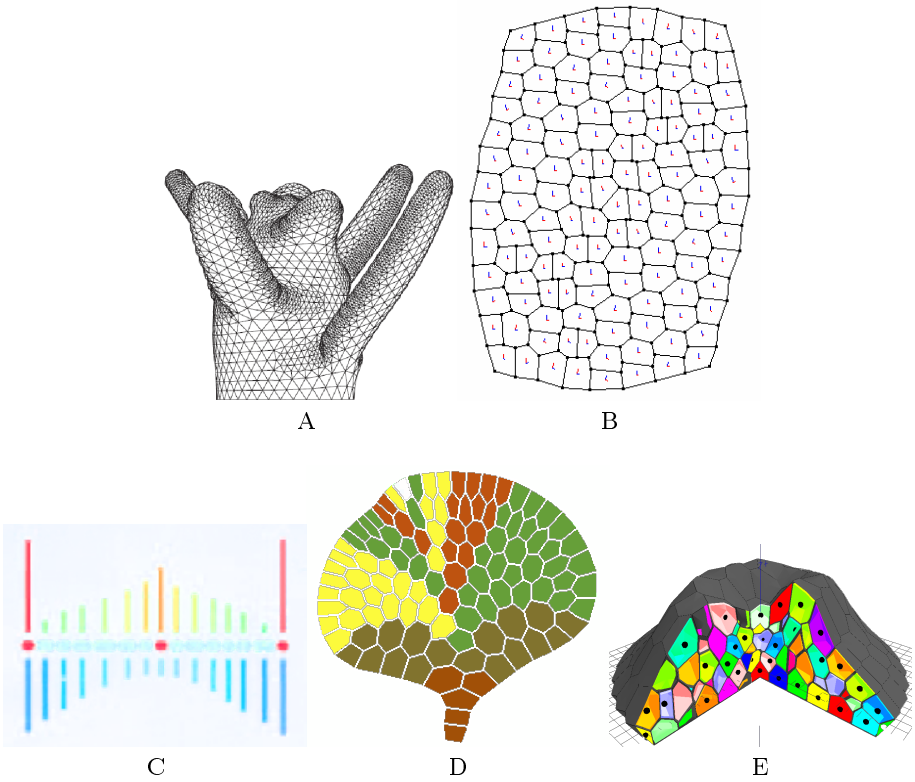

Figure 4.1: A classification of different tissue representations. Figures 4.1A, 4.1B show the examples of continous and discrete tissue representations respectively (figures taken from Smith et al. [2006a], Rudge and Haseloff [2005]). Figures 4.1C, 4.1D, 4.1E show examples of tissue representations containing 1,2,3-manifold cell topology respectively (figures taken from Coen et al. [2004], Prusinkiewicz and Lindenmayer [1990], Stoma et al. [2007]).

The models in this thesis are mechanistic, fairly abstract, giving rather qualitative than quantitative results concerning the reality. The simulation are held at a cellular level and they are usually executed in a local, single processor environment. Since the structure must account for the simulation of $(DS)^2$-system, it is required that tissue editing operations are performed efficiently.

4.2.1 Tissue models

Modelling of vegetal tissues is a frequent task in contemporary plant biology. It requires developing specific data structures thus, this is a frequently analyzed issue. Despite this fact, this problem does not necessary have a unique solution: the tissue representation must be properly adjusted to various applications,

which are usually diverse.

4.2.1.1 Continuous and discrete tissues

Vegetal tissue representation may be based on global or local point of view. Both concepts are established on two different views on living organism: the *cell* and the *organismal* theories Kaplan and Hagemann [1991].

In the first case a tissue is considered as a *continous* volume, where cells are providing the compartmentalization of this structure. It is called *continous* representation. This approach was used in a Smith et al. [2006a] model showing a SAM development with a formation of primordia (figure 4.1). The tissue was represented as a mesh and growth was achieved by the insertion of new mesh faces (more faces were inserted in the primordia locations leading to the outgrowth of bumps). It is important to note, that the subdivision into cells was not required in this model, since the author assumed that primordia placement is governed by a global mechanism and not local one.

In the second case it is assumed, that a set of autonomous cells forms a tissue. Each cell grows and develops independently. However, cells might exchange information (e.g. by cell signaling) and interact (e.g. by mechanical constraints). This communication provides a synchronization at tissue level. The tissue development is a result of the integration of the development of all cells. This approach is used in the model presented by Rudge and Haseloff [2005] based on a self-reproducing cell, which has a dynamically changing state and geometry (figure 4.1). In this particular model, cell signaling is simulated by diffusion of morphogens and genetic regulation. These processes could be specified by a script program. The model provides a platform to explore coupled interactions between genetic regulation, spatio-mechanical factors, and signal transduction in multicellular organisms. The cells are modelled as 2D polygons with elastic properties (the cell walls are simulated by springs). Growth is achieved by changing springs parameters. The cell growth and cell division algorithms are based on biological observations (e.g. each cell has a main axis of growth and a cell divisions occur accordingly).

The continous approach is especially useful when the modelled process is global and its source does not lay in the interactions between the cells. In this case, the cell structure still can be accessed when required, however its access might be an expensive operation. The discrete approach has advantages over continuous one in the cell-based, mechanistic models. In such models it is often required to access cells frequently, because cells works like agents* and require communication. One of the difficult issues resulting from this type of representation is

the integration of the interactions (e.g. in the case of growth: if cell A grows isotropically and its neighbour cell B grows anisotropically, how does the cell wall between A and B grow?).

4.2.1.2 Topological structure of the tissue

The second criterion of the classification might be the type of cell neighbourhood relation in the data structure (called *cell topological structure* of the tissue). In the simplest case the representation does not contain any topology. Tissue representations based on *sets* or *multisets* are good examples. In such a representation each cell is an element of the set. The elements are not ordered by definition thus, no relation between them is assumed. This representation is useful when the cells are simply assumed to be aggregated.

A second type of representation is based on a simple, sequential cell topological structure, like *lists*. A good example is the model of *Anabema* presented by Lindenmayer [1968], Prusinkiewicz and Lindenmayer [1990] (figure 4.1). In this model, the authors study a theory of growth for filamentous organisms. They considered *in silico* treatments where inputs are received by each cell from both directions along the filament and the change of state and the output of a cell is determined by its present state and the two inputs it receives.

Another representations are based on cell topological structures allowing to describe neighbourhood in one layer of cells, like *branching structures* (e.g. based on L-systems) or *planar graphs*. An example of a representation based on branching structure is a model of the fern gametophyte *Microsorium linguaeforme* proposed by Prusinkiewicz and Lindenmayer [1990]. This representation, based on *map L-systems*, enables to simulate the development of the apical cell of the gametophyte. It divides repetitively, giving a rise each time to a new apical cell and a primary (initial) segment cell. The segment cells subsequently develop into multicellular segments. The division wall of an apical cell is attached to the thallus* border on one side and to a previously created division wall on the other side (figure 4.1).

Another class of models uses topological structures which are able to express any cell neighbourhood found in plant tissues (e.g. *graphs*). An example of this approach is a model of a carpel of *Arabidopsis thaliana* proposed by Stoma et al. [2007]. In this model, all cells are represented as polyhedra. It is assumed that each wall between two cells remains planar and therefore, it is represented as a polygon in space. The model uses the shell theory to compute strains and mechanical constraints in the meristem with a finite elements method (figure 4.1).

Using topology is required for algorithms that deal with the information exchanged between the cells (e.g. cell signalling, diffusion of morphogens, etc.). More general topology (i.e. allowing to express any type of cell neighbourhood) requires more complex data structure, and as a consequence, often the algorithms with higher complexity.

4.2.1.3 Connection between cell/wall geometry and cell/wall topology

Another criterion of classification might be the type of the link between cell/wall geometry and cell/wall topology used in the tissue representation. Usually, it is possible to compute topologies from geometries and vice versa. The main drawback of such an approach is the error introduced while this computation and its computational complexity. However, representing explicitely all topologies and geometries makes the structure cumbersome to modify, since the synchronization of cell/wall topology/geometry after a change in the tissue (e.g. cell division, cell removal, etc.) is required.

Representations without both geometries First class of representations do not include any explicit geometry. If necessary, the cell or wall geometry can be *imposed* or *computed*. An example of this approach is a model of *Anabema* presented by Lindenmayer [1968], Prusinkiewicz and Lindenmayer [1990], already mentioned before. In this model the cell geometry is necessary only to provide the visualisation of the development of the organism. It is imposed on the system by regular positioning of the consecutive cells (in topological sense) on the file of rectangles [Prusinkiewicz and Lindenmayer, 1990].

This approach is used in the models which do not require exact geometry, because when geometry is inferred from cell/wall topology a certain error appears. Computing of geometry might be also expensive algorithm. One of the biggest advantages of this approach is the simplicity, since it is required to store only topological information

Representations without wall geometry An example of a structure, which does not include the wall geometry is included in the Cellerator framework Shapiro and Mjolsness [2001], Shapiro et al. [2003]. The structure is designed to describe single and multi-cellular signal transduction networks (STN). Multi-compartment systems are represented as *graphs* with STNs embedded in each node. Interactions include mass-action, enzymatic and allosteric models. Reactions are translated into differential equations and can be solved numerically

to generate predictive time courses or output as systems of equations that can be read by other programs. It is important to note, that using a system of properties it is possible to extend this representation to include wall topology.

Representations without cell/wall topology Another class of representation dual to the previous one, does not include the topology at all. When the topology is required, it is *computed* from geometry. An example of this approach is the general representation based on polygons or polyhedra proposed by Lück and Lück [1983]. The cell and wall topologies in this representation is inferred from the contacts between geometrical objects (polygons in 2D or polyhedra in 3D).

Another example of structure, where the cell and wall topology is computed is the one proposed by Bodenstein [1986]. In this method the topological neighbourhood is assumed for every pair of cells (represented as disks), when the distance between their centres is smaller than given neighbourhood constant. This approach was extended by Jönsson et al. [2006], where the cells are represented as spheres. It is important to note, that this concept allows the authors to model L1 layer of 3D, volumic cells in the meristem, using simple, *planar graph-based* cell topological structure.

An alternative approach was proposed by Sulsky et al. [1984], where the both wall geometry and topology is computed using the Voronoi diagrams. In their model, Voronoi diagrams are introduced as a suitable representation for a two-dimensional cell sheet. These polygons are defined in terms of a finite number of points, making numerical simulations tractable. Cells can change their neighbours and shape in response to deforming forces without leaving gaps in the tissue. Using this representation allowed the authors to simulate the rounding of uneven tissue and engulfment of two intact tissues. The Voronoi-based approach is also used in multiple works by Honda et al. [2004].

In this approach cell/wall topology and wall geometry is computed on demand based on cell geometry. This is usually less efficient then the usage of explicit topological structure, thus this approach is not recommended for models strongly dependent on topological algorithms. Also, this approach may lead to the issues with structures dynamically changing in time (e.g. cell sliding, changes is wall. Similarly to representation without geometry, one of the main advantages is the simplicity, since it is not required to synchronize the the geometrical representation with the topological one.

Representations with topology and geometry Another class of representation uses in parallel both geometrical and topological structures. An example

of this approach is already described model by Rudge and Haseloff [2005], where the cell geometry is stored in a graph of walls and the topology in a graph of cells. A similar approach is used in Smith et al. [2006c] representation, whose model is used to simulate auxin fluxes in growing shoot meristem. The cell topological structure in this model is expressed in the VV environment [Smith et al., 2006a], which ease the manipulation of 2-manifold topology in growing object. This representation allows the authors to simulate L1 layer of shoot apical meristem cells as a mesh.

This approach makes it possible to have an efficient access to both, topological and geometrical structure. There is no additional error resulting from computation of these substructures. It is, though, required to synchronize both structures, which can be a difficult task.

4.2.1.4 Recent SAM representations

Particulary interesting in the context of this thesis are representations proposed to model the development of SAM. Recently, three such a data structures were proposed.

Jönsson et al. [2006]: The cells are modelled as spheres, with centres laid dome-like shape (described by half sphere glued to a cylinder). The cells are considered as neighbours, when they overlap. Only the epidermis of the meristem is considered.

The growth is modelled using mechanics. The centres of each pair of neighbouring cells are connected with a spring which rest length depends on the sum of the radii of the spheres. Thus, the springs are exerting forces repulsing the cells from each other. This repulsion process results in overall cell movement from the meristem centre (the centre of the half-sphere) to the periphery (bottom of the cylinder). The radius of each sphere is constantly increasing. A cell divides, when it reaches a certain volume.

This representation results in unrealistic cell behaviour (e.g. like cell walls sliding on each other or empty space appearing between the cells).

Smith et al. [2006c]: The cells are modelled as 2D polygons building up a mesh. The representation uses VV language as a paradigm [Smith et al., 2006a] to deal with $(DS)^2$ systems. Only the most external cell walls are modelled explicitly. These walls form a hyperbolic, dome shaped, polygonal surface with "bumps" located in the places of primordia.

The growth of the cells is the result of moving polygon vertices on the surface away from the centre of the tissue. The cell divisions are performed using the algorithm proposed by Nakielski [2000].

In this representation both cell growth and proliferation were calibrated with biological data gained from the study of development of *Arabidopsis*.

Barbier [2005]: The cells are modelled using Voronoi domains in 2D.

The growth of the SAM is simulated using mechanical model. Centres of each pair of neighbouring cells are connected with a spring pushing them away. The main flaw of the model, mentioned by the author, was unrealistic cell behaviour (after cell division closely cells might change their neighbours, which does not occur in the SAM).

4.2.2 WalledTissue structure

One of the main goals of this thesis was to perform various *in silico* experiments concerning in particular auxin transport and growth issues. This task required to develop computer programs and to perform simulations. The code developed during this thesis is available as an OpenAlea module [Pradal et al., 2008], called `mersim`. One of the key components of this package is the data structured used to model tissues. This structure is called WalledTissue and is described in this chapter.

The structure is an example of discrete representation, since the cell interactions are one of the key elements of the performed simulations and it is important to execute them efficiently. The structure uses a planar graph to store cell topology, which makes it possible to represent a one layer of cells in 3D space. This property is used in physical-based simulations, where the tissue shape is deformed by various forces. The structure contains explicit cell wall topology and geometry, which has two main advantages: *i*) cell geometry is exact and no approximation error is present *ii*) the structure allows for fast access to cell and wall geometry, allowing for fast computation of deformations. These properties are useful in the simulations focused on development. The exact cell wall geometry makes it possible to simulate simplastic* growth and avoids the introduction of non-realistic cell behaviour (e.g. sliding cells, changes in cell neighbourhood). Fast access to cell wall geometry allows for easy integration of the structure with particle solver (this property is intensively used in the physical-based simulations). In the particle solver cell wall vertices are treated as particles and their displacement is computed from the forces.

4.2.2.1 Data digitising

The *in silico* models within `mersim` module can be build on the basis of real meristem images. The digitising is semi-automatic. Two different protocols are possible to acquire the data from images: one based on a Merrysim software developed by Pierre Barbier Barbier [2005] and the second one based on the CellTissue software developed by Jerome Chopard. The first protocol requires to use a dedicated "tissue edition" software, whereas for the second one, it is necessary to use third party software, which is able to export the figure in SVG format (e.g. Inkscape).

Briefly, both methods involve the following steps. Firstly, the membranes of the individual cells are identified on the images. This information is used to automatically reconstruct a graph, where the nodes represent the cells, and the edges describe the cell neighbourhood relation (details in the next section).

Secondly, any required number of additional relation can be specified. These relation must be a subset of cell neighbourhood relation. These relations are used in the models described in this thesis e.g. to simulate active transport of auxin mediated by PIN.

Thirdly, a specific information describing the properties of virtual tissue is added. This mechanism is used in the models described in this thesis e.g. to describe the identity of cells in virtual tissues (to specify initial or boundary conditions for simulations). A short comparison between these protocols is given in the table 4.1.

Here I demonstrate the example code required for tissue initialization starting from Merrysim tissue presented in figure 4.2:

```
# using default properties, removing all default cell properties
const=TissueConst()
const.cell_properties ={}
# reading tissue
tissue = read_walled_tissue( file_name="/home/stymek/mdata/08-12-05-2cell", const=const )
# displaying tissue (see figure 4.2)
tissue_visualization(tissue, "pylab_graph", show_wall_ids=True)
tissue_visualization(tissue, "cells_with_walls", cell_color=Green, wall_color=Black)
```

4.2.2.2 Structure core

The representation was designed to store vegetal tissues, in which the cells can not move, contrary to their animal counterparts. The geometry of each polygonal cell is described by explicit walls (i.e. they correspond to the projection of

Property	Merrysim	CellTissue
Interface of cell editor	Identification of cells requires a dedicated software. The interface of this software is well adjusted to the task, however it requires a process of learning.	Identification of cells requires any software able to write SVG files (e.g. Inkscape). In case when the user is used to editing SVG files, the interface does not require learning. Additionally, interface itself may provide useful features (e.g. copy, paste, undo, etc.).
Extensibility	The extensions require editing Merrysim code. It requires skills in C++ programming, however extensions may concern any aspect of tissue editing.	The extension possibility depends on the software. In the case of Inkscape it is possible. It requires skills in Python programming, however the extensions are limited by the Inkscape API.
3D reconstruction	Assuming that the image is acquired using confocal microscopy it is possible to use Merrysim software to acquire reproduce 3D information from the confocal stack of images.	No reconstruction is currently possible.

Table 4.1: Comparision of tissue digitalization protocols.

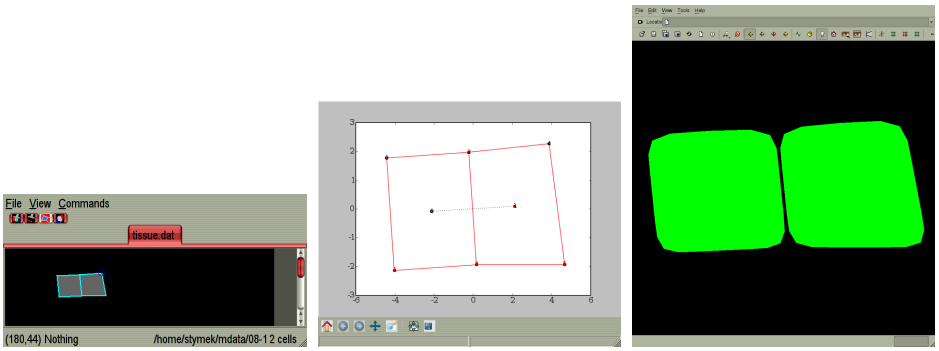

A B C

Figure 4.2: Tissue initialization using Merrysim protocol.
Figure 4.2A shows a screen shot of the `Merrysim` tissue editor in which two cells were created. Figure 4.2B shows a screen shot of tissue visualization in `PyLab`, whereas 4.2C an OpenGL visualization created using `PlantGL`.

anticlinal* cell walls). Internally, the data structure works on two complementary graphs: cell neighbourhood (C, N) and walls (V, W). The vertices of these graphs are called respectively *cells* (C) and *wall vertices* (V), and edges respectively *cell neighbourhood* (N) and *walls* (W) (figure 4.3). The wall graph is linked with an object describing *wall* geometry, which allows for explicit access to *wall vertex* coordinates.

Special operations are provided to operate on tissue. Let us assume that: $c \in C, v \in V, n \in N, w \in W$. Each subgraph of the structure can be inspected with standard graph API (e.g. `neighbours(`$c \vee w$`)`, `degree(`$c \vee w$`)`, `edge(`$c1, c2 \vee w1, w2$`)`, etc.). Additionally, two new operations, executed in constant time, are added to the structure to make it possible to explore the relation between the graphs (and therefore the *cell* to *wall* relation):

Operation	**Time**	**Description**
`cell_shape(`c`)`	$O(1)$	Returns an ordered list of *wall vertices* v surrounding a cell.
`wv2cells(`v`)`	$O(1)$	Returns a list of *cells* in which *wall vertex* v is present.

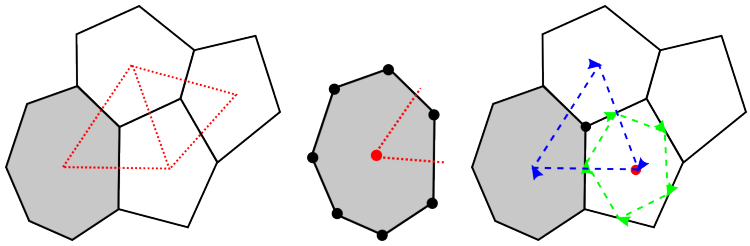

Figure 4.3: The tissue representation in WalledTissue structure.
The figure 4.3A presents *wall* graph (in black) and *cell neighbourhood* graph (in red). The figure 4.3B presents different elements of graphs: black circles depict *wall vertices*, red circles depict *cells*, red lines depict *cell neighbourhood*, black lines depict *walls*. The figure 4.3C presents the relations between *wall* graph and *cell neighbourhood* graph. Each *wall vertex* has an access to ordered *cells* which it belongs to. Each *cell* has a list of ordered *wall vertices* which describe its shape.

These are key operations of the tissue representation. After each modification of the graph the data structure updates itself to keep the `cell_shape` and `wv2cells` working.

The mutation of the structure assumes that only dedicated operations are allowed:

Operation	**Time**	**Description**
`remove_cell`(c)	$O(C)$	Removes *cell* from cell neighbourhood graph (and all its *wall vertices* from the wall graph if they are not a part of other cells).
`divide_cell`($c, w1, w2$)	$O(C)$	Replaces the *cell* c with two cells connected by a new *wall* w. The *wall vertices* of w "belong" to $w1, w2$. Requirement: $w1, w2 \in c \bigwedge w1 \neq w2$

After initialization (which can be performed as described in 4.2.2.1), tissue is augmented by performing `divide_cell` and decreasing by `remove_cell` operations. An example of `divide_cell` operation performed on a single cell is

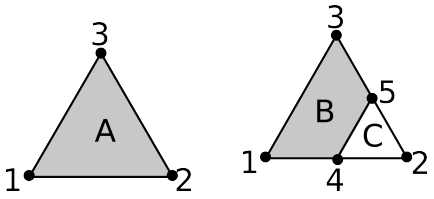

Operation	Before (figure A)	After (figure B)
cell_shape(A)	[1,2,3]	-
cell_shape(B)	-	[1,4,5,3]
cell_shape(B)	-	[4,2,5]
wv2cells(1)	[A]	[B]
wv2cells(2)	[A]	[C]
wv2cells(3)	[A]	[B]
wv2cells(4)	-	[B,C]
wv2cells(5)	-	[B,C]

Figure 4.4: Operation of topological cell division.
Figures present a result of `cell_shape` and `wv2cells` operations in WalledTissue structure presented before (4.4A) and after (4.4B) a division `divide_cell`$(A,(1,2),(2,3))$. Since the changes in cell neighbourhood graph (CNG) and wall graph (WG) are explicitely visible on the figure, thus their description here is omitted.

presented in figure 4.4.

Here I demonstrate an example of code modifying previously read tissue. Firstly, 50 cell division operations are performed (according to two different geometrical strategies) and they are followed by 25 cell remove operations. Results are presented in figure 4.5.

```
tissue2=tissue.copy()
for t in [tissue,tissue2]:

    for i in range(50):


        # first cell from the tissue is selected for division
        # this cell changes in every step of iteration
        if t=tissue: strategy="shortest_wall"
        else: strategy="shortest_wall_with_shrinking"
        t.divide_cell(t.cells()[0], strategy=strategy)

    tissue_visualization(tissue, "cells_with_walls", cell_color=Green, wall_color=Black)
    for i in range(25):

        # a random cell is removed
        t.remove_cell(t.cells()[int(random()*len(t.cells()))])

    tissue_visualization(tissue, "cells_with_walls", cell_color=Green, wall_color=Black)
```

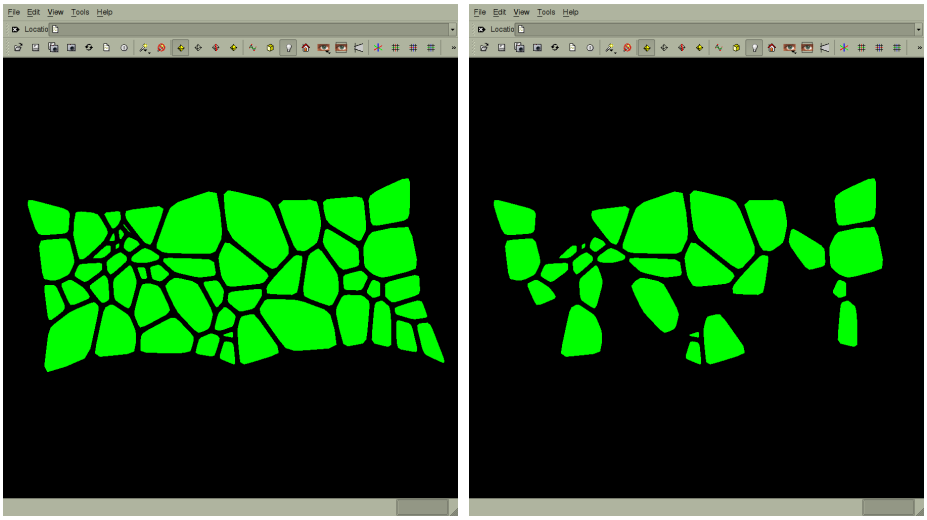

A B

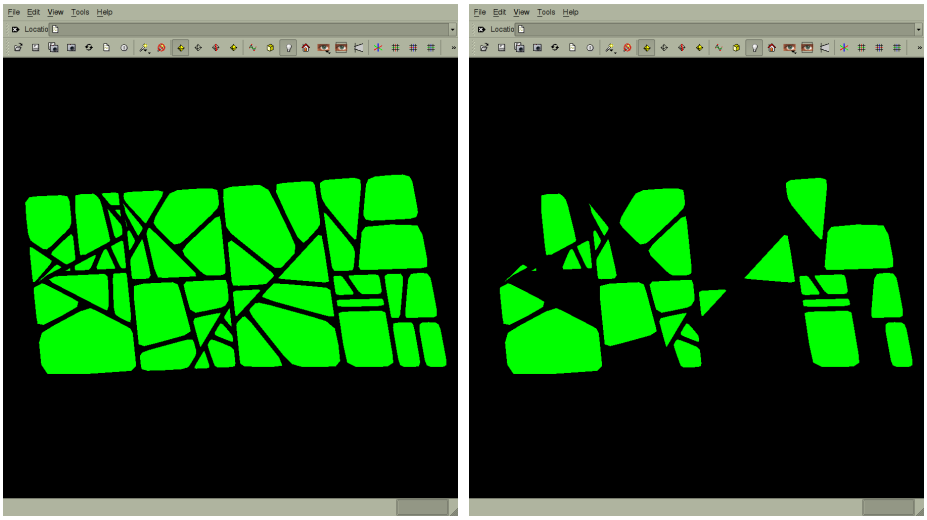

C D

Figure 4.5: A result of a series of cell divisions with different strategies followed by cell removal operation on the tissue presented in figure 4.2.
Figure 4.5A-4.5B show cell modified by cell division strategy "shrinking" the division wall, whereas 4.5C-4.5D uses the same cell division strategy, however no "shrinking" is performed. For additional information concerning "shrinking" please look in Nakielski [2000].

4.2.2.3 WalledTissue properties

While modelling tissue, it is often required to store different information concerning different attributes (e.g. *cell* identity, morphogen concentration in *wall*, *tissue* age, etc). WalledTissue contains a uniform system to manage its properties. Properties are specified for each type of object in the structure. They are accessed using a unified API. In the description `X` stands for *cell*, *wv* (wall vertex), *cn* (cell neighbourhood), *wall* and x for the identificator of an object:

Operation	Time	Description
`X_property`(x, p, pv)	$O(1)$	If pv is specified sets `X` x property p to pv, else returns the current value of p property for x.

Here I present an example of code changing the properties of the previously loaded tissue:

```
L1=[],wv_positions=[]
# the tissue was initialized in such a way that "L1_cell" is a valid
# property for every cell
tissue.cell_property(1,"L1_cell", True)
for i in tissue.cells():

     if tissue.cell_property(i, "L1_cell"): L1.append(i)

for wv in tissue.wvs():

     # wv positions are stored in "position" property
     wv_positions.append(tissue.wv_property(wv, "position"))

>>> L1=[1], wv_positions=[(1.0,2.0,1.0), ..., (5.0,3.2,1.0)]
```

Additionally, the structure API allows for selective properties save, load, import between tissues and script specified initialization. Properties are closely related with visualization, which can create properties dependent tissue visualization. Internally, the representation of the system of properties is based on hash maps*.

4.2.2.4 WalledTissue visualization

A common helper operation performed on tissue is its visualization. Mersim package defines a pack of strategies [Gamma et al., 1995] to provide different visualization of WalledTissue structure. For each type of graph element default geometry is specified (i.e. *Point* for vertices, *Segment* for edges), which can

be used as a basis of the visualization. Different views of WalledTissue were already presented in figures 4.2, 4.5. Additional visualizations are presented in figure 4.6.

4.2.3 Cell division algorithm

In most plants, a typical mature cell is surrounded by a cell walls. Because meristematic cells are "glued" together along their walls, plant organs grow symplasticaly [Erickson, 1986]. The symplastic growth is defined as coordinated growth of cells within the organ [Nakielski, 2000], where the neighbouring cells do not slide with respect to each other and the organ as a whole maintains its physical integrity. During such a growth, the cells are deformed (usually they also increase in volume) and new cells are formed by divisions (which can be viewed as replacing the parent cell by two daughter cells). It is important to note, that cell growth and cell division can be view as separated, superimposed processes. In this case, it is possible to define a cell division algorithm, which depends only on current tissue geometry (and does not need to take into account any previous developmental state of the tissue).

Cell division patterns are varying in different plant species, tissues, and even in different locations of the same organs (e.g. SAM) Kwiatkowska and Dumais [2003], Kwiatkowska [2004a,b, 2006]. Detailed studies of cell division patterns with respect to cell were not studied extensively in this thesis.

In the context of this thesis, the purpose of geometrical division is to keep the cell shapes in virtual tissue during development close to cell shapes observed *in vivo* in SAM tissue. Furthermore, to allow maximum generality, this operation is based only on geometrical factors (e.g. this is opposite to the algorithm proposed by Nakielski [2000], whose algorithm requires not only the geometry, but also a primary direction of cell growth) and works efficiently on meshes. In many approaches, algorithms describing growth and tissue geometry usually emphasize rules acting at the cellular level Prusinkiewicz and Lindenmayer [1990].

Both, topological and geometrical component of WalledTissue structure are updated by the algorithm. The update of topological component is an extension of the algorithm proposed in VV and can be found in the thesis of Colin Smith Smith et al. [2006a]. Original VV algorithm works on triangular mesh* and its extension used in WalledTissue works on polygonal mesh*.

They are two major questions concerning cell division in the tissue *i*) when does the cell divide? *ii*) how does the cell divide (figure 4.7)?

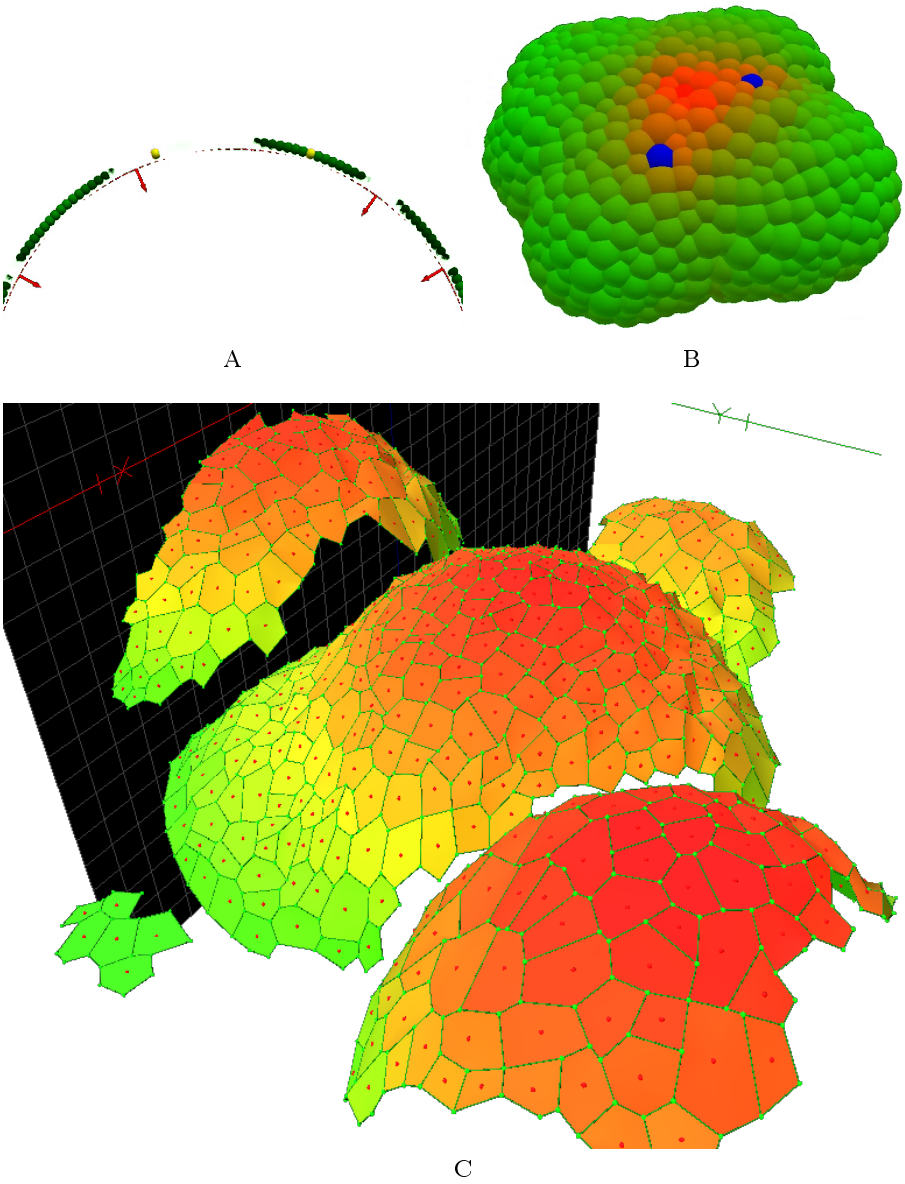

Figure 4.6: Different visualisation of WalledTissue structure.
Figure 4.6A shows 1-manifold tissue, with visualization imposing *cell* position. *Cells* are represented by spheres (colour depends on *cell* properties). Figure 4.6B shows 2-manifold tissue with 3D geometry, where growth was driven by mechanics (as described in 3), *Cells* are visualized again as spheres. Figure 4.6C shows a reconstructed tissue (using algorithm specified in 4.2.2.1), where *cells* are represented as polygons (color depends on z component of cell position) and *wall vertices* as small spheres.

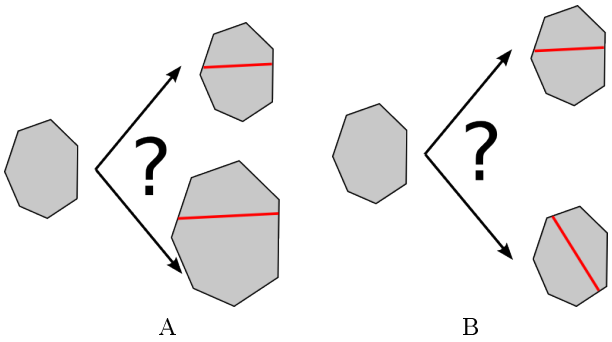

Figure 4.7: Questions concerning cell division.
When a cell should divide (figure 4.7A)? How a cell should divide (figure 4.7B)?

The first question is intuitively related to growth and cell age. Usually, in meristematic tissues a single cell grows during all its life and after being mature enough. Therefore, cell age and cell volume are proportional. The observations of meristematic tissues shows, that maximum area of L1 cells do not exceed 150% of average of these walls [Nakielski, 2000]. Therefore, a cell is chosen to be divided, when a critical value of its volume is exceeded.

The second question is more difficult to answer. It is reduced to the following problem: a cell is selected for the division. How a new cell wall (dividing the cell into two daughter cells) should be inserted? To answered this question we analysed cell division templates in real SAM tissue (figure 4.8). This inspection lead to the most common scenarios of cell divisions observed in the SAM:

1. the new wall is dividing cell into two new cells of similar volume (B, C),
2. the new wall is the shortest possible wall connecting dividing the cell into two parts and crossing the centre of the mass of cell (A,B),
3. the new wall is perpendicular to the old ones (A,C).
4. the new wall is formed in the middle of old walls (A, C).

These observations allowed us to formulate a different division strategies used in the thesis. The division algorithm is accessible through `mersim` module. The example of growth and cell divisions is presented in figure 4.9

4.2.4 Structure limits

WalledTissue can only be used for modelling structures with a mesh-like topology. However, an important question is whether this method can be extended

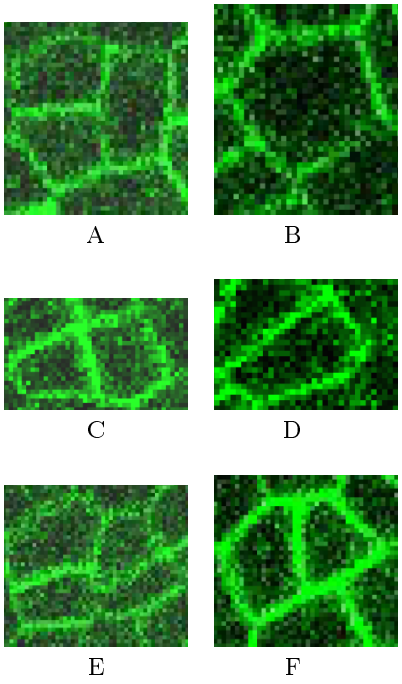

Figure 4.8: Illustration of common cell divisions patterns.
Images from Jan Traas.

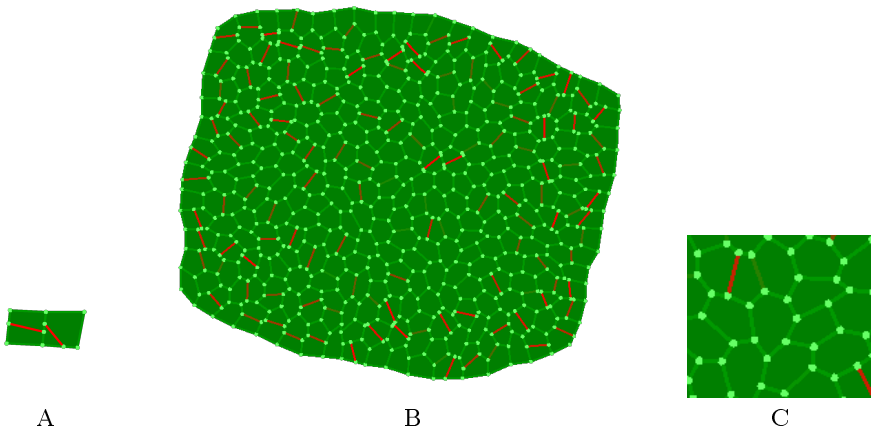

Figure 4.9: Cell division algorithm.
The system is initiated with 2 rectangular cells (figure 4.9A), After a period of growth and cell divisions number of cells increases (figure 4.9B). Zoom of the fragment of tissue shows, that *in silico* cell shapes are resembling real cell shapes (figure 4.9C).

to handle a wider class of topologies.

The volumetric tissue is an important example of structure which requires 3 manifold topology. Examples of such a representation are tetrahedral or cubic vertex sets or voxel structures.

WalledTissue requires, that the cell neighbourhood is defined in a rotational order i.e. for each set of cell neighbours we can define a cyclic ordering function. In a volumetric structure, a cell has a neighbourhood for which there is no obvious rotational order. In general, there is no obvious local ordering around a vertex in the non-planar case. However, it is important to note, that some specific cases can be handled. For example, a voxel structure always has six neighbours in the up, down and four adjacent positions. A simple neighbourhood ordering can be used when there is a fixed number of neighbours with a fixed orientation. Such a requirement imposes the regularity of the geometrical representation.

Some data structures were proposed for arbitrary discrete volumetric structures. Two examples are G-maps and the group-based fields used in MGS Giavitto et al. [2002], Giavitto and Michel [2003].

In the case of G-maps, the connectivity of each dimension of the structure is maintained with an arrays of arrays, each array containing arrays representing the next lower dimension down to a set of labels for dimension zero. At each modification of the connectivity, each level of arrays must be updated. For objects with more than one or two dimensions, the analysis becomes complicated. Moreover, G-maps are just a data structure, lacking operations to describe transformations to the structure (therefore efficient simulations of DS^2-systems require non-trivial structure extension).

Group-based fields in MGS can be used to describe any discrete structure of arbitrary dimension, provided that the user can come up with a group that describes the connectivity. It is technically possible to always find a group that describes the connectivity of a structure, however, doing so in practice is often difficult. It should be noted, that the examples provided in Giavitto et al. [2002], Giavitto and Michel [2003] mostly deal with planar cases.

Summary

Research contributions

The research presented in this thesis is focused on *in silico* experiments devoted to morphogenesis. One of the main objectives of this work was to make a step towards better understanding of the mechanisms governing the plant development and in particular, phyllotaxis. Frequently, the models presented in this thesis were able to verify common biological hypotheses, however sometimes they also raised new questions. Not surprisingly, many issues remain unsolved and should be the subject of future work. In this summary I extract the main scientific achievements of this thesis and in the end I propose a set of perspectives for future work.

WalledTissue data structure The tissue structure described in Chapter 4 provides a flexible, computationally inexpensive representation used to model virtual tissues (2.1), developing tip of the shoot apex with auxin fluxes (2.2), as well as physical based simulation of the SAM (Chapter 3), demonstrating the utility of this structure. This structure is a part of OpenAlea module `mersim`, which makes it easier to reuse and to share the code. The module includes various components (e.g. tissue constructors, cell division strategies, growth algorithms, tissue visualizations, transport and diffusion processes, etc.) thus, provides a framework for the study of tissue at cellular scale.

Exploration of *flux-based* auxin transport hypothesis I described our work on the *flux-based* concept introduced with the canalization hypothesis by Sachs [1969]. We revised models that demonstrated vein formation and showed some new properties of *flux-based* mechanizm. We showed that constant auxin synthesis allows for vein formation from sink to source, the concentration of auxin inside of a vein is not necessary lower than in the tissue and how to update the equation describing the transport to take into the account the geometry of

the tissue. On the example of vasculature regeneration, we showed that the flux-based mechanizm has the ability to dynamically reconfigure and adjust for the new conditions, which resembles the PIN reconfigurations observed in the L1 of the SAM.

Auxin-transport based model of phyllotaxis The *flux-based* patterning mechanism discussed in the previous section was inspired by experimental work aimed at understanding the development of vasculature. Since the molecular basis for the *flux-based* mechanizm is hypothesized to involve the same components as the transport-based mechanizm required for phyllotaxis, we decided to check if the *flux-based* polarization is a plausible candidate for the patterning mechanizm in the L1. We adapted the *flux-based* model to the SAM and followed the conceptual model of phyllotaxis proposed by Reinhardt et al. [2003]. One of the main advantages of this phyllotaxis model, is the fact that we demonstrated that the same *flux-based* mechanizm is sufficient to explain the events observed not only in L1, but also in the rib zone of the meristem. Up to our knowledge, it is the first model at cellular resolution which explains both, finding the location for a primordium and vasculature formation below it. Since the model proposed in Chapter 2 is an alternative to the *concentration-based* models proposed by Jönsson et al. [2006], Smith et al. [2006c], we compared them and suggested that the ordering of the events of vasculature development and PIN reorientation on the surface might be used to discriminate among the models.

Physical-based modelling framework The framework presented in Chapter 3 allowed us to perform *in silico* experiments in which we investigated the development of the SAM including the feedback between growth and auxin. The simplistic, physical-based model made it possible to demonstrate that wall hardening and isotropic growth are sufficient to reproduce continuous growth of *pin*-shaped meristem. Our framework allowed us to express growth tropisms as a function described by physiological processes. Using this framework we performed the simulations of development in which growth was a function of auxin concentration. We reproduced *in silico* the experiment described by Reinhardt et al. [2000a], in which a patch of auxin was manually placed on the peripheral zone of the meristem, which triggered the primordium initiation. The model revealed a circumferential stress in the boundary zone. We presented a preliminary work in which the auxin-transport model was changing the growth of meristem by altering the mechanical properties of the cell walls. Although we did not observed regular phyllotaxis, the framework is an upgrade comparing to the previous models, since it includes a feedback loop between auxin transport

and shape evolution.

Perspectives

This work, unsurprisingly, leaves many important questions which can be investigated further in the context of this thesis.

Flux-based issues Important issues concern *flux-based* mechanizm. In this thesis we followed the idea of Sachs [1969], according to which the flux of auxin increases its polar transporter distribution in the direction of transport. This mechanizm was used in the computer models which explain various phenomena (e.g. vasculature formation, leaf venation, phyllotaxis). However, nowadays we have only a little of understanding what are the molecular basis of such a mechanizm. It is, therefore, of a great importance to identify the molecular components of this process and as a consequence, to validate the plausibility of *flux-based* models. This discovery would probably allow us to go one step further with the modelling, allowing us to finetune fairly abstract mechanizm used in the contemporary models to stay in better agreement with the real process.

Except of the polarization mechanizm itself, in the auxin transport models the assumption concerning auxin synthesis, endocytosis and transport efficiency as well as PIN synthesis and endocytosis are also crucial for the *in silico* experiments thus, they require further experimental investigation. Closely related to these issues is the problem of a reliable auxin marker, able to faithfully report auxin concentrations. So called DR5::GFP is tissue dependent and often does not provide unequivocal answers, leaving out a big margin for speculations. For example, it is an important question if the regions of DR5::GFP activation correspond to locations with high auxin concentrations or low concentration and high directional fluxes.

Phyllotaxis issues The *flux-based* model of phyllotaxis requires a rapid leak of auxin from L1 inside the meristem dome. The exact mechanizm of this process, however, has not been identified yet. Interestingly, the images show lower expression levels of AUX pumps in the primordia L1 cells, which might explain such a leak. However, since these data have not been investigated in this context, they do not answer this question in a meaningful way (e.g. we do not know how strong are the AUX pumps; we do not know if other efflux carriers do not overtake the function of AUX pumps). These issues should be studied more carefully.

Better understanding of the polarization mechanizm on a molecular level, should facilitate validating the requirement of the *flux-based* phyllotaxis model to use different feedback of auxin flux on PIN polarization in L1 and rib zone of the meristem, which leads to laminar or canalization-like regimes.

It would be also interesting to build up a volumetric model of apical meristem, where not only L1 but also the rib zone would be explicitely represented. In such a model it would be possible to study the issue of vasculature development together with the patterning in L1 within only one model, which might indicate new difficulties and different, possibly testable conditions. The main difficulties would be dealing with the growth in a volumetric structure, as well as much higher computational complexity (e.g. the L1 of *Arabidopsis* SAM contains about 300 cells, whereas the number of cells in whole meristem is in order of thousands).

Physical-based simulations It would be very interesting to extend the proposed physical-based framework and to simulate a 3D, volumetric representation of the meristem. With such a model, the compression forces could also be studied, which might be important in various developmental processes (as discussed in 3.6). This model might require to exchange the MSS approach by more suited to 3D FEM method.

Another interesting perspective might be using of the proposed MSS framework to simulate growth of real meristem and to reproduce a regular, spiral phyllotaxis. First question which remains unanswered is whether *flux-based* and *concentration-based* patterning mechanisms are compatible with the increased local outgrowth in the region of the primordia. The physical-based approach seems suitable to investigate this questions, since it allows for straightforward introduction of growth tropisms. This can be done by extending the physical-based model presented in 3.5 by including more intensive primordia outgrowth and the mechanizm keeping the realistic primordia shape.

Second question is inspired by the physical-based model and concerns the stability of the patterning mechanisms and their resistance to growth errors. Both, *concentration-based* and *flux-based* mechanisms are able to produce stable, spiral phyllotaxis patterns assuming a regular growth (the regular, spiral patterns were obtained only on structures with geometrical, imposed growth [Smith et al., 2006c, Stoma et al., 2008]). The physical-based growth in the framework described in 3.2 is less regular then the descriptive growth used in 2.2. It is therefore possible, that the lack of stability in obtained phyllotaxis patterns in a model described in 3.5 was due to less stable growth. This issue might be investigated further by analysing growth of the real meristems and selecting

possible sources of phyllotaxis errors (e.g. like discretization of the meristem, due to compartmentalization into cells; errors in radial trajectories and velocities of vertices). These errors can be and then reproduced inside of the model with descriptive growth and they influence on the stability of the patterns can be tested.

Computer related issues Despite its simplicity, WalledTissue appeared to be a useful data structure for modelling a cellular processes. Since it is entirely developed in Python, it should be rewritten in a faster, compiled language. This would lead to faster execution times, and together with re-implementing of expensive algorithms (e.g. mechanical solvers, physiological processes) it should move current limits of real time simulations from 100 cells to about 1000 cells.

Second important goal should be designing of 3D, volumetric cell structure, allowing us to simulate not only the surface of the meristem, but also its internal parts. This should allow for accomplishing the targets of creating of 3D volumic model of meristem, as well as mechanical simulations with compression forces.

Bibliography

M. Aida, T. Ishida, H. Fukaki, H. Fujisawa, and M. Tasaka. Genes involved in organ separation in arabidopsis: An analysis of the cup-shaped cotyledon mutant. *The plant cell*, 9(6):841–857, 1997.

P. Atela, C. Golé, and S. Hotton. A dynamical system for plant pattern formation: A rigorous analysis. *Journal of Nonlinear Science*, V12(6):641–676, November 2002. doi: 10.1007/s00332-002-0513-1.

Orna Avsian-Kretchmer, Jin-Chen Cheng, Lingjing Chen, Edgar Moctezuma, and Z. Renee Sung. Indole acetic acid distribution coincides with vascular differentiation pattern during arabidopsis leaf ontogeny. *Plant Physiol*, 130 (1):199–209, Sep 2002. doi: 10.1104/pp.003228.

A. Bandyopadhyay, J. J. Blakeslee, O. R. Lee, J. Mravec, M. Sauer, B. Titapiwatanakun, S. N. Makam, R. Bouchard, M. Geisler, E. Martinoia, J. Friml, W. A. Peer, and A. S. Murphy. Interactions of pin and pgp auxin transport mechanisms. *Biochemical Society Transaction*, 35:137–141, 2007. URL `http://www.biochemsoctrans.org/bst/035/0137/bst0350137.htm`.

Barbier. *Toward a dynamic model of the shoot apical meristem of Arabidopsis thaliana.* PhD thesis, Universite Montpellier II, December 2005.

P. Barbier de Reuille, I. Bohn-Courseau, K. Ljung, H. Morin, N. Carraro, C. Godin, and J. Traas. Computer simulations reveal properties of the cell-cell signaling network at the shoot apex in arabidopsis. *PNAS*, 103(5):1627–1632, 2006.

Bonnie Bartel. Auxin biosynthesis. *Annual Review of Plant Physiology and Plant Molecular Biology*, 48(1):51–66, 1997. doi: http://dx.doi.org/10.1146/annurev.arplant.48.1.51. URL `http://dx.doi.org/10.1146/annurev.arplant.48.1.51`.

M. K. Barton and R. S. Poethig. Formation of the shoot apical meristem in arabidopsis thaliana: an analysis of development in the wild type and in the

shoot meristemless mutant. *Development*, 119(3):823–831, November 1993. URL http://dev.biologists.org/cgi/content/abstract/119/3/823.

Tobias I. Baskin. On the alignment of cellulose microfibrils by cortical microtubules: A review and a model. *Protoplasma*, 215(1):150–171, March 2001. doi: http://dx.doi.org/10.1007/BF01280311. URL http://dx.doi.org/10.1007/BF01280311.

Tobias I. Baskin. Anisotropic expansion of the plant cell wall. *Annual Review of Cell and Developmental Biology*, 21(1):203–222, 2005. doi: http://dx.doi.org/10.1146/annurev.cellbio.20.082503.103053. URL http://dx.doi.org/10.1146/annurev.cellbio.20.082503.103053.

R. Benjamins, A. Quint, D. Weijers, P. Hooykaas, and R. Offringa. The pinoid protein kinase regulates organ development in arabidopsis by enhancing polar auxin transport. *Development*, 128(20):4057–4067, October 2001. ISSN 0950-1991. URL http://dev.biologists.org/cgi/content/abstract/128/20/4057.

Sally R. M. Bennett, John Alvarez, Gerd Bossinger, and David R. Smyth. Morphogenesis in pinoid mutants of arabidopsis thaliana. *The Plant Journal*, 8(4):505–520, 1995. doi: http://dx.doi.org/10.1046/j.1365-313X.1995.8040505.x. URL http://dx.doi.org/10.1046/j.1365-313X.1995.8040505.x.

Rishikesh P. Bhalerao, Jan Eklöf, Karin Ljung, Alan Marchant, Malcolm Bennett, and Göran Sandberg. Shoot-derived auxin is essential for early lateral root emergence in arabidopsis seedlings. *The Plant Journal*, 29 (3):325–332, 2002. doi: http://dx.doi.org/10.1046/j.0960-7412.2001.01217.x. URL http://dx.doi.org/10.1046/j.0960-7412.2001.01217.x.

Joshua J. Blakeslee, Wendy A. Peer, and Angus S. Murphy. Auxin transport. *Current Opinion in Plant Biology*, 8(5):494–500, October 2005. doi: http://dx.doi.org/10.1016/j.pbi.2005.07.014. URL http://dx.doi.org/10.1016/j.pbi.2005.07.014.

Joshua J. Blakeslee, Anindita Bandyopadhyay, Ok R. Lee, Jozef Mravec, Boosaree Titapiwatanakun, Michael Sauer, Srinivas N. Makam, Yan Cheng, Rodolphe Bouchard, Jiri Adamec, Markus Geisler, Akitomo Nagashima, Tatsuya Sakai, Enrico Martinoia, Jiri Friml, Wendy A. Peer, and Angus S. Murphy. Interactions among pin-formed and p-glycoprotein auxin transporters in arabidopsis. *Plant Cell*, 19(1):131–147, January 2007. doi: 10.1105/tpc.106.040782.

L. Bodenstein. A dynamic simulation model of tissue growth and cell patterning. *Cell differentiation*, 19(1):19–33, July 1986. ISSN 0045-6039. URL `http://view.ncbi.nlm.nih.gov/pubmed/3755380`.

David Bourg. *Physics for Game Developers*. O'Reilly Media, Inc., 1st edition, November 2001. ISBN 0596000065. URL `http://www.amazon.ca/exec/obidos/redirect?tag=citeulike09-20\&path=ASIN/0596000065`.

U. Brand. Dependence of stem cell fate in arabidopsis on a feedback loop regulated by clv3 activity. *Science*, 289:617–619, 2000.

A. Braun. Vergleichende untersuchung über die ordnung der schuppen an den tannenzapfen als einleitung zur untersuchung der blattstellung überhaupt. *Nova Acta Academiae Caesareae Leopoldino Carolinae Germanicae Naturae Curiosorum*, 15:195–402, 1831.

A. Braun. Dr.schimpers vorträge über die möglichkeit eines wissenschaftlichen verständnisses der blattstellung...flora. *Iena*, 18:145–191, 1835.

Cristel C. Carles and Jennifer C. Fletcher. Shoot apical meristem maintenance: the art of a dynamic balance. *Trends in Plant Science*, 8(8):394–401, August 2003. doi: http://dx.doi.org/10.1016/S1360-1385(03)00164-X. URL `http://dx.doi.org/10.1016/S1360-1385(03)00164-X`.

Nicholas Carr, Wendy Doniger, Benjamin M. Friedman, Leslie H. Gelb, David Gelernter, Murray Gell-Mann, Vartan Gregorian, Thomas Nagel, Donald Norman, Don M. Randel, Sutherland O. Houndwood, and Michael Wesch. *Encyclopedia Britannica*. 2008.

Ilda Casimiro, Alan Marchant, Rishikesh P. Bhalerao, Tom Beeckman, Sandra Dhooge, Ranjan Swarup, Neil Graham, Dirk Inzé, Goran Sandberg, Pedro J. Casero, and Malcolm Bennett. Auxin transport promotes arabidopsis lateral root initiation. *Plant Cell*, 13:843–852, 2001. URL `http://plancellalainsun.freetcp.com/cgi/content/abstract/13/4/843`.

J. L. Celenza, P. L. Grisafi, and G. R. Fink. A pathway for lateral root formation in arabidopsis thaliana. *Genes & Development*, 9:2131–2142, 1995. URL `http://genesdev.cshlp.org/cgi/content/abstract/9/17/2131`.

J. M. Chapman and R. Perry. A diffusion model of phyllotaxis. *Ann Bot*, 60(4):377–389, October 1987. URL `http://aob.oxfordjournals.org/cgi/content/abstract/60/4/377`.

Youfa Cheng, Xinhua Dai, and Yunde Zhao. Auxin biosynthesis by the yucca flavin monooxygenases controls the formation of floral organs and vascular

tissues in arabidopsis. *Genes Dev.*, 20(13):1790–1799, July 2006. doi: 10.1101/gad.1415106.

N. G. Cholodny. Wuchshormone und tropismen bei den pflanzen. *Biologisches Zentralblatt*, 47:604–626, 1927.

S. Christensen, N. Dagenais, J. Chory, and D. Weigel. Regulation of auxin response by the protein kinase pinoid. *Cell*, 100(4):469–478, 2000.

S. E. Clark. Clavata1, a regulator of meristem and flower development in arabidopsis. *Development*, 119:397–418, 1993.

E. Coen, A. G. Rolland-Lagan, M. Matthews, J. A. Bangham, and P. Prusinkiewicz. The genetics of geometry. *Procedings of the National Acadamy of Science U S A*, 101(14):4728–4735, April 2004. ISSN 0027-8424. doi: http://dx.doi.org/10.1073/pnas.0306308101. URL `http://dx.doi.org/10.1073/pnas.0306308101`.

D. J. Cosgrove. Wall extensibility: its nature, measurement and relationship to plant cell growth. *New Phytolo.*, 124:1–23, 1993.

D. J. Cosgrove. Plant cell enlargement and the action of expansins. *BioEssays : news and reviews in molecular, cellular and developmental biology*, 18(7):533–540, July 1996. ISSN 0265-9247. doi: http://dx.doi.org/10.1002/bies.950180704. URL `http://dx.doi.org/10.1002/bies.950180704`.

D. J. Cosgrove. Relaxation in a high-stress environment: the molecular bases of extensible cell walls and cell enlargement. *The Plant cell*, 9(7):1031–1041, July 1997. ISSN 1040-4651. doi: http://dx.doi.org/10.1105/tpc.9.7.1031. URL `http://dx.doi.org/10.1105/tpc.9.7.1031`.

D. J. Cosgrow. Expansive growth of plant cell walls. *Plant Physiol. Biochem.*, 28:109–124, 2000.

C. F. Curtiss and J. O. Hirschfelder. Integration of stiff equations. *Proceedings of the National Academy of Sciences of the United States of America*, 38(3):235–243, March 1952. ISSN 0027-8424.

Carolin Delker, Anja Raschke, and Marcel Quint. Auxin dynamics: the dazzling complexity of a small molecules message. *Planta*, 227(5):929–941, April 2008. doi: http://dx.doi.org/10.1007/s00425-008-0710-8. URL `http://dx.doi.org/10.1007/s00425-008-0710-8`.

H. Dermen. Periclinal cytochimeras and origin of tissues in stem and leaf of peach. *American Journal of botany*, 40:154–168, 1953.

Pavel Dimitrov and Steven W. Zucker. A constant production hypothesis guides leaf venation patterning. *PNAS*, 103(24):9363–9368, June 2006. doi: 10.1073/pnas.0603559103.

S. Douady and Y. Couder. Phyllotaxis as a physical self-organized growth process. *Physical Review Letters*, 68(13):2098+, March 1992. doi: http://dx.doi.org/10.1103/PhysRevLett.68.2098. URL `http://dx.doi.org/10.1103/PhysRevLett.68.2098`.

S. Douady and Y. Couder. Phyllotaxis as a dynamical self organizing process part ii: The spontaneous formation of a periodicity and the coexistence of spiral and whorled patterns. *Journal of Theoretical Biology*, 178(3):275–294, February 1996a. doi: 10.1006/jtbi.1996.0025.

S. Douady and Y. Couder. Phyllotaxis as a dynamical self organizing process part i: The spiral modes resulting from time-periodic iterations. *Journal of Theoretical Biology*, 178(3):255–273, February 1996b. doi: http://dx.doi.org/10.1006/jtbi.1996.0024. URL `http://dx.doi.org/10.1006/jtbi.1996.0024`.

Jacques Dumais and Charles R. Steele. New evidence for the role of mechanical forces in the shoot apical meristem. *Journal of Plant Growth Regulation*, 19:7–18, 2000.

Leah Edelstein-Keshet. *Mathematical Models In Biology*. McGraw-Hill Companies, 1st edition, January 1988. ISBN 0075549506.

J. F. Emery, S. K. Floyd, J. Alvarez, Y. Eshed, N. P. Hawker, A. Izhaki, S. F. Baum, and J. L. Bowman. Radial patterning of arabidopsis shoots by class iiihd-zip and kanadi genes. *Current biology*, 13:1768–1774, 2003.

Ralph O. Erickson. Symplastic growth and symplasmic transport. *Plant Physiol.*, 82(4):1153+, December 1986. URL `http://www.plantphysiol.org/cgi/content/abstract/82/4/1153`.

Y. Eshed, A. Izhaki, S. F. Baum, S. K. Floyd, and J. L. Bowman. Asymmetric leaf development and blade expansion in arabidopsis are mediated by kanadi and yabby activities. *Development*, 131:2997–3006, 2004.

Francois G. Feugier, A. Mochizuki, and Y. Iwasa. Self-organization of the vascular system in plant leaves: Inter-dependent dynamics of auxin flux and carrier proteins. *Journal of Theoretical Biology*, 236(4):366–375, October 2005. doi: 10.1016/j.jtbi.2005.03.017.

Leonardo Fibonacci and Laurence E. Sigler. *Fibonacci's Liber Abaci*. Springer, 1st edition, September 2002. ISBN 0387954198. URL `http://www.amazon.ca/exec/obidos/redirect?tag=citeulike09-20\&path=ASIN/0387954198`.

Jiri Friml. Auxin transport – shaping the plant. *Current Opinion in Plant Biology*, 6(1):7–12, February 2003. doi: 10.1016/S1369526602000031.

Jiri Friml, Justyna Wisniewska, Eva Benkova, Kurt Mendgen, and Klaus Palme. Lateral relocation of auxin efflux regulator pin3 mediates tropism in arabidopsis. *Nature*, 415:806–809, 2002.

Hironori Fujita and Atsushi Mochizuki. Pattern formation of leaf veins by the positive feedback regulation between auxin flow and auxin efflux carrier. *J Theor Biol*, 241(3):541–551, Aug 2006. doi: 10.1016/j.jtbi.2005.12.016.

E. Gamma, R. Helm, R. Johnson, and J. Vlissides. *Design Patterns: Elements of Reusable Object-Oriented Software*. Addison-Wesley Professional, January 1995.

Leo Gälweiler, Changhui Guan, Andreas Müller, Ellen Wisman, Kurt Mendgen, Alexander Yephremov, and Klaus Palme. Regulation of polar auxin transport by atpin1 in arabidopsis vascular tissue. *Science*, 282(5397): 2226–2230, December 1998. doi: 10.1126/science.282.5397.2226.

M. Geisler and A. Murphy. The abc of auxin transport: The role of p-glycoproteins in plant development. *FEBS Letters*, 580(4):1094–1102, 2006. URL `http://linkinghub.elsevier.com/retrieve/pii/S0014579305014249`.

Geitmann and Anja. Plant and fungal cytomechanics: quantifying and modeling cellular architecture. *Canadian Journal of Botany*, 84(4):581–593, April 2006. ISSN 0008-4026. URL `http://www.ingentaconnect.com/content/nrc/cjb/2006/00000084/00000004/art00012`.

Niko Geldner, Jiri Friml, York-Dieter Stierhof, Gerd Jurgens, and Klaus Palme. Auxin transport inhibitors block pin1 cycling and vesicle trafficking. *Nature*, 413(6854):425–428, 2001. doi: 10.1038/35096571.

J. L. Giavitto, C. Godin, O. Michel, and P. Prusinikiewicz. Computational models for integrative and developmental biology. *LaMI Rapport de Recherche*, (72-2002), March 2002.

Jean-Louis Giavitto and Olivier Michel. Modeling the topological organization of cellular processes. *Biosystems*, 70(2):149–163, July 2003. doi: http://

dx.doi.org/10.1016/S0303-2647(03)00037-6. URL http://dx.doi.org/10.1016/S0303-2647(03)00037-6.

T. H. Giddings and L. A. Staehelin. *Microtubule-mediated control of microfibril deposition; a reexamination of the hypothesis*. Academic Press, London, UK, 1991.

E. M. Gifford and G. E. Corson. The shoot apex in seed plants. *Botanical Review*, 37:143–229, 1971.

Pedro Gil, Elizabeth Dewey, Jiri Friml, Yunde Zhao, Kimberley C. Snowden, Jo Putterill, Klaus Palme, Mark Estelle, and Joanne Chory. Big: a calossin-like protein required for polar auxin transport in arabidopsis. *Genes and Development*, 15:1985–1997, 2001.

Mary H. Goldsmith, Timothy H. Goldsmith, and Monroe H. Martin. Mathematical analysis of the chemosmotic polar diffusion of auxin through plant tissues. *PNAS*, 78(2):976–980, February 1981. doi: http://dx.doi.org/10.1073/pnas.78.2.976. URL http://dx.doi.org/10.1073/pnas.78.2.976.

Olivier Grandjean, Teva Vernoux, Patrick Laufs, Katia Belcram, Yuki Mizukami, and Jan Traas. In vivo analysis of cell division, cell growth, and differentiation at the shoot apical meristem in arabidopsis. *Plant Cell*, 16(1): 74–87, January 2004. doi: 10.1105/tpc.017962.

William M. Gray. Hormonal regulation of plant growth and development. *PLoS Biology*, 2(9):e311+, September 2004. doi: http://dx.doi.org/10.1371/journal.pbio.0020311. URL http://dx.doi.org/10.1371/journal.pbio.0020311.

P. B. Green. Multinet growth in the cell wall of nitella. *J. Biophys. biochem. Cytol.*, (7):289–297, 1960.

P. B. Green. Surface of the shoot apex: a reinforcement-field theory for phyllotaxis. *Journal of cell science. Supplement*, 2:181–201, 1985. ISSN 0269-3518. URL http://view.ncbi.nlm.nih.gov/pubmed/3867672.

Veronica A. Grieneisen, Jian Xu, Athanasius F. Maree, Paulien Hogeweg, and Ben Scheres. Auxin transport is sufficient to generate a maximum and gradient guiding root growth. *Nature*, 449(7165):1008–1013, October 2007. doi: 10.1038/nature06215.

Tom Guilfoyle. Plant biology: Sticking with auxin. *Nature*, 446(7136):621–622, April 2007. ISSN 0028-0836. doi: http://dx.doi.org/10.1038/446621a. URL http://dx.doi.org/10.1038/446621a.

Tom Guilfoyle, Gretchen Hagen, Tim Ulmasov, and Jane Murfett. How does auxin turn on genes? *Plant Physiol.*, 118(2):341–347, October 1998. doi: http://dx.doi.org/10.1104/pp.118.2.341. URL `http://dx.doi.org/10.1104/pp.118.2.341`.

Tom J. Guilfoyle and Gretchen Hagen. Auxin response factors. *Current Opinion in Plant Biology*, 10(5):453–460, 2007.

Olivier Hamant, Marcus Heisler, Henrik Jönsson, Pawel Krupinski, Magalie Uyttewaal, Plamen Bokov, Francis Corson, Patrik Sahlin, Arezki Boudaoud, Elliot Meyerowitz, Yves Couder, and Jan Traas. Mechanics of morphogenesis at the shoot apical meristem of arabidopsis thaliana: an interdisciplinary view. *In editorial.*

Heisler, M., Jonsson, and H. Modeling auxin transport and plant development. *Journal of Plant Growth Regulation*, 25(4):302–312, December 2006. ISSN 0721-7595. doi: 10.1007/s00344-006-0066-x.

Marcus G. Heisler, Carolyn Ohno, Pradeep Das, Patrick Sieber, Gonehal V. Reddy, Jeff A. Long, and Elliot M. Meyerowitz. Patterns of auxin transport and gene expression during primordium development revealed by live imaging of the arabidopsis inflorescence meristem. *Current Biology*, 15(21):1899–1911, November 2005. doi: 10.1016/j.cub.2005.09.052.

Z. Hejnowicz. *Mechanical stress patterns in plant cell walls and their morphogenetical importance.* World Scientific, Singapore, 2000.

L. J. Hickey. *A revised classification of the architecture of dicotyledons leaves*, volume 1. Clarendon Press, 2 edition, 1979.

Regina Himmelspach, Richard E. Williamson, and Geoffrey O. Wasteneys. Cellulose microfibril alignment recovers from dcb-induced disruption despite microtubule disorganization. *The Plant Journal*, 36(4):565–575, 2003. doi: http://dx.doi.org/10.1046/j.1365-313X.2003.01906.x. URL `http://dx.doi.org/10.1046/j.1365-313X.2003.01906.x`.

A. C. Hindmarsh. *ODEPACK, A Systematized Collection of ODE Solvers , R. S. Stepleman et al. (eds.), North-Holland, Amsterdam, (vol. 1 of), pp. 55-64.*, volume 1 of *IMACS Transactions on Scientific Computation.* North-Holland Amsterdam, 1983.

H. Honda, M. Tanemura, and T. Nagai. A three-dimensional vertex dynamics cell model of space-filling polyhedra simulating cell behavior in a cell aggregate. *Journal of theoretical biology*, 226(4):439–453, February 2004.

ISSN 0022-5193. doi: http://dx.doi.org/10.1016/j.jtbi.2003.10.001. URL http://dx.doi.org/10.1016/j.jtbi.2003.10.001.

M R R. Howard, S J J. Millward-Sadler, A S S. Vasilliou, D M M. Salter, and J P P. Quinn. Mechanical stimulation induces preprotachykinin gene expression in osteoarthritic chondrocytes which is correlated with modulation of the transcription factor neuron restrictive silence factor. *Neuropeptides*, November 2008. ISSN 0143-4179. doi: http://dx.doi.org/10.1016/j.npep.2008.09.004. URL http://dx.doi.org/10.1016/j.npep.2008.09.004.

Kenneth E. Iverson. *A Programming Language.* John Wiley & Sons. ISBN 0471430145. URL http://www.amazon.ca/exec/obidos/redirect?tag=citeulike09-20\&path=ASIN/0471430145.

Kenneth E. Iverson. *A Programming Language.1.* John Wiley & Sons, 1962. ISBN 0471430145.

M. C. Jarvis. Structure and properties of pectin gels in plant cell walls. ;:. *Plant Cell and Environment*, 7(3):153–164, 1984.

Roger V. Jean. *Phyllotaxis: A systemic study in plant morphogenesis.* Cambridge University Press, Cambridge, 1994.

Sangho Jeong, Amy E. Trotochaud, and Steven E. Clark. The arabidopsis clavata2 gene encodes a receptor-like protein required for the stability of the clavata1 receptor-like kinase. *Plant Cell*, 11:1925–1934, 1999. URL http://plancellalainsun.freetcp.com/cgi/content/abstract/11/10/1925.

Eric Jones, Travis Oliphant, and Pearu Peterson. Scipy: Open source scientific tools for python, 2001.

H. Jonsson and M. Heisler. Modeling auxin transport and plant development. *Journal of Plant Growth Regulation*, 25(4):302–312, December 2006. ISSN 0721-7595. doi: http://dx.doi.org/10.1007/s00344-006-0066-x. URL http://dx.doi.org/10.1007/s00344-006-0066-x.

H. Jönsson, M. G. Heisler, B. E. Shapiro, E. M. Meyerowitz, and E. Mjolsness. An auxin-driven polarized transport model for phyllotaxis. *Proc Natl Acad Sci U S A*, 103(5):1633–1638, January 2006. ISSN 0027-8424. doi: 10.1073/pnas.0509839103.

Jaap A. Kaandorp and Shay Gueron. Particle based modelling methods applied in biology. *Future Generation Computer Systems*, 17(7):v–vi, May 2001. doi: http://dx.doi.org/10.1016/S0167-739X(00)00060-1. URL http://dx.doi.org/10.1016/S0167-739X(00)00060-1.

Donald R. Kaplan and Wolfgang Hagemann. The relationship of cell and organism in vascular plants. *BioScience*, 41(10):693–703, 1991. doi: http://dx.doi.org/10.2307/1311764. URL `http://dx.doi.org/10.2307/1311764`.

R. A. Kerstetter, K. Bollman, R. A. Taylor, K. Bomblies, and R. S. Poethig. Kanadi regulates organ polarity in arabidopsis. *Nature*, 411:706–709, 2001.

R. A. A. Kerstetter and S. Hake. Shoot meristem formation in vegetative development. *The Plant cell*, 9(7):1001–1010, July 1997. ISSN 1040-4651. doi: http://dx.doi.org/10.1105/tpc.9.7.1001. URL `http://dx.doi.org/10.1105/tpc.9.7.1001`.

Sharon Kessler, Brad Townsley, and Neelima Sinha. L1 division and differentiation patterns influence shoot apical meristem maintenance. *Plant Physiol.*, 141(4):1349–1362, August 2006. doi: http://dx.doi.org/10.1104/pp.105.076075. URL `http://dx.doi.org/10.1104/pp.105.076075`.

Bruce K. Kirchoff. Shape matters: Hofmeister's rule, primordium shape, and flower orientation. *International Journal of Plant Sciences*, 164(4):505–517, 2003.

Jürgen Kleine-Vehn, Pankaj Dhonukshe, Ranjan Swarup, Malcolm Bennett, and Jií Friml. Subcellular trafficking of the arabidopsis auxin influx carrier aux1 uses a novel pathway distinct from pin1. *The Plant Cell*, 18:3171–3181, 2006.

Donald E. Knuth. Two notes on notation. *Am. Math. Monthly*, 99(5):403–422, May 1992. ISSN 0002-9890. doi: 10.2307/2325085.

A. J. Koch and H. Meinhardt. Biological pattern formation: from basic mechanisms to complex structures. *Reviews of Modern Physics*, 66(4):1481+, October 1994. doi: http://dx.doi.org/10.1103/RevModPhys.66.1481. URL `http://dx.doi.org/10.1103/RevModPhys.66.1481`.

Eric M. Kramer. Pin and aux/lax proteins: their role in auxin accumulation. *Trends in Plant Science*, 9(12):578–582, December 2004. doi: http://dx.doi.org/10.1016/j.tplants.2004.10.010. URL `http://dx.doi.org/10.1016/j.tplants.2004.10.010`.

Eric M. Kramer and Malcolm J. Bennett. Auxin transport: a field in flux. *Trends in Plant Science*, 11(8):382–386, August 2006. doi: 10.1016/j.tplants.2006.06.002.

Eric M. Kramer, Nicholas L. Frazer, and Tobias I. Baskin. Measurement of diffusion within the cell wall in living roots of arabidopsis thaliana. *J. Exp.*

Bot., 58(11):3005–3015, August 2007. doi: http://dx.doi.org/10.1093/jxb/erm155. URL `http://dx.doi.org/10.1093/jxb/erm155`.

Cris Kuhlemeier. Phyllotaxis. *Trends in Plant Science*, 12(4):143–150, April 2007.

U. Kutschera. The role of the epidermis in the control of elongation growth in stems and cleoptiles. *Bot. Acta*, (105):246–252, 1992. URL `http://kbd.kew.org/kbd/detailedresult.do?id=87329`.

Dorota Kwiatkowska. Structural integration at the shoot apical meristem: models, measurements, and experiments. *Am. J. Bot.*, 91(9):1277–1293, September 2004a. doi: http://dx.doi.org/10.3732/ajb.91.9.1277. URL `http://dx.doi.org/10.3732/ajb.91.9.1277`.

Dorota Kwiatkowska. Surface growth at the reproductive shoot apex of arabidopsis thaliana pin-formed 1 and wild type. *J. Exp. Bot.*, 55(399):1021–1032, May 2004b. doi: http://dx.doi.org/10.1093/jxb/erh109. URL `http://dx.doi.org/10.1093/jxb/erh109`.

Dorota Kwiatkowska. Flower primordium formation at the arabidopsis shoot apex: quantitative analysis of surface geometry and growth. *Journal of Experimental Botany*, 57(3):571–580, February 2006. ISSN 0022-0957. doi: http://dx.doi.org/10.1093/jxb/erj042. URL `http://dx.doi.org/10.1093/jxb/erj042`.

Dorota Kwiatkowska and Jacques Dumais. Growth and morphogenesis at the vegetative shoot apex of anagallis arvensis l. *J. Exp. Bot.*, 54(387):1585–1595, June 2003. doi: http://dx.doi.org/10.1093/jxb/erg166. URL `http://dx.doi.org/10.1093/jxb/erg166`.

P. Laufs. Cellular parameters of the shoot apical meristem in arabidopsis. *Plant Cell*, 10:1375–1389, 1998.

T. Laux, K. F. Mayer, J. Berger, and G. Jurgens. The wuschel gene is required for shoot and floral meristem integrity in arabidopsis. *Development*, 122 (1):87–96, January 1996. URL `http://dev.biologists.org/cgi/content/abstract/122/1/87`.

M. Lenhard, G. Jurgens, and T. Laux. The wuschel and shootmeristemless genes fulfil complementary roles in arabidopsis shoot meristem regulation. *Development*, 129:3195–3206, 2002.

A. Lindenmayer. Mathematical models for cellular interaction in development, parts i and ii. *Journal of Theoretical Biology*, 18(3):280–315, 1968.

Karin Ljung, Rishikesh P. Bhalerao, and Goran Sandberg. Sites and homeostatic control of auxin biosynthesis in arabidopsis during vegetative growth. *The Plant Journal*, 28(4):465–474, 2001. doi: 10.1046/j.1365-313X.2001.01173.x.

Karin Ljung, Anna K. Hull, Mariusz Kowalczyk, Alan Marchant, John Celenza, Jerry D. Cohen, and Göran Sandberg. Biosynthesis, conjugation, catabolism and homeostasis of indole-3-acetic acid in arabidopsis thaliana. *Plant Molecular Biology*, 49(3):249–272, June 2002. doi: 10.1023/A:1015298812300.

Karin Ljung, Anna K. Hull, John Celenza, Masashi Yamada, Mark Estelle, Jennifer Normanly, and Göran Sandberg. Sites and regulation of auxin biosynthesis in arabidopsis roots. *The Plant Cell*, 17:1090–1104, 2005. URL `http://plancellalainsun.freetcp.com/cgi/content/abstract/17/4/1090`.

T. L. Lomax, G. K. Muday, and P. H. Rubery. *Auxin transport*. Kluwer, Dordrecht, Netherlands, 2 edition, 1995. URL `http://www.abebooks.com/products/isbn/9780792329848/Plant-Hormones-Physiology-Biochemistry-and-Molecular-Biology/`.

J. A. Long, E. I. Moan, J. I. Medford, and M. K. Barton. A member of the knotted class of homeodomain proteins encoded by the stm gene of arabidopsis. *Nature*, 379:66–69, 1996.

M. Lucas, C. Godin, C. Jay-Allemand, and L. Laplaze. Auxin fluxes in the root apex co-regulate gravitropism and lateral root initiation. *J. Exp. Bot.*, 59 (1):55–66, January 2008. doi: http://dx.doi.org/10.1093/jxb/erm171. URL `http://dx.doi.org/10.1093/jxb/erm171`.

Jacqueline Lück and Hermann B. Lück. Generation of 3-dimensional plant bodies by double wall map and stereomap systems. In *Proceedings of the 2nd International Workshop on Graph-Grammars and Their Application to Computer Science*, pages 219–231, London, UK, 1983. Springer-Verlag. ISBN 3540123105. URL `http://portal.acm.org/citation.cfm?id=647559.730201`.

Yoshio Masuda. Auxin-induced cell elongation and cell wall changes. *Journal of Plant Research*, 103(3):345–370, 1990. doi: http://dx.doi.org/10.1007/BF02488646. URL `http://dx.doi.org/10.1007/BF02488646`.

J. Mattsson, Z. R. Sung, and T. Berleth. Responses of plant vascular systems to auxin transport inhibition. *Development*, 126(13):2979–2991, Jul 1999.

Klaus F. X. Mayer, Heiko Schoof, Achim Haecker, Michael Lenhard, Gerd Jurgens, and Thomas Laux. Role of wuschel in regulating stem cell fate in the arabidopsis shoot meristem. *Cell*, 95:805–815, 1998.

J. R. Mcconnell, J. Emery, Y. Eshed, N. Bao, J. Bowman, and M. K. Barton. Role of phabulosa and phavoluta in determining radial patterning in shoots. *Nature*, 411:709–713, 2001.

Roeland M. Merks, Yves Van de Peer, Dirk Inze, and Gerrit T. Beemster. Canalization without flux sensors: a traveling-wave hypothesis. *Trends in Plant Science*, 12(9):384–390, September 2007. doi: 10.1016/j.tplants.2007.08.004.

L. Michaelis and M. L. Menten. Die kinetik der inwertin wirkung. *Biochem.*, (49):333–369, 1913.

G. J Mitchison. A model for vein formation in higher plants. *Proceedings of the Royal Society of London*, 207:79–109, 1980a.

G. J. Mitchison. The dynamics of auxin transport. *Proceedings of the Royal Society of London. Series B, Biological Sciences*, 209(1177):489–511, 1980b. URL `http://www.jstor.org/stable/35461`.

G. J. Mitchison. The polar transport of auxin and vein pattern in plants. *Philosophical Transactions of the Royal Society of London*, 295:461–471, 1981.

Gloria K. Muday, Wendy A. Peer, and Angus S. Murphy. Vesicular cycling mechanisms that control auxin transport polarity. *Trends in Plant Science*, 8(7): 301–304, July 2003. doi: http://dx.doi.org/10.1016/S1360-1385(03)00132-8. URL `http://dx.doi.org/10.1016/S1360-1385(03)00132-8`.

Axel Müller, Petra Düchting, and Elmar Weiler. A multiplex gc-ms/ms technique for the sensitive and quantitative single-run analysis of acidic phytohormones and related compounds, and its application to arabidopsis thaliana. *Planta*, 216(1):44–56, November 2002. doi: http://dx.doi.org/10.1007/s00425-002-0866-6. URL `http://dx.doi.org/10.1007/s00425-002-0866-6`.

J. Nakielski. Tensorial model for growth and cell division in the shoot apex. In A. Carbone, M. Gromov, and P. Prusinkiewicz, editors, *Pattern Formation in Biology, Vision and Dynamics*, pages 252–267. World Scientific Publishing Co. Pte. Ltd., Signapore, 2000.

Jerzy Nakielski and Zygmunt Hejnowicz. *The description of growth of plant organs: a continuous approach based on the growth tensor.* Kluwer Academic Publishers, Hingham, MA, USA, 2003. ISBN 1-4020-1567-4.

Jennifer Normanly. Auxin metabolism. *Physiologia Plantarum*, 100(3):431–442, 1997. doi: http://dx.doi.org/10.1111/j.1399-3054.1997.tb03047.x. URL `http://dx.doi.org/10.1111/j.1399-3054.1997.tb03047.x`.

K. Okada, J. Ueda, M. K. K. Komaki, C. J. J. Bell, and Y. Shimura. Requirement of the auxin polar transport system in early stages of arabidopsis floral bud formation. *The Plant cell*, 3(7):677–684, July 1991. ISSN 1040-4651. doi: 10.1105/tpc.3.7.677.

Yoko Okushima, Hidehiro Fukaki, Makoto Onoda, Athanasios Theologis, and Masao Tasaka. Arf7 and arf19 regulate lateral root formation via direct activation of lbd/asl genes in arabidopsis. *Plant Cell*, 19(1):118–130, January 2007. doi: http://dx.doi.org/10.1105/tpc.106.047761. URL `http://dx.doi.org/10.1105/tpc.106.047761`.

D. Otsuga, B. Deguzman, M. J. Prigge, G. N. Drews, and S. E. Clark. Revoluta regulates meristem initiation at lateral positions. *Plant Journal*, 25:223–236, 2001.

T. Paciorek, E. Zazímalová, N. Ruthardt, J. Petrášek, Y. D. Stierhof, J. Kleine-Vehn, D. A. Morris, N. Emans, G. Jürgens, N. Geldner, and J. Friml. Auxin inhibits endocytosis and promotes its own efflux from cells. *Nature*, 435:1251–1256, 2005. URL `http://www.cababstractsplus.org/google/abstract.asp?AcNo=20053136163`.

Jan Petrasek, Jozef Mravec, Rodolphe Bouchard, Joshua J. Blakeslee, Melinda Abas, Daniela Seifertova, Justyna Wisniewska, Zerihun Tadele, Martin Kubes, Milada Covanova, Pankaj Dhonukshe, Petr Skupa, Eva Benkova, Lucie Perry, Pavel Krecek, Ok R. Lee, Gerald R. Fink, Markus Geisler, Angus S. Murphy, Christian Luschnig, Eva Zazimalova, and Jiri Friml. Pin proteins perform a rate-limiting function in cellular auxin efflux. *Science*, 312(5775):914–918, May 2006. doi: 10.1126/science.1123542.

C. Pradal, F. Boudon, C. Nouguier, J. Chopard, and C. Godin. Plantgl : a python-based geometric library for 3d plant modelling at different scales. Technical report, INRIA, November 2007.

C. Pradal, S. Dufour-Kowalski, F. Boudon, C. Fournier, and C. Godin. Openalea: A visual programming and component-based software platform for plant modeling. *Functional Plant Biology*, in revision, 2008.

W. Press, S. Teukolsky, W. Vetterling, and B. Flannery. *Numerical Recipes in C: The Art of Scientific Computing*. Cambridge University Press, New York, NY, second edition, 1992.

Timothy E. Proseus, Joseph K. Ortega, and John S. Boyer. Separating growth from elastic deformation during cell enlargement. *Plant Physiol.*, 119(2):

775–784, February 1999. doi: http://dx.doi.org/10.1104/pp.119.2.775. URL http://dx.doi.org/10.1104/pp.119.2.775.

Timothy E. Proseus, Guo-Li Zhu, and John S. Boyer. Turgor, temperature and the growth of plant cells: using chara corallina as a model system. *J. Exp. Bot.*, 51(350):1481–1494, September 2000. doi: http://dx.doi.org/10.1093/jexbot/51.350.1481. URL http://dx.doi.org/10.1093/jexbot/51.350.1481.

P. Prusinkiewicz and A. Lindenmayer. *The algorithmic beauty of plants*. Springer-Verlag, New York, 1990. URL http://www.algorithmicbotany.org/papers/#abop.

Przemyslaw Prusinkiewicz. Structured dynamical systems.

Venugopala G. Reddy, Marcus G. Heisler, David W. Ehrhardt, and Elliot M. Meyerowitz. Real-time lineage analysis reveals oriented cell divisions associated with morphogenesis at the shoot apex of arabidopsis thaliana. *Development*, 131(17):4225–4237, September 2004. doi: 10.1242/dev.01261.

Robyn C. Reed, Shari R. Brady, and Gloria K. Muday. Inhibition of auxin movement from the shoot into the root inhibits lateral root development in arabidopsis. *Plant Physiol.*, 118(4):1369–1378, December 1998. doi: http://dx.doi.org/10.1104/pp.118.4.1369. URL http://dx.doi.org/10.1104/pp.118.4.1369.

W. T. Reeves. Particle systems—a technique for modeling a class of fuzzy objects. *ACM Trans. Graph.*, 2(2):91–108, April 1983. ISSN 0730-0301. doi: http://dx.doi.org/10.1145/357318.357320. URL http://dx.doi.org/10.1145/357318.357320.

Didier Reinhardt and Cris Kuhlemeier. Plant architecture. *EMBO Rep*, 3(9):846–851, Sep 2002. doi: 10.1093/embo-reports/kvf177.

Didier Reinhardt, Therese Mandel, and Cris Kuhlemeier. Auxin regulates the initiation and radial position of plant lateral organs. *Plant Cell*, 12(4):507–518, April 2000a.

Didier Reinhardt, Therese Mandel, and Cris Kuhlemeier. Auxin regulates the initiation and radial position of plant lateral organs. *Plant Cell*, 12 (4):507–518, April 2000b. URL http://www.plantcell.org/cgi/content/abstract/12/4/507.

Didier Reinhardt, Eva-Rachele Pesce, Pia Stieger, Therese Mandel, Kurt Baltensperger, Malcolm Bennett, Jan Traas, Jiri Friml, and Cris Kuhlemeier.

Regulation of phyllotaxis by polar auxin transport. *Nature*, 426(6964):255–260, November 2003. doi: 10.1038/nature02081.

Didier Reinhardt, Martin Frenz, Therese Mandel, and Cris Kuhlemeier. Microsurgical and laser ablation analysis of leaf positioning and dorsoventral patterning in tomato. *Development*, 132(1):15–26, Jan 2005. doi: 10.1242/dev.01544.

Anne-Gaelle Rolland-Lagan and Przemyslaw Prusinkiewicz. Reviewing models of auxin canalization in the context of leaf vein pattern formation in arabidopsis. *The Plant Journal*, 44(5):854–865, December 2005. ISSN 0960-7412. doi: 10.1111/j.1365-313X.2005.02581.x.

P. H. Rubery and A. R. Sheldrake. Carrier-mediated auxin transport. *Planta*, 118(2):101–121, June 1974. doi: 10.1007/BF00388387.

Tim Rudge and Jim Haseloff. A computational model of cellular morphogenesis in plants. 2005.

Adam Runions, Martin Fuhrer, Brendan Lane, Pavol Federl, Anne-Gaëlle Rolland-Lagan, and Przemyslaw Prusinkiewicz. Modeling and visualization of leaf venation patterns. *ACM Trans. Graph.*, 24(3):702–711, July 2005. ISSN 0730-0301. doi: 10.1145/1073204.1073251.

T. Sachs. Polarity and the induction of organized vascular tissues. *Ann Bot*, 33 (2):263–275, March 1969.

T. Sachs. The control of the patterned differentiation of vascular tissues. *Advances In Botanical Research*, 9:151–262, 1981. URL `http://kbd.kew.org/kbd/detailedresult.do?id=64880`.

Tsvi Sachs. Collective specification of cellular development. *BioEssays*, 25(9): 897–903, August 2003. ISSN 1521-1878. doi: http://dx.doi.org/10.1002/bies.10328. URL `http://dx.doi.org/10.1002/bies.10328`.

Michael Sauer, Jozef Balla, Christian Luschnig, Justyna Wisniewska, Vilem Reinohl, Jiri Friml, and Eva Benkova. Canalization of auxin flow by aux/iaa-arf-dependent feedback regulation of pin polarity. *Genes Dev.*, 20(20):2902–2911, October 2006. doi: 10.1101/gad.390806.

S. Savaldigoldstein and J. Chory. Growth coordination and the shoot epidermis. *Current Opinion in Plant Biology*, 11(1):42–48, February 2008. ISSN 13695266. doi: http://dx.doi.org/10.1016/j.pbi.2007.10.009. URL `http://dx.doi.org/10.1016/j.pbi.2007.10.009`.

Enrico Scarpella, Philip Francis, and Thomas Berleth. Stage-specific markers define early steps of procambium development in arabidopsis leaves and correlate termination of vein formation with mesophyll differentiation. *Development*, 131(14):3445–3455, July 2004. doi: 10.1242/10.1242/dev.01182.

Enrico Scarpella, Danielle Marcos, Jiri Friml, and Thomas Berleth. Control of leaf vascular patterning by polar auxin transport. *Genes Dev.*, 20(8):1015–1027, April 2006. doi: 10.1101/gad.1402406.

K. F. Schimper. Beschreibung des symphytum zeyheri und seiner zwei deutschen verwandten der s.bulborum schimp und s.tuberosum jacq. geiger's mag. *Pharm*, 29:1–92, 1830.

A. Schmidt. Histologische studien am phanerogamen vegetationspunkten. *Botanisches Archiv*, 8:345–404, 1924.

H. Schoof, M. Lenhard, A. Haecker, K. Mayer, G. Jürgens, and T. Laux. The stem cell population of arabidopsis shoot meristems is maintained by a regulatory loop between the clavata and wuschel genes. *Cell*, 100(6): 635–644, 2000. URL `http://linkinghub.elsevier.com/retrieve/pii/S009286740080700X`.

J. C. Schoute. On whorled phyllotaxis i. *Rec. Trav. bot. neerl*, 19:184–206, 1922.

B. Shapiro and E. Mjolsness. Developmental simulations with cellerator. In *Second International Conference on Systems Biology*, November 2001.

B. E. Shapiro, A. Levchenko, E. M. Meyerowitz, B. J. Wold, and E. D. Mjolsness. Cellerator: extending a computer algebra system to include biochemical arrows for signal transduction simulations. *Bioinformatics*, 19(5):677–678, March 2003. ISSN 1367-4803. URL `http://view.ncbi.nlm.nih.gov/pubmed/12651737`.

Patrick D. Shipman and Alan C. Newell. Phyllotactic patterns on plants. *Physical Review Letters*, 92(16):168102+, April 2004. doi: 10.1103/PhysRevLett.92.168102.

L. E. Sieburth. Auxin is required for leaf vein pattern in arabidopsis. *Plant Physiol*, 121(4):1179–1190, Dec 1999.

Richard Smith. *Simulation Models of Phyllotaxis and Morphogenesis in Plants*. PhD thesis, August 2007.

Richard Smith, Cris Kuhlemeier, and Przemyslaw Prusinkiewicz. Inhibition fields for phyllotactic pattern formation: a simulation study. *Canadian Journal of Botany*, 84(11):1635–1649, 2006a.

Richard S. Smith, Soazig Guyomarc'h, Therese Mandel, Didier Reinhardt, Cris Kuhlemeier, and Przemyslaw Prusinkiewicz. A plausible model of phyllotaxis. *PNAS*, 103(5):1301–1306, January 2006b.

Richard S. Smith, Soazig Guyomarc'h, Therese Mandel, Didier Reinhardt, Cris Kuhlemeier, and Przemyslaw Prusinkiewicz. A plausible model of phyllotaxis. *PNAS*, 103(5):1301–1306, January 2006c. doi: http://dx.doi.org/10.1073/pnas.0510457103. URL `http://dx.doi.org/10.1073/pnas.0510457103`.

Mary Snow and Robert Snow. A theory of the regulation of phyllotaxis based on lupinus albus. *Philosophical Transactions of the Royal Society of London. Series B, Biological Sciences*, 244(717):483–513, 1962.

Eldra P. Solomon and Linda R. Berg. *Biology*. Brooks Cole, international ed edition, February 2007. ISBN 0495114197. URL `http://www.amazon.ca/exec/obidos/redirect?tag=citeulike09-20\&path=ASIN/0495114197`.

T. Steeves and I. Sussex. *Patterns in Plant Development*. Prentice Hall, Inc., Englewood Cliffs, New Jersey, 1972.

T. Steeves and I. Sussex. *Patterns in Plant Development*. Cambridge University Press, 2 edition, 1989. URL `http://books.google.com/books?hl=pl\&#38;lr=\&#38;id=7GCTLqM3FDcC\&#38;oi=fnd\&#38;pg=PP15\&#38;dq=Steeves+and+Sussex,+1989\&#38;ots=QG60zZFTxE\&#38;sig=EqptcDc9O11QYWzgoz95hV-LOiY`.

R. N. Stewart and L. G. Burk. Independence of tissues derived from apical layers in ontogeny of the tobacco leaf and ovary. *American Journal of botany*, 57:1010–1016, 1970.

Pia A. Stieger, Didier Reinhardt, and Cris Kuhlemeier. The auxin influx carrier is essential for correct leaf positioning. *The Plant Journal*, 32(4):509–517, 2002. doi: http://dx.doi.org/10.1046/j.1365-313X.2002.01448.x. URL `http://dx.doi.org/10.1046/j.1365-313X.2002.01448.x`.

Szymon Stoma, Jérôme Chopard, Christophe Godin, and Jan Traas. Using mechanics in the modelling of meristem morphogenesis. In *Functional-structural plant*, November 2007.

Szymon Stoma, Mikael Lucas, Jérôme Chopard, Marianne Schaedel, Jan Traas, and Christophe Godin. Flux-based transport enhancement as a plausible unifying mechanism for auxin transport in meristem development. *PLoS Comput Biol*, 4(10):e1000207+, October 2008. doi: http://dx.doi.org/10.1371/journal.pcbi.1000207. URL `http://dx.doi.org/10.1371/journal.pcbi.1000207`.

D. Sulsky, S. Childress, and J. K. Percus. A model of cell sorting. *Journal of Theoretical Biology*, 106(3):275–301, February 1984. doi: http://dx.doi.org/10.1016/0022-5193(84)90031-6. URL `http://dx.doi.org/10.1016/0022-5193(84)90031-6`.

Ranjan Swarup, Joanna Kargul, Alan Marchant, Daniel Zadik, Abidur Rahman, Rebecca Mills, Anthony Yemm, Sean May, Lorraine Williams, Paul Millner, Seiji Tsurumi, Ian Moore, Richard Napier, Ian D. Kerr, and Malcolm J. Bennett. Structure-function analysis of the presumptive arabidopsis auxin permease aux1. *The Plant Cell*, 16:3069–3083, 2004.

Ranjan Swarup, Eric M. Kramer, Paula Perry, Kirsten Knox, Ottoline H. M. Leyser, Jim Haseloff, Gerrit T. S. Beemster, Rishikesh Bhalerao, and Malcolm J. Bennett. Root gravitropism requires lateral root cap and epidermal cells for transport and response to a mobile auxin signal. *Nature Cell Biology*, 7(11):1057–1065, October 2005. ISSN 1465-7392. doi: 10.1038/ncb1316.

K. V. Thimann and F. Skoog. On the inhibition of bud development and other functions of growth substance in vicia faba. *Royal Society of London Proceedings Series B*, 114:317–339, February 1934. URL `http://adsabs.harvard.edu/cgi-bin/nph-bib_query?bibcode=1934RSPSB.114..317T`.

Kenneth V. Thimann. *Plant growth hormones*. Academic Press, New York, USA, 1948.

Kenneth V. Thimann. *Hormone action in the whole life of plants*. The University of Massachusetts, Amherst,MA, 1977.

Boosaree Titapiwatanakun and Angus S. Murphy. Post-transcriptional regulation of auxin transport proteins: cellular trafficking, protein phosphorylation, protein maturation, ubiquitination, and membrane composition. *J. Exp. Bot.*, pages ern240+, September 2008. doi: http://dx.doi.org/10.1093/jxb/ern240. URL `http://dx.doi.org/10.1093/jxb/ern240`.

A. M. Turing. The chemical basis of morphogenesis. *Philosophical Transactions of the Royal Society of London. Series B, Biological Sciences*, 237(641):37–72, August 1952.

Tim Ulmasov, Gretchen Hagen, and Tom J. Guilfoyle. Arf1, a transcription factor that binds to auxin response elements. *Science*, 276(5320):1865–1868, June 1997. doi: http://dx.doi.org/10.1126/science.276.5320.1865. URL `http://dx.doi.org/10.1126/science.276.5320.1865`.

T. Vernoux, J. Kronenberger, O. Grandjean, P. Laufs, and J. Traas. Pin-formed 1 regulates cell fate at the periphery of the shoot apical meristem. *Development*, 127(23):5157–5165, December 2000. URL `http://dev.biologists.org/cgi/content/abstract/127/23/5157`.

Anne Vieten, Michael Sauer, Philip B. Brewer, and Jiri Friml. Molecular and cellular aspects of auxin-transport-mediated development. *Trends in Plant Science*, 12(4):160–168, April 2007. doi: 10.1016/j.tplants.2007.03.006.

Chunfang Wei, Philip M. Lintilhac, and Jason J. Tanguay. An insight into cell elasticity and load-bearing ability. measurement and theory. *Plant Physiol.*, 126(3):1129–1138, July 2001. doi: http://dx.doi.org/10.1104/pp.126.3.1129. URL `http://dx.doi.org/10.1104/pp.126.3.1129`.

Jonathan D. B. Weyers, Neil W. Paterson, Richard A'brook, and Zhi-Yong Peng. Quantitative analysis of the control of physiological phenomena by plant hormones. *Physiologia Plantarum*, 95(3):486–494, 1995. doi: http://dx.doi.org/10.1111/j.1399-3054.1995.tb00867.x. URL `http://dx.doi.org/10.1111/j.1399-3054.1995.tb00867.x`.

Andrew Witkin. Physically based modeling: principles and practice. 2001.

Andrew W. Woodward and Bonnie Bartel. Auxin: Regulation, action, and interaction. *Annals of Botany*, 95(5): 707–735, 2005. URL `http://pt.wkhealth.com/pt/re/abot/abstract.00008707-200504000-00001.htm;jsessionid=LRtb8Lf6T1BLLzcWfzWLgQTHmvYbJw2vCKsQnTX2Mxy8B0D2B5JN!383905440!181195628!8091!-1`.

Appendix A

ODE/PDE equation in $(DS)^2$-systems

A differential equation (DE) describes the relation of an unknown function with its derivatives of various orders. Differential equations arise in many areas of science and technology, usually when continuously changing quantities (modelled by functions) and their rates of change (expressed as derivatives) are expressed. The intuitive example may be found in classical mechanics: Newton's Laws allow one to relate a body position, velocity, acceleration, various forces and express it as a differential equation. This equation enables tracing of the body position changing in time.

Differential equations are mathematically studied from several different perspectives, mostly concerned with their solutions. Not all differential equations have the solutions given by explicit formulas. If an explicit formula for the solution is not available (e.g. not known, not existing), the solution may be numerically approximated using computers.

The work in this thesis requires solving of differential equations. These equations are used to describe different processes taking place in vegetal tissues such as growth, deformations, transport of morphogens, etc. The systems studied in this thesis, as mentioned before, are frequently $(DS)^2$-systems. Solving of differential equations in such a systems needs particular adaptations. In this section I describe these adaptations. In general, solving of differential equations is a very broad topic thus, here I focus only on its precisely chosen parts. As a result, this text introduces only basic concepts which are required to understand the ODE systems in the context of this thesis.

For this thesis two applications of differential equation systems are particularly important: i) particle-based systems, used to calculate the displacement based on the forces in the system, ii) chemosmotic systems, changing the concentration of morphogens in the tissue. The systems are described in details in Chapter 2 and 3, therefore in this place I focus only on numerical solving. In the first part I introduce the basic definitions and concepts required for clarity of the description of solving algorithm. Next, I explain how the solving algorithms are chosen and adjusted to a given task. It is demonstrated on the example of a system describing Decay Law.

A.1 Math primer

A.1.1 Differential equation

Let us consider first order differential equation (ODE), which can be denoted:

$$\frac{dy\left(t\right)}{dt} = f\left(y\left(t\right), t\right) \tag{A.1}$$

This equation describes the change of y function by the change of its parameter t. This change depends on the y function itself as well as on its argument t. The analytical solution of equation A.1 is the function y which after inputing to this equation changes it to an identity.

A.1.2 Numerical solving

Solving of such an equation in algebraic way is not always possible, since the algebraic form of the solution does not necessary exist for all the problems. In this case we can use the numerical methods to find the *approximation* of the solution. One of the simplest methods which allows us to solve such an equation in numerical way is the Euler method. Assuming that the initial conditions y_0 and function $f\left(y, t\right)$ is known, the value of function y in all its domain using the following formula can be found:

$$y\left(t + \Delta t\right) \approx y\left(t\right) + \Delta t f\left(y\left(t\right), t\right) \tag{A.2}$$

The issue of finding the value of function y knowing the y_0 and function $f\left(y, t\right)$ is called *initial value problem*. This equation is based on the observation, that to evaluate function y value in the point $t + \Delta t$ it is sufficiently to know its value

in the t, and to make a linear approximation on the Δt segment, which is given by function derivate $f(y(t), t)$. The key requirement for using the numerical method is discretization. In the example above, it is related to considering the value of continous function f only in finite number of consecutive points, placed in the distance of Δt from each other. It is important to note, that the accuracy of the approximation increases with the decrease of this distance (Δt). Usually, the equation A.2 is written in the algorithmic way:

$$y_{n+1} := y_n + hf(y_n, t),$$

where $y_n = y(t_0 + nh)$; $h = \Delta x$ and is called the step length.

A.1.3 Precision

One of the important properties of such an approximation is its precision. Numerical methods introduce two type of errors. The first is caused by the finite precision of computations (e.g. due to floating-point representation). The second is due to the difference between the mathematical solution and the approximate solution obtained when the simplifications are made to the mathematical equations, to make them more amenable to calculations. Precision is described by comparing the approximation result y_n to the exact value of function $y(t_0 + nh)$. The absolute value of approximation error e is defined as $e_n = |y_n - y(t_0 + nh)|$.

A.1.4 Solvers

The Euler method, presented in equation A.2, is only an example of a solver finding the approximation of A.1. In the literature we can find different methods, exhibiting different properties (short overview of methods I used during the thesis is presented in the table A.1). Each solver, due to different algorithm approximating the solution, can achieve different error in the same interval of integration. Also, the execution time for one step can differ between the solvers, due to the different complexity of the algorithm. The overall time of the integration increases with the increase of step's number. However, usually, the error decreases with the decrease of h. Therefore, the more precision is required, the longer are the calculations.

A.1.5 Method order

An important property concerning the precision of the method is the dependency between the error and step size. This property is usually measured using the comparison of the method result to the result of Taylor series decomposition of the function. The numerical method is called of order n if it gives the results similar with n factor of Taylor series. It is important to note that for the method of order $n/2$ the decrease of error is proportional to 2^n. For example, by comparing the the Taylor series to the Euler method:

$$y\left(t+h\right)=\sum_{n=0}^{\infty}\frac{y^{(n)}\left(t\right)}{n!}h^{n}=y\left(t\right)+h\frac{dy\left(t\right)}{dt}+O\left(h^{2}\right),$$

we see that the two first factors are present in its development. This means that this method is a first order method $(n=1)$.

A.1.6 A system of n first order equations

The equation A.1 can be generalised to describe not the single equation y and its relation with its first derivative, but to describe the relation of n functions y_i and all its first derivatives. Assuming that $Y=\left(y_1,...,y_n\right)^T$ is a vector of functions, it can be written in the following form:

$$\frac{dY\left(t\right)}{dt}=f\left(Y\left(t\right),t\right)$$

This notation describes the system of n differential equations. It is important to note, that y_i refers to the linear combination of all the other functions which belong to Y. This system can be efficiently solved by adapting the algorithms used to solve a single equation Witkin [2001].

A.1.7 The reduction of n order equation to a system of n first order equations

The equation A.1 can be generalised to describe not only the relation between the function y and its first derivative, but to describe the the relation of a function y and all its $1,2,..,n$-th derivatives. It can be written in the following form:

$$\frac{d^{(n)}y\left(t\right)}{dt^{(n)}}=f\left(y\left(t\right),y^{(1)}\left(t\right),...,y^{(n-1)}\left(t\right),t\right)$$

Then this equation can be transformed into the system of n equation in the following way:

1. We define a family of unknown functions: $\forall 1 \leq k \leq n . y_k := y^{(k-1)}$
2. We rewrite the original system using the n first order equations:
   (a) $\forall 1 \leq k \leq n-1 . y'_k = y_{k-1}$
   (b) $y'_n = f(y_1, y_2, ..., y_{n-1}, t)$

This technique is frequently used in computer science, because solving a system of first order equations can be easily expressed in the algorithmic way (look in [Press et al., 1992, Witkin, 2001]) and is much simpler than dealing with n-th order equations.

A.1.8 Choosing and adapting the solver

The order of method and the step h are two factors which give us direct control over the precision of the calculation. Usually, the increase of the precision of the calculation (e.g. by decreasing the h or choosing higher order method), results in the elongation of the computation time. Therefore, an important issue while solving the ODE equation is to find a method and a step h which allow us to find the solution with a given precision and in the shortest possible time. Usually, it is done by trying different solvers with different steps h on a simplified equation system for which we know the solution (e.g. we are able to find it in an analytical way) and check the error of the calculation and the time required for the integration. This issue can be illustrated on the classical example: finding the solution of Decay Law, which is describe with the following equation:

$$\frac{dr(t)}{dt} = -kr(t)$$

And the initial condition is: $r(0) = 1$, which describes the system configuration in time $t = 0$. The analytical solution of this equation is a function $r(t) = e^{-kt}$. Knowing this, we can check the behaviour of different solving methods and the step size required to achieve desired precision.

Figure A.1 show different behaviour of ODE solvers (Euler method, Runge-Kutta of order 4 and LSODE) applied to Decay Law equation system. The solvers are using different step size h. Figure (A.1A) shows the solution found by the solvers, (A.1B) shows the error of the solvers, (A.1C) average time required

for each solver to integrate the function on increasing interval. Analysing these results, we can choose which method gives us desired precision, not exceeding the maximal allowed time required for the calculation (if we have time constraints).

A.2 Particle-based system solving

The particle-based systems are frequently used in many different applications Reeves [1983], Kaandorp and Gueron [2001]. Newton's Laws allows expressing of a position of a body as a second order differential equation involving various forces acting on this body. As it was demonstrated earlier, a differential equation of order n can be converted to a system of n equation of first order. It means that to compute all the displacement in the system containing k particles we need to solve a system of $2k$ independent, first order differential equations. Another system of equation may be required to compute the forces in the system. However, in the systems I use in my work, the equations describing the forces are explicit and not in the form of differential equations (e,g. they describe processes like elasticity, turgor pressure). The mechanical solver I use for mechanical-based simulation uses the method well-suited for this type of problems: Runge-Kutta of 4th order (for the problem analysis look in Bourg [2001], Witkin [2001], for method implementation Press et al. [1992]). This method allowed me for high precision of calculation with relatively big steps h, which lead to relatively fast calculations.

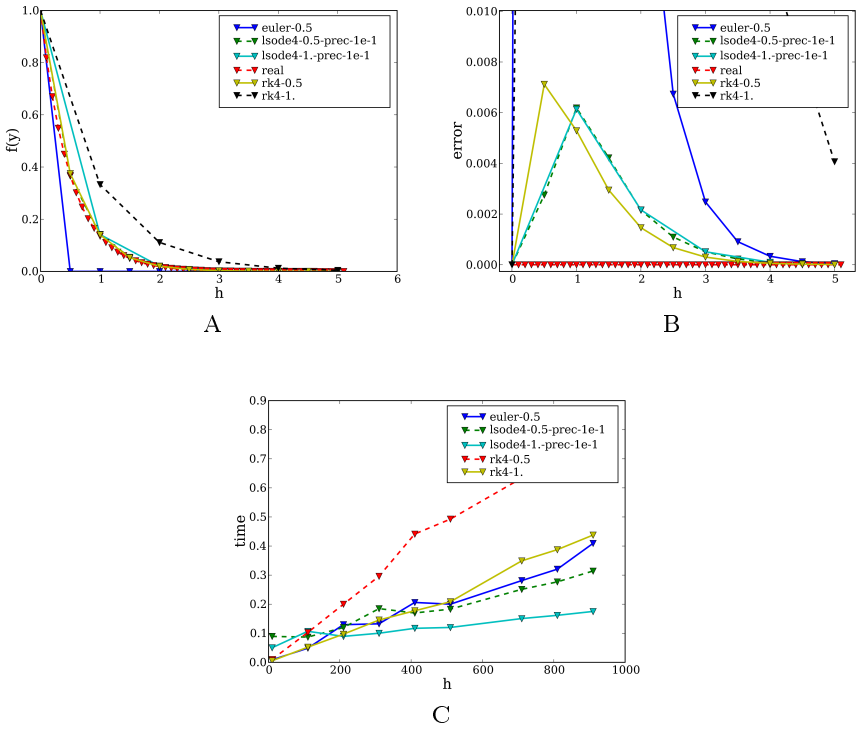

Figure A.1: Figures show the behaviour of different ODE solvers applied to Decay Law equation system.
Curves correspond to different solvers: Euler method, Runge-Kutta of order 4 and LSODE solver for different steps h (which is specified as a second element after "-" in the line description in the legend). The LSODE curve description contains also a third item which describes another solver parameter: the required precision. Figure A.1A shows the solution found by the solvers. Figure A.1B shows the error of the solvers. Figure A.1C average time required for each solver to integrate the function on increasing interval (each point in the line is one simulation for given).

Name	Order	Algorithm	Remarks
forward-Euler	1	$y_{n+1} := y_n + hf(y_n, t_n)$	Fast, simple to implement, imprecise method, mostly used in the case of linear relationships or simple tasks requiring only low precision.
Parabolic extrapolation	2	$y_{n+1} := y_{n-1} + 2hf(y_n, t_n)$ $y_{n+2} := y_n + 2hf(y_{n+1}, t_{n+1})$	More precise then forward-Euler. The second order precision is achieved by introducing the oscillations. Method is sensitive to initial conditions.
Middle point	2	$k_1 := hf(y_n, t_n)$ $k_2 := hf(y_n + k_1/2, t_n + h/2)$ $y_{n+1} := y_n + k_2$	Second order method, which contrary to Parabolic extrapolation does not introduce the oscillations. Faster then Runge-Kutta 4th, however still giving precise solutions.
Runge-Kutta 4th	4	$k_1 := hf(y_n, t_n)$ $k_2 := hf(y_n + k_1/2, t_n + h/2)$ $k_3 := hf(y_n + k_2/2, t_n + h/2)$ $k_4 := hf(y_n + k_3, t_n + h)$ $y_{n+1} := y_n + (k_1 + 2k_2 + 2k_3 + k_4)/6$	The fourth order allow us to apply the method even in difficult numerical problems. It is highly recommended in the situations when we can allow ourselves for longer time of the integration.

Table A.1: ODE solvers implemented during the thesis.

Appendix B

Glossary

B.1 Biology

acropetal Growing or developing upwards from the base or point of attachment, so that the oldest parts are at the base and the youngest are at the tip (Wikipedia).

basipetal Growing or developing from apex to base, so that the oldest parts are nearest the apex and the youngest are nearest the base.

dicots Dicotyledons, or "dicots", is a name for a group of flowering plants whose seed typically has two embryonic leaves or cotyledons (Wikipedia).

epidermis The epidermis is the outer single-layered group of cells covering a plant, especially the leaf and young tissues of a vascular plant including stems and roots (Wikipedia).

gymnosperms are a group of spermatophyte seed-bearing plants with ovules on the edge or blade of an open sporophyll, which are usually arranged in cone-like structures (Wikipedia).

phenotype A phenotype is any observable characteristic or trait of an organism: such as its morphology, development, biochemical or physiological properties, or behavior (Wikipedia).

phloem In vascular plants, phloem is the living tissue that carries organic nutrients (known as photosynthate), particularly sucrose, a sugar, to all parts of the plant where needed (Wikipedia).

plastochrone is the time between consecutive organ formation. Usually it is constant (Wikipedia).

procambium lies just inside of the protoderm and develops into primary xylem and primary phloem. It also produces the vascular cambium, a secondary meristem (Wikipedia).

rheology is the study of the flow of matter. It considers mainly liquids, but also soft solids or solids under conditions in which they flow rather than deform elastically (Wikipedia).

scanning electron microscope (SEM) is a type of electron microscope that images the sample surface by scanning it with a high-energy beam of electrons in a raster scan pattern. The electrons interact with the atoms that make up the sample producing signals that contain information about the sample's surface topography, composition and other properties such as electrical conductivity (Wikipedia).

stem cells are cells found in most, if not all, multi-cellular organisms. They are characterized by the ability to renew themselves through mitotic cell division and differentiating into a diverse range of specialized cell types (Wikipedia).

thallus from Latinized Greek θαλλος (thallos), meaning a green shoot or twig, is an undifferentiated vegetative tissue of some non-mobile organisms, which were previously known as the thallophytes (Wikipedia).

vascular tissue is a complex conducting tissue, formed of more than one cell type, found in vascular plants. The primary components of vascular tissue are the xylem and phloem (Wikipedia).

xylem In vascular plants, xylem is one of the two types of transport tissue, phloem being the other. The word "xylem" is derived from classical Greek ξυλον (xylon), "wood", and indeed the best known xylem tissue is wood, though it is found throughout the plant. Its basic function is to transport water (Wikipedia).

B.2 Computer science

API An application programming interface (API) is a set of declarations of the functions (or procedures) that an operating system, library or service provides to support requests made by computer programs (Wikipedia).

approximation An approximation (represented by the symbol $\approx$) is an inexact representation of something that is still close enough to be useful. Although approximation is most often applied to numbers, it is also frequently applied to such things as mathematical functions, shapes, and physical laws (Wikipedia).

complex system A complex system is a system composed of interconnected parts that as a whole exhibit behaviour not obvious from the properties of the individual parts (Wikipedia).

computing, distributed deals with hardware and software systems containing more than one processing element or storage element, concurrent processes, or multiple programs, running under a loosely or tightly controlled regime (Wikipedia). v

computing, parallel is a form of computation in which many calculations are carried out simultaneously,[1] operating on the principle that large problems can often be divided into smaller ones, which are then solved concurrently ("in parallel") (Wikipedia).

discretization In mathematics, discretization concerns the process of transferring continuous models and equations into discrete counterparts (Wikipedia).

graph In mathematics and computer science, a graph is the basic object of study in graph theory. Informally speaking, a graph is a set of objects called points, nodes, or vertices connected by links called lines or edges (Wikipedia).

GUI is a type of user interface which allows people to interact with electronic devices such as computers, hand-held devices (MP3 Players, Portable Media Players, Gaming devices), household appliances and office equipment (Wikipedia).

hash map In computer science, a hash table, or a hash map, is a data structure that associates keys with values. The primary operation it supports efficiently is a lookup: given a key (e.g. a person's name), find the corresponding value (e.g. that person's telephone number). It works by transforming the key using a hash function into a hash, a number that is used as an index in an array to locate the desired location ("bucket") where the values should be (Wikipedia).

Appendix C

Communication&Diffusion

C.1 Posters

OpenAlea

An open-source platform for the integration of heterogenous FSPM components

S. Dufour-Kowalski[1], C. Pradal[2], N. Dones[3], P. Barbier de Reuille[4], F. Boudon[5], J. Chopard[1], D. DaSilva[6], J.-B. Durand[7], F Ferraro[3], C. Fournier[3], Y. Guédon[5], A. Ouangraoua[8], C. Smith[4], S. Stoma[1], F. Théveny[3], H. Sinoquet[3] and C. Godin

[1]INRIA, Sophia Antipolis, France; [2]CIRAD, Montpellier, France; [3]INRA, Clermont-Ferrand, France; [4]Université Montpellier2, Montpellier, France; [5]INRA, Thiverval Grignon, France; [6]Université Bordeaux 1, LaBRI, Talence, France; [7]INPG, LJK/IMAG, Grenoble, France; [8]INRA, 34060 Montpellier, France

A collaborative approach

The open source OpenAlea project's goal is to share and reuse heterogeneous models from the FSPM community

The open source development model provides a framework to efficiently develop a software platform in a scientific context. It improves:

(a) **scientific collaboration** by providing free access to published scientific models;
(b) **model comparison** by providing access to the source code for the entire community;
(c) **synergy** by enhancing the collaboration between multidisciplinary research teams;
(d) **economies of scale** by sharing development, distribution and maintenance cost; and
(e) **software quality** by enforcing common rules and best practices.

Free Licensing
The OpenAlea platform is distributed under a free license (GNU LGPL) allowing external components to choose their own license (including proprietary). Each modeler is responsible for the development of its modules but takes advantage of the facilities provided by the platform.

Coding and Modeling sprints
Developers and modelers start collaboration and work together in pairs on a common objective during coding and modeling sprint sessions, encouraging communication, feedback and exchanges.

Collaborative environment
Documentation, source code, forum, bug tracking and binary distributions are freely available on a collaborative web space (http://openalea.gforge.inria.fr).

Diffusion
Available models are distributed and shared via the network and are easily installable throught the OpenAlea installation framework. License, author and copyright information are included in each package.

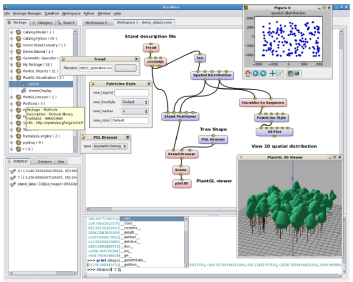

Visualea: OpenAlea visual programming interface. Modules are represented by boxes with inputs and outputs. The graph represents the program flow, here, a stand generation process (Da Silva et al. FSPM07).

First integrated components

Plant Architecture analysis

Multiscale plant architecture databases are constructed from field mesurement using different methods (digitiser, topology mapping, etc). 3D plants structures are reconstructed and various tools are available to explore their topology and their geometry (Godin et al. 1999).

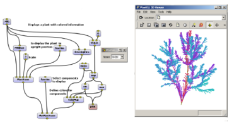

The hidden Markov tree models are used to identify tree entities with similar characteristics (length, presence/absence of flowers,...), and to characterise how they change within the trees (gradients). Here, each category of entities corresponds to one of the 8 hidden states. The restoration of the hidden states leads to a visual labelling of the entities using the 8 classes. See (Durand et al. FSPM 2007).

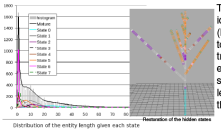

Multiple change-point models are used to identify growth phases along tree main axis (Guédon et al. FSPM 2007).

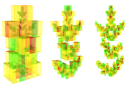

$$D_b = \lim_{\delta \to 0} \frac{\log N_\delta}{\log \frac{1}{\delta}} \delta$$

The fractal dimension of a plant characterizes the complexity of plant foliage. It can be estimated using the Box Counting Method. It uses tools to discretize the plant volume in voxels at different scales δ. The number of voxels intercepted by the plant, N_δ, is counted. Using a range of decreasing scale δ, fractal dimension is assessed by a linear regression between the log of these 2 quantities (Da silva et al. 06).

Plant geometry modeling

PlantGL is a graphic library dedicated to plant modeling. It contains a hierarchy of geometric objects that can be assembled into a scene graph, a set of algorithms to manipulate them and some visualization tools (Pradal et al. 2007). Plant and forest mockups can be build and analysed interactively. For instances :

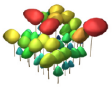

Stands are generated by positioning and deforming coarse representations of individuals using a distribution method based on Gibbs process that simulates tree competition (Boudon et al. 2007).

Different tree architectures can be generated procedurally. The model defined by Weber and Penn (Weber and Penn, 1995) is used for tree generation and is based on a set of allometric rules. Fundamental parameters are, for instance, the overall appearance of the tree, the size of the lower part of the tree without branches, the max branching order, and the curvature of the axes.

Ecophysiological processes

The Drop model simulates rainfall interception and distribution by plants. It has been applied on 3D banana plants mock-ups. DropTri provides meshing algorithms for digitised leafs and DropInt computes water flows, interception and splashing on a virtual plant or a plot (Dufour-Kowalski et al. FSPM 2007).

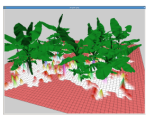

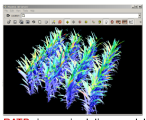

Caribu is a model for lighting 3D virtual plant canopies. It uses the nested radiosity algorithm (Chelle et al., 1998), and gives a precise estimation of light absorption at the level of small canopy elements (typically 1 cm^2). The model is composed of: MCSAIL, that computes turbid medium equations on a layered canopy and CANESTRA, that computes radiosity and projection.

RATP is a simulation model computing radiation interception, transpiration and carbon gain of tree canopies for a range of spatial scales. The tree structure is abstracted with a set of voxels fitting the canopy shape and accounting for the spatial distribution of leaf area density. Radiation interception is computed from the turbid medium analogy. Transpiration and photosynthesis are derived from the energy balance and the biochemical Farquhar's model (Sinoquet et al. 2001).

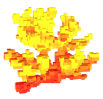

Meristem Modeling

The Phyllotaxis toolkit provides tools to visualise and analyse various standard phyllotaxis model properties (divergence angles, time between primordia creation, etc). We show here an implementation of Snow&Snow inhibitory field based model. Others, like auxin transport based family (Johnson et. al 2006, Smith et al. 2006) are also available.

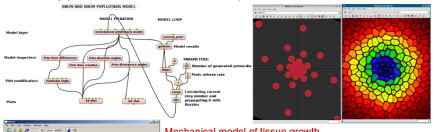

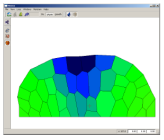

Mechanical model of tissue growth.
At tissue scale, a set of interconnected modules make it possible to simulate the growth of plant organs. Physiology modules are used to compute the change of the state of cells (i.e. chemical concentrations, genetic state) taking into account the state of adjacent cells. A mechanical model of cells is used to compute cell deformation and growth under turgor pressure (Chopard et al. 2007). This information is then integrated at tissue scale to compute the growth achieved by the tissue throughout time.

References

Boudon F. & Le Moguedec G. 2007, Déformation asymétrique de houppiers pour la génération de représentations paysagères réalistes. REFIG.
Chelle M. & Andrieu B. 1998, The nested radiosity model for the distribution of light within plant canopies. Ecological Modelling.
Chopard J. et al. 2007, Toward a formal expression of morphogenesis: a mechanics based integration of cell growth at tissue scale. IPCAT07.
Da Silva D. et al. 2006, A Critical Appraisal of the Box Counting Method to Assess the Fractal Dimension of Tree Crowns. ISVC 2006.
Da Silva D. et al. 2007, Modeling of light transmission under heterogeneous forest canopy: model description and validation. FSPM07.
Dufour-Kowalski S. et al. 2007, A software for the simulation of rainfall distribution on 3D plant architecture: PyDROP. FSPM07.
Durand J.B. et al. 2007, Segmentation-based approaches for characterising plant architecture and assessing its plasticity at different scales. FSPM07.
Guédon Y. et al. 2007, Identifying and characterizing the ontogenetic component in tree development. FSPM07.
Godin, C. et al. 1999, Exploration of plant architecture databases with the AMAPmod software illustrated on an apple-tree hybird family. Agronomie.
Jönsson H. et al. 2006, An auxin-driven polarized transport model for phyllotaxis. Natl Acad Sci USA.
Pradal C. and al. 2007, The architecture of OpenAlea: A visual programming and component based software for plant modeling. FSPM07.
Pradal C. and al. 2007, PlantGL : A python-based geometric library for plant modeling at different scales. RR - INRIA.
Sinoquet H. et al., 2001, RATP: A model for simulating the spatial distribution of radiation absorption, transpiration and photosynthesis. Plant, Cell and Environment.
Smith RC. et al., 2006, A plausible model of phyllotaxis. PNAS.
Weber J., and Penn, J. 1995, Creation and rendering of realistic trees. SIGGRAPH 1995.

Web : http://openalea.gforge.inria.fr

INRIA CIRAD INRA

Figure C.1: FSPM in Napier, 2007.

Auxin transport in the SAM: Canalization as a unifying concept for auxin transport in plant development

Szymon Stoma, Christophe Godin, Jan Traas.

Modelling phyllotaxis

Several macroscopic models at the tissue level have been proposed to explain phyllotaxis:

Minimum-space (van Iterson 1907, Snow&Snow 1962):
The primordium initiation requires a "minimum space" free of all other organs before it can occur.

Inhibitory-based models (Schoute 1913, Couder&Douady 1996, Smith et al. 2007):
The primordium produces an inhibitor (or takes away a stimulator) which prevents other primordia to form.

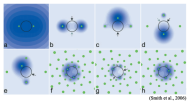

Green dots represent primordia centers. The intensity of blue colour describes the strength of the inhibitory field (blue is depicting high values). The figures present the formation of consecutive primordia.

(Smith et al., 2006)

At the cellular level polar active auxin transport (by a family of membrane transporters of the PIN family) seems to play an important role (Reinhardt et al. 2003). At this level one model has been proposed that can explain the macroscopic behaviour:

The cells probe their environment and 'pump' auxin to the neighbours with a higher concentration (Up-The-Gradient: Jönsson et al. 2006, Smith et al. 2006). As a consequence, PIN transporters polarise towards the auxin maximum. This model can explain phyllotaxis.

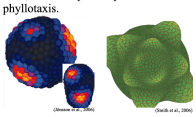

Both figures present L1 cells in the meristem. The concentration of auxin is marked with colour gradients (in the left: from blue to red and in the right: from dark green to light green for low to high values respectively). In the left figure the concentration of auxin in the cell is marked with the intensity of red colour (red is depicting high values).

(Jönsson et al., 2006) (Smith et al., 2006)

A conceptual problem

While an Up-The-Gradient model has been proposed for phyllotaxis, a completely different auxin transport mechanism has been proposed for other patterning mechanisms in the plant, in particular venation in leaves and stems: the Canalization concept (Sachs 1979).

Canalization assumes that auxin flux controls the localisation of auxin transporters. The cells sense an initial flux, which is subsequently reinforced by the PIN transport system.

Since it seems strange that the plant would use two distinct mechanisms involving the same molecular elements, we wondered whether the Canalization could be used as well to explain the genesis of phyllotactic patterns.

Canalization equation system

The Canalization system could be denoted:

$$\frac{\partial c_i}{\partial t} = \sum_{n \in N_i} J_{i \to n}$$

$$J_{i \to n} = \gamma \left(c_n p_{n,i} - c_i p_{i,n} \right)$$

The concentration of product in the cell changes according to the net flux of auxin between its neighbours. The net flux is the difference between incoming and outcoming product particles. The gamma describes the efficiency of the product transport and the reaction constant for Prod+Tran->$\text{Tran}_{\text{prod}}$ The key concept of Canalization states that the transporter concentration changes with the flux of product, which could be denoted:

$$\frac{\partial p_{i,j}}{\partial t} = \Phi \left(J_{i \to j} \right) + \sigma_p - \theta_p p_{i,j}$$

Canalization-based model can mimic inhibitory-based model

The active transport in the Canalization-based phyllotaxis model mimics the behaviour of inhibitory field, therefore the model is able to reproduce the same patterns as inhibitory based model family. Primordium instead of producing the inhibitor, drains the activator. The role of the activator is played by IAA. As a consequence, the concentration of auxin explicitly corresponds to the inhibitory field. The field is modified by the active transport of auxin, which is governed by PIN proteins. Primordia act as sinks, draining the auxin from the meristem. The auxin concentration gradient is increasing with the overall distance from all primordia and it is smooth (which is the reason why it can mimic the inhibitory field):

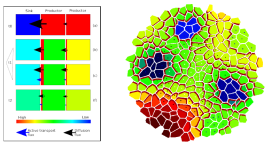

In the left figure the Canalization basics is presented on the example of linear cell system. Left cell unit is a sink and two rightmost cells are auxin sources. The solution to equilibrium state is shown. In the right figure the application of Canalization system on the meristem is shown. The concentration of auxin is marked with small black dots and auxin sour cells with white dots. Primordium cells (marked with small blue dots) act as sinks. The concentration of auxin is marked with colour gradient from dark blue (low) to red (high). Concentration of PIN is marked with cell wall thickness.

New primordium is inserted as an indirect result of the meristem growth. The growth moves primordia away from the meristem centre, which increases the concentration of auxin in the competence zone. The primordium is inserted in the competence zone, when the concentration of auxin exceeds certain threshold. Inserted primordium acts as a sink and modifies the concentration gradient of auxin in whole meristem:

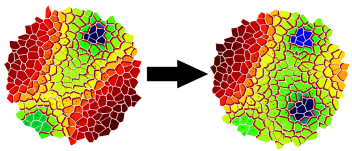

Conclusion

The Canalization-based model shows that the Canalization concept is possible as a unifying hypothesis of auxin transport in the plant. Predictions from Canalization and Up-The-Gradient models have now to be tested using experimental approaches.

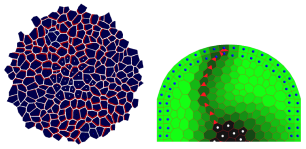

In the left figure the PIN map output from the model is shown. On the right Canalization system was applied to transversal cut of meristem. The vein formation could be observed. Concentration of auxin is marked with colour gradient form black (low) to green (high).

References

Douady, S. and Couder, Y. (1996). Phyllotaxis as a dynamical self organizing process part I: The spontaneous formation of a periodicity and the coexistence of spiral and whorled patterns. Journal of Theoretical Biology, 178(3):275-294.
Sachs, T. and Cohen, D. M. (1977). The Polar Transport of Auxin. Annual Review of Plant Physiology, 28(1):439-470.
Jönsson, H., Heisler, M. G., Shapiro, B. E., Meyerowitz, E. M., and Mjolsness, E. (2006). An auxin-driven polarized transport model for phyllotaxis. Proc Natl Acad Sci U S A, 103(5):1633-1638.
Reinhardt, D., Mandel, T., and Kuhlemeier, C. (2003). Auxin regulates the initiation and radial position of plant lateral organs. Plant Cell, 12(4):507-518.
Reinhardt, D., Pesce, E.-R., Stieger, P., Mandel, T., Baltensperger, K., Bennett, M., Traas, J., Friml, J., and Kuhlemeier, C. (2003). Regulation of phyllotaxis by polar auxin transport. Nature, 426(6964):255-260.
Smith, R., Kuhlemeier, C., and Prusinkiewicz, P. (2006). Inhibition fields for phyllotactic pattern formation: a simulation study. Canadian Journal of Botany, 84(11):1635-1649.
Smith, R. S., Guyomarc'h, S., Mandel, T., Reinhardt, D., Kuhlemeier, C., and Prusinkiewicz, P. (2006). A plausible model of phyllotaxis. PNAS, 103(5):1301-1306.

Canalization-based phyllotaxis model

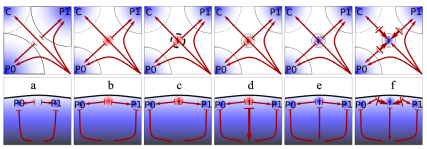

In the Canalization model an initiation of new primordium looks as follow: each primordium acts as a sink, therefore it lowers the concentration of auxin in its closest neighbourhood. The concentration of auxin in primordia is lower than in the neighbourhood. Due to the growth of meristem primordia move away from each other (a), which increases the concentration of auxin in the region between them. The maximum of concentration of auxin gradually appears in the place maximising the distance between all primordia (b). The pumps in L1 close to the maximum point in the direction of the closest primordium (or the centre). The concentration of auxin exceeding certain threshold induces the change of the cell identities in the zone of maximum concentration of auxin. These cells are recruited to the initium (c). The change of cell identities in the initium stimulates formation of the vasculature (d). The vein formed below the initium drains the auxin and converts the initium into a minimum (e). The initium acts as a sink and drags the auxin from the neighbourhood. The flux induced by this process reverses pump polarisations in the direction of initium on the surface (f).

Up-The-Gradient phyllotaxis model

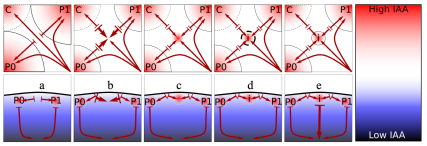

In the Up-The-Gradient model an initiation of new primordium looks as follow: each primordium acts as a sink, therefore it lowers the concentration of auxin in its closest neighbourhood. The concentration of auxin in primordia is higher than in the neighbourhood, because we assume that the removal of auxin from L1 is smaller then the net flux coming to primordia. Due to the growth of the meristem primordia move away from each other (a), which changes the balance between active transport and diffusion. This change reverses pump polarisations in L1 in the direction of place maximising the distance between all primordia (b). This reverse creates the new maximum of the concentration of auxin (c). The concentration of auxin exceeding certain threshold induces the change of the cell identities in the zone of maximum concentration of auxin (d). The change of cell identities in the initium stimulates formation of the vasculature (e).

Figure C.2: MEET in Berlin, 2008.

C.2 Covers

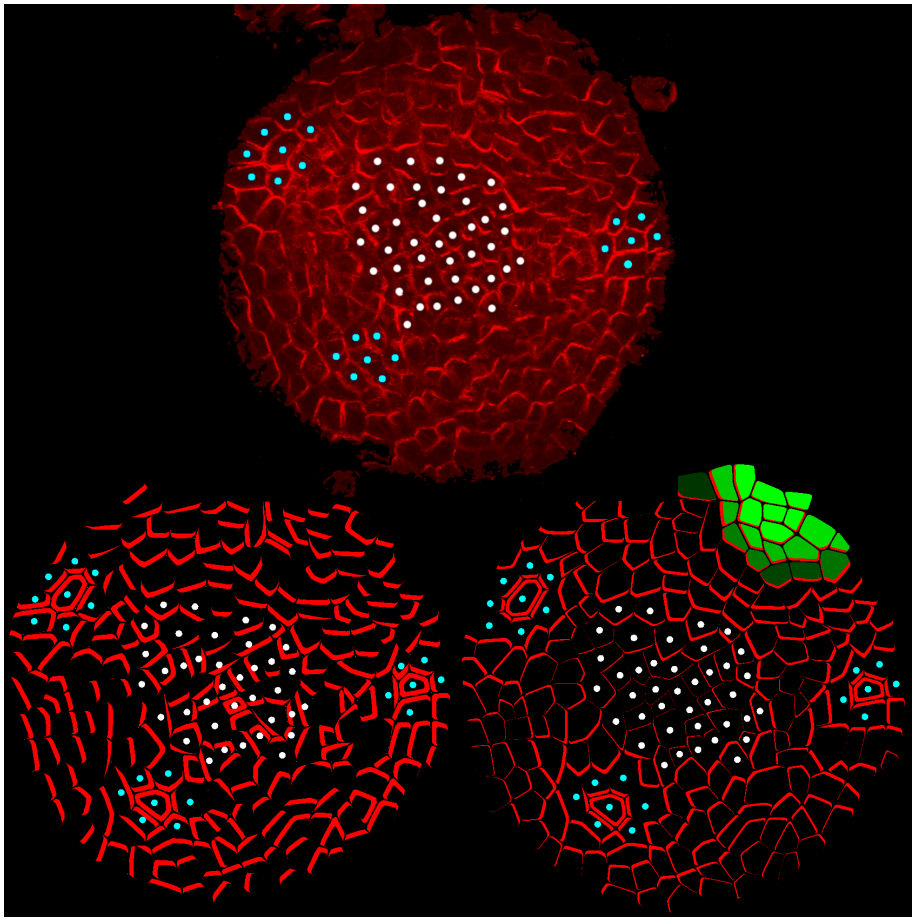

Figure C.3: Cover of October issue of PLOS Computational Biology 2008. Transport of the plant hormone auxin in a virtual meristem: A comparison between simulations and experimental data. Top: observed distribution of auxin transporters (PIN proteins) in shoot apical meristem cells of Arabidopsis. The image was obtained by immunolabelling of the PIN1 auxin-carrier using confocal microscopy. Bottom left: Digitized version of the top image where the efflux carriers have been manually positioned. Bottom right: simulated distribution of efflux carriers (in red) emerging from a flux-based polarization hypothesis of auxin transport. This type of virtual experiment makes it possible to test in silico different hypotheses on mechanisms that are not fully accessible experimentally and to assess their plausibility by comparing predictions with experimental data.

C.3 Original papers

C.3.1 Using mechanics in the modelling of meristem morphogenesis

This annex contains the work presented during the Fifth International Workshop on Functional-Structural Plant Models which was held in November 2007 in Napier, New Zealand.

Using mechanics in the modelling of meristem morphogenesis

Szymon Stoma[1,†], Jérôme Chopard[1,†], Christophe Godin[1,†], Jan Traas[3,‡]

[1] INRIA, 2004 route des lucioles BP 93, 06902 Sophia Antipolis, France
[3] INRA, 147 rue de l'Université, 75338 Paris Cedex 07, France
[†] Virtual Plants, UMR Développement et Amélioration des Plantes, TA A-96/02, 34398 Montpellier Cedex 5, France
[‡] Laboratoire de Reproduction et Développement des plantes, UMR INRA/CNRS/ENS, 46 allée d'Italie, 69364 Lyon Cedex 7, France

Keywords : mechanics ; meristem ; morphogenesis ; shape development

Introduction

Shoot apical meristems are small groups of rapidly dividing, undifferentiated cells, which generate all aerial parts of the plants. Recently, spectacular advances in molecular biology and genetics have provided a wealth of information on meristem functioning. However, the amount of available information is now such, that an integrated view is no longer possible. As a result, researchers have been led to develop computational models in the form of *virtual meristems* to analyse this complexity *in silico* and to test different hypotheses. Only very recently three such models have been described [8, 1, 5]. All three are able to integrate various cell-based processes and show different emerging behaviours (e.g. meristem maintenance, phyllotaxis). This pioneering work has demonstrated that the *in silico* analysis of plant development can be an extremely useful complement to classical experimentation.

Previous models have focused their interrogations on physiological processes in the meristem for a given, predefined, tissue shape. However, in nature, the shape itself is the result of a continuous feedback loop between physiological information and growth. As suggested by [4, 2], the mechanical components of the cells could provide such a link. In this work, we consider the problem of integrating such a feedback loop in meristem development.

The role of mechanics

As physical objects, cells obey mechanical laws. In plants, a major factor controlling cell shape is the cell wall, which resists to the internal turgor pressure and guarantees the final shape of the cell. Turgor (Π_0) induces mechanical constraints ($\underline{\underline{\sigma}}$) into the walls :

$$\mathrm{div}\underline{\underline{\sigma}} = \Pi_0 \tag{1}$$

Being elastic, walls deform and elongate to adjust to this stress. This deformation ($\underline{\underline{\varepsilon}}$) depends on mechanical properties of each wall which is caracterized by set of parameters (called tensor of elasticity, $\underline{\underline{\underline{\underline{K}}}}$):

$$\underline{\underline{\sigma}} = \underline{\underline{\underline{\underline{K}}}}(\underline{\underline{\varepsilon}} - \underline{\underline{\varepsilon^0}}) \tag{2}$$

The equations of mechanics (1 and 2) allow us to compute the elongation ($\underline{\underline{\varepsilon}} - \underline{\underline{\varepsilon^0}}$) of each wall (and thus each cell) for a given state (turgor pressure). However, to obtain a given shape, elastic deformations are not sufficient and plants must add material into the walls to achieve some plastic deformation. One biochemical hypothesis [3] is that cells add material to fill the void between cellulose microfibrils in the wall. The more the wall is stretched, the more gaps are being created between fibrils, the more material must be added to the wall. This modifies the reference state ($\underline{\underline{\varepsilon^0}}$) of the wall and thus growth is increased in the direction for which ($\underline{\underline{\varepsilon}} - \underline{\underline{\varepsilon^0}}$) reaches maximum. By synthesising expansins (e.g. auxin) that change cell walls' elasticity ($\underline{\underline{\underline{\underline{K}}}}$ and then $\underline{\underline{\varepsilon}}$) or wall *repair* rate (parameter G in equation 3), meristem shape can emerge fom cell physiological properties.

Mechanical model of meristem surface

In *Arabidopsis*, the external cell layer (called L1) plays a crucial role in meristem functioning [6]. To build up a mechanical model of this surface, we projected the L1 cells on the external surface of the meristem to obtain a polygonal mesh. Each polygonal cell is surrounded by the edges that stand for the projection of

its anticlinal walls, assuming an infinitely small thickness of the walls. A junction between edges is called a vertex. The behaviour of all inner cells of the meristem is summarized by an overall turgor pressure that perpendiculary pushes the surface and prevents the L1 layer from collapsing (as expressed in (d) on figure 1).

To describe the mechanical properties of a meristem the representation described above is expressed in terms of a mass-spring system (MSS). Each edge e_i has an associated spring while masses are attached to the vertices. The mechanical behaviour of each spring is characterised by two parameters: a stiffness K_i and a rest length l_i^0. Growth is expressed as a change of spring rest length l^0 depending on the current spring tension :

$$\frac{\partial l_i^0}{\partial t} = \begin{cases} 0 & \text{if} \quad [l_i(t) - l_i^0] < \text{threshold} \\ G[l_i(t) - l_i^0] & \text{else} \end{cases} \tag{3}$$

where G is a growth rate. This change, in turn, induces a new mechanical state. A solver for particle systems [9] was designed to trace the shape evolution of the mesh.

This model was used to reproduce *in silico* the change of shape of the *Arabidopsis pin1* mutant depicted by Reinhardt [7]. This paper describes the emergence of a young primordium near the position of an applied patch of auxin. Cells with high auxin concentration grow faster, possibly due to the change in the mechanical properties of their walls. We simulate this behaviour by changing the mechanical parameters K of the springs associated with edges of the cells with high auxin concentration. In our model this resulted in faster, local growth in the *auxin-positive* region (in red on figure 1 (a)). The *bump* shaped structure, that appears, reproduces the appearance of a young primordium (simulation output presented in figure 1 (a)).

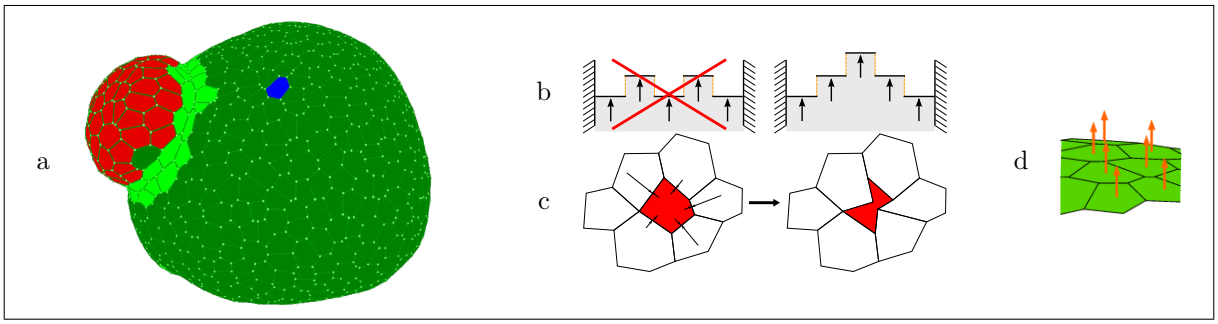

Figure 1: Model of meristem surface

This figure shows in (a) the modelling of *primordium* induction by an auxin patch applied in the red region. On (b), solid bars (horizontal segments, in black) are linked by elastic springs (vertical segments, in yellow). Extremities of the system are fixed. A pressure applied from bottom on the system will push all the bars to top. Crest formation is thus impossible. The red cell in (c) collapses due to the load of its neighbors. The explicit L1 layer representation (green poligons) with implicit inner cells (represented as pressure force – orange arrows) in (d).

Modelling only surface cells with 1D walls as springs is an efficient way to address meristem shape modelling. It allows fast computation of meristem shapes when testing different parameters of this complex system. In addition, the use of springs seems to be compatible with what is known on the biological system. In particular the concept of growing springs yielding to an inner force is clearly coherent with the idea of cell wall synthesis permitting the cells to yield to inner pressure. However, the implicit representation of the inner cells as a generalised pressure makes it impossible to generate more complex shapes (see figure 1 (b)). To model a crest instead of a bump, for instance, we need to explicitely represent the interior of the meristem. In addition, the use of MSS is suitable for small shape deformations but becomes less straight forward when dealing with more complex deformations. Because the link between two springs has no rotational constraint, cells under external load tend to collapse (see figure 1 (c)).

Mechanical model of meristem volume

To address complex shape changes, we need to model explicitly the interior of the meristem. The simplest conceptual way to do it consists of implementing a full 3D model of a tissue. In this model, all cells are

represented as polyhedra as shown on figure 2 (a). We assume that the wall between two cells remains planar and can thus be represented as a polygon in space. Wall mechanical properties are summarized by the two principal directions of the elasticity tensor in this plane. This assumption allows us to use the shell theory to compute deformations and constraints in the meristem with a finite elements method. As in the previous model, growth is computed as a function of the amount of deformation of the mesh standing for the meristem, parameterized by the physiological state of each individual cell.

The young carpels formed by the young Arabidopsis flower, arise together as a cylindrical shape on the top of the floral meristem. They provide a typical example of complex structure (see figure 2 (b)) previously described on figure 1 (b). The model makes it possible to simulate the result of a differentiation of a ringlike domain cells around the meristem center. These cells grow out more quickly than their neighbours, which is caracterized by a more rapid extension of the cell walls in the model. A 3D representation of this meristem shows the formation of the cylindrical *style tube* (see figure 2 (c))

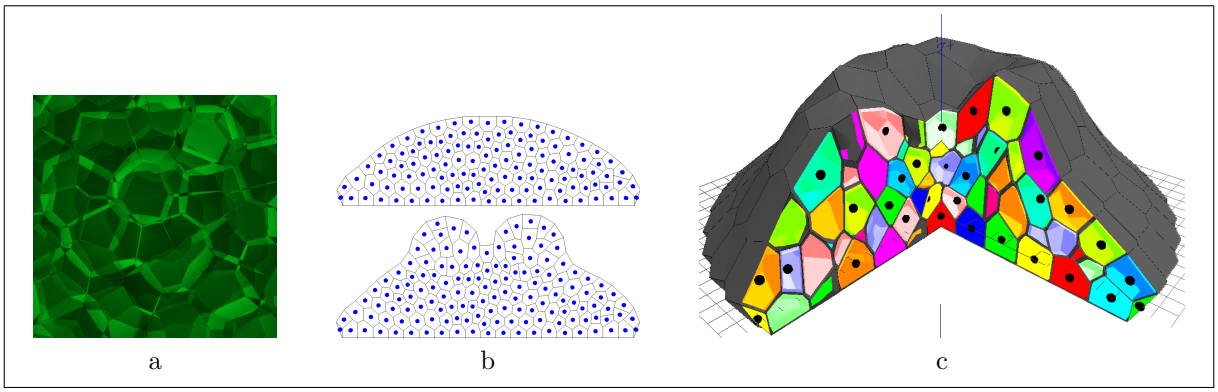

Figure 2: Carpel formation

(a) 3D meristem representation where cells appear as polyhedra. (b) Simulation of carpel development. From an initial state (on top) with a bump shaped meristem, the simulation runs to a crest shaped tissue (on bottom). (c) 3D representation of the final state of the simulation depicted in (b) that shows the formation of the *style tube*.

Conclusion

In the talk, we shall present the application of mechanical models to the integrated simulation of primordia generation and carpel development. We shall discuss how these models relate physiological information to meristem morphogenesis. By closing the feedback loop, they provide, a useful complement to previous models that mainly concentrated on physiological processes.

References

[1] Pierre Barbier de Reuille, Isabelle Bohn-Courseau, Karin Ljung, Halima Morin, Nicola Carraro, Christophe Godin, and Jan Traas. Computer simulations reveal properties of the cell-cell signaling network at the shoot apex in arabidopsis. *PNAS*, 103(5):1627–1632, 2006.

[2] Enrico Coen, Anne-Gaëlle Rolland-Lagan, Mark Matthews, J. Andrew Bangham, and Przemyslaw Prusinkiewicz. The genetics of geometry. *PNAS*, 101(14):4728–4735, 2004.

[3] Daniel J. Cosgrove. Growth of the plant cell wall. *Nature reviews*, 6:850–861, 2005.

[4] Jacques Dumais and Charles R. Steele. New evidence for the role of mechanical forces in the shoot apical meristem. *Journal of Plant Growth Regulation*, 19:7–18, 2000.

[5] Henrik Jönsson, MArcus G. Hesler, Bruce E. Shapiro, Elliot M. Meyerowitz, and Eric Mjolsness. An auxin-driven polarized transport model for phyllotaxis. *PNAS*, 103(5):1633–1638, 2006.

[6] Sharon Kessler, Brad Townsley, and Neelima Sinha. L1 division and differentiation patterns influence shoot apical meristem maintenance. *Plant Physiology*, 141:1349–1362, 2006.

[7] Didier Reinhardt, Therese Mandel, and Cris Kuhlemeier. Auxin regulates the initiation and radial position of plant lateral organs. *The Plant Cell*, 12:507–518, 2000.

[8] Richard S. Smith, Soazig Guyomarc'h, Therese Mandel, Didier Reinhardt, Cris Kuhlemeier, and Przemyslaw Prusinkiewicz. A plausible model of phyllotaxis. *PNAS*, 103(5):1301–1306, 2006.

[9] Andrew Witkin. Physically based modeling. Technical report, Pixar AnimationStudio, 2001.

C.3.2 *Flux-Based* Transport Enhancement as a Plausible Unifying Mechanism for Auxin Transport in Meristem Development

This anex contains the paper published in October issue of PLOS Computational Biology 2008.

OPEN ACCESS Freely available online

PLoS COMPUTATIONAL BIOLOGY

Flux-Based Transport Enhancement as a Plausible Unifying Mechanism for Auxin Transport in Meristem Development

Szymon Stoma[1,2], Mikael Lucas[1], Jérôme Chopard[1], Marianne Schaedel[2], Jan Traas[2]*, Christophe Godin[1]*

1 Virtual Plants Project-Team, UMR DAP, INRIA, Montpellier, France, **2** Laboratoire de Reproduction et Développement des Plantes, Université de Lyon 1, INRA, CNRS, ENS-Lyon, Lyon, France

Abstract

Plants continuously generate new organs through the activity of populations of stem cells called meristems. The shoot apical meristem initiates leaves, flowers, and lateral meristems in highly ordered, spiralled, or whorled patterns via a process called *phyllotaxis*. It is commonly accepted that the active transport of the plant hormone auxin plays a major role in this process. Current hypotheses propose that cellular hormone transporters of the PIN family would create local auxin maxima at precise positions, which in turn would lead to organ initiation. To explain how auxin transporters could create hormone fluxes to distinct regions within the plant, different concepts have been proposed. A major hypothesis, *canalization*, proposes that the auxin transporters act by amplifying and stabilizing existing fluxes, which could be initiated, for example, by local diffusion. This convincingly explains the organised auxin fluxes during vein formation, but for the shoot apical meristem a second hypothesis was proposed, where the hormone would be systematically transported towards the areas with the highest concentrations. This implies the coexistence of two radically different mechanisms for PIN allocation in the membrane, one based on flux sensing and the other on local concentration sensing. Because these patterning processes require the interaction of hundreds of cells, it is impossible to estimate on a purely intuitive basis if a particular scenario is plausible or not. Therefore, computational modelling provides a powerful means to test this type of complex hypothesis. Here, using a dedicated computer simulation tool, we show that a *flux-based* polarization hypothesis is able to explain auxin transport at the shoot meristem as well, thus providing a unifying concept for the control of auxin distribution in the plant. Further experiments are now required to distinguish between *flux-based* polarization and other hypotheses.

Citation: Stoma S, Lucas M, Chopard J, Schaedel M, Traas J, et al. (2008) *Flux-Based* Transport Enhancement as a Plausible Unifying Mechanism for Auxin Transport in Meristem Development. PLoS Comput Biol 4(10): e1000207. doi:10.1371/journal.pcbi.1000207

Editor: Jason A. Papin, University of Virginia, United States of America

Received May 9, 2008; **Accepted** September 16, 2008; **Published** October 31, 2008

Copyright: © 2008 Stoma et al. This is an open-access article distributed under the terms of the Creative Commons Attribution License, which permits unrestricted use, distribution, and reproduction in any medium, provided the original author and source are credited.

Funding: This work was partially funded by the European RTN SY-STEM and the ANR Virtual Carpel projects.

Competing Interests: The authors have declared that no competing interests exist.

* E-mail: jan.traas@ens-lyon.fr (JT); christophe.godin@inria.fr (CG)

Introduction

During plant development, organs are continuously created by small populations of cells called *apical meristems*. The so-called shoot apical meristem (SAM) generates all the aerial parts of the plant. The SAM is a highly organized structure, composed of a central zone required to maintain the meristem and a surrounding peripheral zone, that is competent to initiate new organ primordia [1]. The young organs are usually initiated in highly ordered spiralled or whorled patterns. This remarkable arrangement of organs is called phyllotaxy and varies according to particular plant species and growth conditions. Over the last two centuries, phyllotaxy has been extensively studied and different models for this patterning process have been proposed. From a mechanistic point of view, it is now widely accepted that phyllotaxy emerges from a process of local lateral inhibition: each primordium creates an inhibitory field in its vicinity where no other primordium can develop. This basic inhibitory field hypothesis (see [2] for a review), is potentially able to generate a wide range of phyllotactic patterns [2–6].

Hypotheses concerning the physiological nature of these inhibitory fields were proposed only recently [7]. They rely on the signalling role of a key hormone called *auxin*, that plays a crucial role in primordium formation [1]. Auxin is actively transported throughout the plant from cell to cell by carriers that are located at the cell plasma membranes [8]. During auxin transport influx carriers of the AUX/LAX family, facilitate auxin import into the cells. This is in contrast to the PIN-FORMED (PIN) proteins, which facilitate efflux [9]. Interestingly, PIN proteins often accumulate on one particular side of the cell, thus suggesting that auxin is evacuated preferentially via that side. Importantly, PIN carriers often show locally coherent orientations between groups of neighbouring cells, indicating that PIN orientation is coordinated at the level of tissues [7,10]. It is therefore possible to imagine how cells could transport auxin from cell to cell throughout the plant, thereby creating fluxes that lead to local hormone maxima and minima [11,12]. These differences in concentration would subsequently be interpreted in terms of differential gene expression and growth rates.

At the SAM, auxin importers and exporters are mainly expressed at the meristem surface [7]. When auxin transport is inhibited, organ initiation is severely affected or even totally absent [13]. In addition, the cells at the SAM orient their PIN proteins

Author Summary

Plants continuously generate new organs through the activity of populations of stem cells called meristems. The shoot apical meristem (SAM) initiates leaves, flowers, and lateral organs in highly ordered, spiraled, or whorled arrangements via a process called phyllotaxis. Auxin, a plant hormone, plays an essential role in this process. It is actively transported from cell to cell by specific membrane-associated transporters. In the SAM, this coordinated transport creates organized auxin fluxes resulting in hormone accumulation at precise positions, where organ formation is triggered. One key question in this process is to understand how auxin transport is coordinated. To address this issue, we have investigated a specific hypothesis, the canalization hypothesis, whereby every cell senses and attempts to stabilize existing hormone fluxes. Because such a patterning process would require the interaction of hundreds of cells, it is impossible to estimate on a purely intuitive basis whether it would be able to generate the observed organ positions. We, therefore, developed a computational approach to test this hypothesis and showed that a flux-based mechanism is indeed able to generate phyllotactic patterns and is consistent with biological data describing meristem development.

towards the young primordia and it is now currently thought that organs are initiated at auxin accumulation points, while the hormone is depleted in their neighbourhoods [7]. The young primordia would thus create drainage basins in their vicinity which would be equivalent to the inhibitory fields proposed previously. While the coherent behaviour of PIN proteins in cell populations is well established, the actual mechanism behind this phenomenon is still not well understood. So far two basic concepts have been proposed.

A first hypothesis is based on the pioneering work of Sachs (1969) on vascular tissue differentiation in plants [14]. Sachs proposed that auxin transport is facilitated during the process of vascular tissue induction. He suggested that the positive feedback between flux and transport is able to amplify small fluxes and can potentially create *canals* of auxin between auxin sources and sinks that subsequently differentiate into vein tissues. This positive feedback between flux and transport is at the basis of the *flux-based* polarization mechanism we study in this work. The *canalization* hypothesis was then formalized by Mitchison [15,16] who developed a mathematical model of this process that increases membrane permeability of cell plasma membrane on the sides where the net flux of auxin is positive. This model was then further studied in the context of leaf venation pattern by several authors [17–20] who interpreted the *canalization* hypothesis as a feedback mechanism between auxin fluxes and PIN transporters and studied the properties of such a coupling both on a fixed shape and during leaf development. From the biological point of view, recent experiments tend to support the *canalization* hypothesis, at least in the inner tissues of the plant [21–23]. However, whether it could also account for the behaviour of auxin transporters in other parts of the plant such as the shoot and root apical meristem or leaf margins remains an open question.

More recently, a second concept was proposed to explain auxin transport at the SAM surface [24,25]. Based on the observation that PIN carriers point to primordia initiation sites in the SAM which supposedly correspond to auxin maxima, it was hypothesized that relative concentrations of auxin in neighbouring cells differentially drive the polarization of PIN1 to the corresponding portion of the membrane between each cell and its neighbours [24]. The cells would thus tend to export auxin against the auxin concentration gradient (referred to here as *concentration-based* hypothesis), thus amplifying differences in local auxin concentrations and creating *local maxima* or *spots* of auxin [22]. The comparision of *concentration-based* and *flux-based* polarization hypothesis is presented in Figure 1, Using computational modelling, several authors were able to show that *concentration-based* hypothesis can produce spiralled and whorled phyllotactic patterns. In a recent article, Merks et al. proposed a modified *concentration-based* hypothesis [26]. Although it requires further development, it is potentially able to explain the formation of veins in internal tissues. Could it, therefore, represent a unifying mechanism for the control of auxin fluxes throughout the plant? A major argument against this idea is that the model does not seem to be compatible with the presence of stable auxin maxima in tissues. This is typically the case at the root meristem, where a continuous, stable auxin maximum is maintained with incoming and outgoing fluxes [27]. In a recent study, Sauer et al. suggested that cell-type specific factors could decide whether one or the other mechanism would be used [23], but this remains to be proven.

Since the *concentration-based* hypothesis can not, on its own, provide a unifying mechanism for the control of auxin fluxes in the plant, we investigated whether *flux-based* polarization hypothesis, as the other major concept in the field could provide a realistic alternative. Since such cell-cell signalling based patterning processes involve the interactions between hundreds of cells it is impossible to estimate on a purely intuitive basis if a particular scenario is plausible or not. In this context, computational

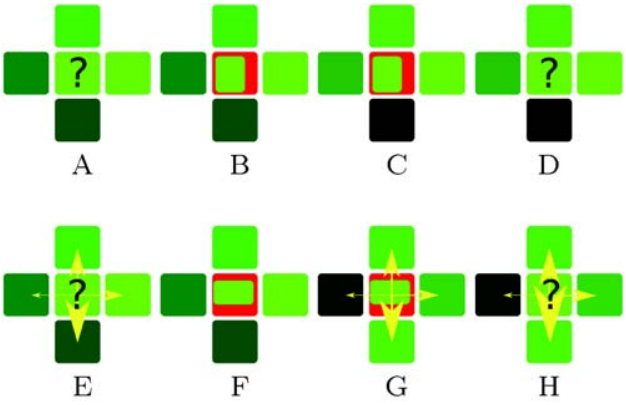

Figure 1. Comparison of two PIN orientation hypotheses. The concentration of auxin in the cells is marked with green (the brighter green, the higher the concentration), the fluxes are depicted with yellow arrows, and PIN concentration at the membranes are indicated by red lines with variable thickness (the thicker the line the higher the concentration). Note that the fluxes might be independent from the concentrations. (E–H) show the principle of the *concentration-based* hypothesis and (A–D) show the principle of *flux-based* polarization hypothesis. In both cases the key question is how the cell marked with "?" should allocate the PINs to its membranes (A,E). In the case of the *concentration-based* hypothesis this cell makes the decision based on the *concentrations* in the neighbouring cells. The higher its neighbours auxin concentration, the more PIN will be inserted in the membrane (F). *Flux-based* polarization depends on the *net flux* between neighbouring cells. The higher the *net flux* to its neighbour the more PIN will be inserted in the membrane (B). In both cases the newly allocated PINs change the concentrations and fluxes (C,G), leading to the next iteration of the scenario (D,H).
doi:10.1371/journal.pcbi.1000207.g001

modelling provides a powerful means to test this type of hypotheses. We therefore designed a set of models and showed that the *flux-based* polarization mechanism is able to:

1. generate spiral phyllotactic patterns observed in the SAM,
2. produce provascular strands below primordia in the subepidermal meristem layers,
3. reproduce stable auxin maxima as observed in the root meristems.

We therefore conclude that flux-based polarization could provide a unifying principle for the guidance of auxin fluxes in the plant. In addition, our model leads to a set of testable predictions, that should be able to distinguish between the *flux-based* and *concentration-based polarization* hypotheses.

Models

Biological Assumptions

To model auxin transport in a tissue we used a set of auxin related hypotheses derived from biological observations taken from the literature (see also introduction):

1. **The Auxin quantity in a cell changes as a result of active transport and diffusion between cells and local creation/degradation** [28], as in previous models [10,24,25].
2. **Auxin is created locally in every cell** (suggested by Reinhard et al. [29], also used in other models [17,24,25]). At this stage all precise locations of auxin synthesis is not well defined, but several of the YUCCA genes involved in auxin synthesis are expressed at the shoot meristem [30].
3. **Auxin is degradated locally in every cell**, e.g., see [31].
4. Auxin is transported from the cell into the inter-cellular space according to the chemiosmotic model [32]. Briefly, this supposes that it is difficult for auxin to leave the cell by diffusion because of the neutral pH of the cytoplasm, whereas it can enter it more freely from the acidic inter-cellular space. Therefore, the plant has developed a system of transporters that facilitates the transport from cell to cell [8,33]. At the meristem, only PIN transporters seem to be polarized, while the AUX/LAX influx carriers are homogeneously distributed over the membrane. We model this overall transport process using a simplified system. First, we assume direct flux of auxin from cell to cell by omitting the wall compartment. Second, due to the symmetry of influx carriers, only PIN is simulated explicitly. Therefore, **we model auxin redistribution in the meristem as a result of passive diffusion between cells and polar transport which is governed by PIN**. A similar approach was also used in other transport models [10,17,24–26].
5. **PIN concentration in a cell membrane is up-regulated by auxin flux through this membrane** [14]. This hypothesis is explained in detail in the Mathematical Formalization section.

To design the model of phyllotaxis, we extended the auxin related hypotheses with a set of hypotheses related to phyllotaxis:

1. The shoot apical meristem is a dome shaped structure, containing up to thousands of cells. **We distinguish the epidermal layer, called L1, that is one cell thick from the subepidermal cells that makes up the rest of the dome.**
2. **The L1 layer is itself composed of a central zone surrounded by a peripheral zone (also called competence zone)**. These zones exhibit different properties [34] as explained below.
3. **Primordia can appear only in the peripheral zone of the meristem** [**1**]. Once a primordium is initiated, it moves away from the meristem summit following a radial trajectory, due to cell growth throughout the L1 [2,35].
4. **In the L1, primordium cells act as sinks by redirecting auxin from the L1 layer downwards**. This hypothesis is justified by the presence of vascular strands below each primordium which would transport auxin downwards [7]. We assume that a primordium can easily remove any amount of auxin (the saturation level is much higher than the amount of auxin available in meristem).
5. Longitudinal sections show that provascular strands are approximately three cells wide (data not shown). Therefore we assume that **a primordium is constructed from a central cell and all its direct neighbours**.
6. **A new primorium is formed as a response to high auxin accumulation in a cell of the competence (peripheral) zone** [1].
7. **Auxin and PIN reallocation are fast processes. PIN proteins can be reallocated within one or two hours ([23], our own unpublished results). Growth occurs at a slower timescale. Typically, a cell doubles its volume in 24 h** [36]. Therefore, as a simplification, we consider auxin concentrations and PIN localisation to be in equilibrium at the time scale used to model growth.
8. **Auxin is concentrated in the L1 and accesses the inner layers via primordia**. Because of the presence of **AUX/LAX** auxin importers, it has been proposed that auxin is concentrated in the L1 layer. It is mainly transported to the inner tissues via the provascular strands in the primordia.

Flux-Based Polarization Model

The model is essentially based on the *flux-based* polarization hypothesis derived from the *canalization* concept, introduced by Sachs [14] who suggested that auxin transport is increased during the vascular induction by the auxin flux itself, leading to the canalization of the flux (for earlier mathematical formalizations see also [15–18,37]. The model is inspired by the original Mitchison model revisited by Rolland-Lagan and Prusinkiewicz [16,18].

Conservation law for the transport of auxin. We denote a_i ($\mathrm{mol\cdot m^{-3}}$) the concentration of auxin in a cell i and $p_{i,n}$ ($\mathrm{mol\cdot m^{-2}}$) the concentration of PIN proteins in the membrane facilitating transport from cell i to cell n. V_i ($\mathrm{m^3}$) denotes cell volume and N_i denotes the set of neighbouring cells of cell i. If i and n are two neighbouring cells, then $S_{i,n}$ ($\mathrm{m^2}$) denotes the exchange surface between these two cells. We assume that the auxin variation rate results from the combination of three processes: (i) diffusion, (ii) active transport of auxin by PIN, and (iii) local cell auxin synthesis and decay (see Auxin Hypotheses 1–4).

$$\frac{\partial a_i}{\partial t} = -\frac{1}{V_i}\sum_{n\in N_i} S_{i,n}J^D_{i\to n} + \\ -\frac{1}{V_i}\sum_{n\in N_i} S_{i,n}J^A_{i\to n} + \alpha_a - \beta_a a_i, \quad (1)$$

where $J^D_{i\to n}$, $J^A_{i\to n}$ are the fluxes of auxin ($\mathrm{mol\cdot m^{-2}\cdot s^{-1}}$) due to

diffusion from cell i to its neighbouring cell n, active transport from cell i to n respectively. By convention, out-going fluxes are positive, incoming fluxes are negative. α_a ($\mathrm{mol{\cdot}m^{-3}{\cdot}s^{-1}}$) is a constant that describes the rate at which auxin is produced in cells and β_a ($\mathrm{s^{-1}}$) defines the rate of auxin decay. Diffusion is modelled using Fick's First Law, $J^D_{i\to n}=\gamma_D(a_i-a_n)$ where γ_D is the constant of permeability reflecting the capability of auxin to move across the membrane ($\mathrm{m{\cdot}s^{-1}}$). In his original paper from 1981, Mitchison proposed to model the flux due to active transport across a *membrane* between cells i and n as $J^A_{i\to n}=\gamma_A(a_i p_{i,n}-a_n p_{n,i})$ where γ_A ($\mathrm{m^3{\cdot}mol^{-1}{\cdot}s^{-1}}$) characterizes the transport efficiency of the PIN pumps. Hence the auxin variation rate in a cell i can be expressed as:

$$\begin{aligned}\frac{\partial a_i}{\partial t} &= -\frac{1}{V_i}\sum_{n\in N_i} S_{i.n}\gamma_D(a_i-a_n)+\\ &-\frac{1}{V_i}\sum_{n\in N_i} S_{i.n}\gamma_A(a_i p_{i,n}-a_n p_{n,i})+\\ &+\alpha_a-\beta_a a_i.\end{aligned} \tag{2}$$

***Flux-based* polarization.** According to Sachs' original concept, *canalization* relies on a feedback mechanism from the auxin fluxes on its transporters. More precisely, we assume that the concentration of PIN proteins $p_{i,n}$ in cell i transporting auxin to cell n changes due to (i) insertion in the *membrane* induced by the flux and (ii) background insertion and removal of PIN from the *membrane*. The net flux of auxin that crosses *membrane* from cell i to cell n is $J_{i\to n}=J^D_{i\to n}+J^A_{i\to n}$.

$$\frac{\partial p_{i,n}}{\partial t}=\Phi(J_{i\to n})+\alpha_p-\beta_p p_{i,n}, \tag{3}$$

where Φ defines the intensity of PIN insertion into the *membrane* due to the feedback of the auxin flux, α_p ($\mathrm{mol{\cdot}m^{-2}{\cdot}s^{-1}}$) describes the rate of background PIN insertion into the *membrane*, and β_p ($\mathrm{s^{-1}}$) the background removal rate from the *membrane*. Depending on the nature of the Φ function, different types of canalization regimes can be obtained ([17] and see below). In this paper we use two types of functions: a linear function $\Phi_L(\mathcal{J}_{i\to n})=\kappa(\mathcal{J}_{i\to n}/\mathcal{J}_{\mathrm{ref}})$ and a quadratic function $\Phi_Q(\mathcal{J}_{i\to n})=\kappa(\mathcal{J}_{i\to n}/\mathcal{J}_{\mathrm{ref}})^2$, where κ ($\mathrm{mol{\cdot}m^{-2}{\cdot}s^{-1}}$) is a constant parameter and $\mathcal{J}_{\mathrm{ref}}$ ($\mathrm{mol{\cdot}m^{-2}{\cdot}s^{-1}}$) is an arbitrary reference flux that makes it possible to keep constant units in the equation. For a negative net flux the Φ functions are truncated to 0, which means that no additional PIN is inserted in the *membranes* for which more auxin particles come in than particles come out.

SAM Model

As mentioned above we suppose that auxin flows essentially in two separated conduits: the L1 layer and the subepidermal layers. The two systems meet at the primordia cells. This very localized coupling between epidermal and subepidermal domains makes it possible to model the transport in each pathway independently and to account for their interaction at the sites of primordia only.

Epidermal model. We represent the L1 layer by a set of polygonal cells forming a 2D surface. Similarly to other models of auxin transport at the SAM [24,25], the inter-cellular space was not modelled as a compartment of its own (however see [38]) and the contact between cells was abstracted as a single separation (referred to as *membrane*) allowing auxin molecules to flow between adjacent cells and PIN molecules to accumulate on either side. To model phyllotaxis we included certain topological and geometrical assumptions. We identify a particular point z as the meristem centre. Different zones of the meristem are defined relatively to this centre z. The centroid of each cell i is denoted by o_i. The central zone, $\mathcal{Z}$, is the set of cells whose centroids have a Euclidean distance to the meristem centre z less than or equal to the constant radius $R_{\mathcal{Z}}$. Similarly, a cell i belongs to the peripheral (or competence) zone $\mathcal{C}$ when the distance between its centroid o_i and the meristem centre z is less than or equal to $R_{\mathcal{C}}$ and greater than $R_{\mathcal{Z}}$. Cells i in the peripheral zone can be promoted to primordia cells (which is denoted by $i\in\wp$).

Subepidermal model. Second, to model the vascular pathways below the primordia, we designed a 2D model of a longitudinal section of the SAM where the connection between the epidermal and subepidermal layers could be explicitly represented. In the subepidermal layer, the definition of the zones $\mathcal{Z}$, $\mathcal{C}$, and of primordia cells $\wp$ is analogous to that of the epidermal model. Cells are also represented as 2D planar polygons whose edges represent cell *membranes*.

Growth of the SAM. To simulate meristem dynamics, we used a purely kinetic description of meristem growth [25]. We explicitly defined the velocity v of every point at the meristem surface in a reference frame attached to the meristem centre z. The velocity $v(x)$ of a point x at the meristem surface is assumed to be proportional to its distance to the meristem centre: $v(x)=\rho\,|x-z|$, thus simulating isotropic radial growth [2]. The constant ρ defines the relative elementary growth rate in the radial direction [39]. Due to this global kinetic process, the vertices of each cell move toward the meristem periphery with a velocity growing exponentially. This makes the cells grow smoothly as they move away from the meristem centre. As soon as a cell surface exceeds a constant threshold $S_{\max}$, the cell divides by creating a new wall inside. The position of this wall is computed using a modification of the optimization criterion introduced by Nakielski [40], i.e., finding a wall that both minimizes the distance between two opposite walls of the cell and that divides the cell into two polygons with the same surface. Then, similarly to [25], the cell vertices of newly created walls are slightly moved toward each other to provide a more realistic aspect. After a cell division event, the auxin concentration and PIN concentration in the *membranes* are inherited by the daughter cells from their parent. Primordium identity is inherited by randomly choosing one daughter of the primordium cell as the new primordium cell. The new *membrane* is initialized with α_p/β_p concentration of PIN on both sides. Finally, to keep a constant size of the overall simulation, a cell i that is too far away from the meristem centre z (its centroid o_i is at a distance greater than R_{sim}) is removed from the simulation.

In order to integrate in a single model the different processes involved in the system, i.e., auxin transport, cell growth, division, PIN allocation, and cell differentiation, we assume that these processes take place at different scales. Auxin transport is supposed to be much faster than growth and cell differentiation so that in the growing meristem, auxin concentrations are always at equilibrium.

Practical Aspects of Simulation

Numerical solving. The non-linear system of equations describing the *flux-based* polarization model is integrated using the Scipy package designed for ODE solving [41]. The integration algorithm uses the Adams predictor-corrector method in the non-stiff case [42]. Solver iterations are performed until a stable state is obtained, i.e., until change in auxin concentration becomes less than a predefined threshold value $\varepsilon_{\min}$ in every cell.

Boundary and initial conditions. The boundary conditions for every simulation are specified in the supplementary material

(Text S1). In most simulations boundary cells do not receive any auxin flux from the outside and we assume fixed, null concentration in sinks. In all simulations we assume that the initial auxin concentrations are null and PIN concentration on both sides of the *membrane* are initiated with a basic amount of PIN α_p/β_p.

Visualisation and simulation environment. The visualization of tissue simulations was carried out with PlantGL, an open-source graphic toolkit for the creation, simulation and analysis of 3D virtual plants [43] available in the OpenAlea software platform for plant modelling [44].

General convention for figures. In all figures representing 1D or 2D tissues, we adopted the following graphical conventions: the absence of auxin in a cell is represented by black while the highest concentration is shown in bright green. Intermediate concentrations are represented by interpolations between these two extremes (see Text S1). PIN transporters at the *membrane* of a cell i are represented as a red line. The thickness of this line is proportional to the amount of PIN.

Supplementary materials. For every figure showing a dynamic system, we provide a corresponding movie to capture system dynamics (Videos S1, S2, S3, S4, S5, S6, S7, S8, S9, S10, S11, S12, S13, S14, S15, S16 and S17). Movies are available as supplementary materials and named after the figures. Supplementary text is provided, specifying equations, parameters, boundary and initial conditions and display specific conventions (Text S1).

Results

The study of systems controlled by *flux-based* polarization is not straightforward as the process relies on a feedback loop between auxin concentrations and auxin fluxes in tissues. To address this problem, we first defined different remarkable properties of the *flux-based* polarization that are essential in the generation of patterns. These properties are illustrated on simplified 1D or 2D "virtual tissues". The sensitivity of the model for different parameters was tested. As expected, the sytem was more dependent on certain parameter values, but overall the results were robust (Text S1). Based on this analysis, we then investigated the ability of *flux-based* polarization to produce phyllotactic patterns at the SAM in a way that is consistent with the current biological knowledge and observations.

Flux-Based Polarization Amplifies Fluxes

The *flux-based* hypothesis, proposes that any small flux between two cells in the system will reinforce itself by increasing the local amount of PIN, thus initiating a positive feedback loop. Initial fluxes may typically be generated by diffusion between zones with different concentrations. We illustrated this phenomenon on a 1-dimensional tissue with two perfect auxin sinks at both extremities (Figure 2A). Auxin is produced in every cell except the sink cells. Initially, the highest flux appears close to the sink cells, due to diffusion. This small initial flux is subsequently reinforced by a polar allocation of PIN transporters favoring the evacuation of auxin in the direction initiated by the original flux. If the auxin sink is maintained, the auxin flux reaches a stable state with the maximum concentration of auxin appearing at the maximal distance from both sinks (Figure 2A). This figure also shows that the concentration of PIN at each cell *membrane* linearly increases from the location of the auxin maximum up to the sinks. This is because each cell is producing auxin at a constant rate α_a and in the stationary state the amount of removed auxin must be balanced by auxin synthesis (if we neglect auxin degradation). It implies that the auxin flux should grow linearly in the direction of the closest sink. If the feedback function Φ is linear, this results in a linearly increasing allocation of PINs to the cell *membranes* in the direction of the closest sink.

Flux-Based Polarization Allows Auxin To Flow with or against Auxin Gradients

Although the molecular mechanism underlying PIN polarization is still unknown, PIN proteins can polarize either *with* or *against* the gradient of auxin [8,22,45]. If a unique transport mechanism is operating in the plant it should thus be able to reproduce this property. In the previous example, auxin fluxes were amplified from regions of high concentration of auxin to regions of low concentration (Figure 2A). Auxin thus flowed *with* the auxin gradient.

To show that *flux-based* polarization can also lead to flow against the gradient, we modified the above 1-dimensional model by weakening the sinks in such a way that they were only able to degrade auxin at a finite constant rate. This simple modification produces a drastic change in the system's behaviour. The auxin gradient is now reversed in the stable state, with highest concentrations at the sink locations and lowest in the places *maximizing* the distance to all sinks (Figure 2B).

To study the conditions for either pumping *with* or *against* the gradient, we considered a system of two cells sharing a *membrane*. One cell is a source of auxin while the other acts as a sink destroying auxin at a constant rate. Once this system reaches a stable state, the net flux across the *membranes* separating the two cells is exactly equal to the rate at which the source creates auxin and leads to a polarization of PIN from the source to the sink. Depending on the model parameters, the system can reach different levels of concentration in both cells. Two regimes may be obtained as shown by the graphs (Figure 2C and 2D). The transition between both regimes, pumping *with* or *against* the gradient, can be obtained by varying different parameters of the model such as the feedback strength and the degradation rate (2).

Flux-Based Polarization Has Two Different Regimes (*Weak* and *Strong*)

Initially, the *flux-based* polarization hypothesis was introduced to model the formation of vascular canals in stem and leaf tissues, as an integral part of the *canalization* concept [15–17,19,37]. Using this mechanism in the meristem may seem in contradiction with the absence of canals at the meristem surface. Feugier et al. [17] demonstrated that a *fluxed-based* polarization mechanism where the feedback function Φ was linear did not result in the formation of canals in a tissue. We further confirmed this by comparing the behaviour of auxin transporters in a 2D sheet of cells showing weak or strong feedback. When the feedback function Φ is non-accelerating (increasing linearly or less rapidly than linearly) the process creates laminar flows transported by homogeneous arrangement of PINs and converging to the sink (Figure 3A). We refer to such a system as a *weak* regime. Conversely, when the feedback function Φ is *accelerating* (increasing more rapidly than linearly), canals appear, creating branching structures in the 2D tissue (Figure 3B). We will call such a system a *strong* regime. In both cases, fluxes may be oriented with or against the gradient, depending on the model parameters and boundary conditions.

The *Weak* Regime Can Produce Fields of Lateral Inhibition of Varying Intensities

As explained earlier, the most widely accepted theory of phyllotaxy relies on the formation of inhibitory fields around each primordium. Recent models propose that these fields are in fact

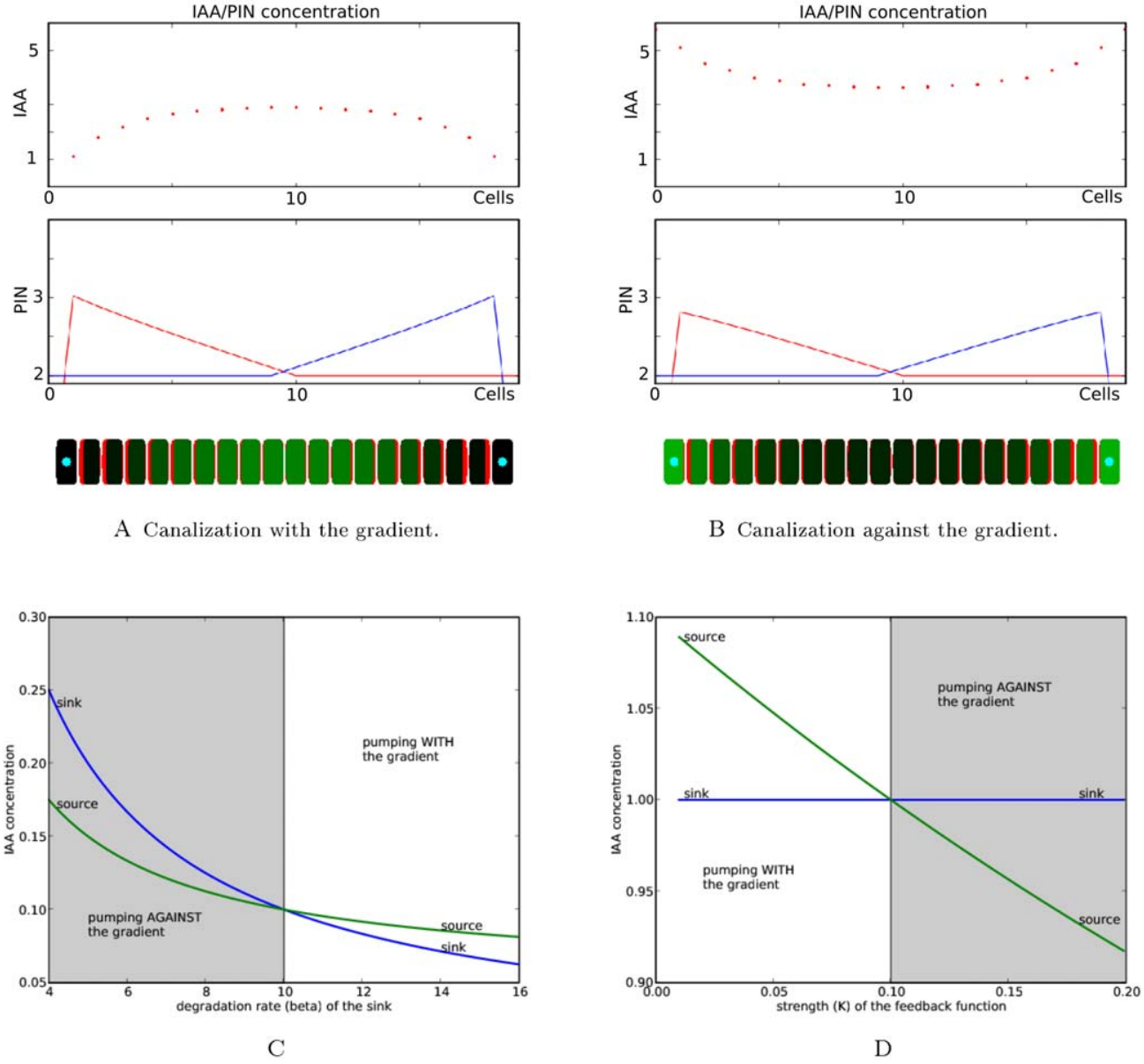

Figure 2. Canalization in a 1-dimensional cellular system. (A,B) show the system consists of 20 linearly aligned cells. Boundary cells are acting as sinks; hence they evacuate or degrade auxin. At the start of the simulation the cells do not contain auxin. Then the simulation runs until a stable state emerges. On the two first plots (A,B) the blue and red lines correspond to PIN concentrations at the right and left side of the membranes respectively. The two systems differ only by the way auxin is removed: in (A) we assume that the removal in the sink cells is very efficient whereas in (B) the removal efficiency is limited. This difference leads us to two different stationary patterns in which the auxin gradients are opposite and the sink cells are minima of auxin (A) or maxima (B). (C,D) present a further analysis of the conditions leading to pumping against or with the gradient. For this purpose a system of two cells sharing one membrane was analysed. (C) presents the concentrations of auxin in the two cells in the stable state as a function of the degradation rate β of the sink. The green curve corresponds to auxin concentrations in the source cell, the blue curve corresponds to auxin concentrations in the sink cell. In the grey region, pumping is carried out against the auxin gradient, while in the white region, pumping follows the gradient. (D) shows similar curves for the variation of the feedback strength κ of flux on PIN synthesis.
doi:10.1371/journal.pcbi.1000207.g002

zones where auxin is depleted [2,3,6]. To show that *flux-based* polarization can indeed be considered as a plausible mechanism, we demonstrate that it can generate such inhibitory fields with varying intensities.

A *weak* regime (as in Figure 3A) leads to the formation of a zone around the sink where auxin is depleted. The intensity of the auxin depletion fields around sinks can be changed by tuning the parameter κ that controls the feedback level of auxin fluxes on PIN insertion in the *membranes*. Figure 4 shows the extent of inhibitory fields (in black) around the blue sinks for increasing values of parameter κ. PIN is regularly distributed throughout the tissue, with a polarity that is determined by the relative distance of the cell to the different sinks. The weak regime thus makes it possible to vary the auxin depletion level around sinks. It therefore provides a plausible explanation for the formation of inhibitory fields during organ initiation at the SAM.

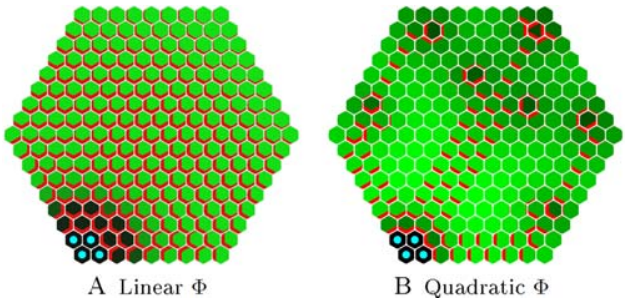

Figure 3. Weak and strong regimes on 2D hexagonal lattices. The sink cells are tagged with blue dots. (A) shows the stable state in case of a weak regime. At the end of the simulation the auxin concentration is progressively increasing with the distance from the sink. PIN, marked in red, is present in all cells leading to a laminar flow over the entire surface. (B) shows the stable state of a strong regime with one sink leading to the formation of canals (where PIN is present) and patches of cells without transporter. This system corresponds to the original *canalization* concept.
doi:10.1371/journal.pcbi.1000207.g003

Flux-Based Polarization as a Source of Patterning in a Growing Structure

The mechanism that controls PIN orientation in cells takes place in a growing structure. Therefore we constructed a dynamic model with dividing and growing cells. As before, we assume that all cells create auxin except for a limited number of cells marked as sinks in which auxin concentration is fixed at 0. To produce phyllotactic patterns, the combination of *flux-based* polarization hypothesis and tissue growth should therefore show a recurrent, temporal patterning property. We show this property in a simplified 1D model by introducing a sink creation threshold, i.e., an auxin concentration at which a new auxin sink is created. In a growing system, neighbouring auxin sinks are pushed apart. Due to the weakening of the sink influence and the constant local hormone production the level of auxin increases in the zone between these two sinks. At a particular auxin threshold (the sink initiation threshold ω), the amount of hormone is sufficient to initiate a new sink at the location which is the farthest from the two sinks (Figure 5A and 5B). As a result of sink creation, some of the PIN pumps reverse toward the new sink, with PIN and auxin patterns similar to that of the previous sinks. By changing the sink initiation threshold ω, it is possible to augment or to decrease the initiation frequency (Figure 5C–F). In the supplementary materials we show in details how the initiation frequency depends on different model parameters (Text S1).

Flux-Based Polarization Model Can Reproduce Observed PIN Maps and Realistic Influence Zones

In Barbier et al. (2006), we showed that the distribution of PIN at the SAM (called "PIN map") has a number of specific features [10]. As illustrated in Figure 6, PIN labelled membranes are pointing towards their nearest primordium (blue dots in Figures 6B and 6C). In addition, a significant number of cells appear to transport auxin to the meristem summit. A plausible model of phyllotaxy should be able to reproduce similar distributions of PIN.

To determine to what extent the *flux-based* polarization model could reproduce realistic PIN maps, we digitized the cell walls on the images of real meristems, immunolabelled to visualize PIN. We recorded the PIN orientation in each cell as described in [10] (called *real PIN maps* as in Figure 6C). The position of each primordium could be clearly identified as indicated by the convergence of PIN toward particular cells and the presence of vascular strands below these primordia seen on other sections of the same meristem (blue dots in Figure 6B, longitudinal image data not shown). We also designated a central zone of about 6 cells in diameter at the meristem summit. This zone is usually free of primordia in the wild type *Arabidopsis* SAM.

We then simulated the emerging arrangement of PIN distributions according to the *flux-based* polarization hypothesis on the digitized maps. Primordia were considered as perfect sinks while all other cells in the meristem were assumed to produce auxin at a fixed rate according to Equation 2. The resulting PIN distributions are shown in Figure 7. Close to the primordia, the simulated PIN arrangements are converging towards the sink cell and look similar to the PIN arrangements on the real PIN maps (Figure 6A). Besides, auxin accumulates at the position where one would expect the next initium in a spiral phyllotaxy (Figure 7A). However, contrary to real PIN maps, virtual PIN patterns did not show any significant converging tendency towards the centre of the meristem. To overcome this discrepancy, we made a second simulation, where the cells in the meristem centre were assumed to degrade auxin at a higher rate. While the convergence of PIN toward the primordia cells is preserved, an additional convergence of PIN toward the centre is now observed, reflecting more faithfully the observed distributions of PIN in the immunolabelling images (compare Figures 6C and 7B). The same result were obtained by reducing the synthesis of auxin in the central zone of the meristem (result not shown).

To go beyond a simple visual inspection for similarity, we computed the so-called *influence zones* of the primordia and of the central zone in the real meristem and compared them to those in the simulated meristems. The influence zone of a region (i.e., a cluster of cells) is the set of meristem cells that are connected to a

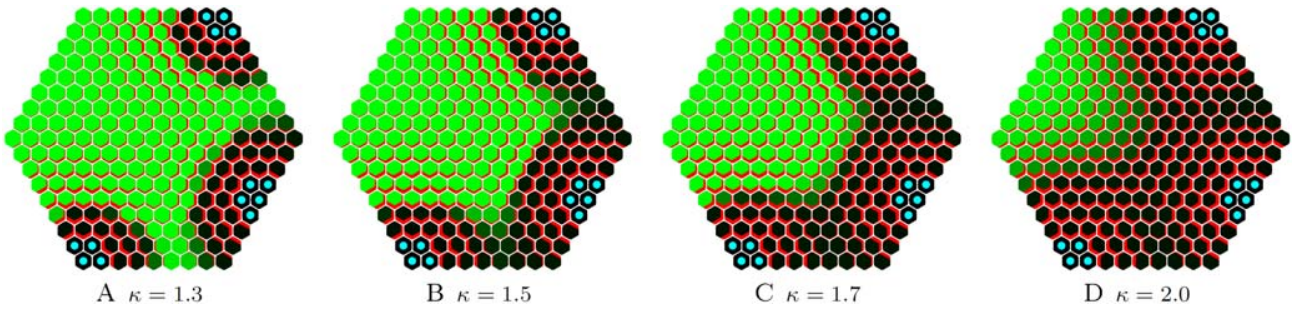

Figure 4. Inhibitory fields induced by a flux-based polarization system. The size of the field changes according to the value of parameter κ which regulates the feedback of fluxes on PIN pumps synthesis.
doi:10.1371/journal.pcbi.1000207.g004

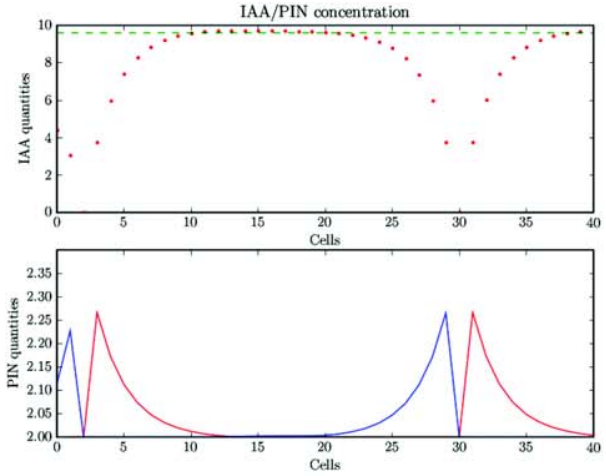

A $\omega = 9.6$

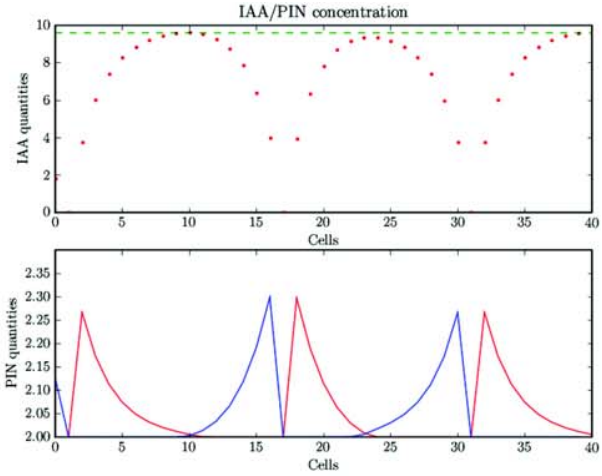

B $\omega = 9.6$

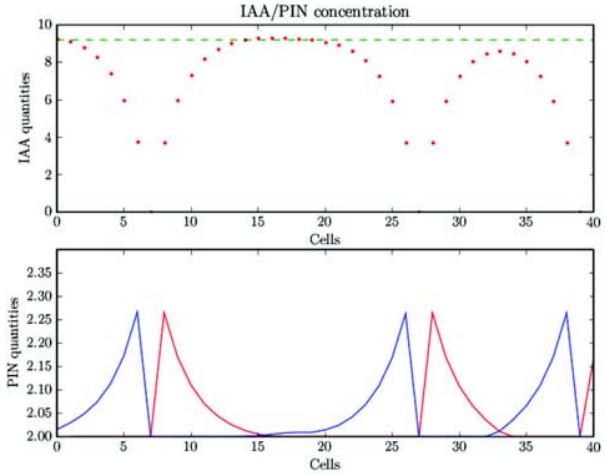

C $\omega = 9.2$

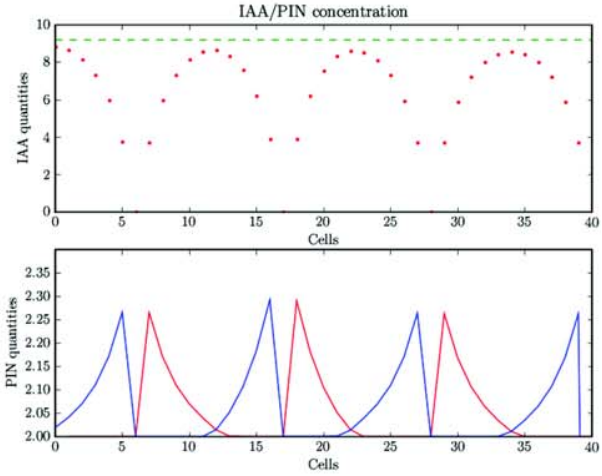

D $\omega = 9.2$

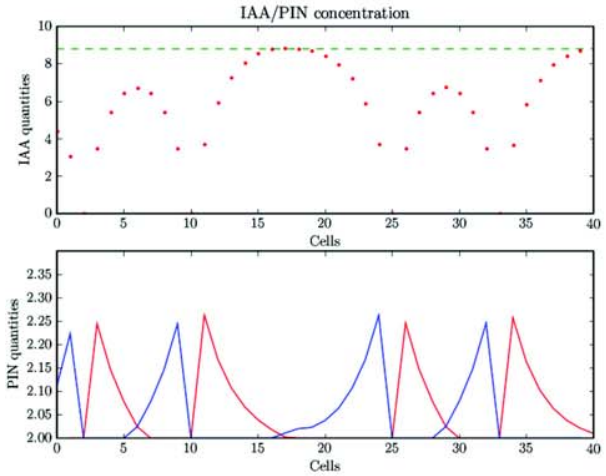

E $\omega = 8.8$

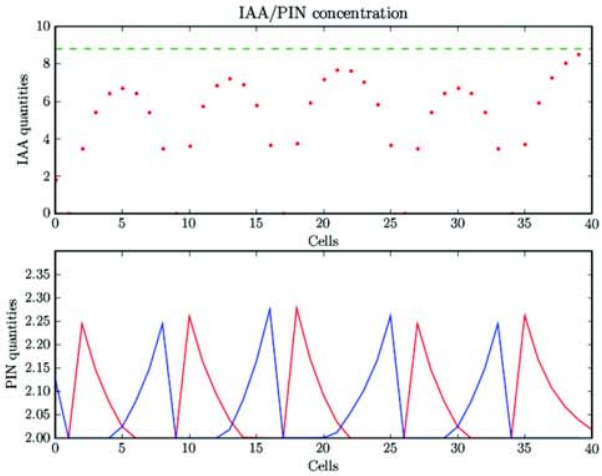

F $\omega = 8.8$

Figure 5. Dynamic patterning with flux-based polarization. (A,B), (C,D), and (E,F) present three simulations with different thresholds ω for primordium initiation. (A,C,E) present the step just before primordium initiation and (B,D,F) present the step just after primordium initiation. The frequency of primordium initiation increases with a decrease of the initiation threshold ω.
doi:10.1371/journal.pcbi.1000207.g005

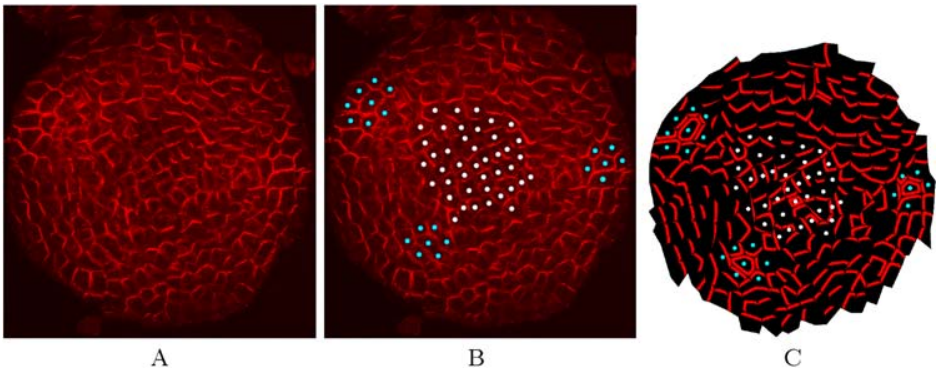

Figure 6. SAM digitalization. (A) shows the PIN distribution in a real meristem obtained using immunolabelling (top view). (B) shows the same image with marked primordia cells (blue dots) and central zone cells (white dots). (C) shows the reproduction of PIN distribution and polarity in a digitized version of the same image.
doi:10.1371/journal.pcbi.1000207.g006

cell of the considered region through a path of PIN arcs oriented in the direction of this region. Figure 8 shows the influence zones of different regions (centre and primordia) on real (Figure 8A–D) and simulated (Figure 8E–L) PIN maps. In real maps, pumps are distributed in such a way that auxin can reach the central zone from all the directions between each pair of primordia (with a small auxin pathway between primordia P_0 and P_2, a larger one between primordia P_0 and P_1 and the largest pathway between P_1 and P_2). Influence zones of the primordia are restricted to the neighbourhood of each primordium and do not extensively overlap with the cells of the central zone. We then computed the influence zones from the first simulation where the central zone did not act as a sink. This showed important differences with the real maps. For the central zone , only two auxin pathways of equivalent width could be observed while the pathway between P_0 and P_2 had disappeared (Figure 8E). In addition, the influence zone of P_0 largely crossed the meristem centre in 8F in contrast to what was observed on the real map. The influence zones of the simulations with auxin depletion in the centre showed better agreement with the influence zones computed from real PIN maps: with three auxin pathways of gradually increasing width going to the meristem centre and the influence zones of primordia being almost non-overlapping with cells in the central zone (Figure 8I–L).

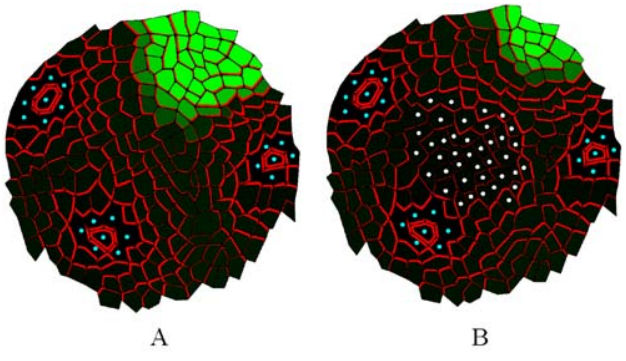

Figure 7. Simulation of auxin transport in a digitized meristem based on the flux-based polarization hypothesis. The cells and primordia of the real meristem shown in Figure 6 were used to initialize the system, and the virtual PIN maps were then calculated based on the flux-based polarization hypothesis. Green intensity is proportional to the virtual auxin concentration. (A) shows a simulation where the centre plays no special role in the auxin flux. (B) shows a simulation where the centre degrades auxin.
doi:10.1371/journal.pcbi.1000207.g007

Formation of Phyllotactic Patterns and Provascular Strands

Based on the preceding results, we designed a dynamic model of phyllotaxy using the *flux-based* polarization hypothesis. The epidermal and subepidermal layers were assumed to be relatively independent, except at the primordia were the two interact by exchanging auxin. This assumption was based on the generally accepted hypothesis that auxin is accumulated in the L1 layer due to the presence of influx carriers of the AUX/LAX family on the cell membranes [7]. This made it possible to simulate auxin transport at the surface and in internal layers separately and to summarize their interactions as boundary conditions. Since in the L1 layer no channels of auxin transport are observed, we supposed that the weak regime prevailed at the surface. For vein formation in inner tissues, we supposed that a strong regime was active.

The simulations using the model characteristics described above resulted in a dynamic pattern of auxin distribution and primordium formation. The following general scenario was observed. In the L1 layer, each primordium evacuates auxin by its provascular system to the inner parts of the meristem. In the L1, the primordium can thus be considered as a sink depleting auxin in its immediate neighborhood. This in turn inhibits the formation of new primordia close to the existing ones (Figure 9A). Due to cell growth, primordia progressively move away from each other, which allows the accumulation of auxin in cells sufficiently distant from these young organs. As a result a new maximum of auxin concentration gradually appears in the region maximally separated from all primordia, thus defining the location of the next initium (Figure 9G). As soon as the auxin concentration exceeds a predefined threshold in a cell belonging to the competent zone surrounding the central zone, this cell and its immediate neighbours acquire primordium identity (Figure 9B). This implies that auxin can leak at the initium location into the inner layers, which triggers the creation of the primordium vascular strand

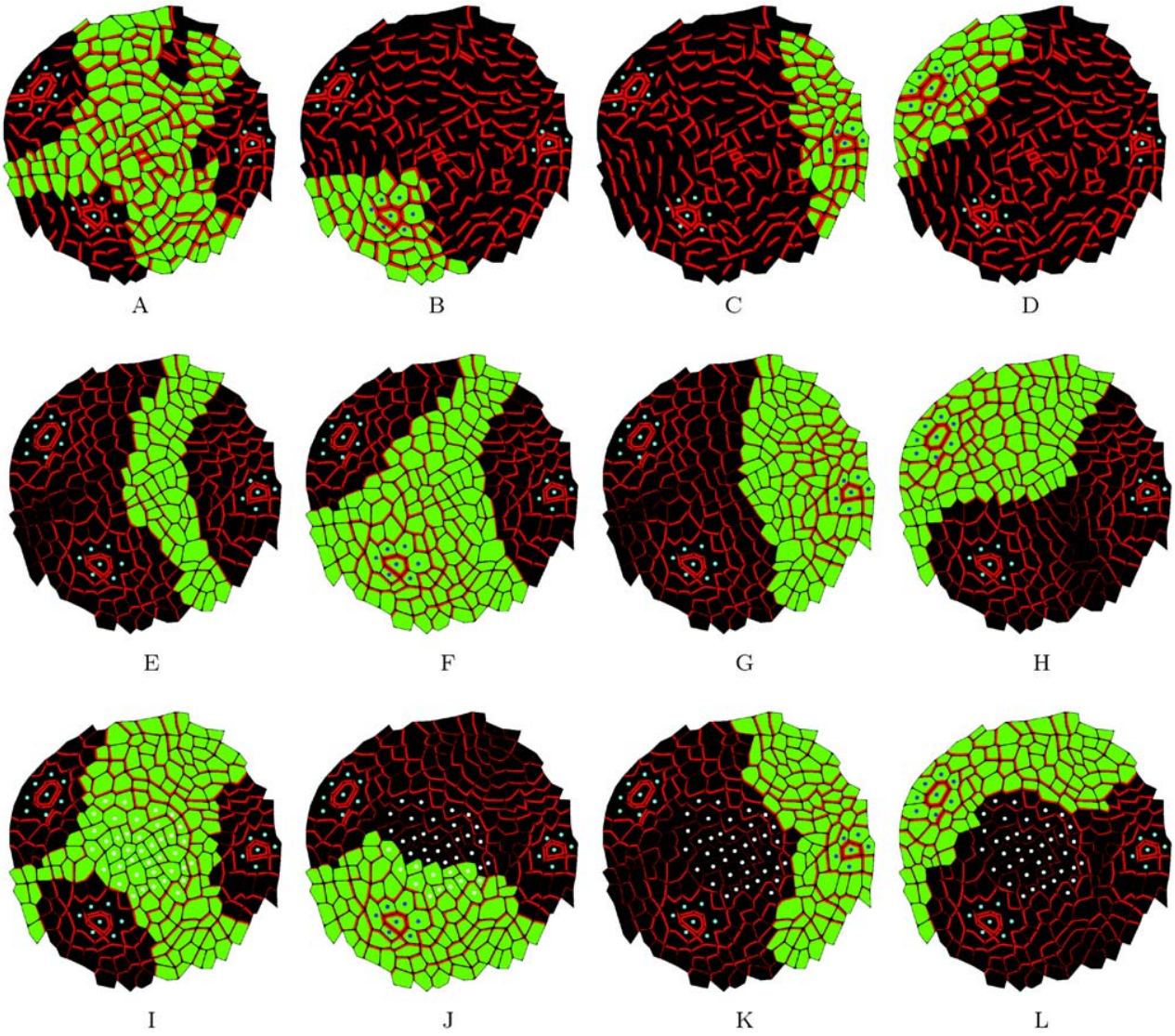

Figure 8. Influence zone analysis. The influence zones calculated for the central zone (first column), P_0 (second column), P_1 (third column), P_2 (fourth column) in real and simulated maps. (A–D) show the influence zones in a real map. (E–H) show the influence zones in digitized maps where PIN labelling was calculated based on the flux-based hypothesis. In this simulation, cells in the central zone are identical to other cells. Primordia (blue cells) are perfect sinks. (I–L) shows a simulation based on the flux-based polarization hypothesis, but here both primordia and cells in the central zone (white cells) are removing auxin. Note that qualitatively the last simulation shows a better match with the original real map.
doi:10.1371/journal.pcbi.1000207.g008

(Figure 9H). The vein being formed below the initium drains the auxin out from the L1 layer and converts the initium into an auxin minimum (Figure 9C and 9H). The flux induced by this process reverses pump polarizations in the direction of the initium in the L1 (Figure 9C and 9I). Then, due to tissue growth, new space becomes available allowing the system to generate a new initium (Figure 9D and 9E). This system is able to produce a stable phyllotactic pattern, with a mean angle close to the golden angle, 137°5 (Figure 9F) observed in *Arabidopsis* and characteristic for spiralled phyllotaxis.

An obvious simplication in this model is the assumption that an instant drop in the auxin concentration occurs when cells of L1 acquire primordium identity. However, modifying the rate at which the auxin concentration changes at the initium showed that an immediate drop gives qualitatively the same patterns as a gradual reduction over time (simulation not included). Since this would add another parameter to the model we kept this simplification.

Discussion

We describe here a *flux-based* model, that provides a realistic explanation for phyllotaxis, predicting patterns of PIN distribution that are very similar to the observed ones. The model leads to a classical inhibitory field scenario where the very young primordia pumps auxin towards the inner tissues, draining the hormone away from their immediate vicinity. As long as these sinks are close to the competence zone, no new primordia can be formed. However, as growth drives the sinks away, auxin concentration can build up again locally because of synthesis and transport, creating a new auxin maximum. The model proposes that the import capacity of the L1 layer at the surface is overridden when a

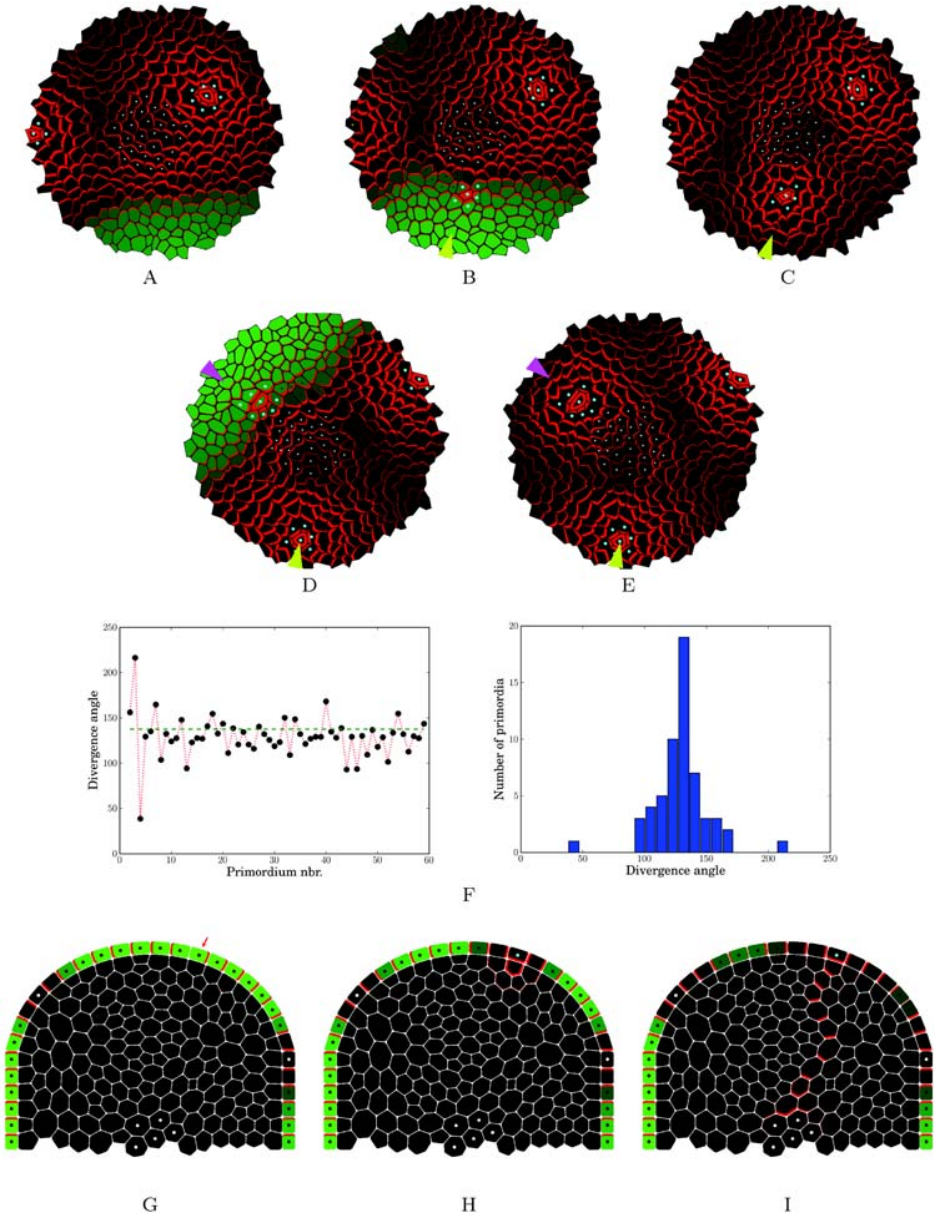

Figure 9. Dynamic models. (A–E) 2D top view of a virtual meristem following the *flux-based* model showing the dynamics of PIN distribution, auxin concentrations and primordia initiation. The sequence shows the initiation of two consecutive primordia (arrowheads). The sequence starts with auxin accumulation in the zone that is the farthest away from the existing primordia. When a threshold is reached, the maximum acquires primordium identity and becomes a sink. (F) shows the variation of the angles between 65 consecutive primordia. Note that the mean value is close to the golden angle (137°5) typical for spiralled phyllotaxis as observed in *Arabidopsis*. (G–I) 2D transversal cut of a virtual meristem following the *flux-based* model showing the dynamics of PIN distribution, leading to the formation of a provascular strand of cells that transport auxin downwards. Detailed description in the text.
doi:10.1371/journal.pcbi.1000207.g009

certain auxin concentration threshold is reached after which the hormone starts to leak away to inner tissues. This initial diffusion-driven flux will be reinforced by *flux-based* polarization. This in turn will rapidly create an auxin transport channel connecting the local surface maximum to the inner vasculature and transforming it into a sink. The main requirement here is that *flux-based* polarization should be relatively weak at the surface, switching to a strong regime in inwards directed fluxes. This switch from one regime to the other could directly depend on the amount of auxin flowing through the cell, but it could also be activated indirectly as part of the differentiation process induced by high auxin concentrations. In such a scenario even a small leakage from the surface to the inner parts would be very rapidly amplified

Flux-Based Polarization Hypothesis as a Unifying Concept

Flux-based polarization provides an alternative explanation for phyllotaxis. Indeed, since it allows for transport with and against gradients, it also provides a plausible explanation for the stable auxin maxima observed in roots and leaves. This is illustrated in Figure 10 where we have reproduced PIN and auxin distributions

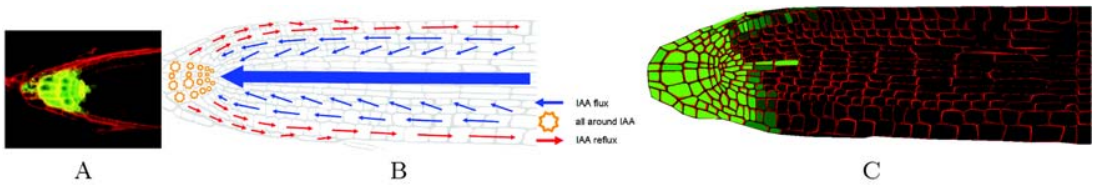

Figure 10. *Flux-based* polarization model of the root meristem. *Flux-based* polarization hypothesis is compatible with the maintenance of an auxin maximum and with the general organization of PIN at the root tip. (A) shows the existence of a stable auxin maximum at the root tip as evidenced by the DR5:GFP marker (Ottenschlager 2003; Grieneisen 2007). At the shoot apex, the general organization of the different PIN transporters in the different tissues suggests a flux going downward via the vascular tissues and than spreading out over superficial layers "like a fountain" (B). (C) shows a digitized root apex based on a real optical section from an *Arabidopsis* root (not shown, image taken by Tom Beeckman). Similarly to PIN maps at the shoot apex, the polarity of PIN was recorded in each cell. This PIN map was used as an initial condition for the simulation. The cellular system was provided with a fixed global quantity of auxin initially divided equally over the tissue. In addition, two border cells of the epidermis were chosen as auxin sinks, to comply with the biological assumption that a fraction of auxin is evacuated from the root tip along the epidermis (Swarup 2005). Auxin arriving in these sink cells is completely depleted at each simulation step. In addition, a permanent auxin source was added on the border of the central vascular system providing auxin in a constant fashion, in accordance to biological auxin source localization in the vascular bundle. Simulations revealed that transporter dynamics based on *flux-based* polarization are sufficient to enable and maintain auxin accumulation in the collumella and quiescent centre (C), as observed in (A). Additionally, realistic transporter distribution profile was maintained by the *flux-based* polarization mechanism.
doi:10.1371/journal.pcbi.1000207.g010

in the root meristem using the flux based hypothesis. An important caveat is that two different regimes are required in the model. As shown previously by Feugier et al., only the weak regime can explain the absence of canals as observed at the meristem surface [17]. In this context it is important to note that the weak regime has some characteristics in common with diffusion. In particular, both processes can lead to auxin transport down the gradient. However, as auxin cannot freely diffuse between the cells, the weak regime is fundamentally different and can only function if the cell is able to sense fluxes. As long as the precise mechanism of PIN localisation is not known, it will be difficult to predict whether each regime would require a completely different cellular mechanism which would go against the idea of a unifying concept. However, it seems reasonable to propose that both regimes correspond to different states of the same flux sensing mechanism. We therefore conclude that the *flux-based* hypothesis remains a potential unifying mechanism for auxin transport throughout the plant.

Confronting the *Flux-Based* Polarization Hypotheses with Experimental Results

Having established that the *flux-based* polarization model can reproduce phyllotactic patterns, it now becomes important to test the hypothesis as rigorously as possible. We have made a first step towards this procedure by comparing the predicted PIN protein patterns with the observed ones. While this in itself is a stringent test, so far not performed on other models, the *flux-based* model should also be coherent with other existing data. In the following paragraphs we will discuss a number of its implications.

Auxin Concentrations at the L1 Layer

Like the *concentration-based* model, the *flux-based* model requires that the patterning process mainly occurs in the L1 layer. This is based on the idea that auxin is concentrated there by auxin importers (AUX1 and LAX proteins) that are strongly expressed in the L1. In addition, the highly organized distribution of PIN at the meristem surface also indicates that the patterning process mainly occurs in the L1 layer. This might seem contradictory with the phenotypes of mutants where the auxin importers are impaired and which are still able to generate primordia. It should be noted, however, that other factors such as the human multiple drug resistance/P-glycoproteins (MDR/PGPs) are also involved in auxin influx [46] and could guarantee the presence of sufficiently high levels of auxin in the L1 layer when the AUX/LAX proteins are inactivated. We therefore conclude that overall our model is in line with the experimental data supporting a major role of the meristem surface in phyllotaxis.

Auxin and the Central Zone

An intriguing aspect of our model concerns the central zone (CZ) cells. Like the *concentration-based* model, the *flux-based* model does not require any particular property of this zone, other than a lack of competence to generate a primordium. We could, however, only obtain realistic patterns of PIN distribution when we attributed a sink function to this zone. This is in line with earlier observations by Barbier et al. (2006) who provided evidence that the CZ receives auxin fluxes [10]. However, the sink function of the CZ required by the *flux-based* model seems in contradiction with the same study showing the presence of relatively high auxin levels there. It is therefore important to note that in the *flux-based* model the concentration in the CZ is not much lower than in the other peripheral zone cells, and is certainly significantly higher than in the primordium cells. Therefore on average the model would predict higher concentrations in the CZ than in the periphery as reported by Barbier et al. (2006). As a result there does not appear to be any conflict between earlier observations and the *flux-based* hypothesis.

Auxin Concentrations and PIN Dynamics

The *flux-based* model scenario proposes that a relatively broad auxin peak leads to an inward flow which rapidly leads to the formation of an auxin sink. It is the formation of this sink that will reorient the PIN transporters in surrounding cells. This scenario seems in contradiction with earlier observations suggesting that (i) the reorientation of PIN transporters precedes the initiation of the young organ and (ii) that an auxin maximum is maintained at the young primordium. There are several explanation for these apparent contradictions.

First, it has not been unambiguously established that the PIN transporters orient before the initiation of the inward flux marked by the formation of the provascular strand. Heisler et al. (2005) showed that there is some reorganisation of PINs before this strand is formed but did not report clear converging transporters [47]. In accordance with this, we have observed the presence of PIN in the internal tissues at a moment where the transporters were not clearly converging

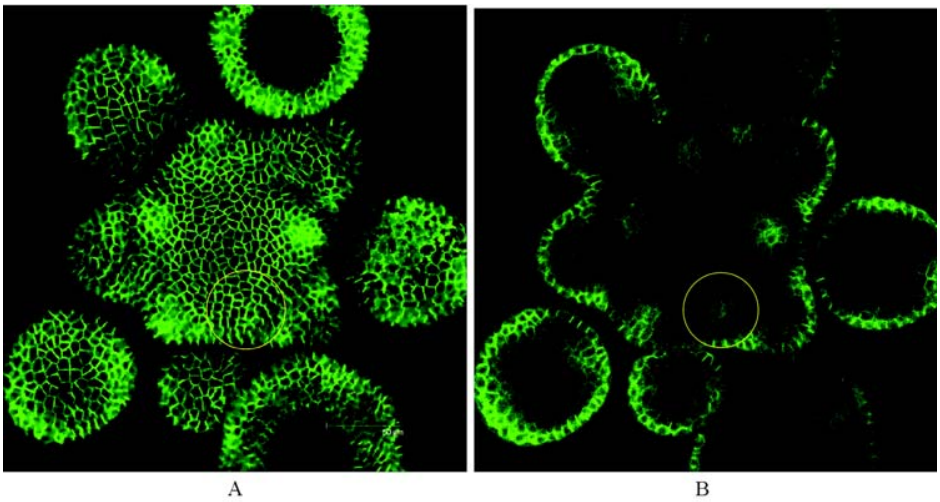

Figure 11. Confocal image of a living meristem expressing a fluorescent version of PIN (PIN1:GFP). (A) shows the higher expression of PIN at the surface around new primordia is clearly observed. The yellow circle indicates the site where the next organ will be initiated. The images show no very obvious reorientation of PIN orientation at this site, although a provascular strand expressing PIN is clearly observed at this site (yellow circle on the individual section of the same meristem in (B)).
doi:10.1371/journal.pcbi.1000207.g011

(Figure 11). We therefore conclude that the precise timing has not been sufficiently well established to draw clear conclusions.

Second, the supposed stable auxin maximum at the young initium has been revealed using the so-called DR5rev promoter driving the green fluorescent protein (GFP). This promoter contains an auxin responsive element and is activated by auxin responsive transcription factors. While it is often presented as a quantitative auxin sensor, it is in fact only a very indirect marker which not only depends on the amount of hormone but also on the capacity of cells to react to it. In addition the fluorescent GFP marker can be stable for prolonged periods, and could therefore mask rapid changes in the activity of the promoter. It is therefore possible that the precise fluctuations in auxin concentrations at the primordium have not been unambiguously established. In addition, DR5rev might not only mark high auxin concentrations but could also be activated by other factors For instance, high levels of another hormone, brassinolide, can activate DR5 in the apparent absence of changes in auxin levels [48]. At this stage, we even cannot exclude that DR5rev reacts to auxin fluxes, although this remains speculative. Interestingly, our simulations show that a *flux-based* activation of DR5rev would give sharp maxima, very comparable to what is observed in vivo (Figure 12).

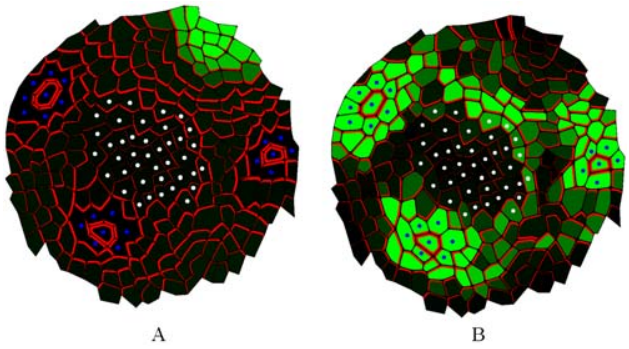

Figure 12. The simulation 7B results showing the predicted levels of auxin concentration (A) and flux intensity (B). The simulation 7B results showing the predicted levels of auxin concentration (A) and flux intensity (B). Note the sharp peaks observed in (B), comparable to DR5rev:GFP peaks observed in vivo [10].
doi:10.1371/journal.pcbi.1000207.g012

General Conclusion

In this study we have shown that the *flux-based* polarization model is a plausible alternative to the existing *concentration-based* model for phyllotaxis. Further experimentation is now required to distinguish between the two models. A careful and quantified description of cell behaviour (e.g., PIN distribution) should be part of this approach. We are further testing this by using transgenic approaches aimed at modifying the capacity of these cells to transport auxin or by changing the auxin content in the same cells. A major scientific question concerns the actual mechanism involved in auxin transport. Indeed a better insight into the process might also help to validate one or the other polarization hypothesis. It is important to note, that both the *flux-based* and *concentration- based* models are obvious abstractions of reality. They both do not, for instance, take into account inter-cellular spaces nor do they indicate how auxin fluxes or auxin concentration gradients are sensed. A process like the *flux-based* polarization mechanism described here could, therefore, be much more complex than just PIN proteins sensing auxin particles flowing through the cell. What is important here is that the overall behaviour of the system can be described accurately by flux-based polarization model with predicted, testable properties.

Supporting Information

Text S1 Equations, parameters, boundary and initial conditions, and display conventions. This file describes all the mathematical and practical details that have been used to perform the simulations used in the paper. In particular, all parameter values are provided for each experiment.
Found at: doi:10.1371/journal.pcbi.1000207.s001 (0.31 MB PDF)

Video S1 Movie presents the dynamics of Figure 2A.
Found at: doi:10.1371/journal.pcbi.1000207.s002 (0.31 MB AVI)

227 **Video S2** Movie presents the dynamics of Figure 2B.

Found at: doi:10.1371/journal.pcbi.1000207.s003 (0.37 MB AVI)

Video S3 Movie presents the dynamics of Figure 3A.
Found at: doi:10.1371/journal.pcbi.1000207.s004 (1.00 MB AVI)

Video S4 Movie presents the dynamics of Figure 3B.
Found at: doi:10.1371/journal.pcbi.1000207.s005 (2.43 MB AVI)

Video S5 Movie presents the dynamics of Figure 4A.
Found at: doi:10.1371/journal.pcbi.1000207.s006 (0.97 MB AVI)

Video S6 Movie presents the dynamics of Figure 4B.
Found at: doi:10.1371/journal.pcbi.1000207.s007 (0.95 MB AVI)

Video S7 Movie presents the dynamics of Figure 4C.
Found at: doi:10.1371/journal.pcbi.1000207.s008 (0.95 MB AVI)

Video S8 Movie presents the dynamics of Figure 4D.
Found at: doi:10.1371/journal.pcbi.1000207.s009 (0.80 MB AVI)

Video S9 Movie presents the dynamics of Figure 5A.
Found at: doi:10.1371/journal.pcbi.1000207.s010 (4.15 MB AVI)

Video S10 Movie presents the dynamics of Figure 5C.
Found at: doi:10.1371/journal.pcbi.1000207.s011 (4.24 MB AVI)

Video S11 Movie presents the dynamics of Figure 5E.
Found at: doi:10.1371/journal.pcbi.1000207.s012 (4.17 MB AVI)

Video S12 Movie presents the dynamics of Figure 7A.
Found at: doi:10.1371/journal.pcbi.1000207.s013 (1.45 MB AVI)

Video S13 Movie presents the dynamics of Figure 7B.
Found at: doi:10.1371/journal.pcbi.1000207.s014 (0.74 MB AVI)

Video S14 Movie presents the dynamics of Figure 9A (part 1).
Found at: doi:10.1371/journal.pcbi.1000207.s015 (8.96 MB AVI)

Video S15 Movie presents the dynamics of Figure 9A (part 2).
Found at: doi:10.1371/journal.pcbi.1000207.s016 (7.38 MB AVI)

Video S16 Movie presents the dynamics of Figure 9G.
Found at: doi:10.1371/journal.pcbi.1000207.s017 (0.92 MB AVI)

Video S17 Movie presents the dynamics of Figure 10A.
Found at: doi:10.1371/journal.pcbi.1000207.s018 (1.66 MB AVI)

Acknowledgments

The authors thank Olivier Hamant, Teva Vernoux, Laurent Laplaze, Pradeep Das, Vincent Mirabet as well as the reviewers for their fruitful comments on the initial version of the manuscript. Figure 11 was provided by Isabelle Courseau. The PIN1:GFP line used to take the image in Figure 11 was a generous gift of J. Friml.

Author Contributions

Conceived and designed the experiments: SS ML JT CG. Performed the experiments: SS ML MS. Analyzed the data: SS JC JT CG. Contributed reagents/materials/analysis tools: SS JC MS CG. Wrote the paper: SS JC JT CG.

References

1. Reinhardt D, Mandel T, Kuhlemeier C (2000) Auxin regulates the initiation and radial position of plant lateral organs. Plant Cell 12: 507–518.
2. Douady S, Couder Y (1996) Phyllotaxis as a dynamical self organizing process Part II: the spontaneous formation of a periodicity and the coexistence of spiral and whorled patterns. J Theor Biol 178: 275–294.
3. Snow M, Snow R (1962) A theory of the regulation of phyllotaxis based on Lupinus albus. Philos Trans R Soc Lond Ser B Biol Sci 244: 483–513.
4. Atela P, Golé C, Hotton S (2002) A dynamical system for plant pattern formation: a rigorous analysis. J Nonlinear Sci 12: 641–676.
5. Shipman PD, Newell AC (2004) Phyllotactic patterns on plants. Phys Rev Lett 92: 168102.
6. Smith R, Kuhlemeier C, Prusinkiewicz P (2006) Inhibition fields for phyllotactic pattern formation: a simulation study. Can J Bot 84(11): 1635–1649.
7. Reinhardt D, Pesce ER, Stieger P, Mandel T, Baltensperger K, et al. (2003) Regulation of phyllotaxis by polar auxin transport. Nature 426: 255–260.
8. Vieten A, Sauer M, Brewer PB, Friml J (2007) Molecular and cellular aspects of auxin-transportmediated development. Trends Plant Sci 12: 160–168.
9. Petrasek J, Mravec J, Bouchard R, Blakeslee JJ, Abas M, et al. (2006) PIN proteins perform a rate-limiting function in cellular auxin efflux. Science 312: 914–918.
10. Barbier de Reuille P, Bohn-Courseau I, Ljung K, Morin H, Carraro N, et al. (2006) Computer simulations reveal properties of the cell-cell signaling network at the shoot apex in Arabidopsis. Proc Natl Acad Sci U S A 103: 1627–1632.
11. Reinhardt D, Kuhlemeier C (2002) Plant architecture. EMBO Rep 3: 846–851.
12. Kuhlemeier C (2007) Phyllotaxis. Trends Plant Sci 12: 143–150.
13. Okada K, Ueda J, Komaki MKK, Bell CJJ, Shimura Y (1991) Requirement of the auxin polar transport system in early stages of Arabidopsis floral bud formation. Plant Cell 3: 677–684.
14. Sachs T (1969) Polarity and the induction of organized vascular tissues. Ann Bot 33: 263–275.
15. Mitchison GJ (1980) A model for vein formation in higher plants. Proc R Soc Lond Ser B 207: 79–109.
16. Mitchison GJ (1981) The polar transport of auxin and vein pattern in plants. Philos Trans R Soc Lond Ser B Biol Sci 295: 461–471.
17. Feugier FG, Mochizuki A, Iwasa Y (2005) Self-organization of the vascular system in plant leaves: inter-dependent dynamics of auxin flux and carrier proteins. J Theor Biol 236: 366–375.
18. Rolland-Lagan AG, Prusinkiewicz P (2005) Reviewing models of auxin canalization in the context of leaf vein pattern formation in arabidopsis. Plant J 44: 854–865.
19. Runions A, Fuhrer M, Lane B, Federl P, Rolland-Lagan AG, et al. (2005) Modeling and visualization of leaf venation patterns. ACM Trans Graph 24: 702–711.
20. Dimitrov P, Zucker SW (2006) A constant production hypothesis guides leaf venation patterning. Proc Natl Acad Sci U S A 103: 9363–9368.
21. Scarpella E, Francis P, Berleth T (2004) Stage-specific markers define early steps of procambium development in arabidopsis leaves and correlate termination of vein formation with mesophyll differentiation. Development 131: 3445–3455.
22. Scarpella E, Marcos D, Friml J, Berleth T (2006) Control of leaf vascular patterning by polar auxin transport. Genes Dev 20: 1015–1027.
23. Sauer M, Balla J, Luschnig C, Wisniewska J, Reinohl V, et al. (2006) Canalization of auxin flow by aux/iaa-arf-dependent feedback regulation of pin polarity. Genes Dev 20: 2902–2911.
24. Jönsson H, Heisler MG, Shapiro BE, Meyerowitz EM, Mjolsness E (2006) An auxin-driven polarized transport model for phyllotaxis. Proc Natl Acad Sci U S A 103: 1633–1638.
25. Smith RS, Guyomarc'h S, Mandel T, Reinhardt D, Kuhlemeier C, et al. (2006) A plausible model of phyllotaxis. Proc Natl Acad Sci U S A 103: 1301–1306.
26. Merks RM, Van de Peer Y, Inze D, Beemster GT (2007) Canalization without flux sensors: a traveling-wave hypothesis. Trends Plant Sci 12: 384–390.
27. Grieneisen VA, Xu J, Maree AF, Hogeweg P, Scheres B (2007) Auxin transport is sufficient to generate a maximum and gradient guiding root growth. Nature 449: 1008–1013.
28. Edelstein-Keshet L (1988) Mathematical Models in Biology. 1st edition. New York: McGraw-Hill Companies.
29. Reinhardt D, Frenz M, Mandel T, Kuhlemeier C (2005) Microsurgical and laser ablation analysis of leaf positioning and dorsoventral patterning in tomato. Development 132: 15–26.
30. Cheng Y, Dai X, Zhao Y (2006) Auxin biosynthesis by the yucca flavin monooxygenases controls the formation of floral organs and vascular tissues in arabidopsis. Genes Dev 20: 1790–1799.
31. Ljung K, Hull AK, Kowalczyk M, Marchant A, Celenza J, et al. (2002) Biosynthesis, conjugation, catabolism and homeostasis of indole-3-acetic acid in arabidopsis thaliana. Plant Mol Biol 49: 249–272.
32. Rubery PH, Sheldrake AR (1974) Carriermediated auxin transport. Planta 118: 101–121.
33. Geldner N, Friml J, Stierhof YD, Jurgens G, Palme K (2001) Auxin transport inhibitors block pin1 cycling and vesicle trafficking. Nature 413: 425–428.
34. Steeves T, Sussex I (1972) Patterns in Plant Development. Englewood Cliffs (New Jersey): Prentice Hall.
35. Reddy VG, Heisler MG, Ehrhardt DW, Meyerowitz EM (2004) Real-time lineage analysis reveals oriented cell divisions associated with morphogenesis at the shoot apex of Arabidopsis thaliana. Development 131: 4225–4237.
36. Grandjean O, Vernoux T, Laufs P, Belcram K, Mizukami Y, et al. (2004) In vivo analysis of cell division, cell growth, and differentiation at the shoot apical meristem in arabidopsis. Plant Cell 16: 74–87.
37. Fujita H, Mochizuki A (2006) Pattern formation of leaf veins by the positive feedback regulation between auxin flow and auxin efflux carrier. J Theor Biol 241: 541–551.
38. Kramer EM, Bennett MJ (2006) Auxin transport: a field in flux. Trends Plant Sci 11: 382–386.

39. Nakielski J, Hejnowicz Z (2003) The description of growth of plant organs: a continuous approach based on the growth tensor. Hingham (Massachusetts): Kluwer Academic Publishers. pp 119–136.
40. Nakielski J (2000) Tensorial model for growth and cell division in the shoot apex. In: Carbone A, Gromov M, Prusinkiewicz P, eds. Pattern Formation in Biology, Vision and Dynamics. Signapore: World Scientific Publishing. pp 252–267.
41. Jones E, Oliphant T, Peterson P (2001) Scipy: Open source scientific tools for python.
42. Curtiss CF, Hirschfelder JO (1952) Integration of stiff equations. Proc Natl Acad Sci U S A 38: 235–243.
43. Pradal C, Boudon F, Nouguier C, Chopard J, Godin C (2007) Plantgl: a python-based geometric library for 3d plant modelling at different scales. Technical report, INRIA.
44. Pradal C, Dufour-Kowalski S, Boudon F, Fournier C, Godin C (2008) Openalea: a visual programming and component-based software platform for plant modeling. Funct Plant Biol, in revision.
45. Heisler M, Jonsson H (2006) Modeling auxin transport and plant development. J Plant Growth Regul 25: 302–312.
46. Blakeslee JJ, Bandyopadhyay A, Lee OR, Mravec J, Titapiwatanakun B, et al. (2007) Interactions among pin-formed and p-glycoprotein auxin transporters in arabidopsis. Plant Cell 19: 131–147.
47. Heisler MG, Ohno C, Das P, Sieber P, Reddy GV, et al. (2005) Patterns of auxin transport and gene expression during primordium development revealed by live imaging of the arabidopsis inflorescence meristem. Curr Biol 15: 1899–1911.
48. Nakamura A, Higuchi K, Goda H, Fujiwara MT, Sawa S (2003) Brassinolide induces iaa5, iaa19, and dr5, a synthetic auxin response element in Arabidopsis implying a cross talk point of brassinosteroid and auxin signaling. Plant Physiol 133: 1–11.

Titre Modélisation du développement du méristème apical caulinaire d'*Arabidopsis*

Résumé Cette thèse présente le résultat de recherches utilisant la modélisation informatique pour améliorer la compréhension du développement du méristème apical caulinaire (SAM), en particulier le processus, appelé phyllotaxie, d'initiation régulière des organes. Ce travail s'intéresse au role de l'auxine, une hormone essentielle à la plante, dans le développement du SAM. Dans cette thèse, j'introduis un modèle de transport de l'auxine à l'échelle cellulaire qui est capable de reproduire la phyllotaxie spiralée observée in vivo. Le transport de l'auxine est facilité par une famille de protéines trans-membranaires appelées PIN. La polarisation de ces transporteurs PIN à l'intérieur d'une cellule est régulée par le flux d'auxine, tel que suggéré originellement par Tsvi Sachs dans son concept de canalisation. Le modèle proposé, basé sur les flux d'auxine, reproduit la distribution des pompes PIN observée in vivo, à la fois dans la couche L1 et dans l'interieur du méristème. La deuxième partie de la thèse concerne la simulation de la croissance du méristème. Dans cette partie, j'introduit un système physique de simulation de la croissance du méristème qui inclus les tropismes. L'auxine est connue pour modifier la rigidité des parois cellulaires et entraine une croissance accrue aux points de forte concentration. Le modèle précédent de transport d'auxine est donc couplé à ce modèle physique de croissance pour obtenir une rétroaction du patron d'accumulation de l'auxine sur la croissance des cellules.

Mots-clés Dévéloppement, arabidopsis, simulations, auxine, croissance, canalisation

Title Modelling development of shoot apical meristem of *Arabidopsis*

Abstract The research presented in this thesis uses computational techniques to heighten our comprehension of shoot apical meristem (SAM) development, and in particular the process of regular organ initiation, called phyllotaxis. This work is focused on the role of an essential plant hormone, auxin, in SAM development. In this thesis, I introduce an auxin-transport model of phyllotaxis at cellular scale, which is able to reproduce spiral phyllotaxis patterns observed in vivo. The auxin-transport is mediated by special membrane carrier molecules, called PIN proteins. The polarization of PIN inside of the cell is regulated by the flux of auxin, as it was suggested in the original canalization concept proposed by Tsvi Sachs. The proposed flux-based model reproduces PIN distribution observed in vivo both, in L1 meristem layer and as well in the rib zone of the meristem. Second part of the thesis is dedicated to the simulations of growth. In this part, I introduce the physical-based framework to simulate growth of the meristem including tropisms. Since auxin modifies rigidity of cell walls leading to an increase in growth rates in the spots of its high concentration, the introduced framework is used to upgrade auxin transport-based model of phyllotaxis. In this upgraded model the transport-based patterning mechanism directly modifies the growth directions of the meristem, allowing us to study the coupling of growth, auxin and PIN distributions.

Keywords development, arabidopsis, computer simulation, growth, auxin, canalization